

**Pressure Sensitive Paint Data on the Transonic
Technology Wing Demonstrator (TST)
in the AEDC Propulsion Wind Tunnel 16T**

**M. E. Sellers
Sverdrup Technology, Inc., AEDC Group**

June 1998

Final Report for Period August to November 1997

Approved for public release; distribution is unlimited.

**ARNOLD ENGINEERING DEVELOPMENT CENTER
ARNOLD AIR FORCE BASE, TENNESSEE
AIR FORCE MATERIEL COMMAND
UNITED STATES AIR FORCE**

NOTICES

When U. S. Government drawings, specifications, or other data are used for any purpose other than a definitely related Government procurement operation, the Government thereby incurs no responsibility nor any obligation whatsoever, and the fact that the Government may have formulated, furnished, or in any way supplied the said drawings, specifications, or other data, is not to be regarded by implication or otherwise, or in any manner licensing the holder or any other person or corporation, or conveying any rights or permission to manufacture, use, or sell any patented invention that may in any way be related thereto.

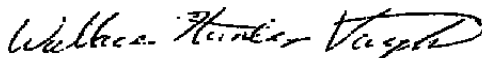
Qualified users may obtain copies of this report from the Defense Technical Information Center.

References to named commercial products in this report are not to be considered in any sense as an endorsement of the product by the United States Air Force or the Government.

This report has been reviewed by the Office of Public Affairs (PA) and is releasable to the National Technical Information Service (NTIS). At NTIS, it will be available to the general public, including foreign nations.

APPROVAL STATEMENT

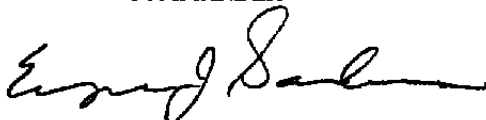
This report has been reviewed and approved.



W. HUNTER VAUGHN
Aircraft Systems Test Division
Test Operations Directorate

Approved for publication:

FOR THE COMMANDER



EUGENE J. SANDERS
Technical Director
Aircraft Systems Test Division

REPORT DOCUMENTATION PAGE			Form Approved OMB No. 0704-0188	
<small>Public reporting burden for this collection of information is estimated to average 1 hour per response, including the time for reviewing instructions, searching existing data sources, gathering and maintaining the data needed, and completing and reviewing the collection of information. Send comments regarding this burden estimate or any other aspect of this collection of information, including suggestions for reducing this burden, to Washington Headquarters Services, Directorate for Information Operations and Reports, 1215 Jefferson Davis Highway, Suite 1204, Arlington, VA 22202-4302, and to the Office of Management and Budget, Paperwork Reduction Project (0704-0188), Washington, DC 20503</small>				
1. AGENCY USE ONLY (Leave blank)		2. REPORT DATE June 1998		3. REPORT TYPE AND DATES COVERED Final Report for Period August - November 1997
4. TITLE AND SUBTITLE Pressure Sensitive Paint Data on the Transonic Technology Wing Demonstrator (TST) in the AEDC Propulsion Wind Tunnel 16T			5. FUNDING NUMBERS PE 65807F JN 3331	
6. AUTHOR(S) Sellers, M. E., Sverdrup Technology, Inc., AEDC Group				
7. PERFORMING ORGANIZATION NAME(S) AND ADDRESS(ES) Arnold Engineering Development Center/DOF Air Force Materiel Command Arnold Air Force Base, TN 37389-6000			8. PERFORMING ORGANIZATION REPORT NUMBER AEDC-TR-98-3	
9. SPONSORING/MONITORING AGENCY NAME(S) AND ADDRESS(ES) Arnold Engineering Development Center/DOF Air Force Materiel Command Arnold Air Force Base, TN 37389-9011			10. SPONSORING/MONITORING AGENCY REPORT NUMBER	
11. SUPPLEMENTARY NOTES Available in Defense Technical Information Center (DTIC).				
12a. DISTRIBUTION AVAILABILITY STATEMENT Approved for public release; distribution is unlimited.			12b. DISTRIBUTION CODE A	
13. ABSTRACT (Maximum 200 words) An improved prototype Pressure Sensitive Paint (PSP) data acquisition and processing system was used to acquire surface pressure data using PSP on the Dornier Alpha Jet with a Transonic Technology (TST) Wing in the AEDC Propulsion Wind Tunnel 16T. A paint formulation developed at the University of Washington was used because of its superior performance characteristics. The process that permits the determination of surface pressure from the paint is described, as well as the image processing that is required. Also, the special illumination and detection components that make up the data acquisition system are presented. Comparisons of conventional pressure measurements and Computational Fluid Dynamics (CFD) results made with the PSP data are presented.				
14. SUBJECT TERMS Pressure Sensitive Paint, flow visualization, TST model, wind tunnel test, surface pressure distribution, transonic flow, spectral characteristics			15. NUMBER OF PAGES 162	
			16. PRICE CODE	
17. SECURITY CLASSIFICATION OF REPORT UNCLASSIFIED	18. SECURITY CLASSIFICATION OF THIS PAGE UNCLASSIFIED	19. SECURITY CLASSIFICATION OF ABSTRACT UNCLASSIFIED	20. LIMITATION OF ABSTRACT SAR	

PREFACE

The work reported herein was conducted by the Arnold Engineering Development Center (AEDC), Air Force Materiel Command (AFMC), under Program Element 65807F, at the request of AEDC/DOT, Arnold AFB, TN 37389-9011. The AEDC Project Managers were Maj. Bret Indermill and Hunter Vaughn. The results of the tests were obtained by Sverdrup Technology, Inc., AEDC Group, support and technical service contractor for the aerospace flight dynamics test facilities at AEDC, AFMC, Arnold AFB, TN. The analysis was performed during the period from October 1997 through November 1997 under AEDC Job Number 3331. This manuscript was approved for publication on May 13, 1998.

A cooperative program between the United States Air Force (USAF) and the German Ministry of Education and Science, Research and Technology (BMBF) was responsible for the execution of the test. The responsibilities of the partners and the objectives of the program are established in a Memorandum of Understanding (MOU) entitled "Wind-Tunnel and Flight Test Data Correlation based on Transonic Technology Demonstrator." The program is structured such that the contribution of the partners is balanced in both cost and technical responsibilities. Technical manager and primary point of contact is Dr. J. W. Davis for the USAF; Dr. E. Stanewsky of DLR (formerly Dr. Lawaczeck) is the point of contact for the BMBF.

CONTENTS

	<u>Page</u>
PREFACE	3
1.0 INTRODUCTION	5
2.0 APPARATUS	5
2.1 Test Article	5
2.2 Pressure Sensitive Paint Theory	5
2.3 Pressure Sensitive Paint	6
2.4 PSP Data System	6
3.0 PROCEDURES	7
3.1 Test Conditions	7
3.2 Data Acquisition	7
3.3 PSP Data Reduction	7
4.0 RESULTS AND DISCUSSION	8
4.1 Pressure Measurement Comparisons	8
4.2 Effects of Paint on Data	9
4.3 PSP to Computational Fluid Dynamics (CFD) Comparisons	10
5.0 SUMMARY	10
REFERENCES	11
NOMENCLATURE	159

ILLUSTRATIONS

<u>Figure</u>	<u>Page</u>
1. TST Model	13
2. Basic Luminescence Process	15
3. Luminescence as Described by the Stern-Volmer Model	16
4. Spectral Characteristics of the FIB7 PSP and Filtered Light Source	17
5. FIB7 PSP Pressure and Temperature Characteristics	18
6. PSP Data Acquisition and Processing System	19
7. TST Conventional and PSP Pressure Coefficient Comparison at Mach Number 0.3 ...	20
8. TST Conventional and PSP Pressure Coefficient Comparison at Mach Number 0.6 ...	32
9. TST Conventional and PSP Pressure Coefficient Comparison at Mach Number 0.835 ..	56
10. PSP Measurement Error Compared to Conventional Measurement	80
11. Pressure vs. Intensity Ratio Data	90

Figure	Page
12. Effects of Paint on Pressure Distribution at Mach Number 0.835	100
13. Reynolds Number Effects on PSP Data at Mach Number 0.835	124
14. Effects of Paint on Model Aerodynamic Coefficients	130
15. TST Pressure Coefficient Distribution at Mach Number 0.835	137
16. TST PSP and CFD Pressure Coefficient Comparison at Mach Number 0.835	147

TABLES

Table	Page
1. TST Wing, Canopy, and Fuselage Pressure Orifice Designation and Location	155
2. Nominal Test Conditions	158

1.0 INTRODUCTION

A demonstration of a prototype Pressure Sensitive Paint (PSP) data acquisition system was performed during a test of the Dornier Alpha Jet with a Transonic Technology (TST) wing in the Arnold Engineering Development Center's (AEDC) Propulsion Wind Tunnel (PWT) 16T in September 1993. For that test, an AEDC paint formulation was applied to the upper wing surface, and an 8-bit video camera was used to acquire images of the painted surface. The specifications of the prototype system and the results of the test are documented in Ref. 1. The model returned to AEDC in August 1997 and was installed in Tunnel 16T for more aerodynamic testing. AEDC has made considerable improvements to the prototype PSP system, and took this opportunity to utilize the new capability to acquire surface pressure data on one-half of the Alpha Jet model. A new paint developed by the University of Washington, designated FIB7, was used because of its superior performance characteristics as compared to the AEDC paint. The 8-bit video camera has been replaced by 16-bit scientific-grade CCD cameras with $1,024 \times 1,024$ -pixel spatial resolution, and the paint illumination system signal-to-noise ratio has been improved. A description of the new PSP system and results from the test are presented herein. Comparisons are made between PSP and conventional pressure measurements and Computational Fluid Dynamics results. Also, the paint's effects on wing surface pressure distribution and vehicle aerodynamic performance are presented.

2.0 APPARATUS

2.1 TEST ARTICLE

The test article was a 1/10-scale model of the Dornier Alpha Jet Technology demonstrator with a TST wing. It was jointly designed by Dornier (fuselage) and Deutsche Aerospace (DASA) (wing). Details of the TST model are presented in Fig. 1. The model was designed to cryogenic testing standards and had a surface finish of $0.2 \mu\text{m}$. Seven canopy and four fuselage pressure orifices were located as shown in Fig. 1a. The starboard wing was instrumented with 169 pressure orifices in the upper and lower surfaces. The pressure orifices were distributed in chordwise rows at five span stations as shown in Fig. 1b. The starboard half of the model (side that was instrumented) was painted with the FIB7 PSP. The wing, canopy, and fuselage pressure orifice designations and locations are listed in Table 1.

2.2 PRESSURE SENSITIVE PAINT THEORY

As described in Refs. 2 and 3, when a luminescent molecule absorbs a photon of appropriate energy, the molecule enters an excited state. From this state, the molecule decays to the ground state through a series of transitions, with at least one resulting in the emission of a photon. Fluorescence is the emission of a photon with a lifetime on the order of 10^{-8} sec and arises from a singlet transition. In contrast, phosphorescence is a delayed emission with a lifetime on the order of 10^{-3} to 100 sec and arises from a triplet-singlet transition. Most luminescent molecules emit very little fluorescence and strong phosphorescence (which is measured). A schematic of the lowest energy level transitions is shown in Fig. 2. Since the energy decay resulting in the photon emission is never complete, the emitted photon will have less energy and, therefore, a longer

wavelength than the original exciting photon. The shift in emission wavelength from the absorption wavelength permits the measurement of emission intensity, or luminescence, with the use of appropriate filters. An alternate transition to the ground state is provided by collision with an oxygen molecule. Rather than emitting a photon, the excess energy of the luminescent molecule is absorbed by the oxygen molecule during a collisional deactivation. Increasing amounts of oxygen increase the collisional deactivations, resulting in a decrease in the amount of luminescence. Since the number of oxygen molecules is directly proportional to the local pressure, low-pressure regions on the surface of a model will be brighter than those of high pressure. The process can be modeled using a simplified form of the Stern-Volmer relation (ignoring temperature effects):

$$\frac{I_0}{I} = 1 + K_q P_{O_2} \quad (1)$$

where I_0 is the PSP luminescence in the absence of oxygen, I and P_{O_2} are the PSP luminescence and partial pressure of oxygen at some pressure, and K_q is the Stern-Volmer constant. Presented in Fig. 3 is a graphic representation of the inverse of Eq. (1) for several Stern-Volmer constants. Paints with a large K_q have higher sensitivity at low absolute pressures and lower sensitivity at high absolute pressures. Paints with a small K_q have a lower, but more constant, sensitivity across the pressure range. Also presented in Fig. 3 is the response of the University of Washington FIB7 PSP at 70°F.

2.3 PRESSURE SENSITIVE PAINT

Two layers of paint typically are applied to the model surface. The first is a white substrate that helps reflect the luminescent light away from the model surface and provides a uniform background. The first layer consisted of the proprietary FIB7 polymer with titanium dioxide. The second, the PSP layer, contains the FIB7 polymer and the luminescent molecule, platinum tetra pentafluorophenyl porphine (PtTFPP). The FIB7 polymer is porous to oxygen molecules permitting contact with the PtTFPP molecules. The absorption and emission spectral characteristics for FIB7 are presented in Fig. 4. Each spectrum was normalized by its peak output. The response of the paint to pressure and temperature was measured in a controlled environment using a special calibration apparatus. The response from a sample of the paint used for the TST test is presented in Fig. 5. The intensity ratio is the inverse of the intensity at each pressure and temperature divided by the intensity at the reference condition (2,000 psfa and 70°F).

2.4 PSP DATA SYSTEM

A schematic of the PSP data acquisition and processing system used during the test is shown in Fig. 6. The starboard half of the model was painted with the FIB7 PSP and illuminated with xenon-arc lamps. Ninety percent or more of the light between 350 and 550 nm was reflected by two cold mirrors, each set at 67.5-deg incidence to the incoming light, through a short wave pass (SWP) filter designed to pass wavelengths below 550 nm and onto the model. The filtered light spectral characteristics are presented in Fig. 4. The filtered light from the xenon-arc lamps passed through optics which spread the light to a diameter of approximately 4 ft at the tunnel centerline. A shutter placed in front of each lamp was opened to pass light only while images were being acquired to reduce photodegradation of the paint. The luminescent light emitted by the paint

passed to the camera detector through a narrow bandpass filter centered at 650 nm with a full width at half maximum of 40 nm. Three scientific-grade CCD cameras were used to obtain black-and-white images of the luminescent surface. The CCD array in each camera had $1,024 \times 1,024$ -pixel spatial resolution and was digitized at 16-bit gray-level resolution.

3.0 PROCEDURES

3.1 TEST CONDITIONS

The test was conducted at nominal Mach numbers of 0.3, 0.6, and 0.835 at Reynolds numbers (based on mean aerodynamic chord) of 1.0, 1.5, 2.0, and 2.7 million. The nominal test conditions established during the test are given in Table 2. After establishing the desired test condition, data were recorded at selected angles of attack using the pitch-pause technique. The angle of attack was varied from 0 to 6 deg.

3.2 DATA ACQUISITION

Model aerodynamic loads data, conventional pressure data, and PSP images were acquired automatically under the control of the facility computer. The facility computer set the requested model attitude and signaled the master personal computer (PC) to acquire PSP data while the facility computer acquired the loads and conventional pressure data. The master PC commanded the power supplies for the xenon-arc lamps on the top wall and upper and lower side wall to increase to full power, and the shutter in front of each lamp to open. The master PC, and a slave PC connected to it, acquired images of the top and side surfaces of the model. After image acquisition was complete, the lamp power was reduced and the shutters were closed. Next, the master PC commanded a third PC to acquire PSP data on the bottom surface. The third PC commanded the lower sidewall and bottom wall lights to increase to full power and open the shutters, after which the PC acquired the image. Again, the light power was reduced and the shutters were closed after image acquisition. All images were stored on the workstation (see Fig. 6) hard drive via Ethernet. The camera exposure times were set for a particular test condition (Mach number and total pressure) to maximize the signal-to-noise ratio. The camera shutter exposure times varied from 0.9 to 5 sec depending on the tunnel conditions. The master PC returned a signal to the facility computer after all images were acquired, allowing the facility computer to move the model to the next attitude. A file containing tunnel conditions and conventional pressure data, one for each data point, was transferred from the facility computer to the workstation via Ethernet.

3.3 PSP DATA REDUCTION

Determining I_0 in Eq. (1) is not practical in the wind tunnel environment. As described in Ref. 2, taking the ratio of an image at a known reference (wind-off) condition to an operating (wind-on) condition eliminates the need to determine I_0 . Also, the effects of nonuniformities in illumination and paint thickness on the amount of luminescence are eliminated. The ratio of wind-off to wind-on using Eq. (1) is:

$$\frac{I_o/I}{I_o/I_{ref}} = \frac{I_{ref}}{I} = \frac{1 + K_q P}{1 + K_q P_{ref}} \quad (2)$$

where I_{ref} and P_{ref} are the PSP luminescence and pressure at a known wind-off condition, and I and P are the PSP luminescence and surface pressure at the wind-on condition. The surface pressure can then be determined from:

$$P = A + B \frac{I_{ref}}{I} \quad (3)$$

where A and B are the calibration coefficients for the paint. Taking the ratio of wind-off to wind-on images assumes the model position and shape in the image remain constant. However, at the wind-on condition, the model moves in the camera's field of view as a result of deflections from operating loads. Using the image registration technique described by Bell (Ref. 4), small targets were placed on the surface at known coordinates so that the wind-on image could be stretched and shifted (registered) to match the wind-off image. The ratio of the wind-off image to the registered wind-on image was computed for each pixel in the image. The constants A and B were determined *in situ* from a least-squares fit of the conventional pressure coefficient (instead of pressure) data and intensity ratio data at known corresponding locations on the model surface. These constants were used to convert intensity ratio to surface pressure coefficient (CP) over the painted surface. A separate curve fit was determined for the top and bottom cameras, using all pressure taps on the upper and lower surface of the wing, respectively, at each data point. The application of the *in situ* calibration accounts for gross temperature changes from the temperature at the wind-off condition but does not account for local temperature variations. The curve fit determined for the top camera was used to convert the image data for the side camera to CP since there were no pressure taps in the view. If the surface temperature were measured globally like pressure, it would be possible to use an *a priori* calibration, determined in a calibration apparatus as a function of intensity ratio and temperature, to convert the intensity ratio data to pressure coefficient. The use of an *a priori* calibration method could eliminate the need for pressure taps. The registration marks were also used to relate the 2-D image coordinate system to the 3-D model coordinate system. The photogrammetry methods described by Bell (Ref. 4) were used to overlay the 2-D images from each camera onto a 3-D mesh grid of the model surface. If a vertex point was visible to more than one camera, the image with the most normal view of the surface was used to supply data at that point. A PLOT3D solution file was generated for each data point with pressure coefficient data at each vertex point in the grid.

4.0 RESULTS AND DISCUSSION

4.1 PRESSURE MEASUREMENT COMPARISONS

A comparison of pressure coefficient (CP) data from conventional pressure and PSP measurements versus wing chord position (X/C) is presented in Figs. 7-9. The data at Mach numbers 0.6 and 0.835 agree very well with the conventional measurements. Although the PSP data at Mach number 0.3 appear to have more noise and do not compare as well as that at 0.6 and 0.835, it is important to remember that PSP is an absolute pressure measurement. Since the data have been non-dimensionalized, the scales for the Mach number 0.3 data are blown up compared to those at 0.6 and 0.835. The error defined as the difference between the conventional pressure measurement and the PSP measurement at corresponding locations is presented in Fig. 10. The Mach number 0.3 data at chord Reynolds number 1.0 have comparable errors to those at the

higher Mach numbers. Recall that the PSP luminescence decreases with increasing pressure (see Fig. 2), resulting in a decrease in the signal-to-noise ratio (SNR). As can be seen in Fig. 10, the PSP measurement error increases as the Reynolds number (i.e., pressure) increases. The *in situ* calibration method also introduces error into the PSP measurement. Presented in Fig. 11 are samples of the conventional pressure measurement vs. intensity ratio data that were used to determine the calibration coefficients for Eq. (3). It is difficult to compute an accurate curve fit when the surface pressure variation and, therefore, luminescence variation, is small across the surface to be calibrated. The data at Mach number 0.3 and 0-deg angle of attack demonstrate this effect. This is one important reason for the development of an *a priori* calibration method that would not require the use of conventional surface pressure measurements.

4.2 EFFECTS OF PAINT ON DATA

The application of PSP to a wind tunnel model can change the shape of the surface to varying degrees depending upon the person applying it and the type of PSP used. Every attempt is made to make the paint layers as thin and smooth as possible. The paint had little or no effect on the wing pressure distribution at Mach number 0.6, and data were not available to make comparisons at Mach number 0.3. Also, the paint had no effect on the canopy pressure data at Mach numbers 0.6 and 0.835. However, the wing pressure distribution at Mach number 0.835 was affected to varying degrees, depending upon the angle of attack and Reynolds number. The effects of the paint on the pressure distribution (determined from the conventional pressure measurements) at Mach number 0.835 are presented in Fig. 12. Included in the plots at Mach number 0.835 and chord Reynolds number 2.7 are data where transition was fixed through the use of boundary-layer trips. Typically, the shock location moves forward as the boundary layer transitions earlier on the upper surface of a wing with supersonic flow. Such is the case with the trips-on data compared to the clean (paint-off) configuration. The paint-on data agreed with the paint off with trips data at the 44-percent span station for 0-deg angle of attack and Rec 2.7 (see Fig. 12s), indicating that the transition location was probably the same. However, at 6-deg angle of attack, the shock location at the 44-, 66-, and 88-percent span stations for the paint-on data was aft of that for the paint-off configuration. The wing notch is between the 44- and 66-percent span locations and most likely affected the boundary layer-shock interactions at these conditions. There were no significant Reynolds number effects at Mach number 0.6. The Reynolds number effects on the PSP pressure distribution at Mach number 0.835 are presented in Fig. 13. The expected trend of higher Reynolds numbers moving the shock location forward can be seen in the data at 0-deg angle of attack. Again, at 6-deg angle of attack, the trend is totally reversed, with the crossover starting between 2- and 4-deg angle of attack. The true Reynolds number effects on the TST model cannot be determined from the PSP data because of the effects the paint had on the pressure distribution.

The effects of the paint and boundary-layer trips (paint off) on the lift, drag, and pitching-moment coefficients are presented in Fig. 14. The paint had little or no effect on the lift and pitching moment coefficients except at angles of attack where separation on the wing was affected. The drag was increasingly affected by the paint as Reynolds number increased to the point of adding approximately 10-15 drag counts at the highest Reynolds number. The boundary-layer trips had a more significant effect on the data than did the paint.

The continuous surface pressure distribution that PSP provides is presented in Fig. 15. The previously discussed Reynolds number effects at Mach number 0.835 can easily be seen with the largest change occurring at the wing notch and root.

4.3 PSP TO COMPUTATIONAL FLUID DYNAMICS (CFD) COMPARISONS

Comparisons of PSP data and CFD Navier-Stokes solutions, using a κ - ϵ (Ref. 5) turbulence model, are presented in Fig. 16. The flow-field solution was generated using the Chimera overset grid approach (Ref. 6). The agreement is very good at the low angles of attack; however, the separation characteristics could not be simulated at the higher angles of attack. The computational effort to tune the turbulence model to improve separation prediction at higher angles of attack will continue to be investigated.

5.0 SUMMARY

An improved Pressure Sensitive Paint (PSP) data acquisition system was used to acquire surface pressure data on one-half of the Dornier Alpha Jet model. A new paint developed by the University of Washington was used because of superior performance characteristics, primarily lower temperature sensitivity, compared to the AEDC paint used in the previous test. A significant improvement was made to the signal-to-noise ratio through the use of new filters in the paint illumination and detection system. Also, the digital cameras provided a significant increase in both resolution and accuracy as compared to the 8-bit video camera used in the previous test. Some conclusions and observations from the test are as follows:

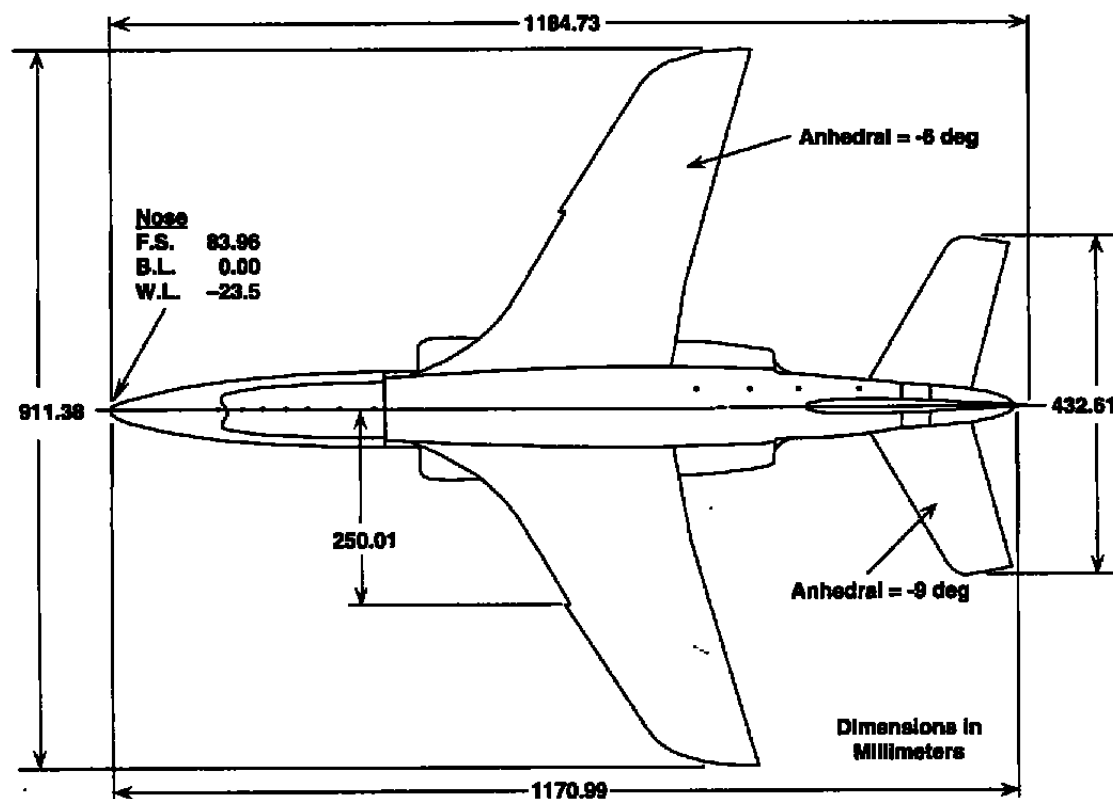
- The pressure sensitive paint data agree very well with conventional pressure measurements.
- An *a priori* calibration method is needed to overcome limitations using the *in situ* method.
- The paint affected the surface pressure distributions at Mach number 0.835 to varying degrees depending upon Reynolds number. The data at Mach number 0.6 were not affected.
- The movement of shock location on the upper wing surface with changes in Reynolds number behaved as expected at most, but not all, test conditions. The unexpected behavior is believed to be a result of boundary layer-shock interactions near the wing notch and root.
- The continuous pressure distribution provided by PSP better defines the shock locations as compared with the sparse conventional pressure measurements.
- The effect of the paint on drag at the lower Reynolds numbers was less than the balance uncertainty and had no effect on the lift and pitching moment. However, the paint added

up to 15 counts of drag at the highest Reynolds number, which was on the order of twice the balance uncertainty, while still having no effect on lift and pitching moment.

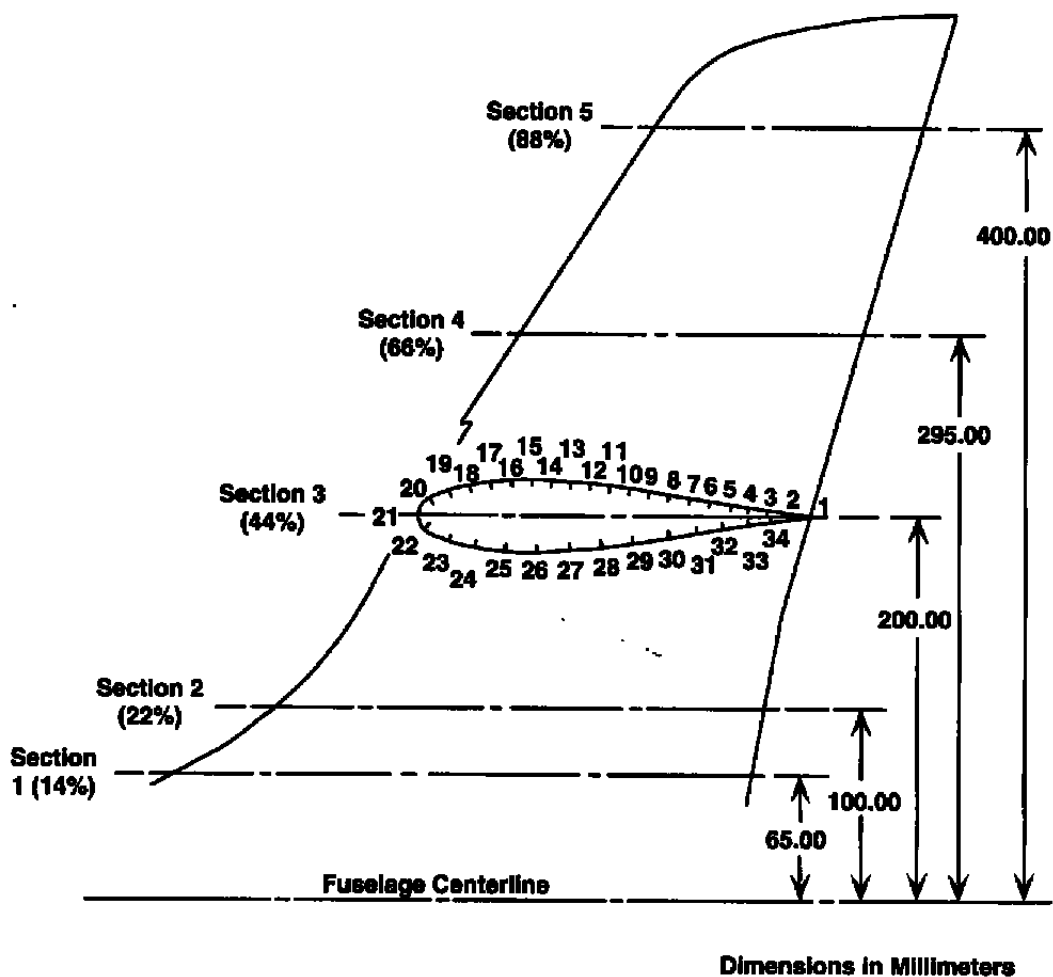
- PSP is a valuable tool for CFD code validation because it can measure a continuous pressure distribution on the model surface in a form similar to CFD results.

REFERENCES

1. Sellers, M. E. "Demonstrations of a Pressure Sensitive Paint Data System in the AEDC Propulsion Wind Tunnel 16T." AEDC-TR-95-8, October 1995.
2. McLachlan, B. G., et al. "Pressure Sensitive Paint Use in the Supersonic High-Sweep Oblique Wing (SHOW) Test." AIAA Paper 92-2686, AIAA 10th Applied Aerodynamics Conference, Palo Alto, CA, June 1992.
3. Morris, M. J., et al. "Aerodynamic Applications of Pressure-Sensitive Paint." AIAA Paper 92-0264, 30th AIAA Aerospace Sciences Meeting, Reno, NV, January 1992.
4. Bell, J. H. and McLachlan, B.G. "Image Registration for Luminescent Paint Sensors." AIAA Paper 93-0178, 31st Aerospace Sciences Meeting, Reno, NV, January 1993.
5. Nichols, R. H. "Development and Validation of a Two-Equation Turbulence Model with Wall Functions for Compressible Flow." AIAA 96-2385, June 1996.
6. Benek, J. A., Steger, J. L., Dougherty, F. C., and Buning, P. G. "Chimera: A Grid-Embedding Technique." AEDC-TR-85-64 (AD-A167466), April 1986.



a. Test article dimensions
Figure 1. TST model.



b. Wing pressure orifice distribution
Figure 1. Concluded.

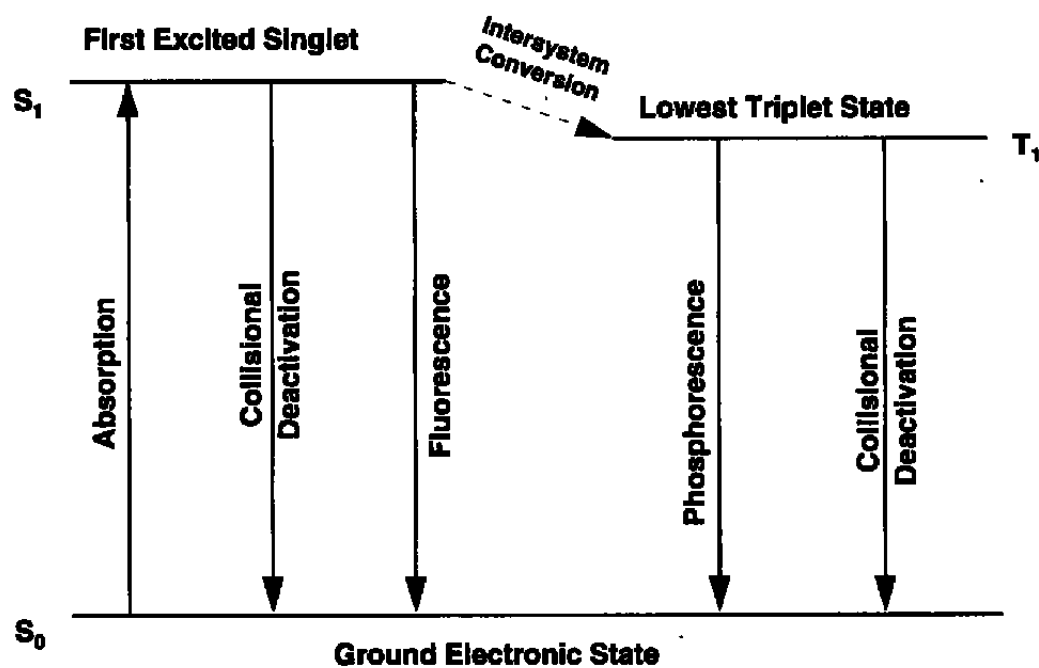


Figure 2. Basic luminescence process.

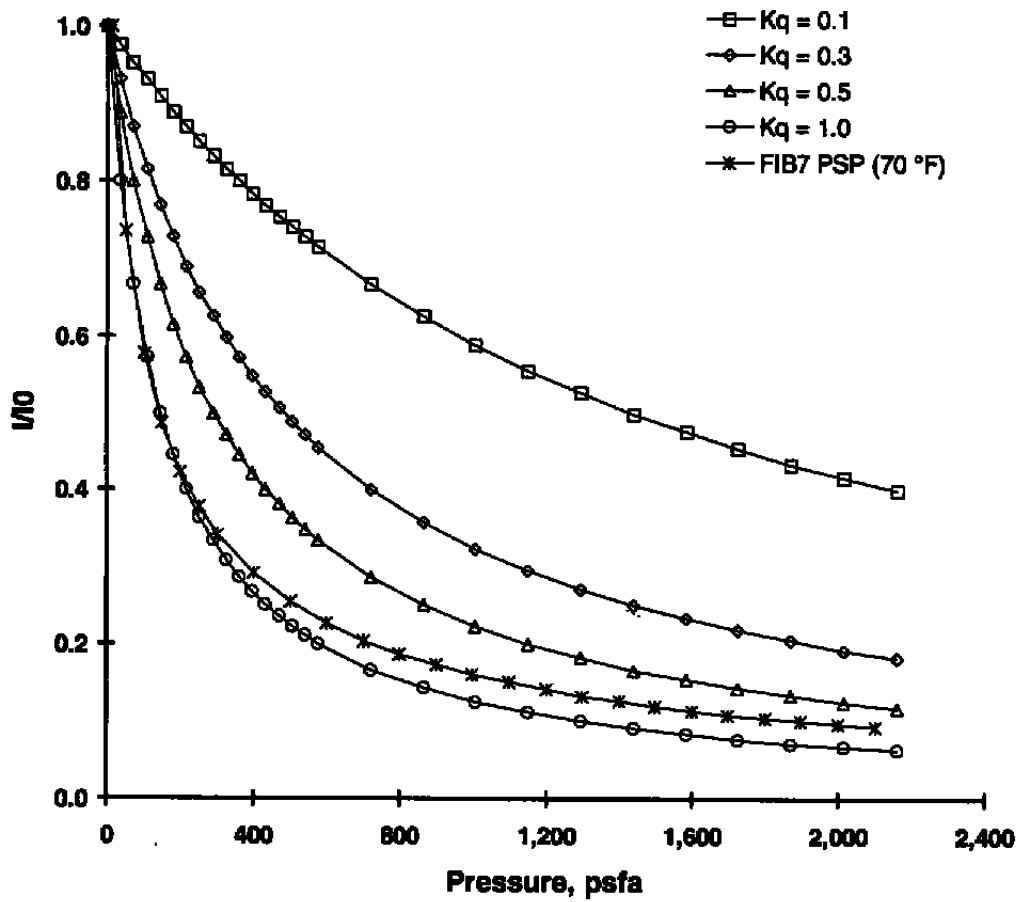


Figure 3. Luminescence as described by the Stern-Volmer Model.

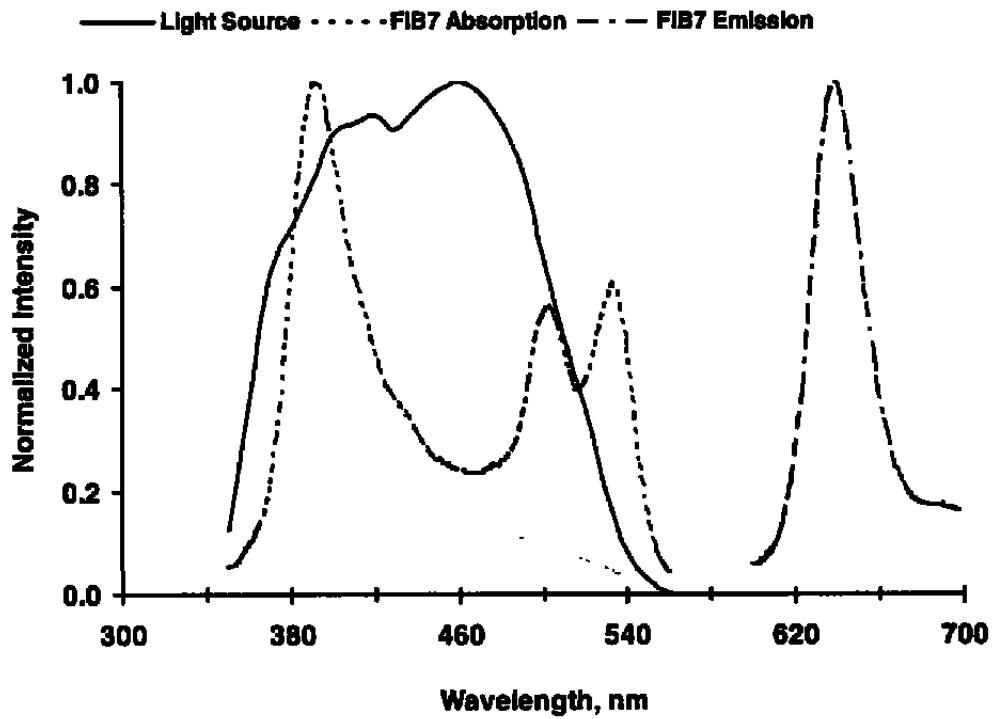


Figure 4. Spectral characteristics of the FIB7 PSP and filtered light source.

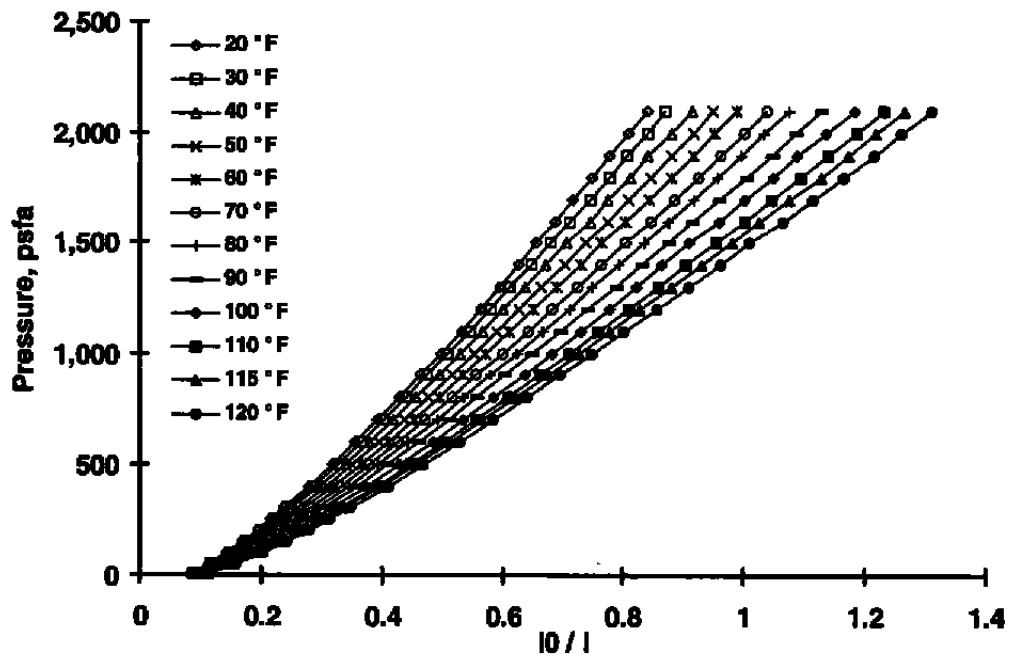


Figure 5. FIB7 PSP pressure and temperature characteristics.

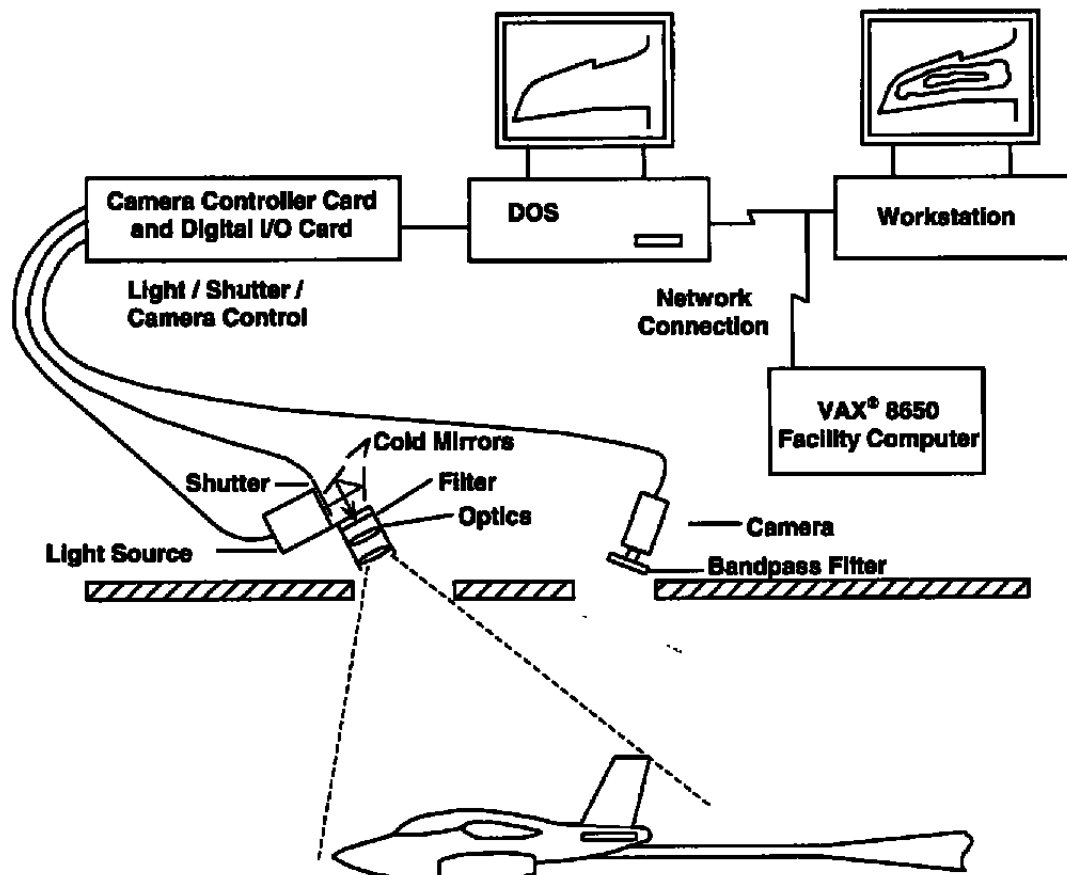
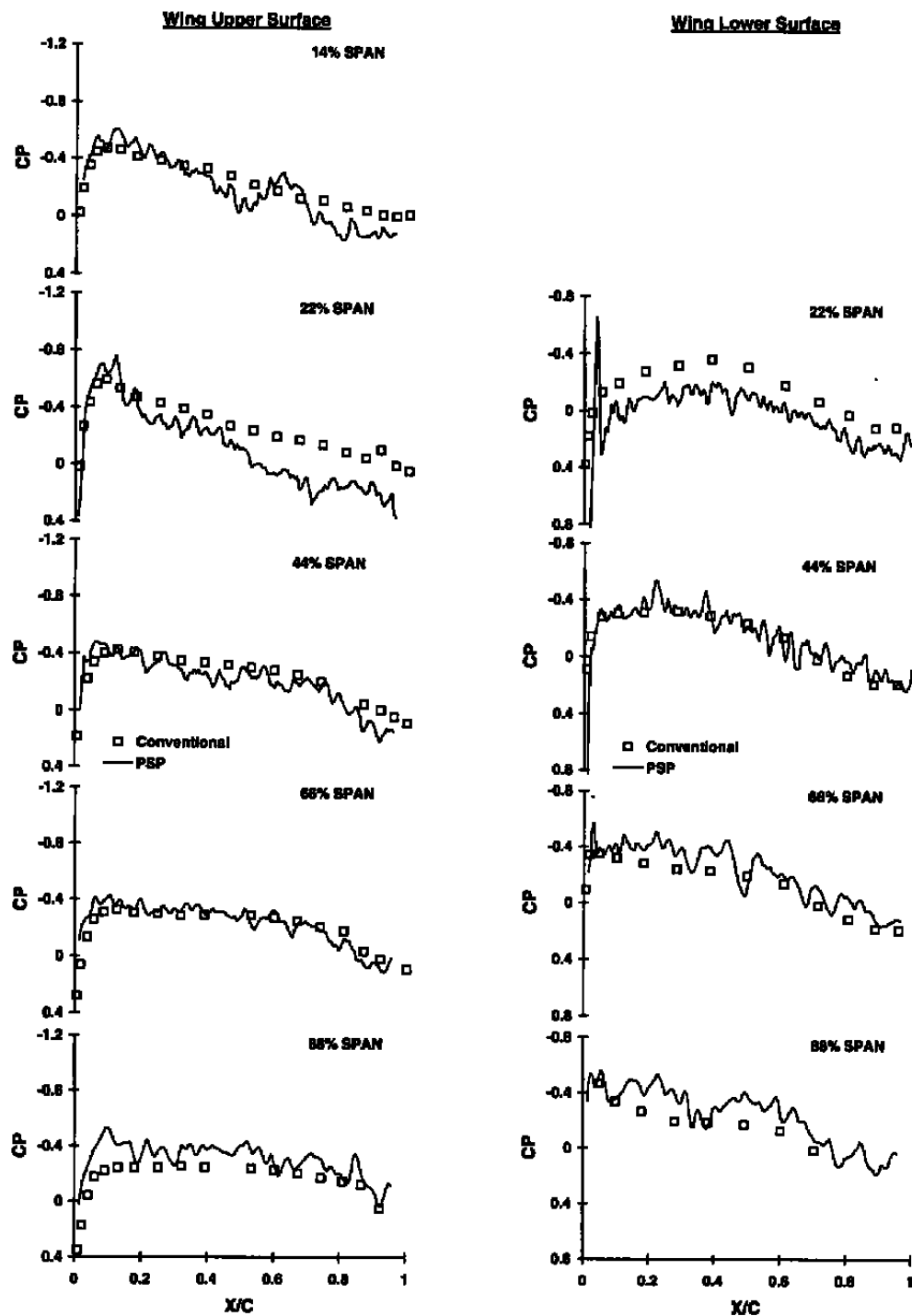
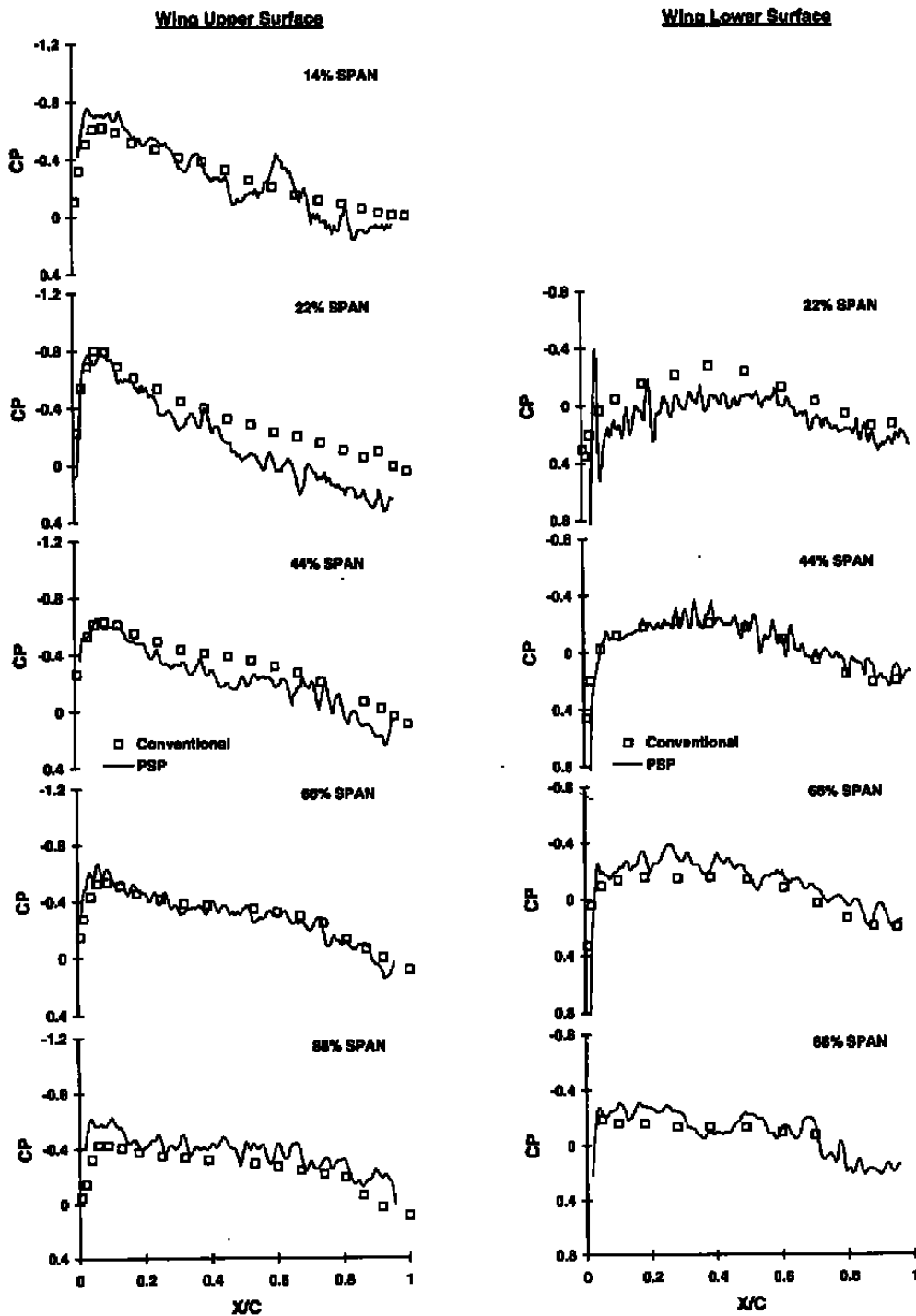


Figure 6. PSP data acquisition and processing system.

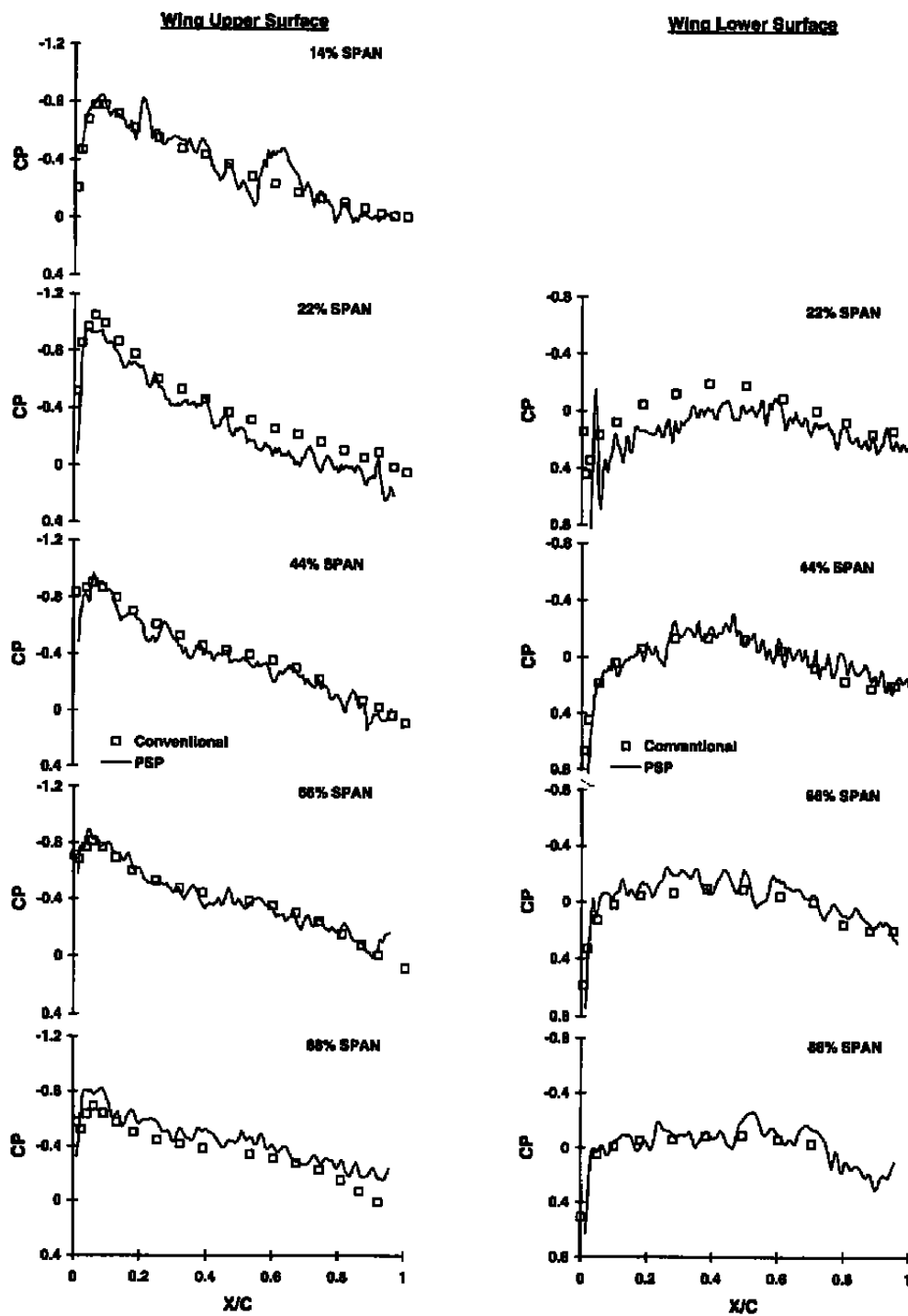


a. Alpha = 0 deg, Rec = 1.0

Figure 7. TSF conventional and PSP pressure coefficient comparison at Mach number 0.3.

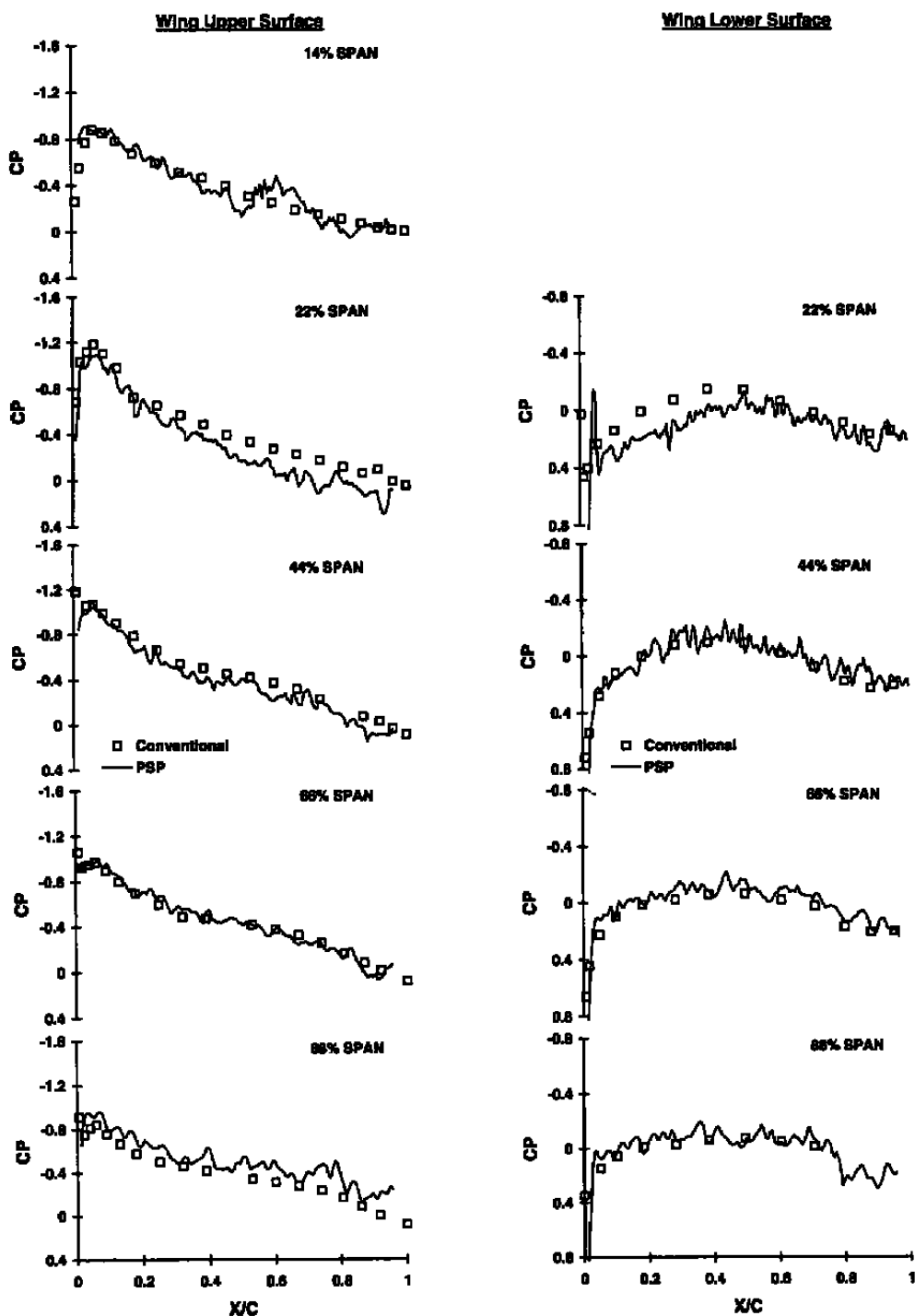


b. $\alpha = 2^\circ$, $Re_c = 1.0$
Figure 7. Continued.

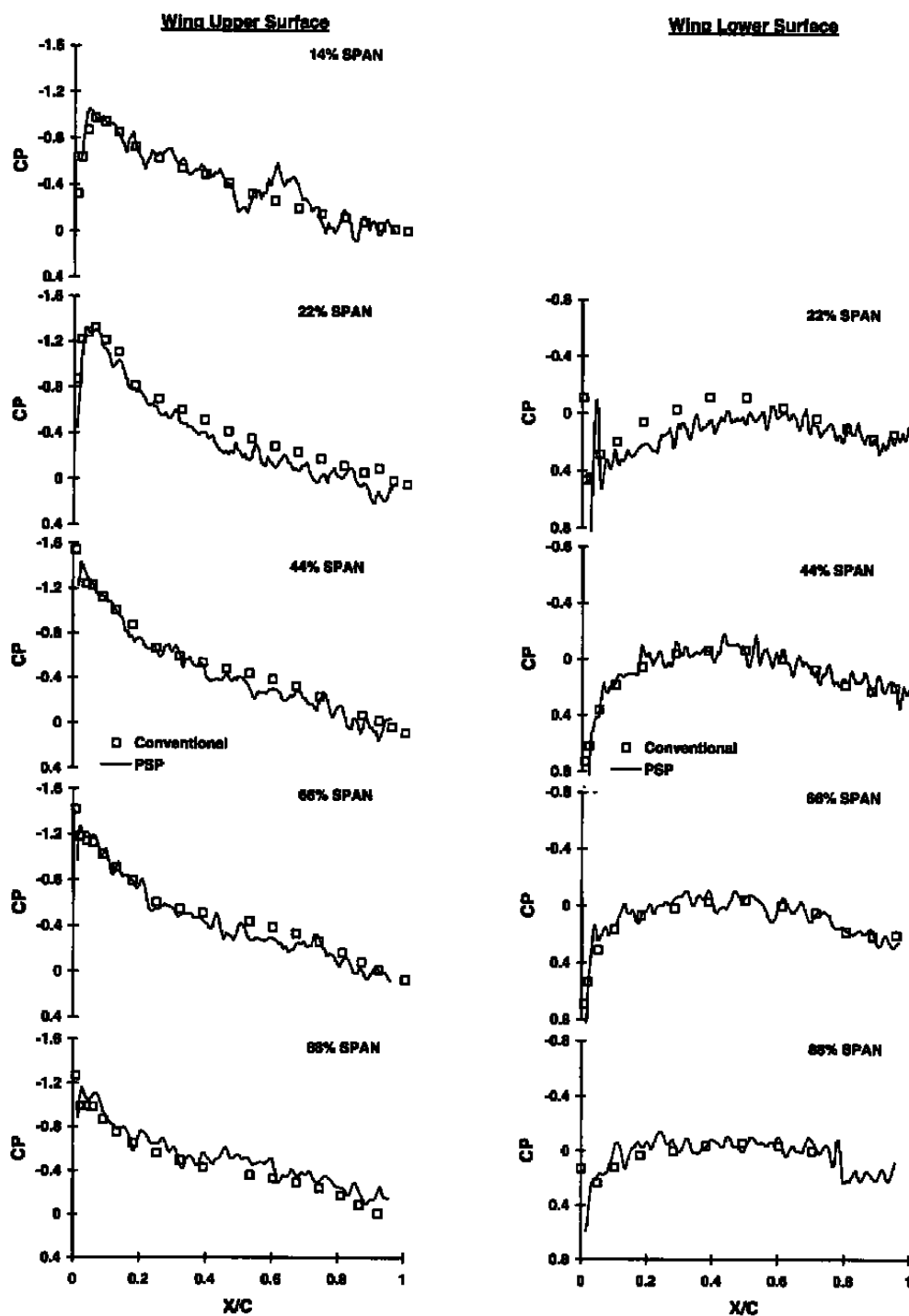


c. Alpha = 4 deg, Rec = 1.0

Figure 7. Continued.

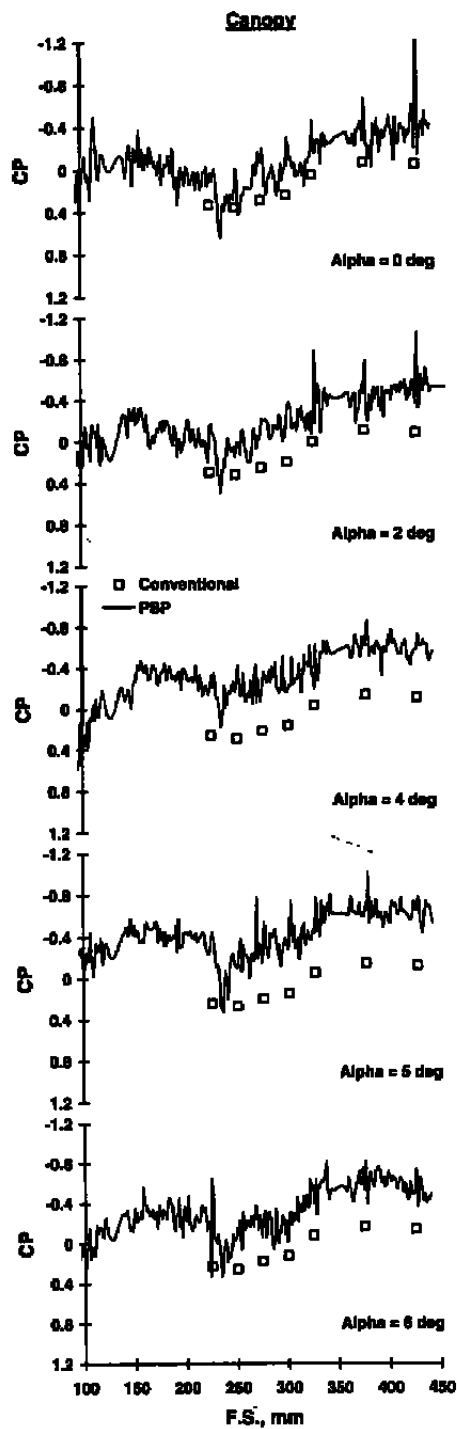


d. $\alpha = 5$ deg, $Re_c = 1.0$
Figure 7. Continued.



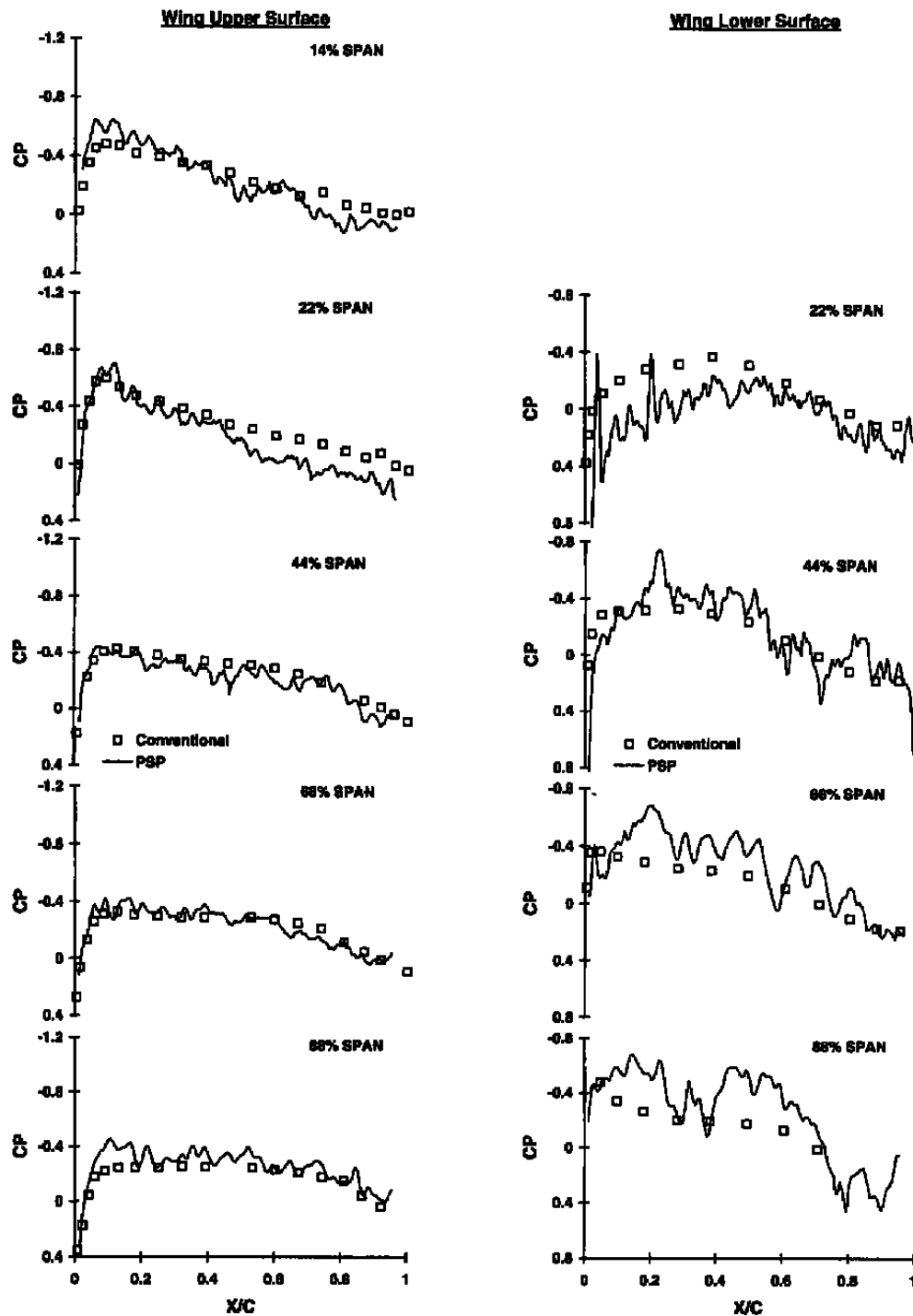
e. Alpha = 6 deg, Rec = 1.0

Figure 7. Continued.



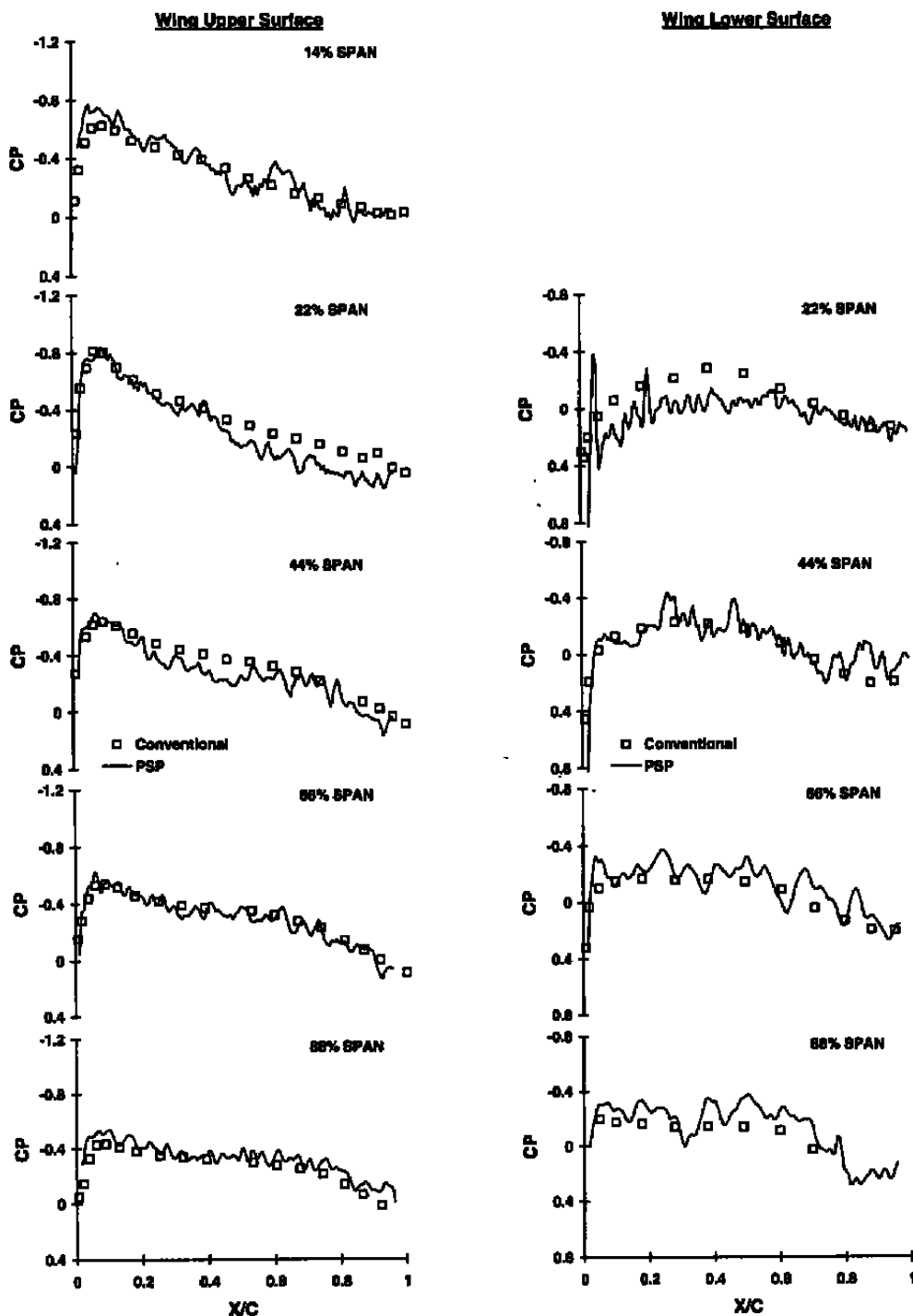
f. Canopy, Rec = 1.0

Figure 7. Continued.

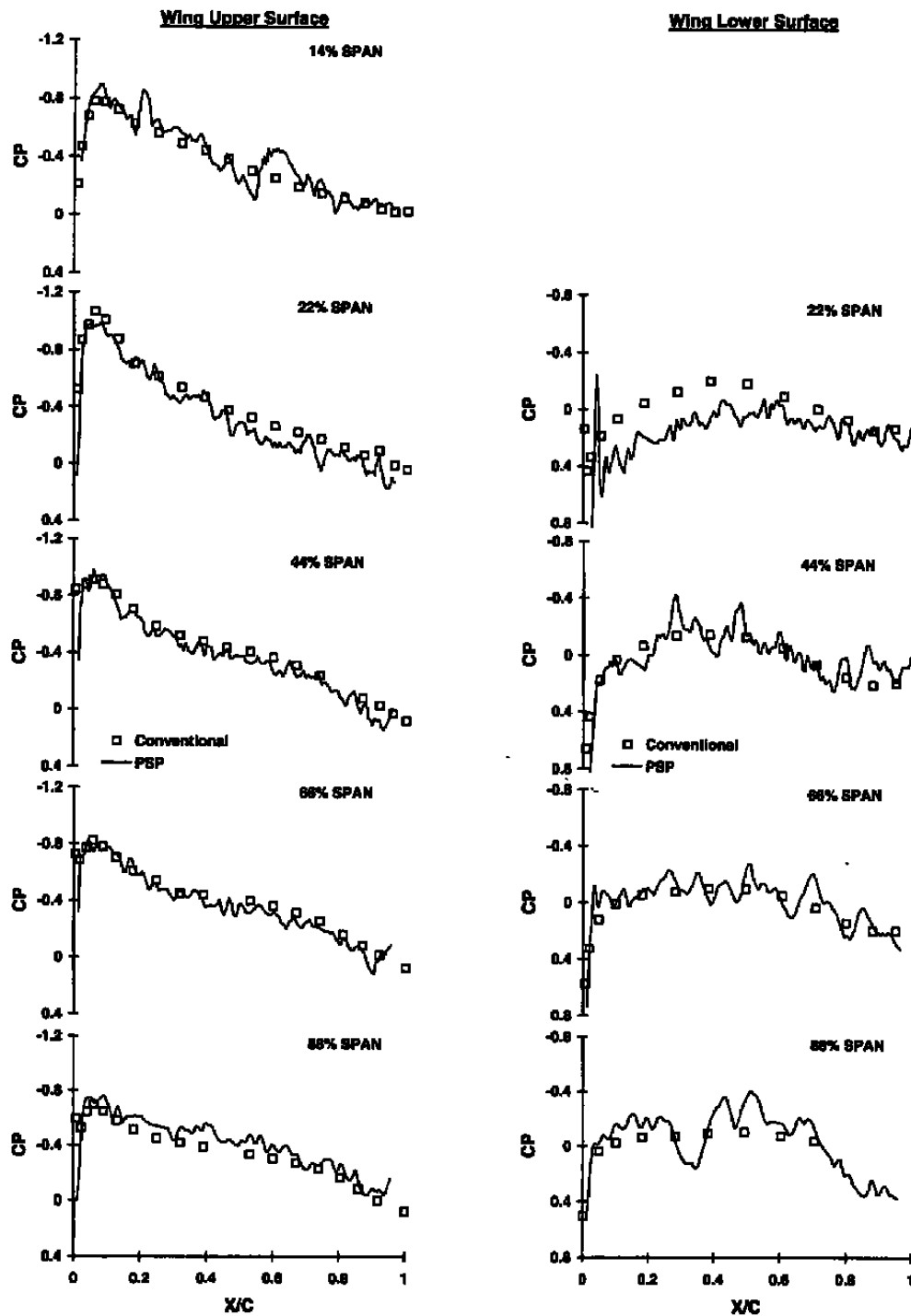


g. Alpha = 0 deg, Rec = 1.5

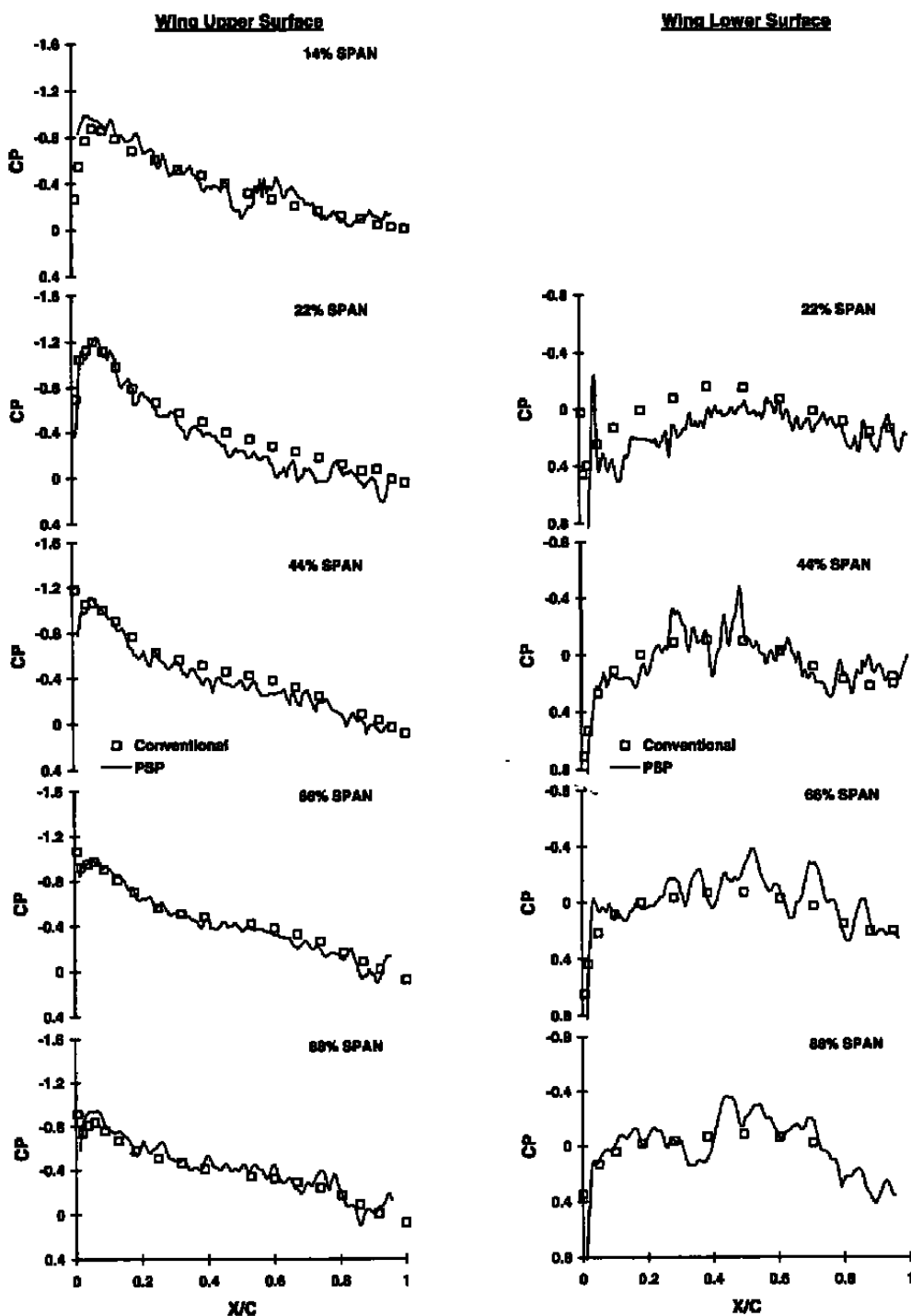
Figure 7. Continued.



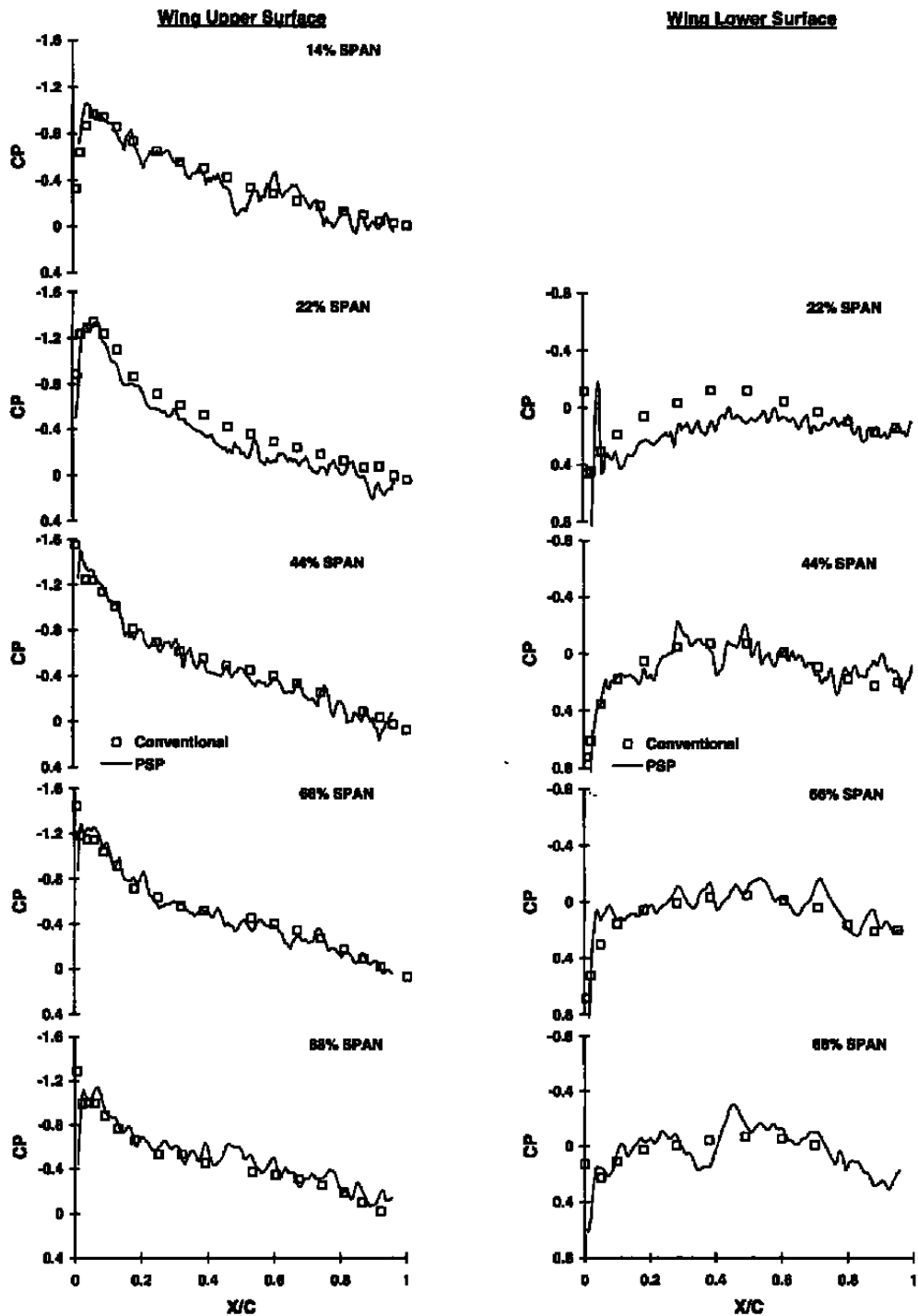
h. Alpha = 2 deg, Rec = 1.5
Figure 7. Continued.



i. Alpha = 4 deg, Rec = 1.5
Figure 7. Continued.

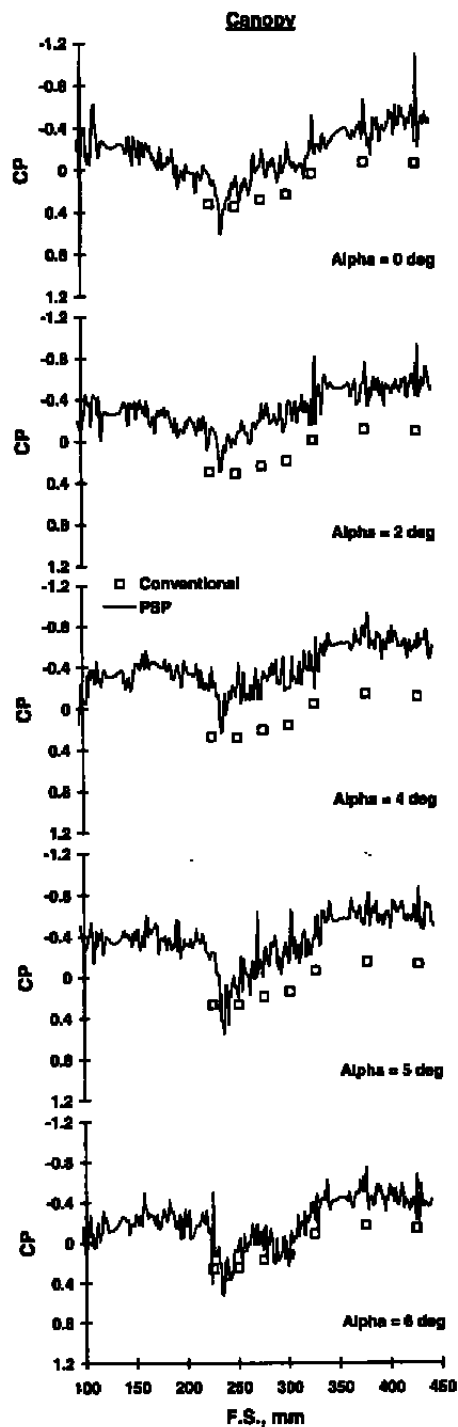


j. Alpha = 5 deg, Rec = 1.5
Figure 7. Continued.

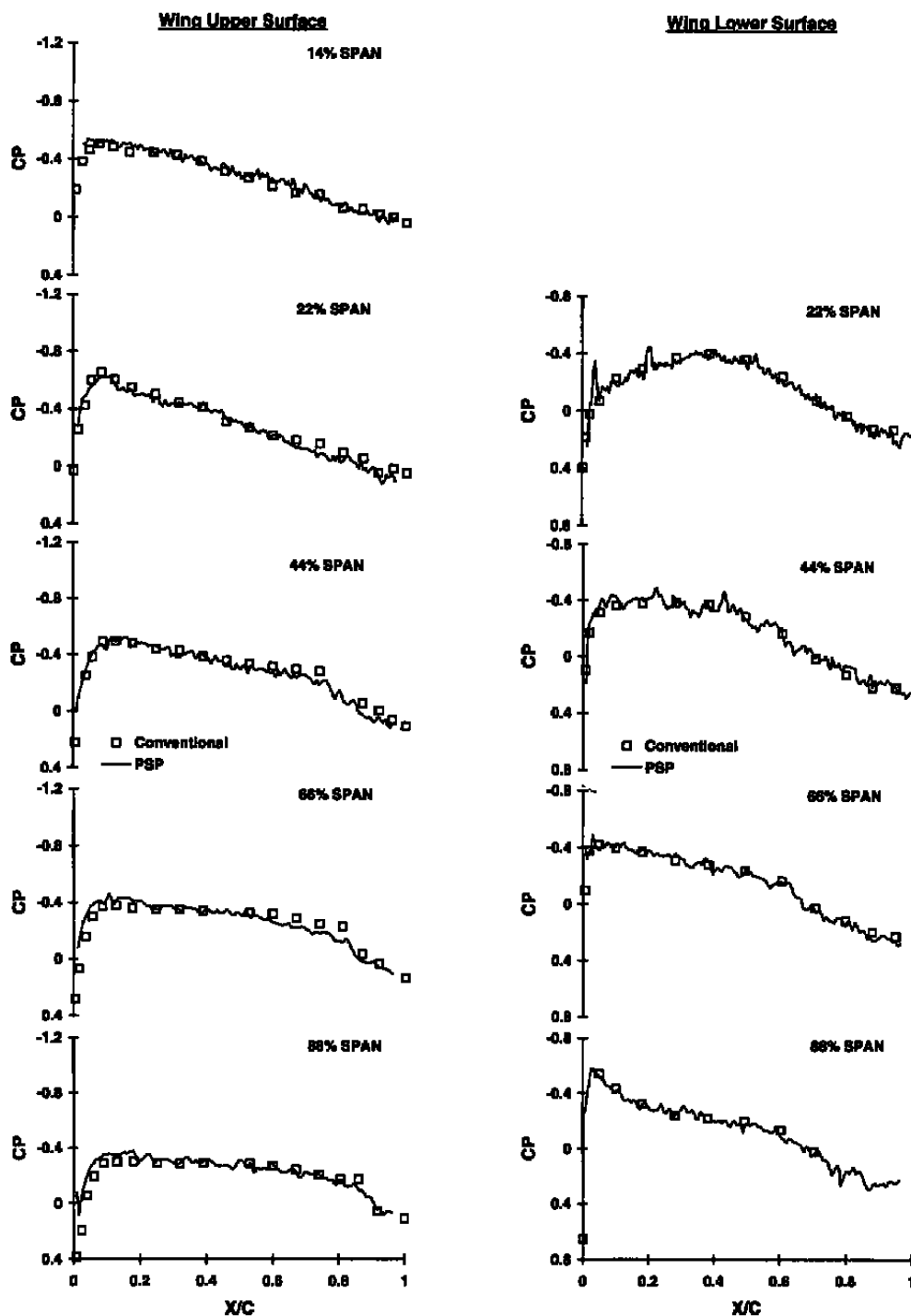


k. Alpha = 6 deg, Rec = 1.5

Figure 7. Continued.

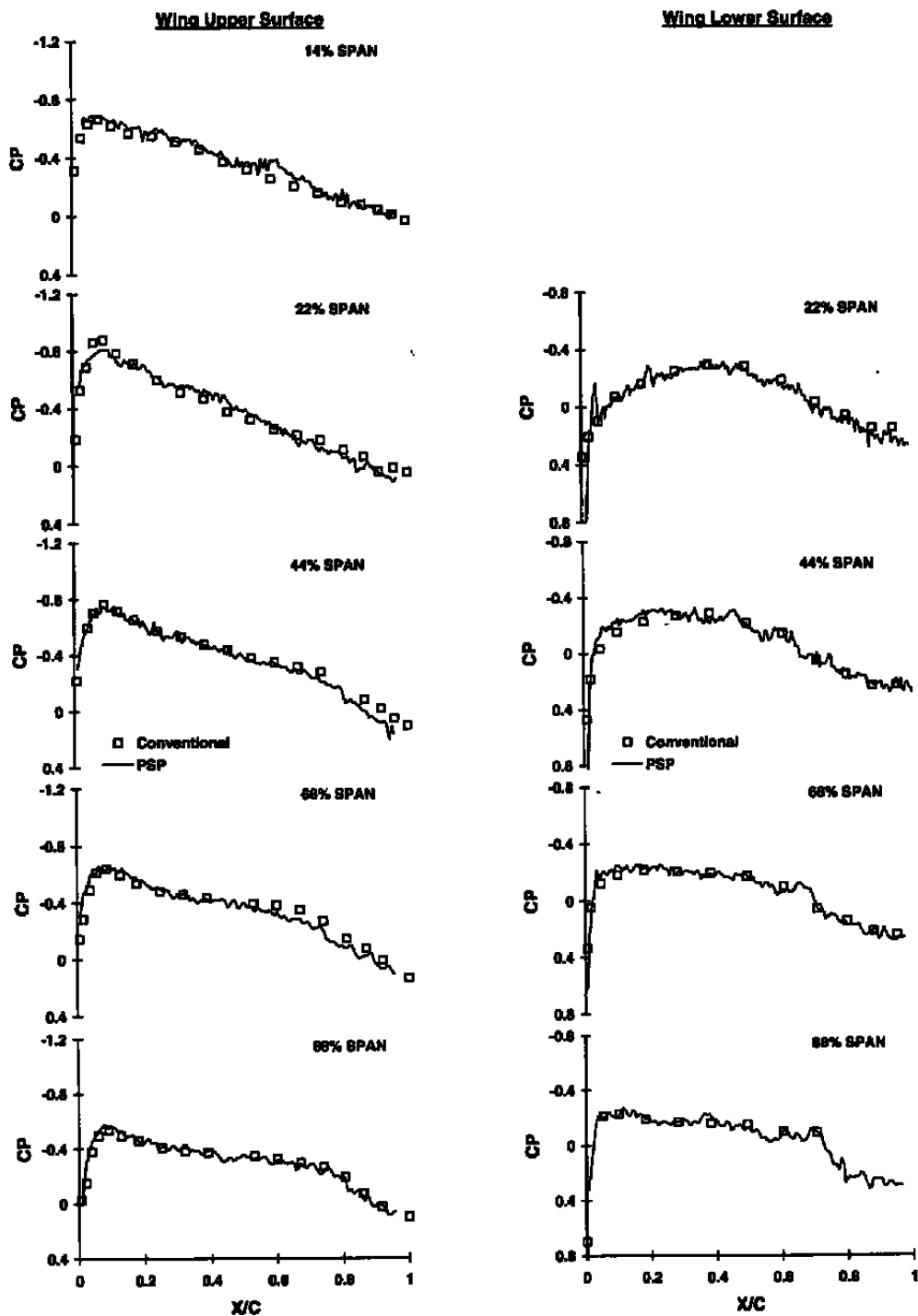


1. Canopy, Rec = 1.5
Figure 7. Concluded.

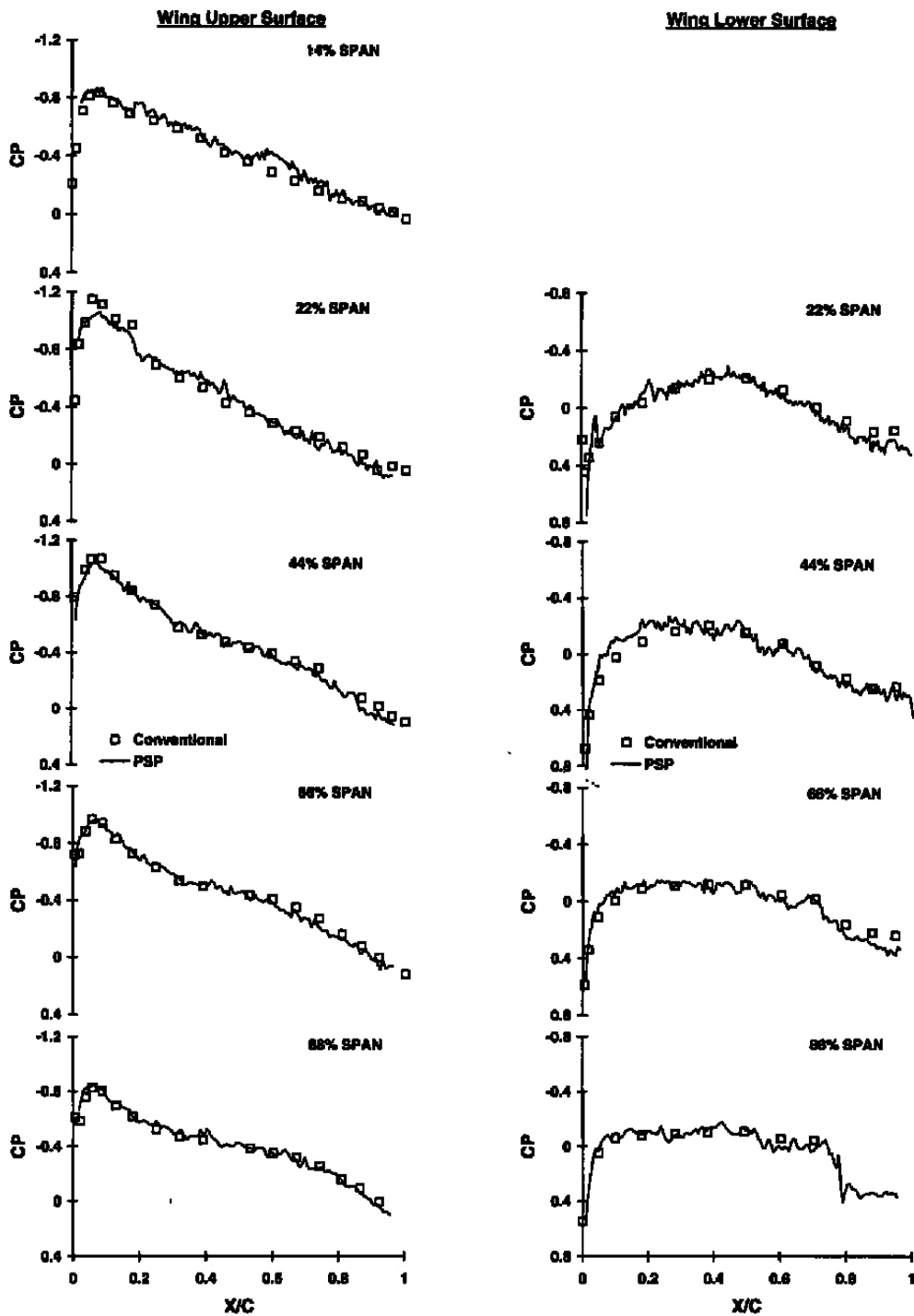


a. Alpha = 0 deg, Rec = 1.0

Figure 8. TST conventional and PSP pressure coefficient comparison at Mach number 0.6.

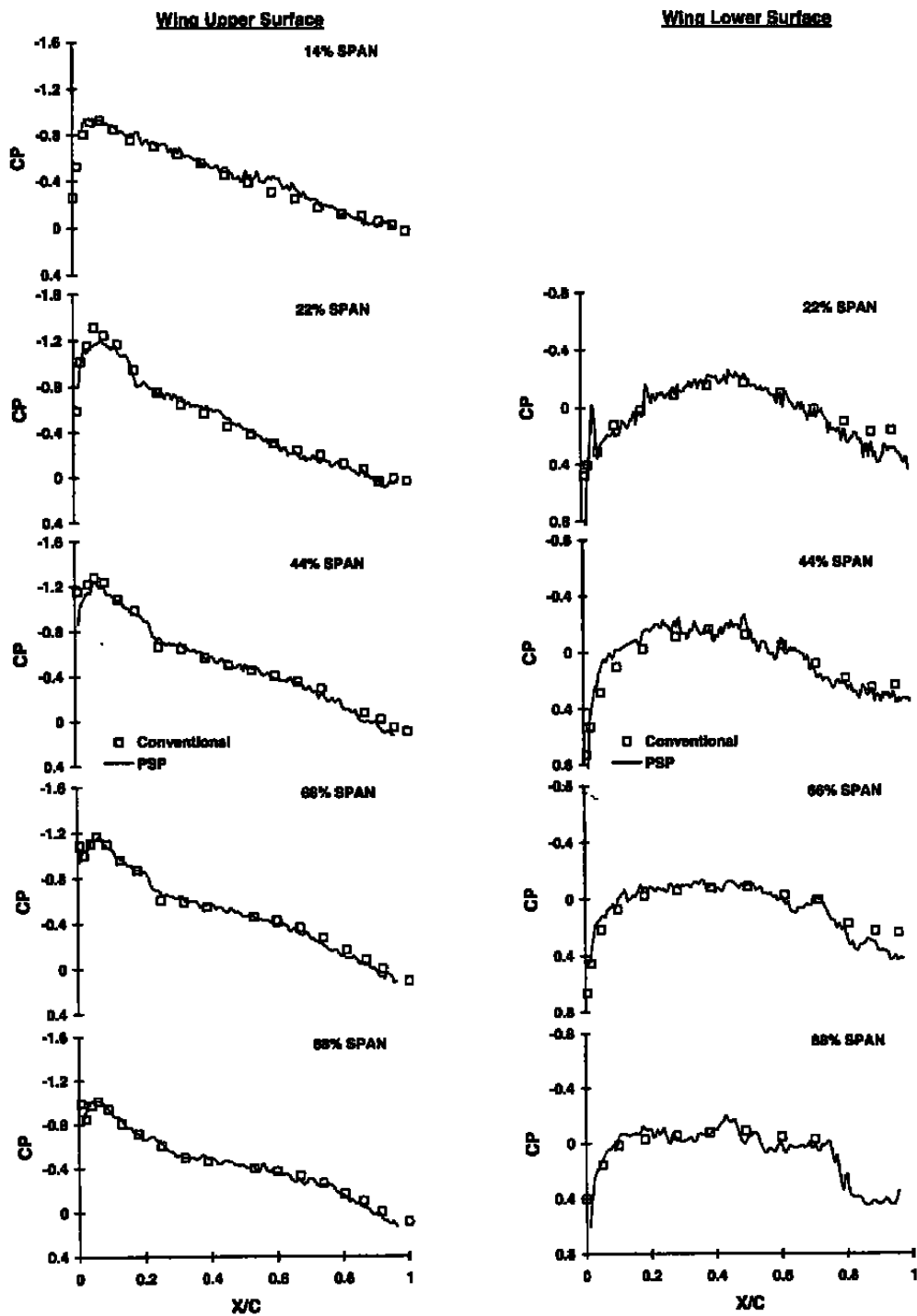


b. $\alpha = 2$ deg, $Re_c = 1.0$
Figure 8. Continued.

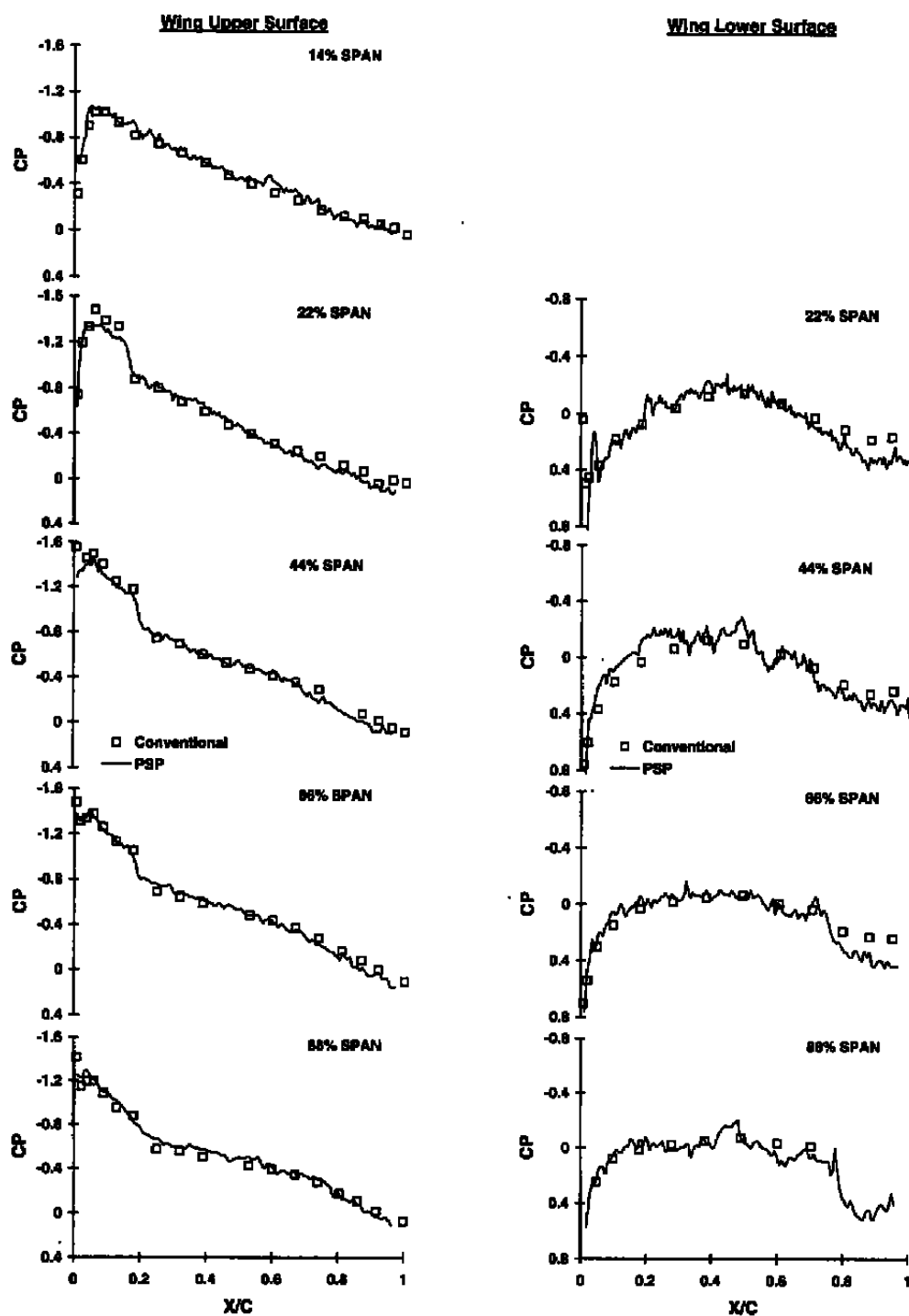


c. Alpha = 4 deg, Rec = 1.0

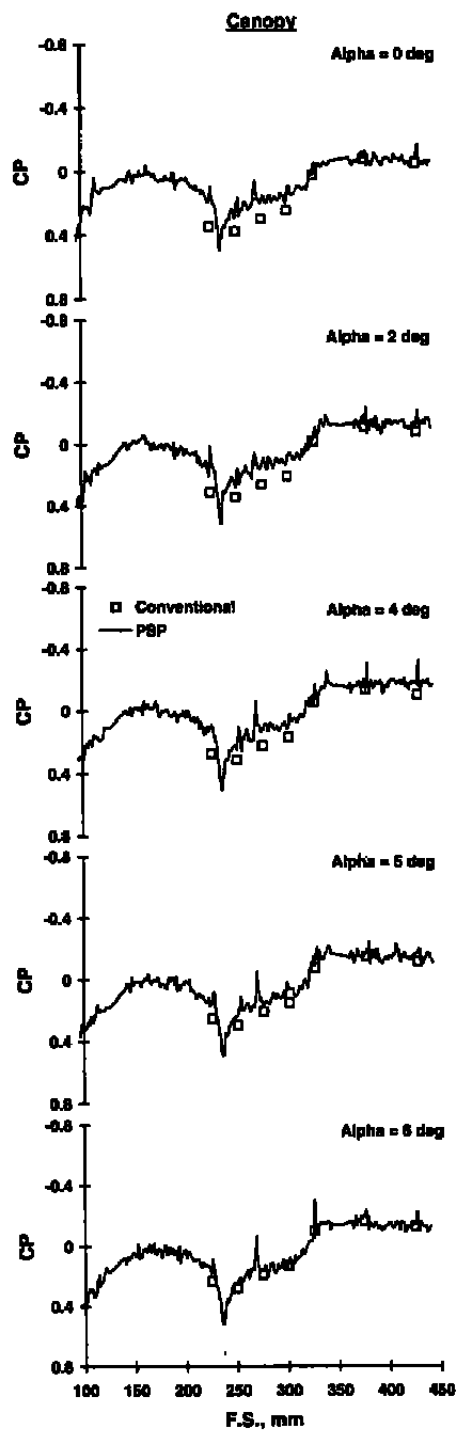
Figure 8. Continued.



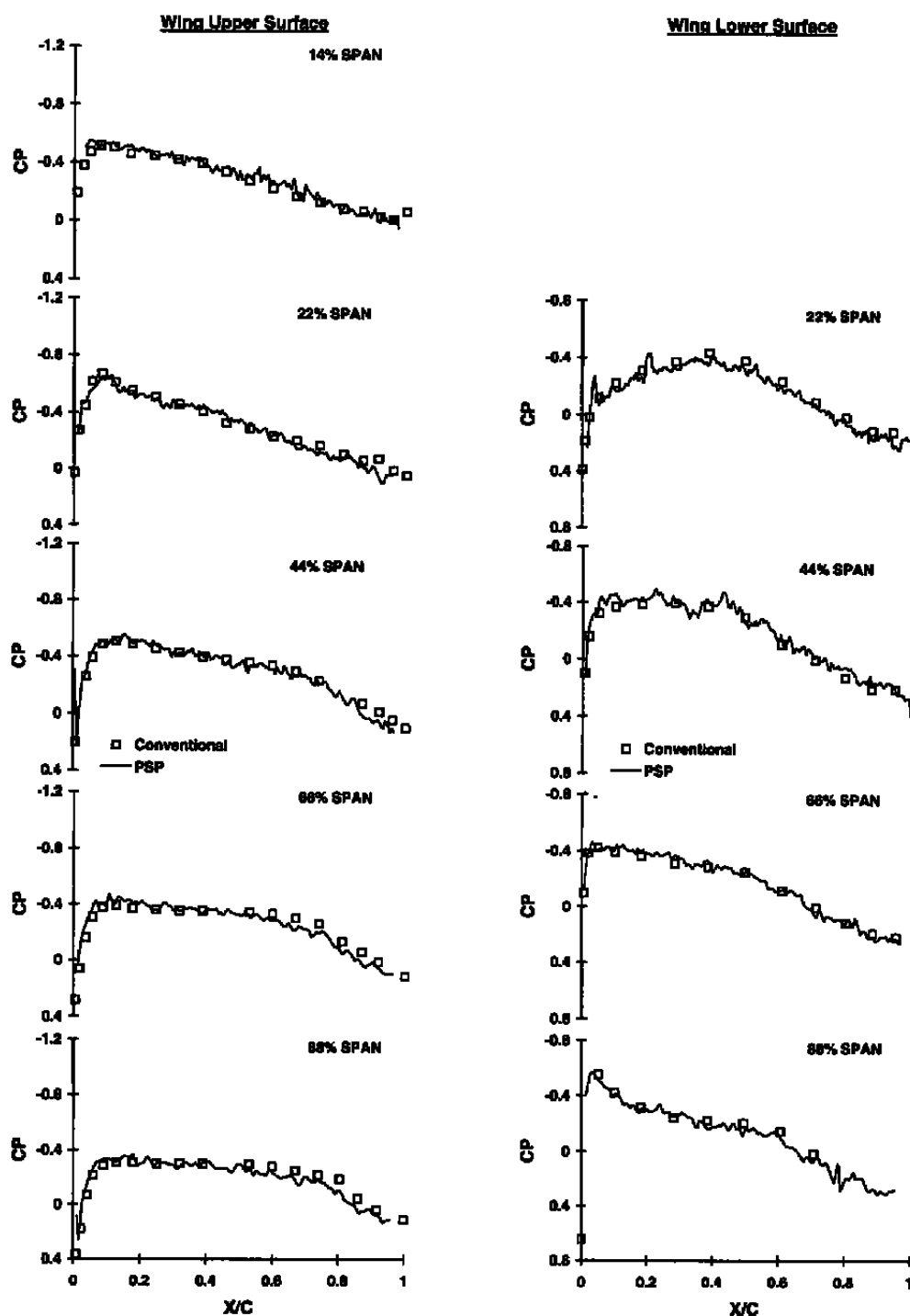
d. $\alpha = 5$ deg, $Re_c = 1.0$
Figure 8. Continued.



e. Alpha = 6 deg, Rec = 1.0
Figure 8. Continued.

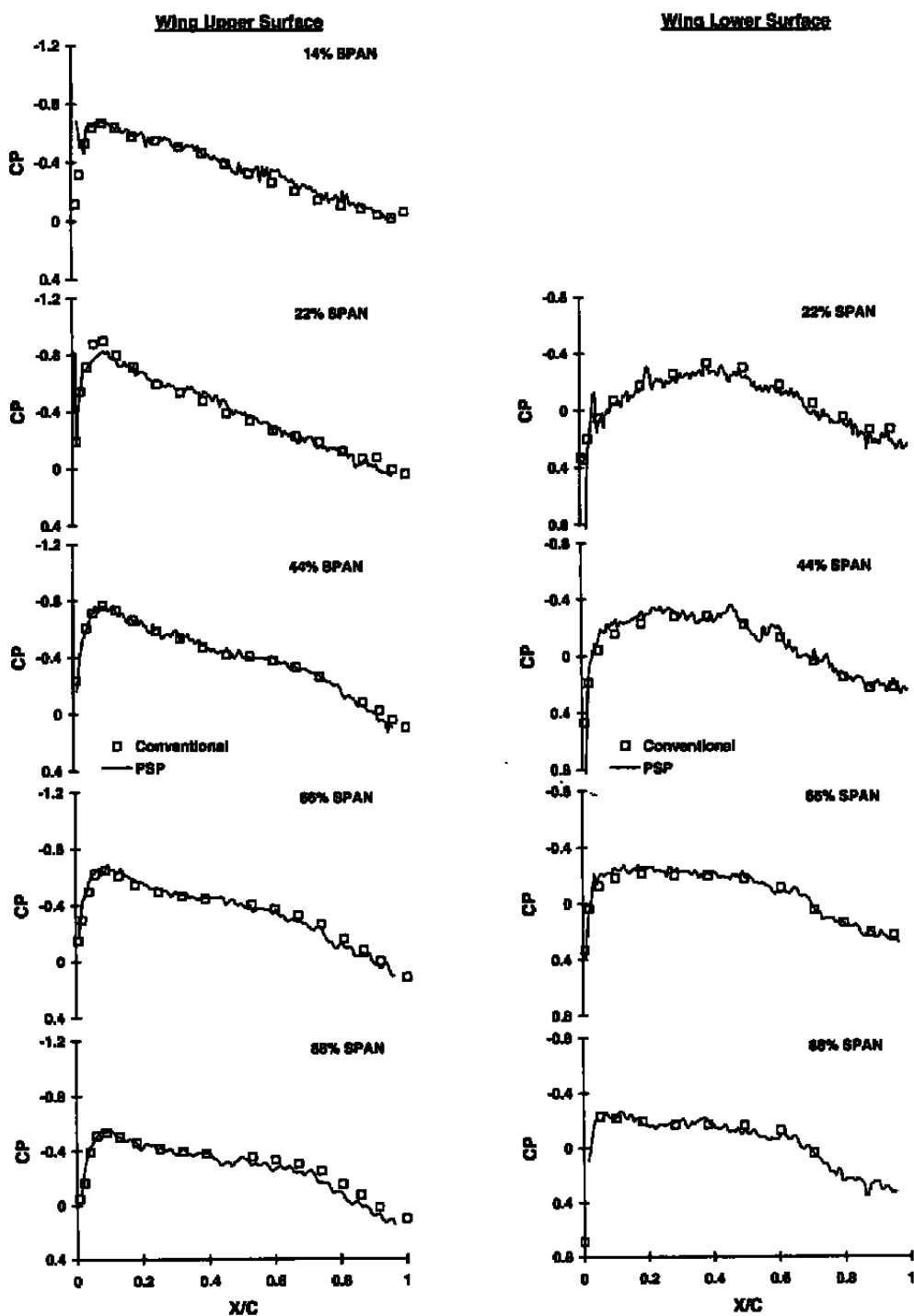


f. Canopy, Rec = 1.0
 Figure 8. Continued.

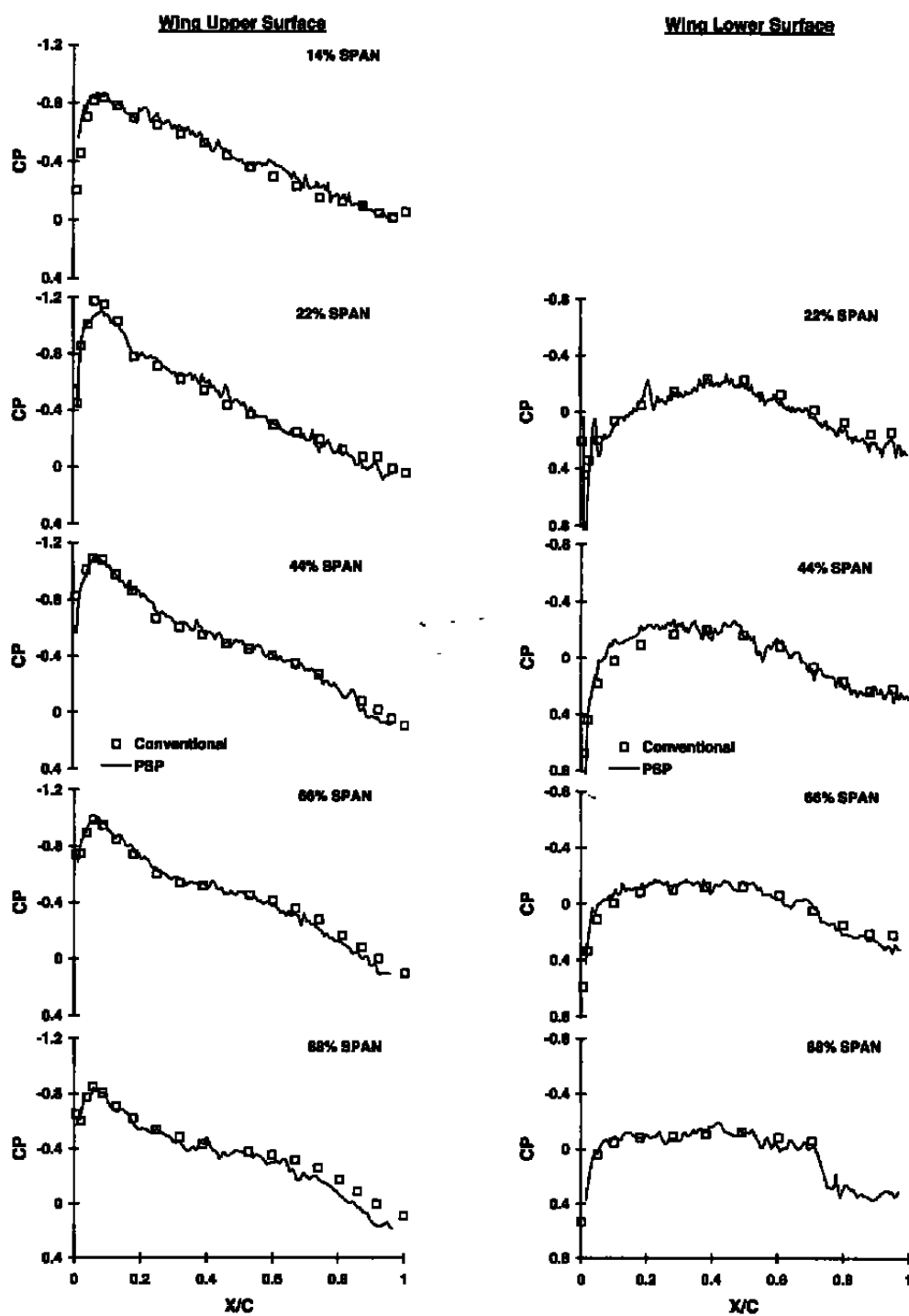


g. Alpha = 0 deg, Rec = 1.5

Figure 8. Continued.

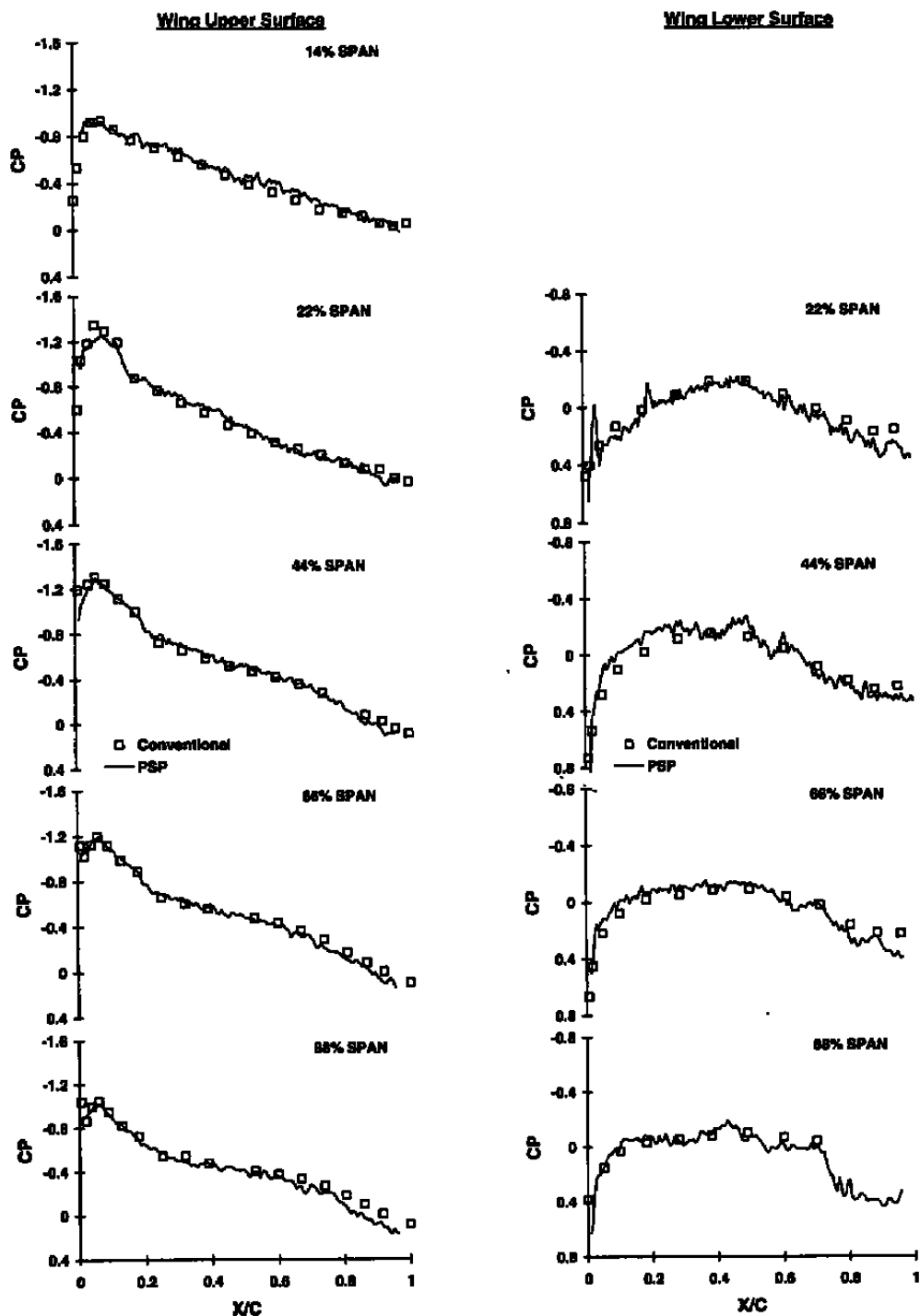


h. Alpha = 2 deg, Rec = 1.5
Figure 8. Continued.

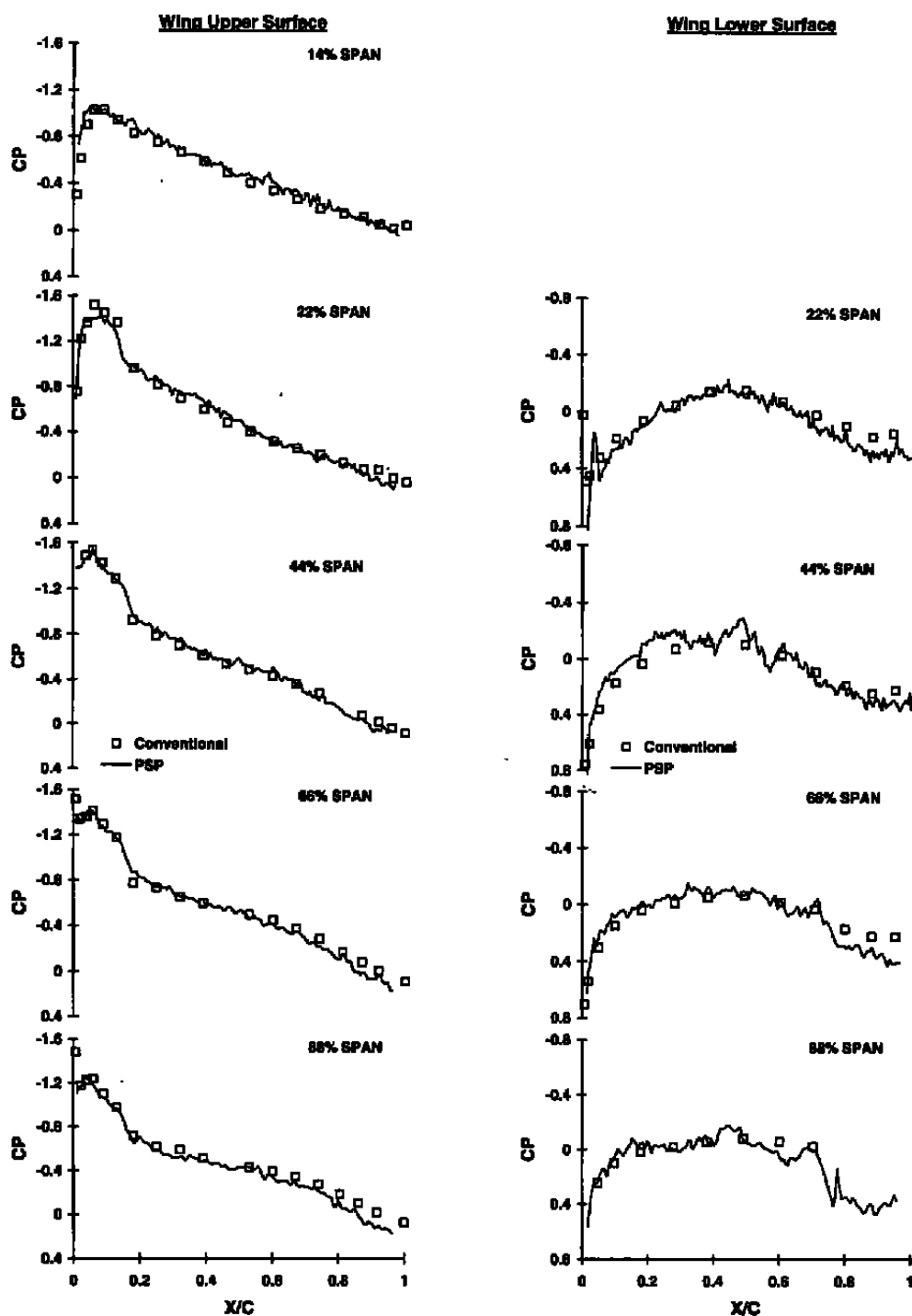


i. Alpha = 4 deg, Rec = 1.5

Figure 8. Continued.

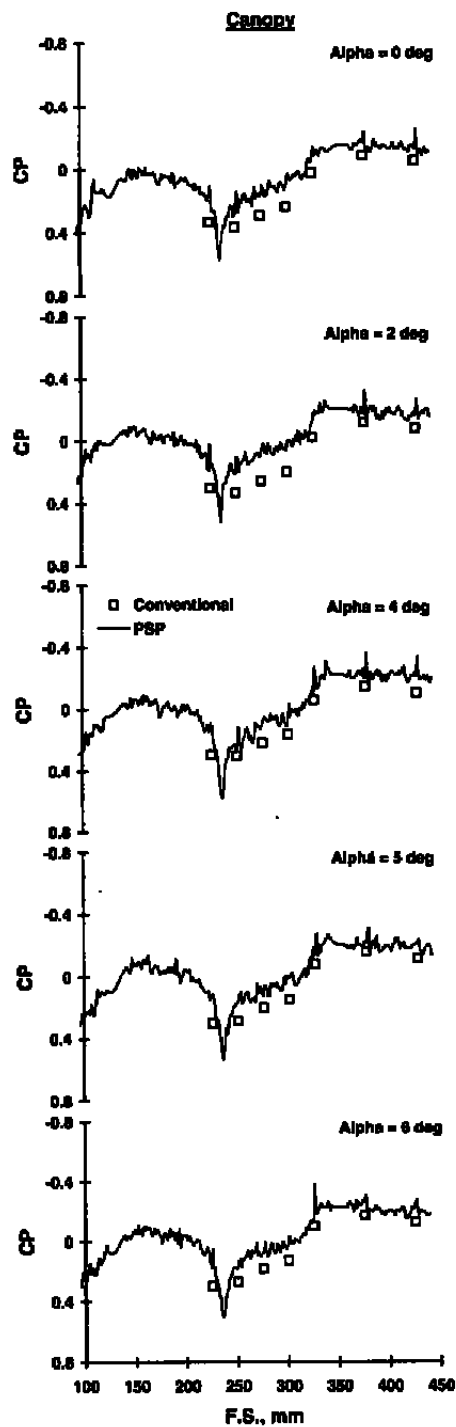


j. Alpha = 5 deg, Rec = 1.5
Figure 8. Continued.

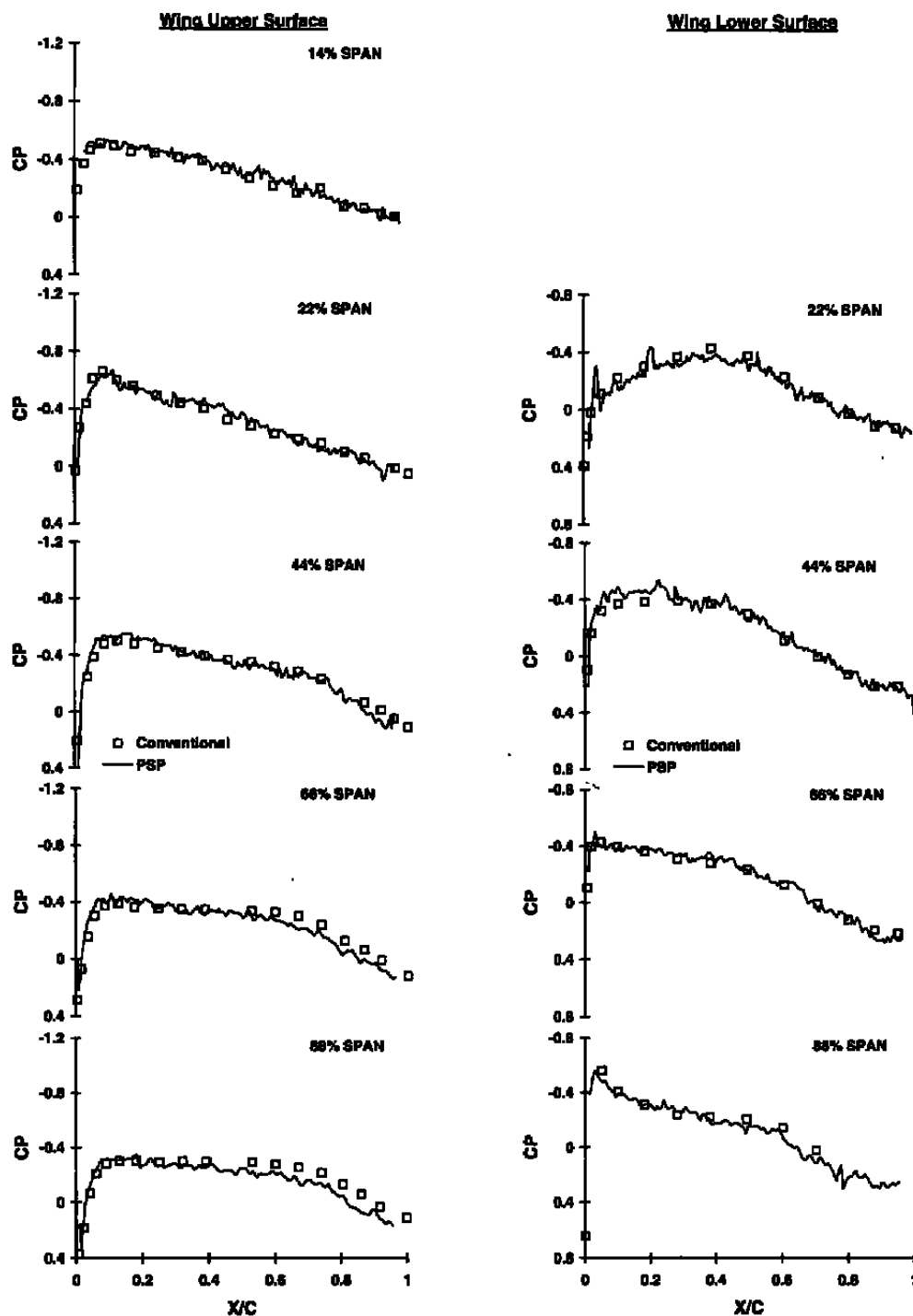


k. Alpha = 6 deg, Rec = 1.5

Figure 8. Continued.

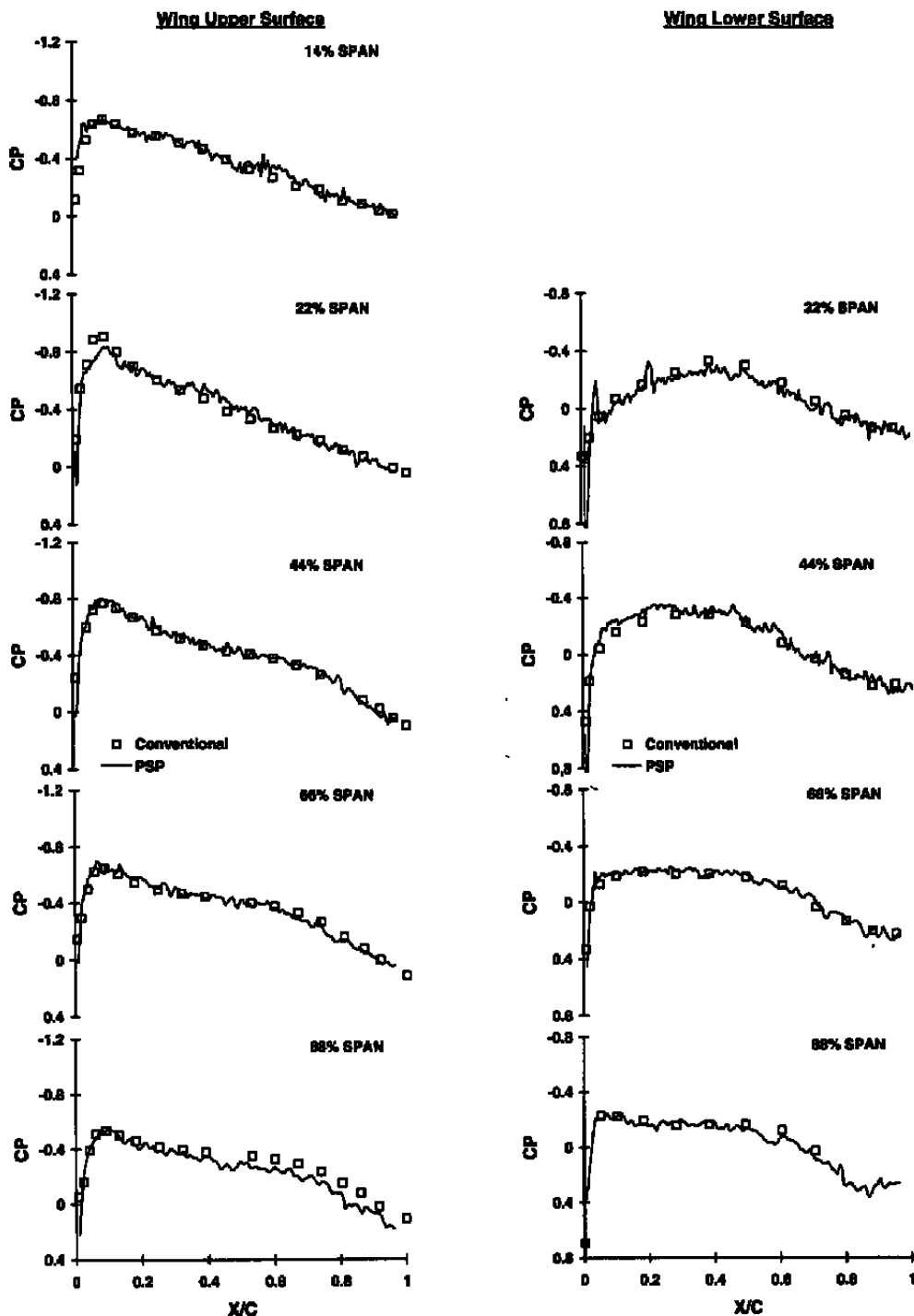


I. Canopy, Rec = 1.5
Figure 8. Continued.

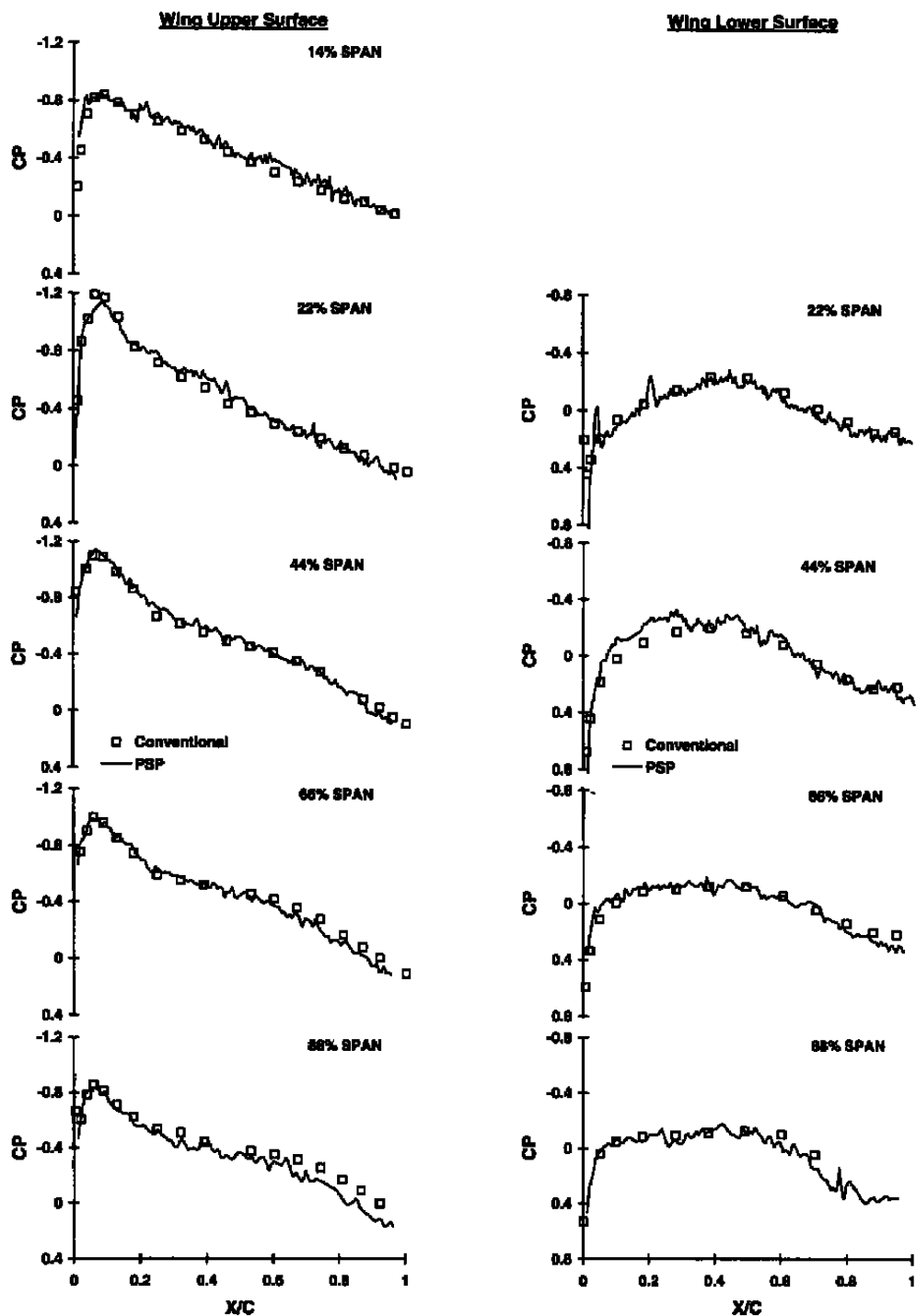


m. Alpha = 0 deg, Rec = 2.0

Figure 8. Continued.

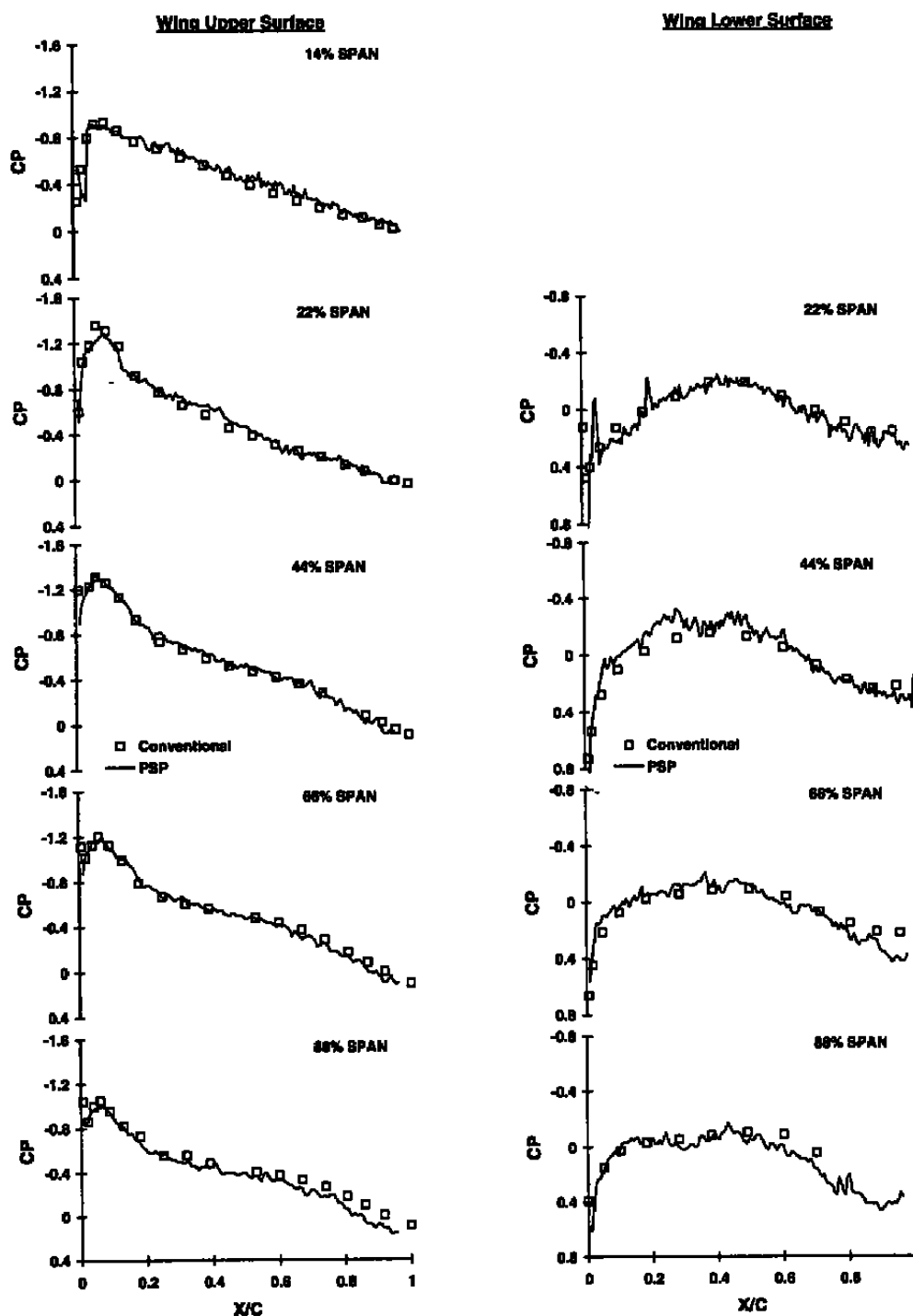


n. Alpha = 2 deg, Rec = 2.0
Figure 8. Continued.

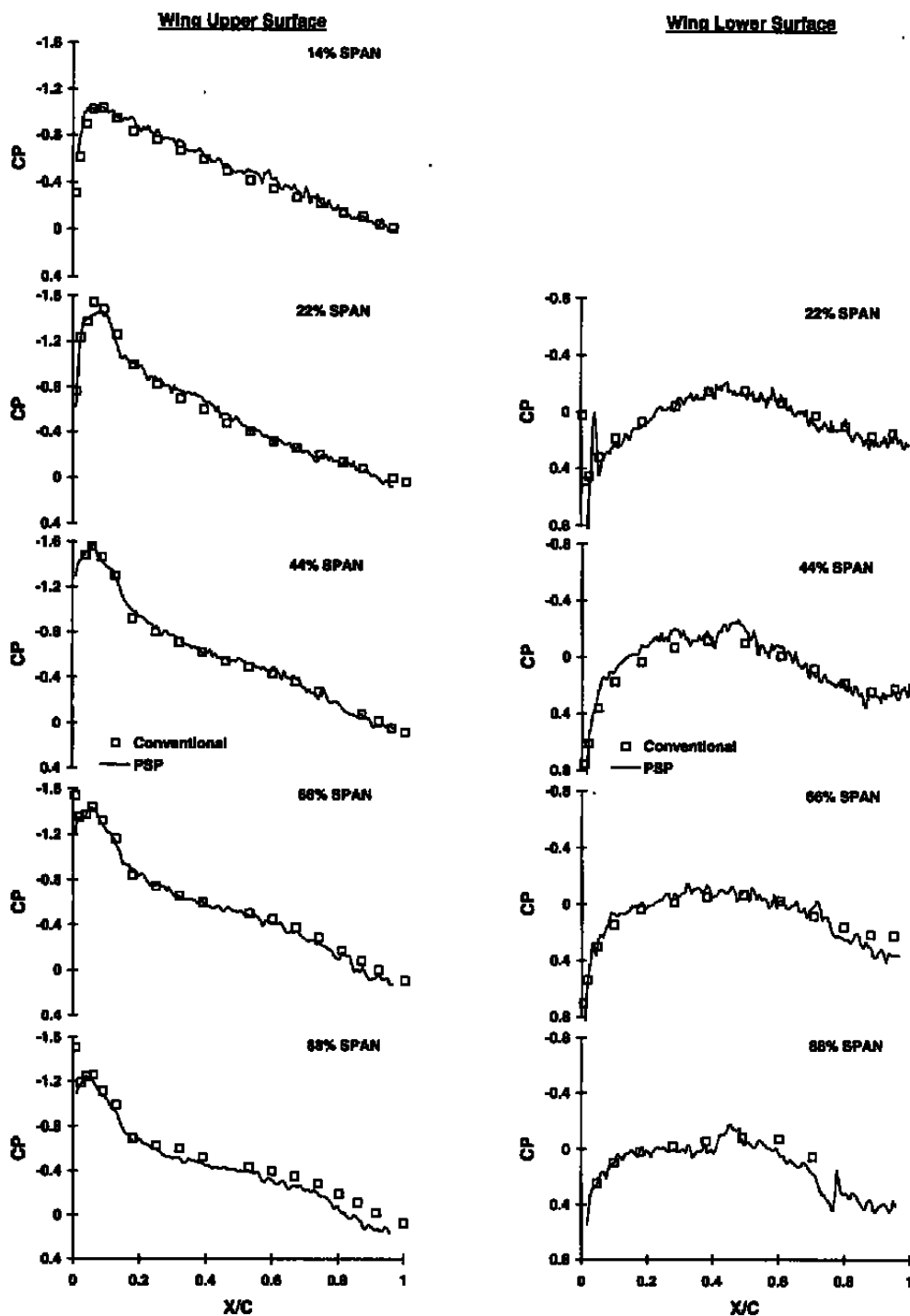


o. Alpha = 4 deg, Rec = 2.0

Figure 8. Continued.

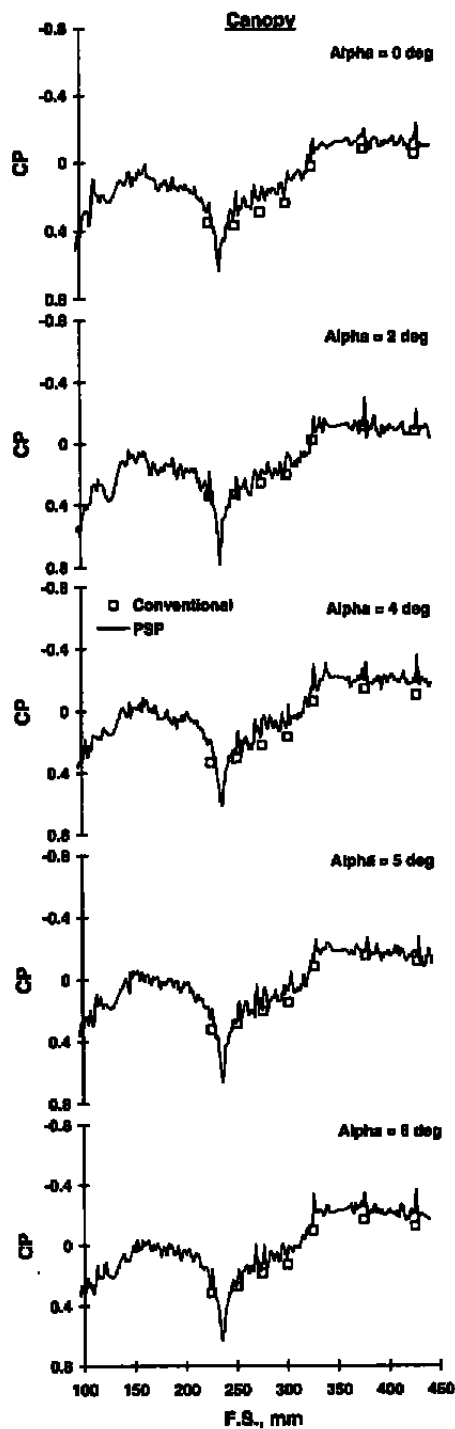


p. Alpha = 5 deg, Rec = 2.0
Figure 8. Continued.



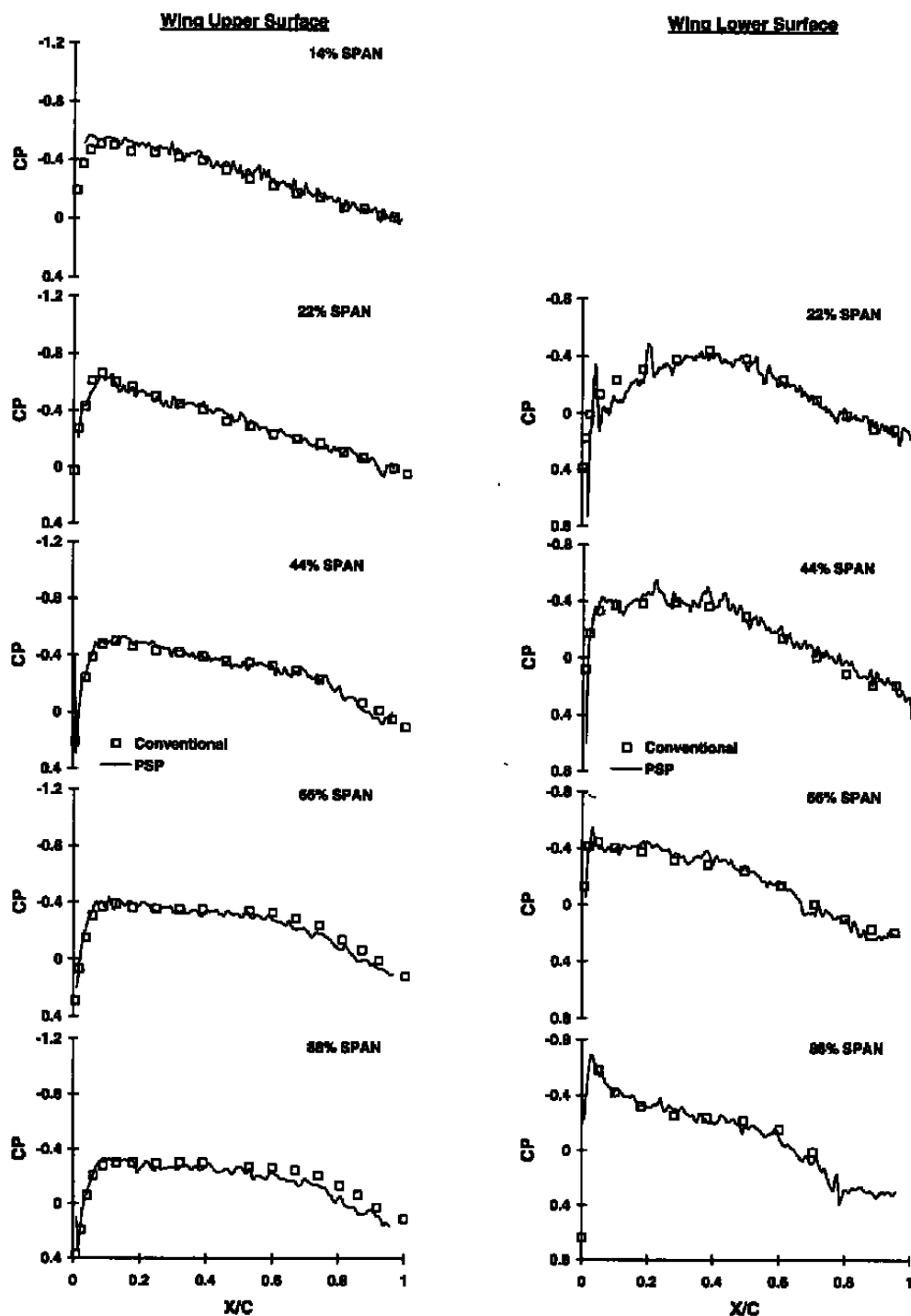
q. Alpha = 6 deg, Rec = 2.0

Figure 8. Continued.



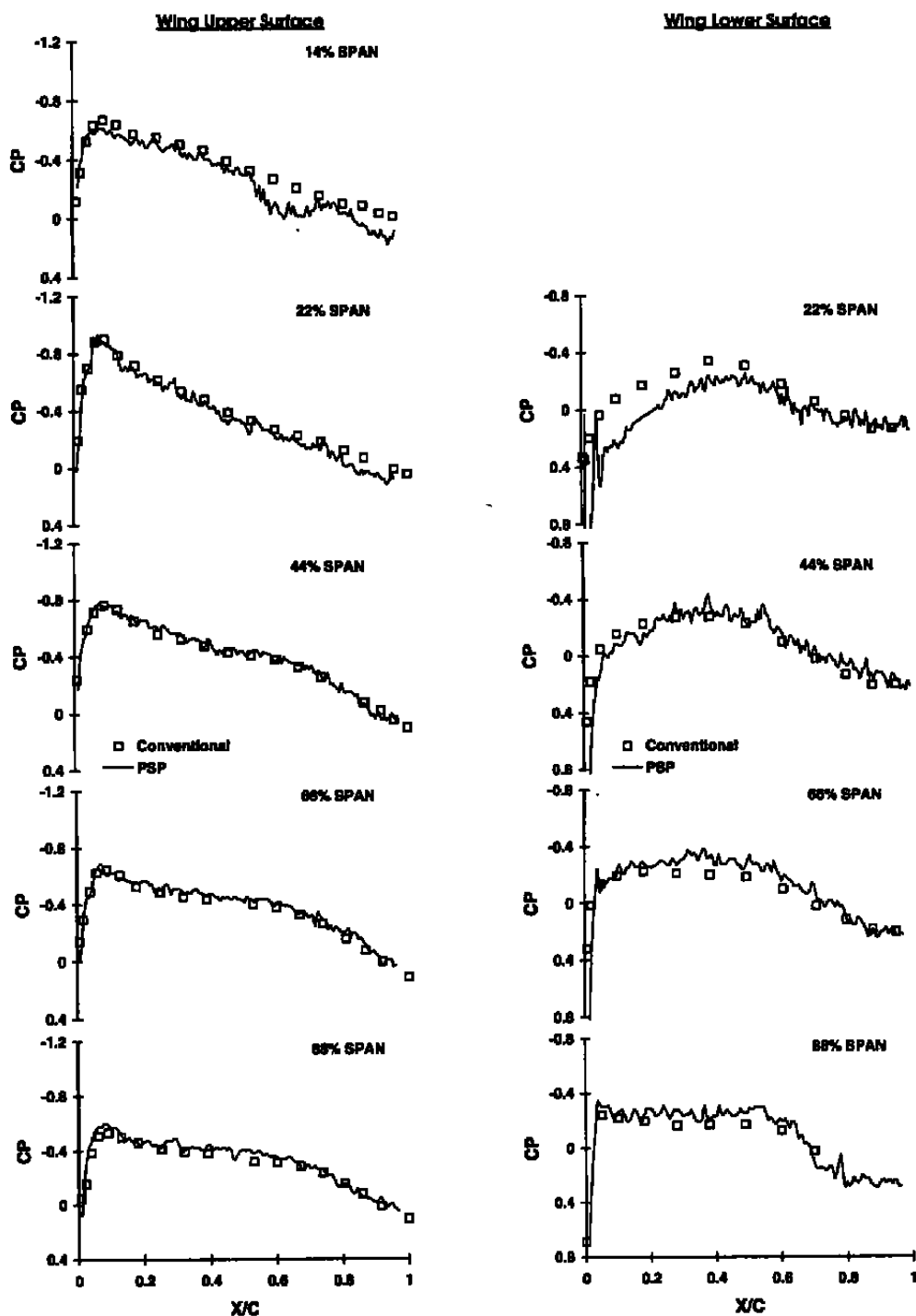
r. Canopy, Rec = 2.0

Figure 8. Continued.

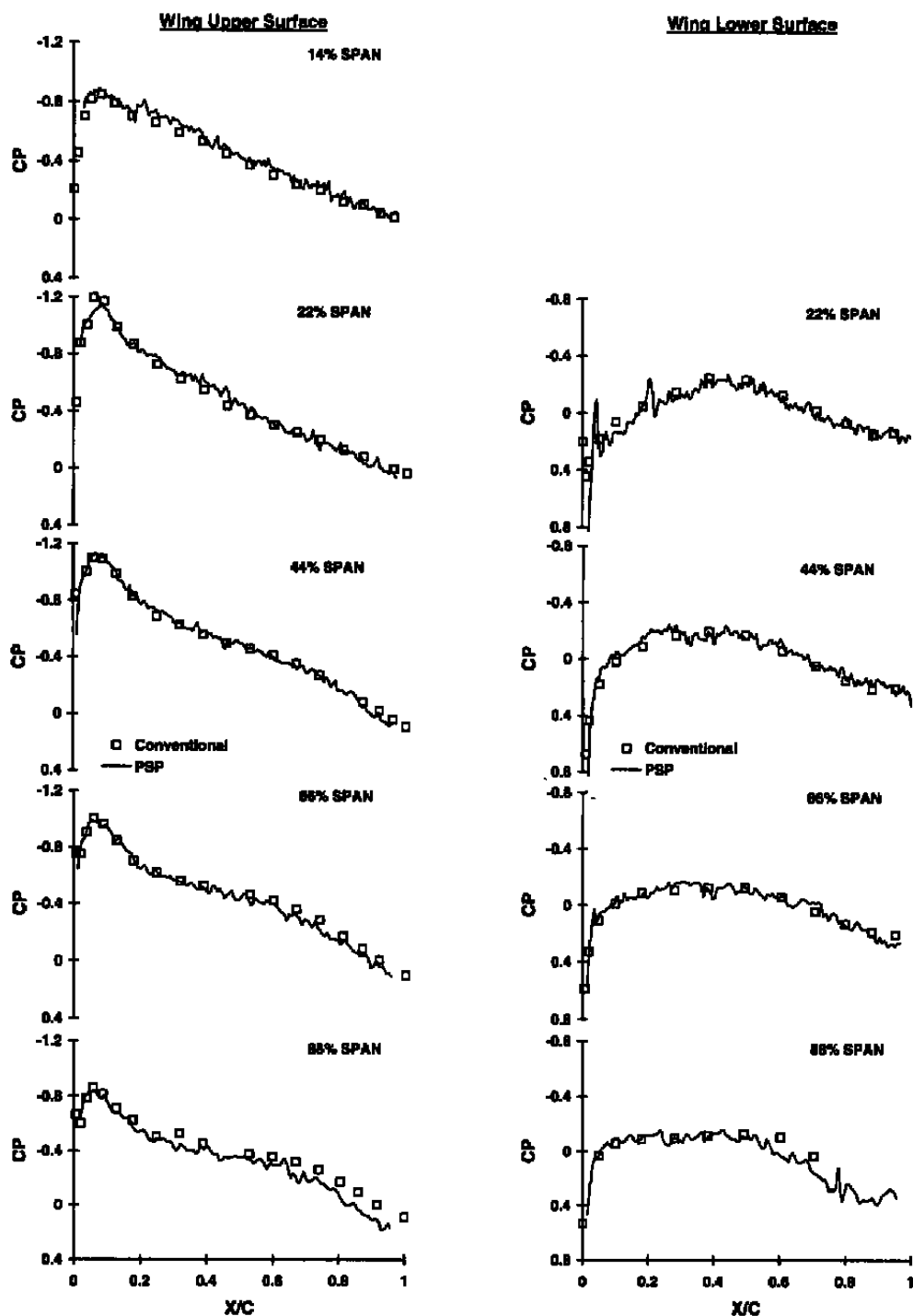


s. Alpha = 0 deg, Rec = 2.7

Figure 8. Continued.

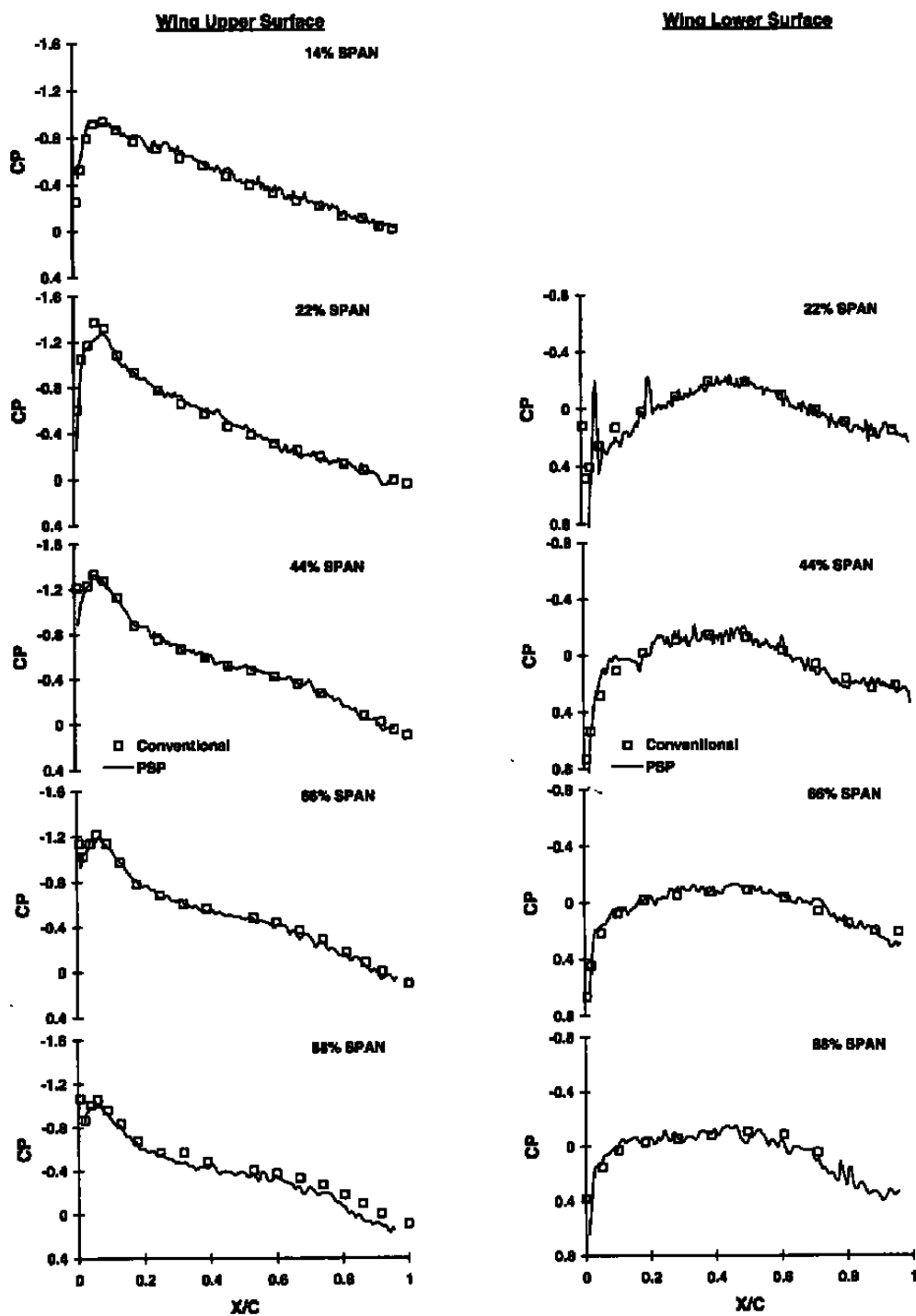


t. Alpha = 2 deg, Rec = 2.7
Figure 8. Continued.

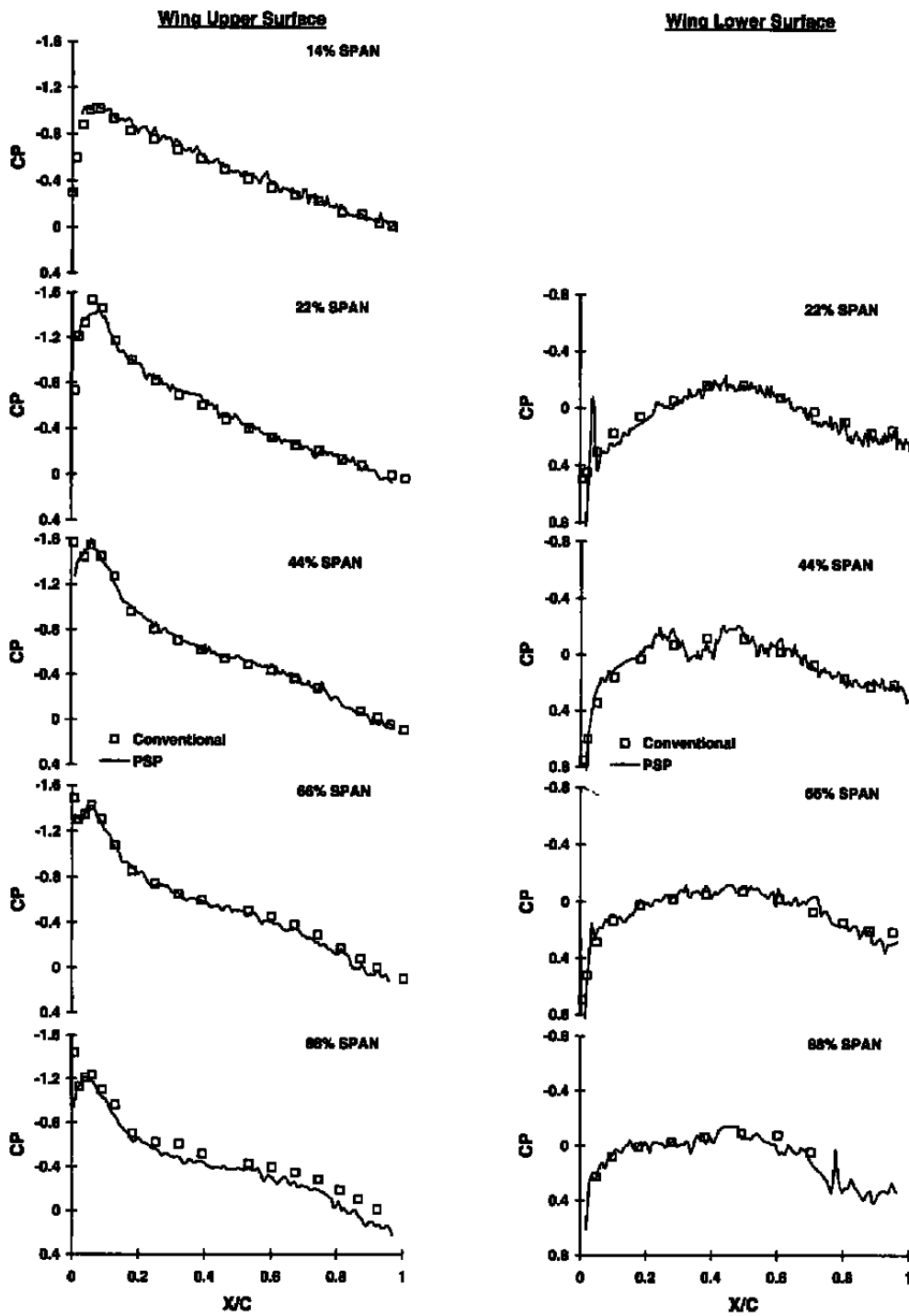


α . Alpha = 4 deg, Rec = 2.7

Figure 8. Continued.

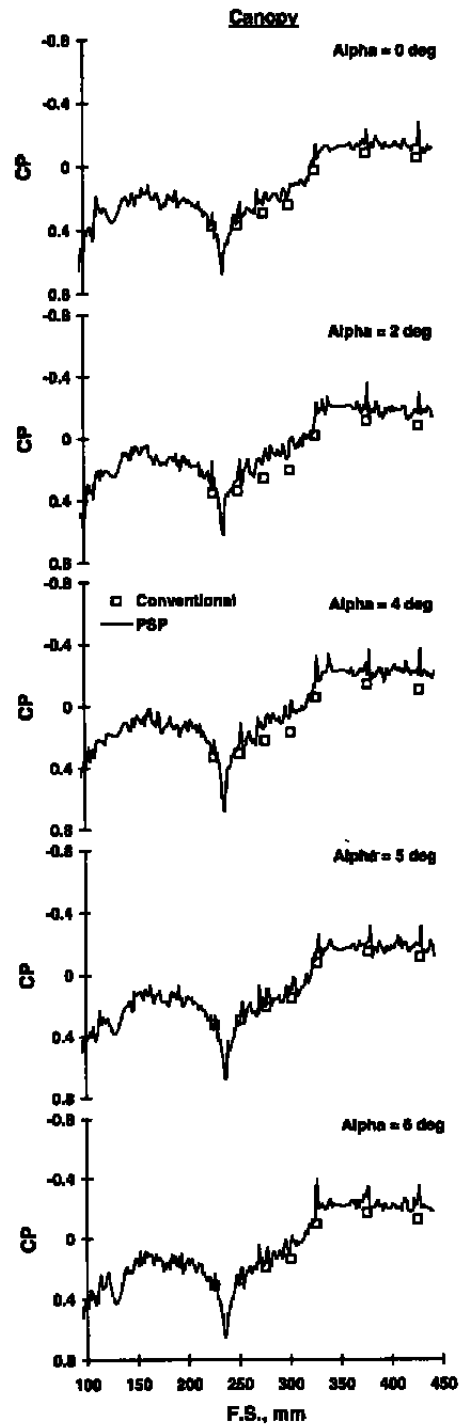


v. $\alpha = 5$ deg, $Re_c = 2.7$
Figure 8. Continued.



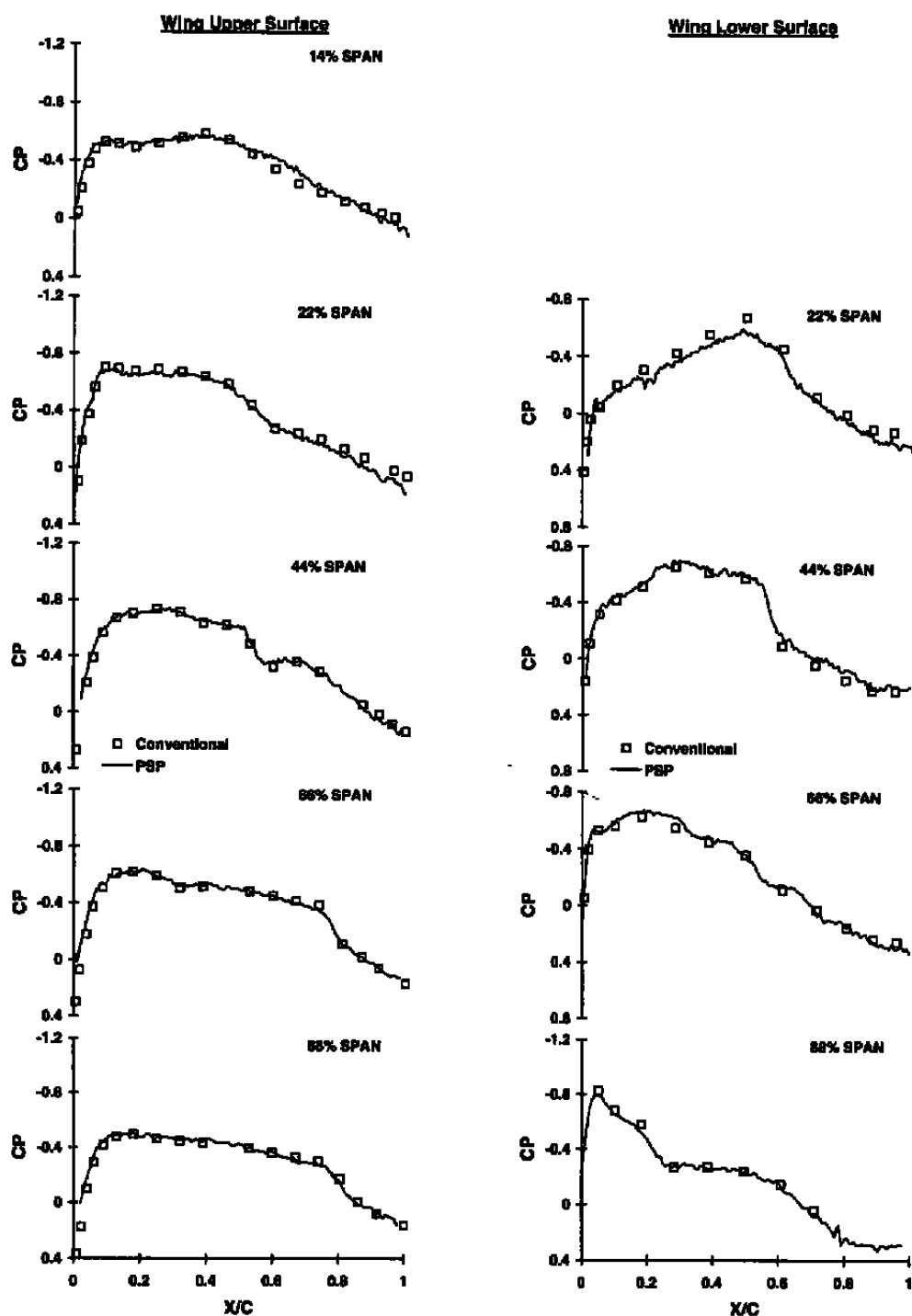
w. Alpha = 6 deg, Rec = 2.7

Figure 8. Continued.



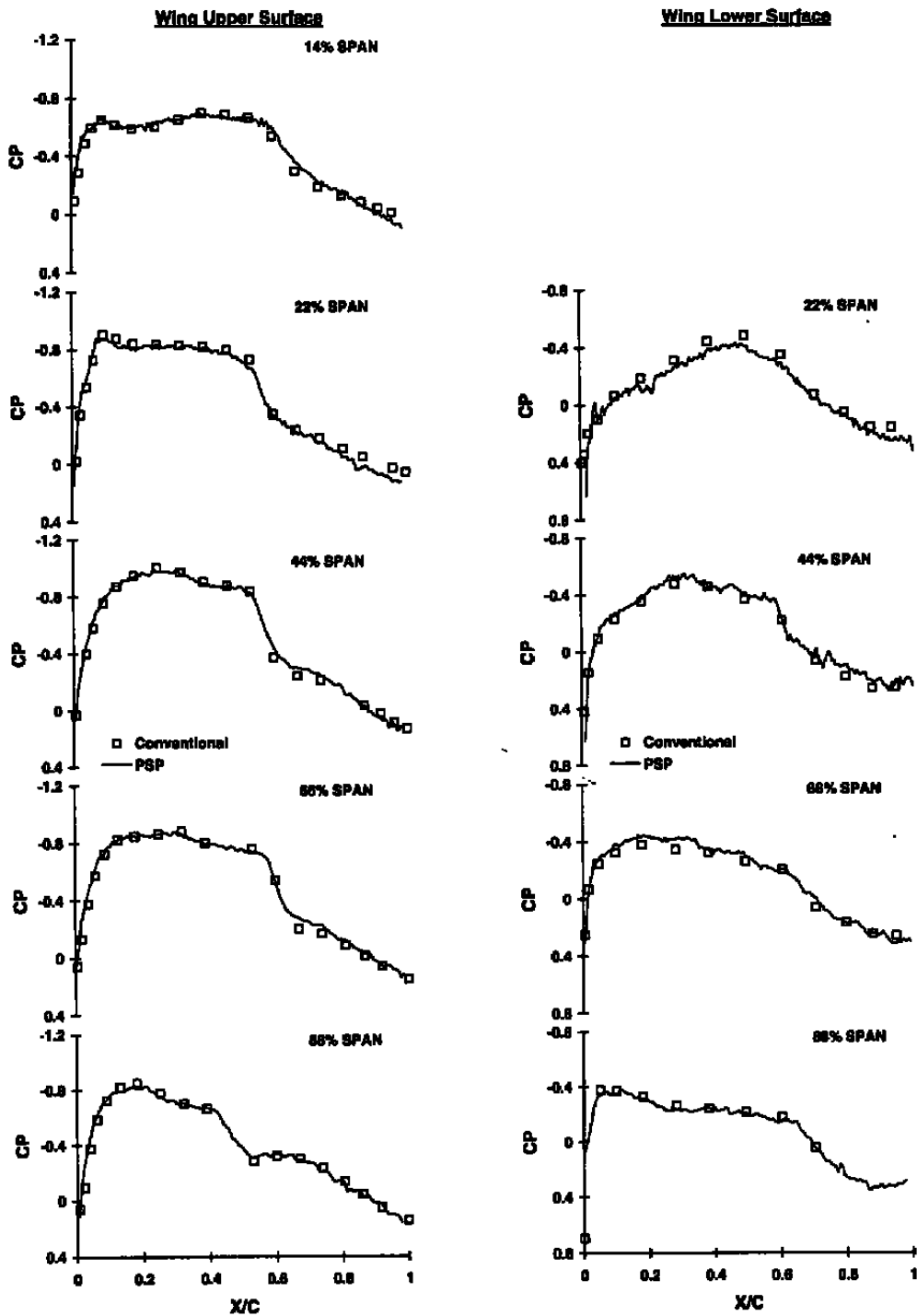
x. Canopy, Rec = 2.7

Figure 8. Concluded.



a. Alpha = 0 deg, Rec = 1.0

Figure 9. TST conventional and PSP pressure coefficient comparison at Mach number 0.835.



b. $\alpha = 2$ deg, $Re_c = 1.0$
Figure 9. Continued.

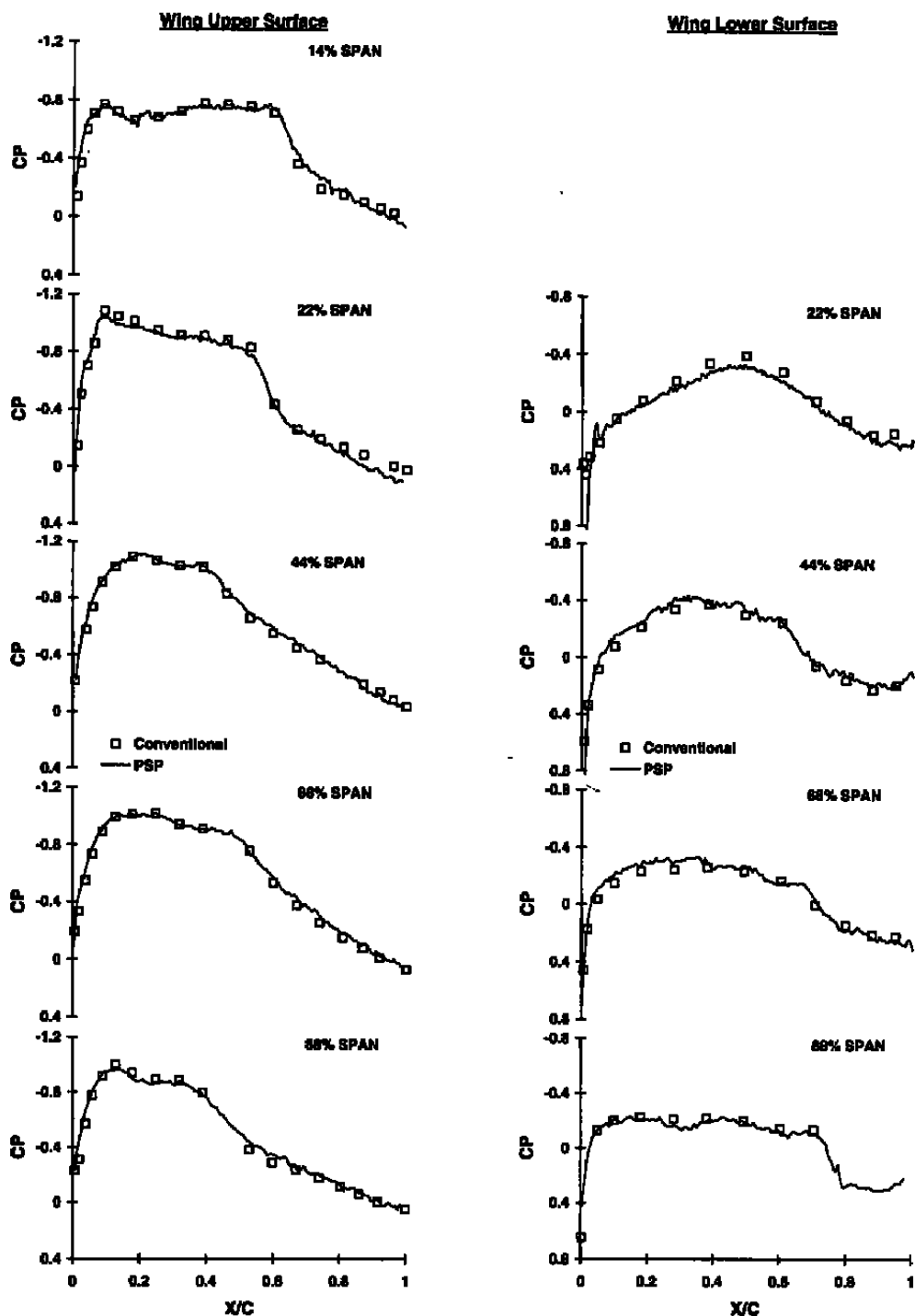
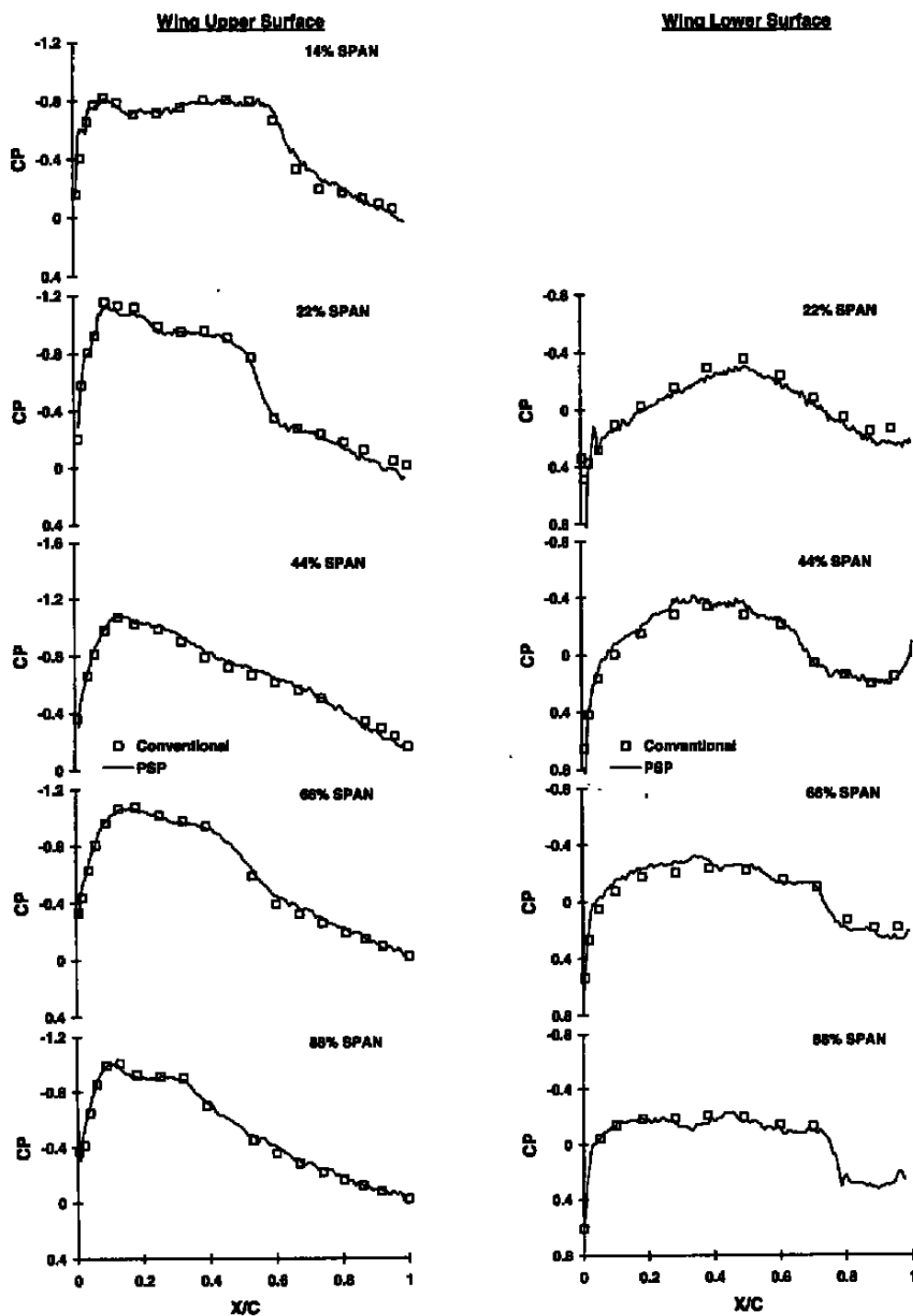
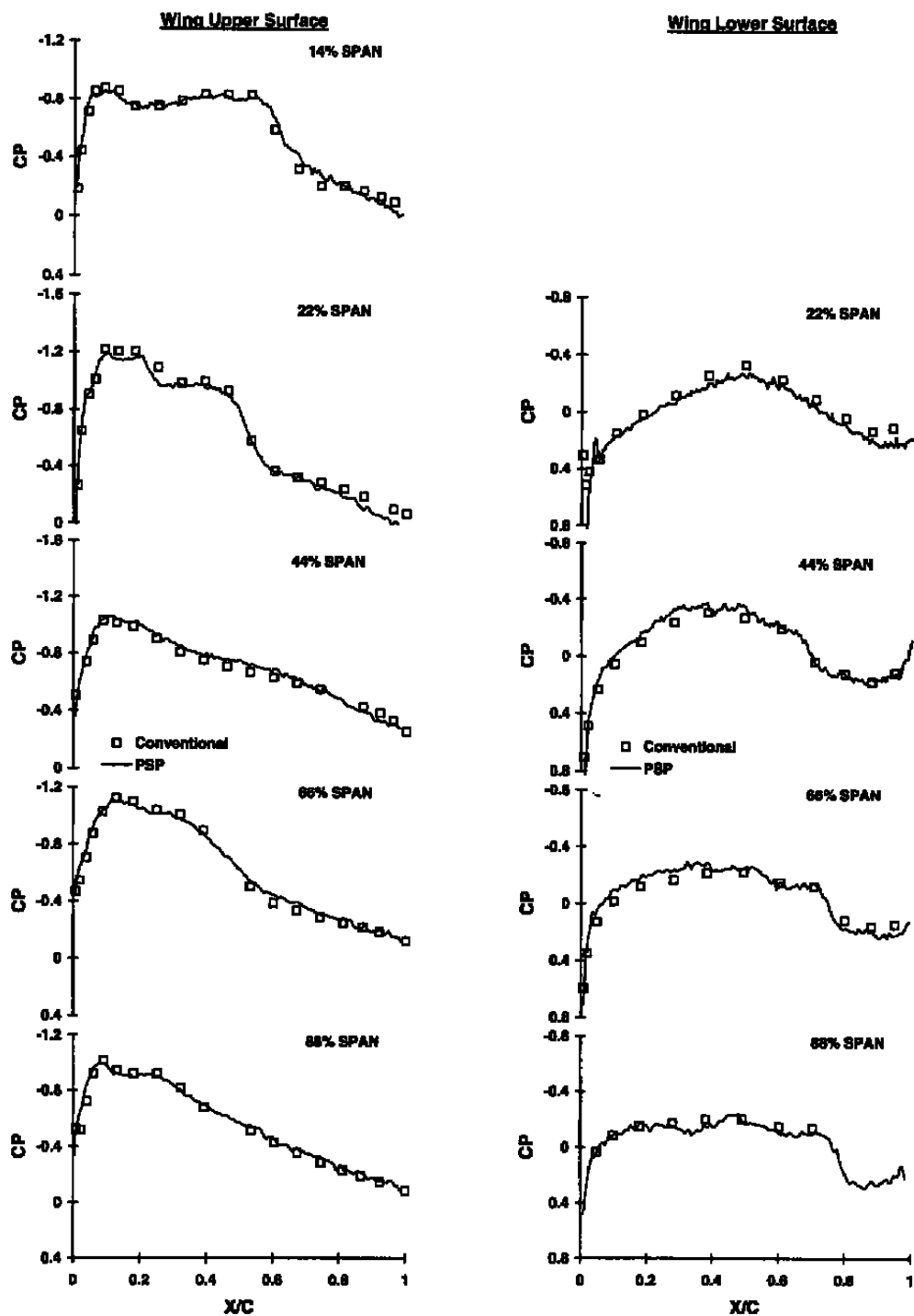
c. $\alpha = 4^\circ$, $Re_c = 1.0$

Figure 9. Continued.

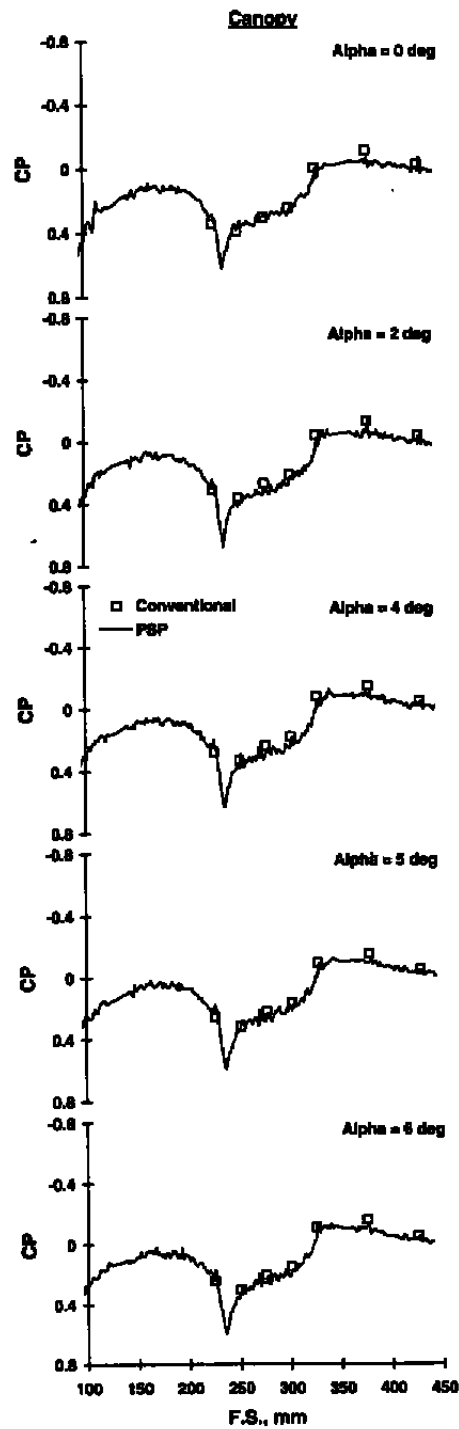


d. Alpha = 5 deg, Rec = 1.0
Figure 9. Continued.

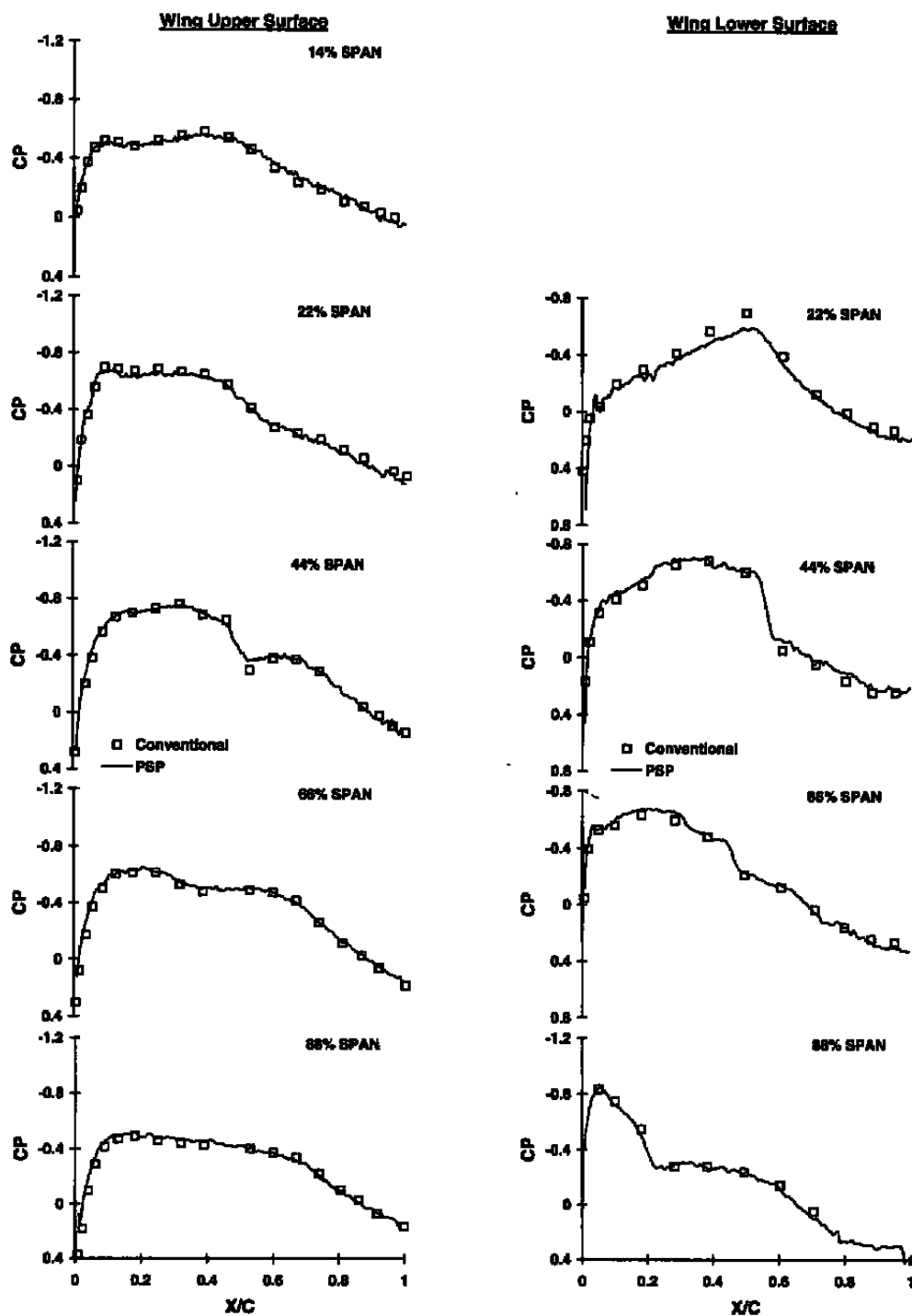


e. Alpha = 6 deg, Rec = 1.0

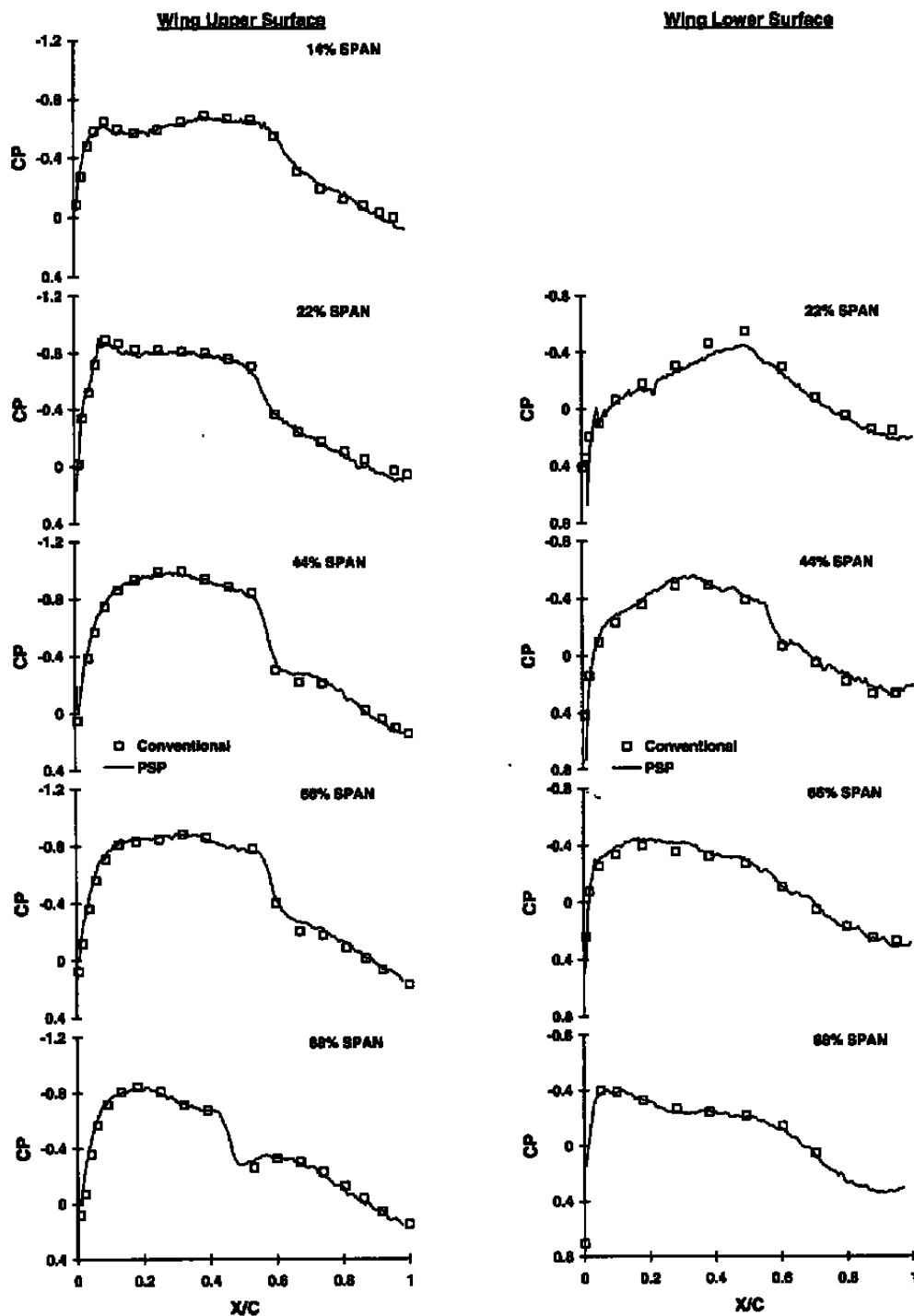
Figure 9. Continued.



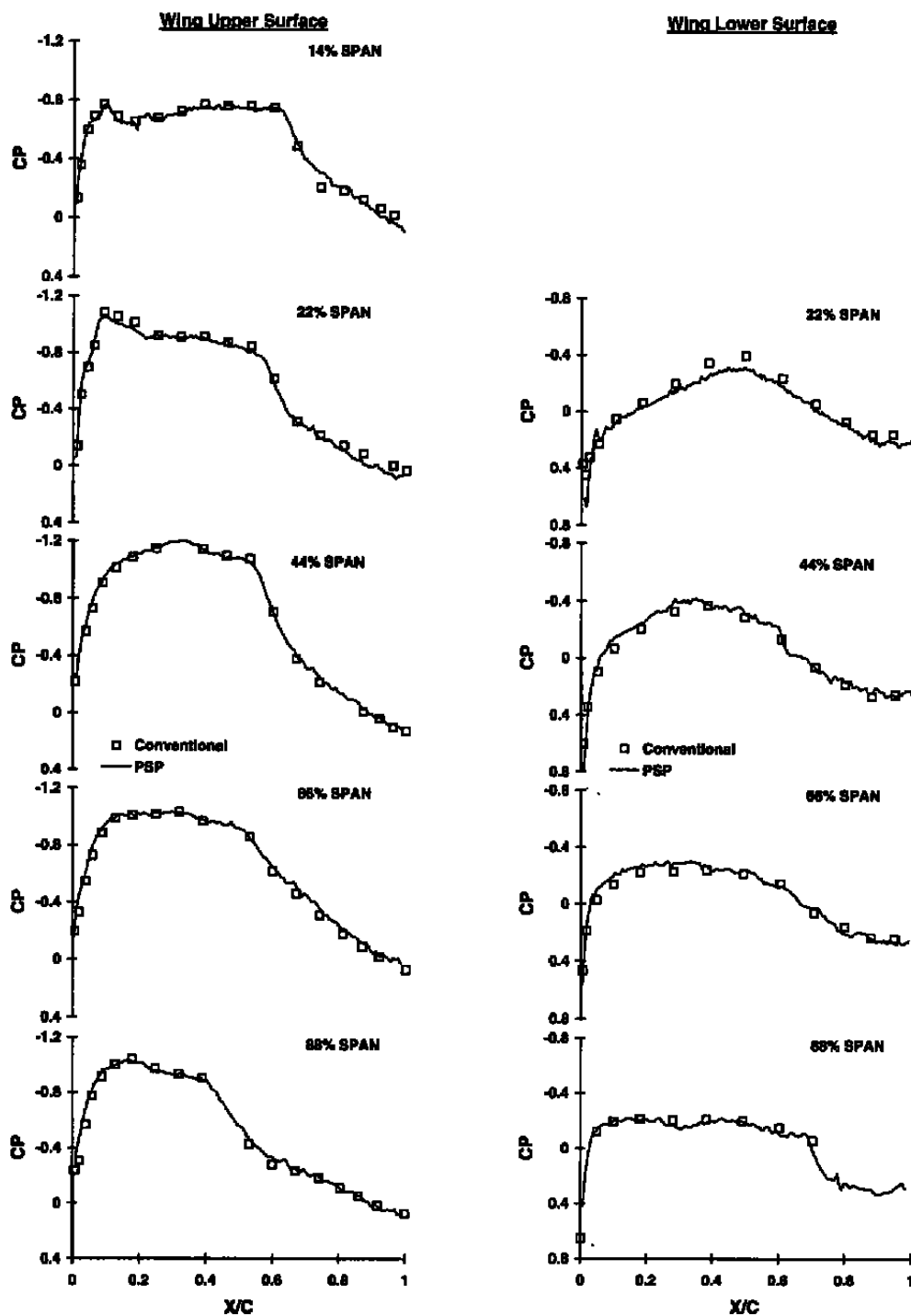
f. Canopy, Rec = 1.0
Figure 9. Continued.



g. Alpha = 0 deg, Rec = 1.6
Figure 9. Continued.

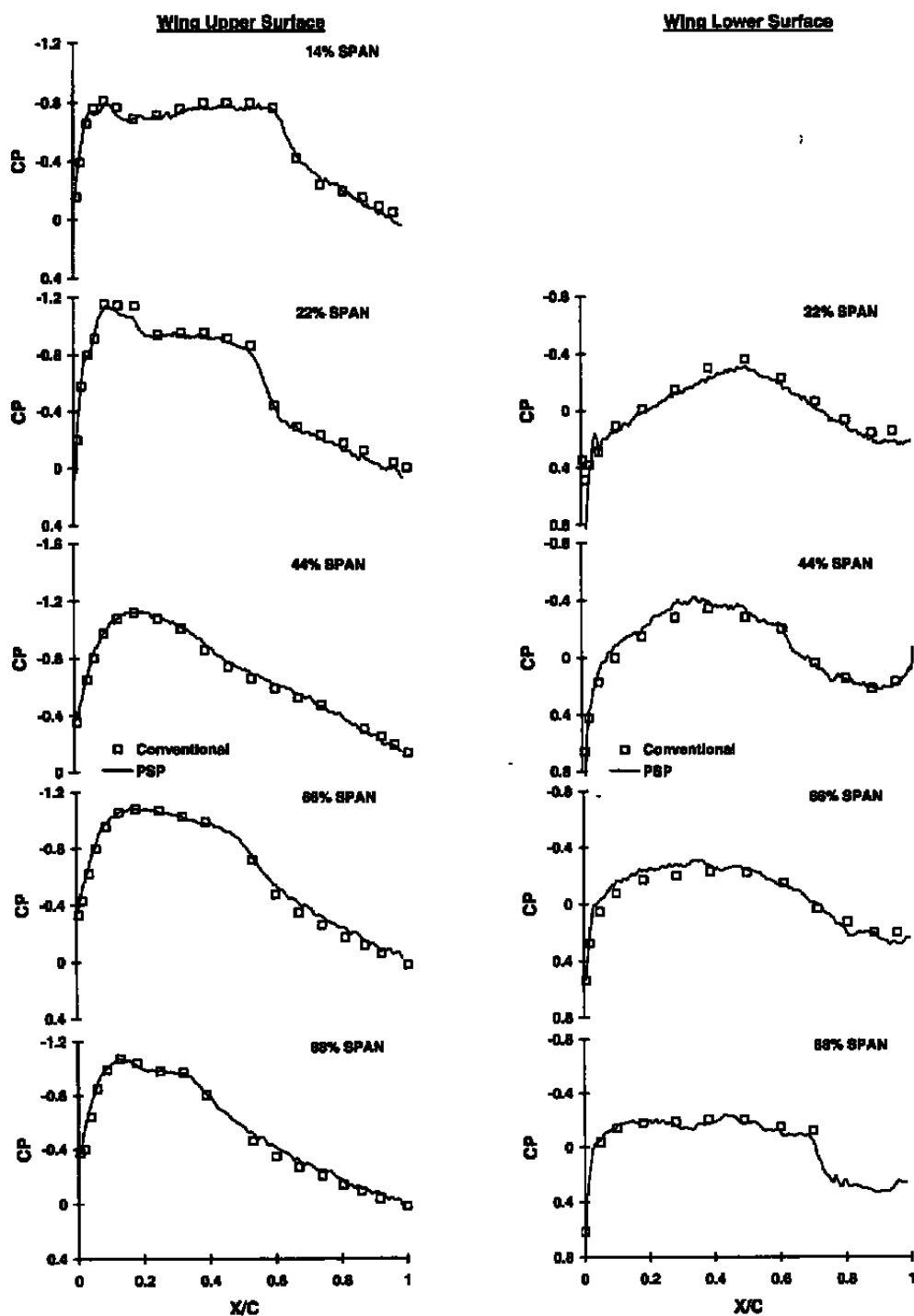


b. Alpha = 2 deg, Rec = 1.5
Figure 9. Continued.

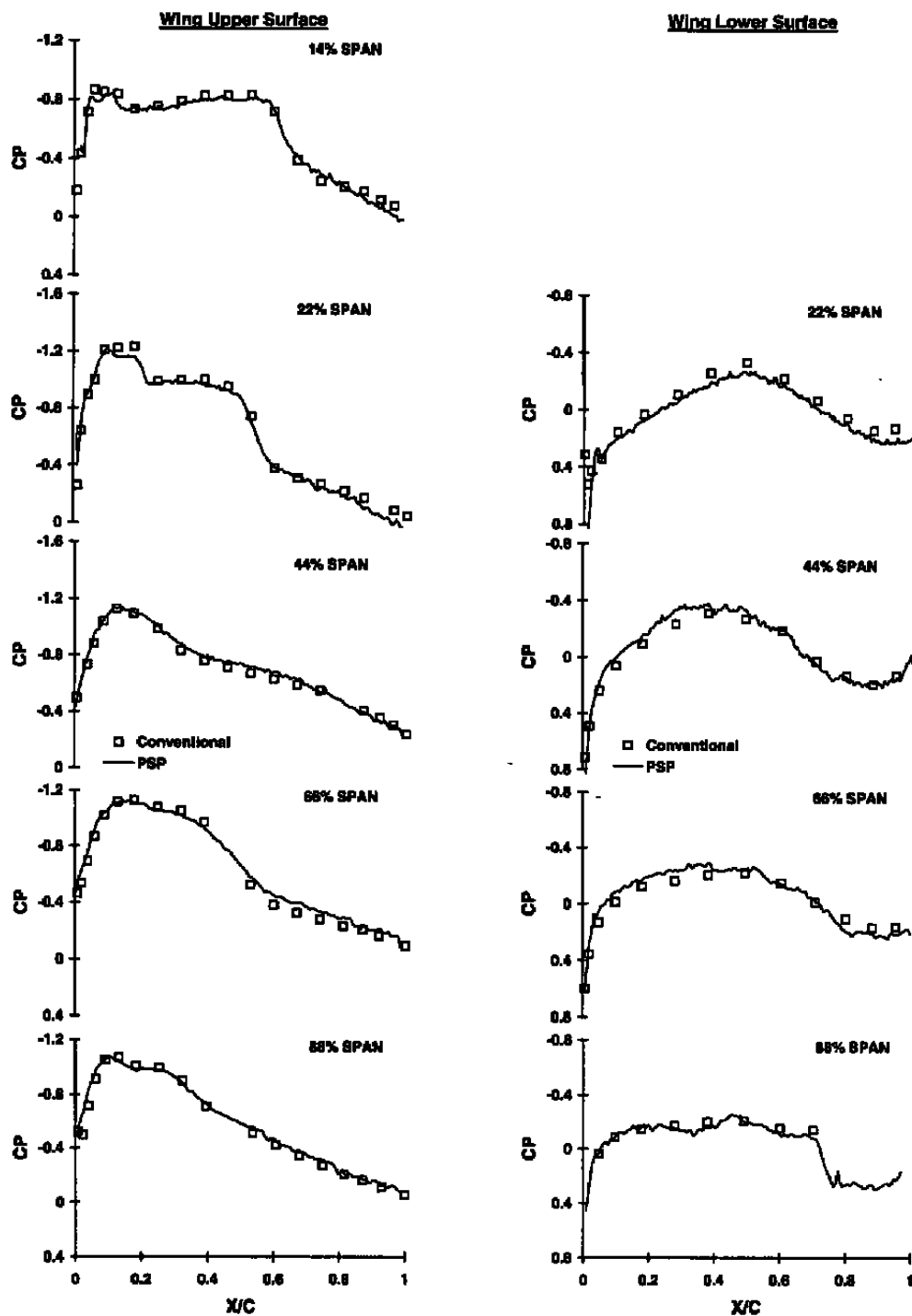


i. $\alpha = 4$ deg, $Re_c = 1.5$

Figure 9. Continued.

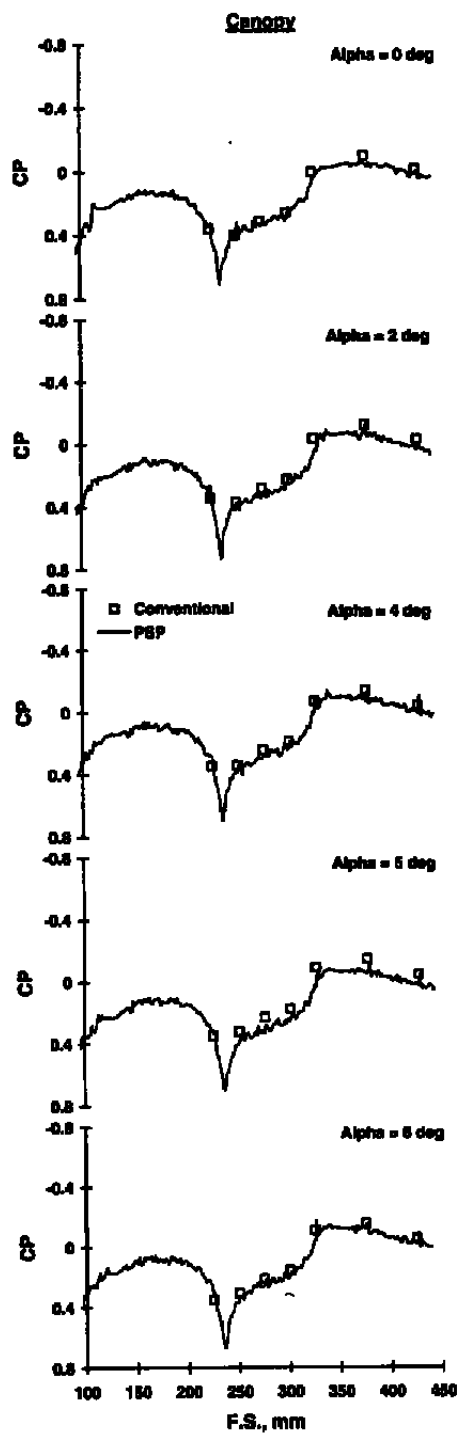


j. Alpha = 5 deg, Rec = 1.5
Figure 9. Continued.



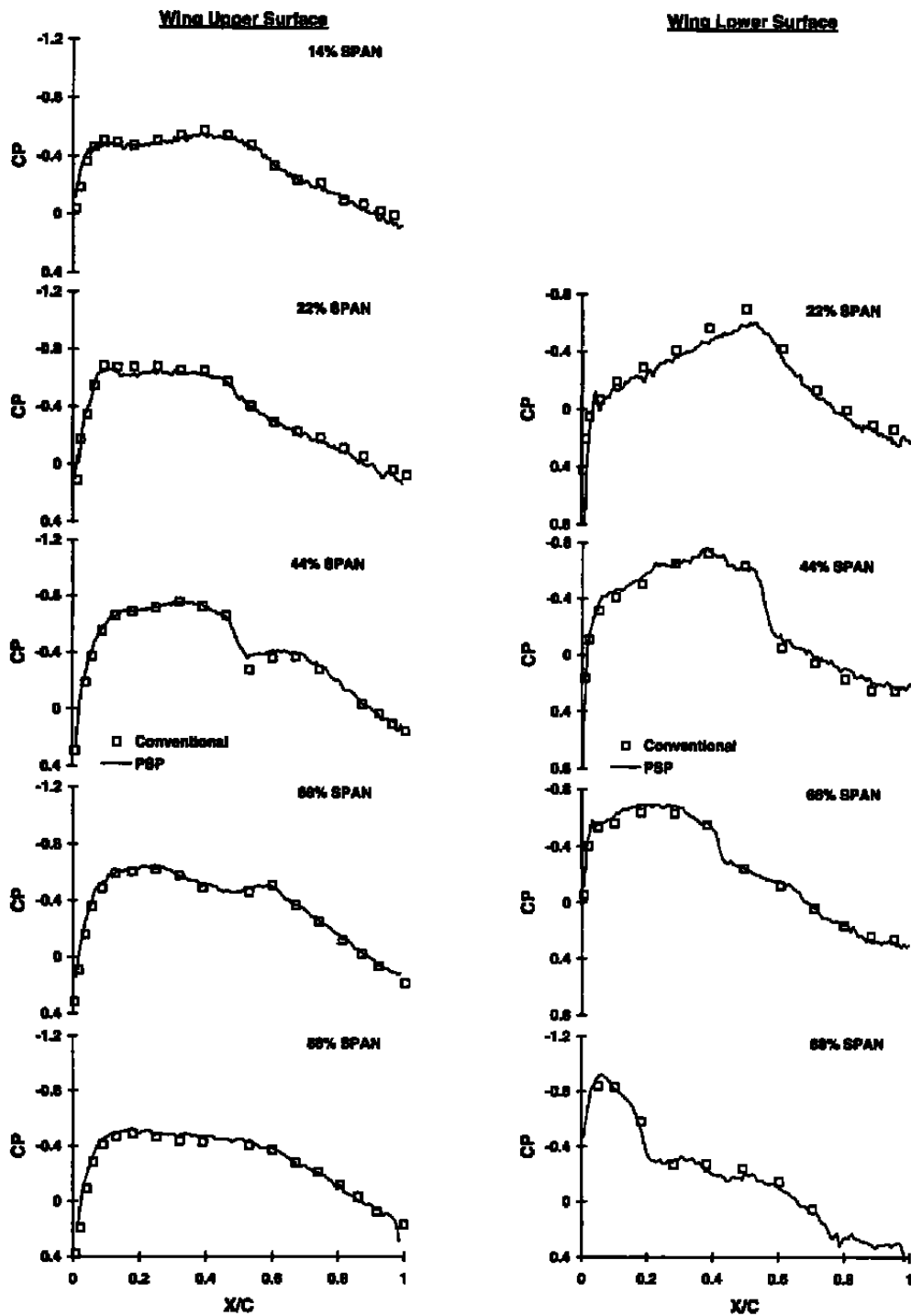
k. Alpha = 6 deg, Rec = 1.5

Figure 9. Continued.



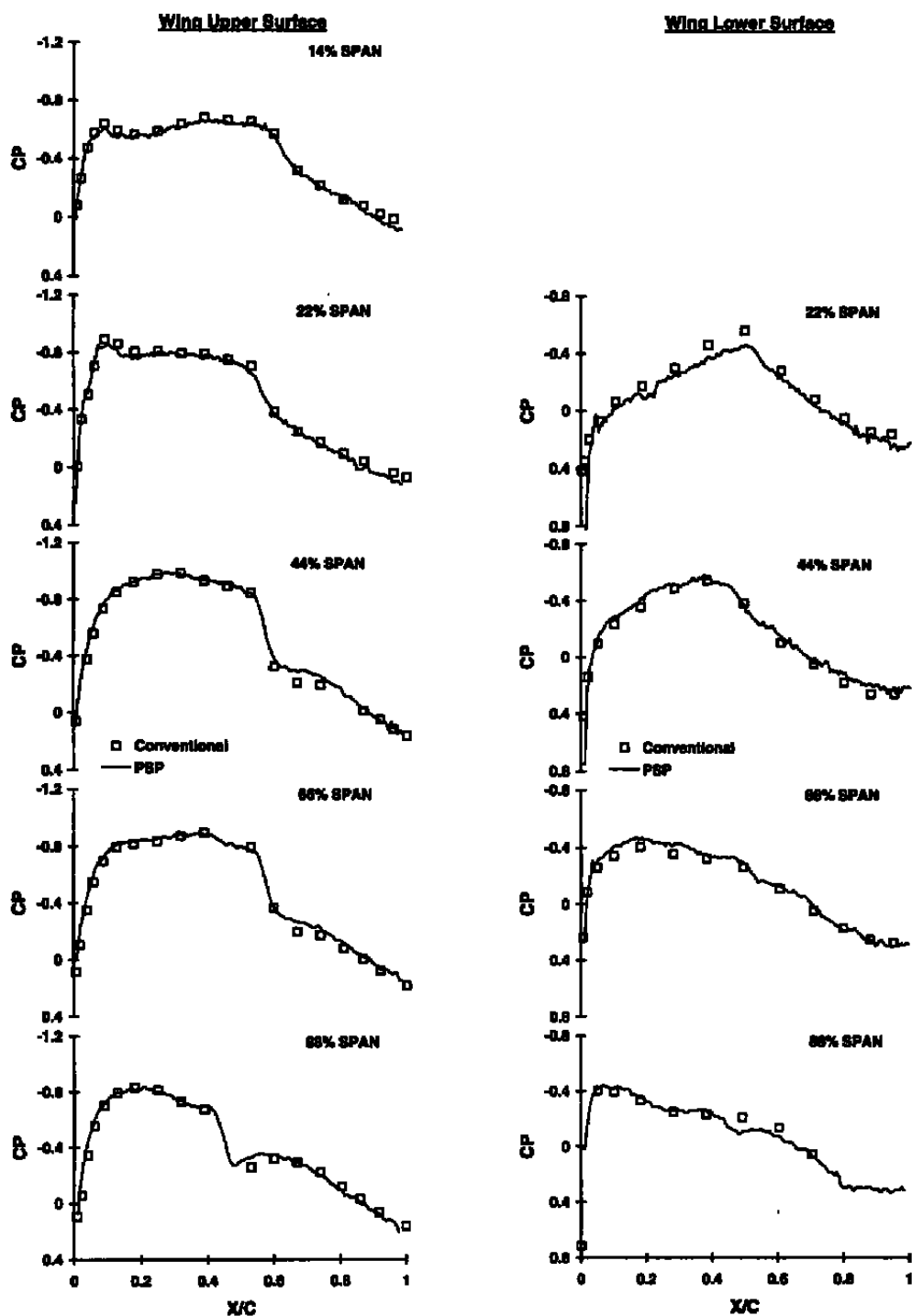
1. Canopy, Rec = 1.5

Figure 9. Continued.



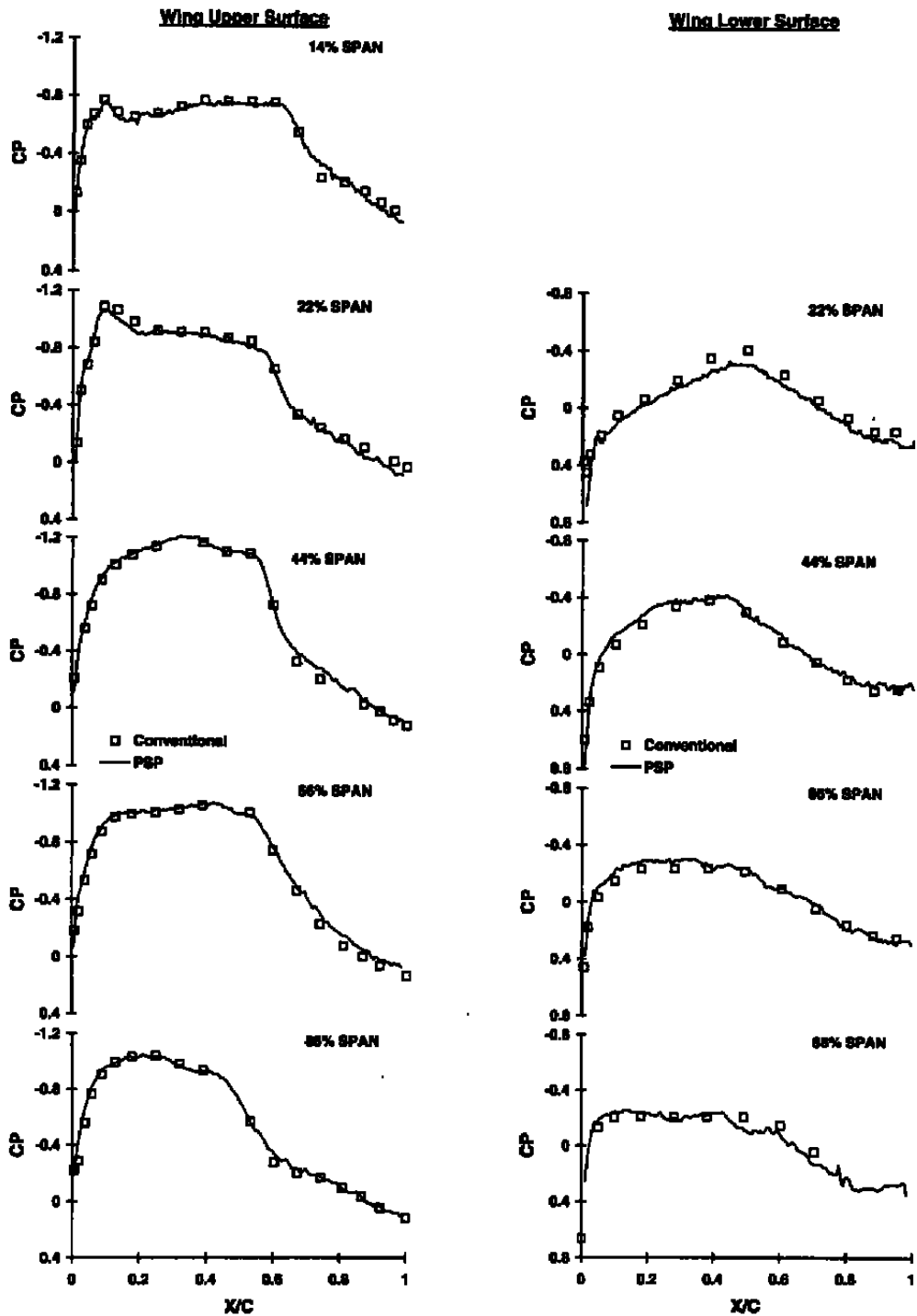
m. $\alpha = 0$ deg, $Re_c = 2.0$

Figure 9. Continued.



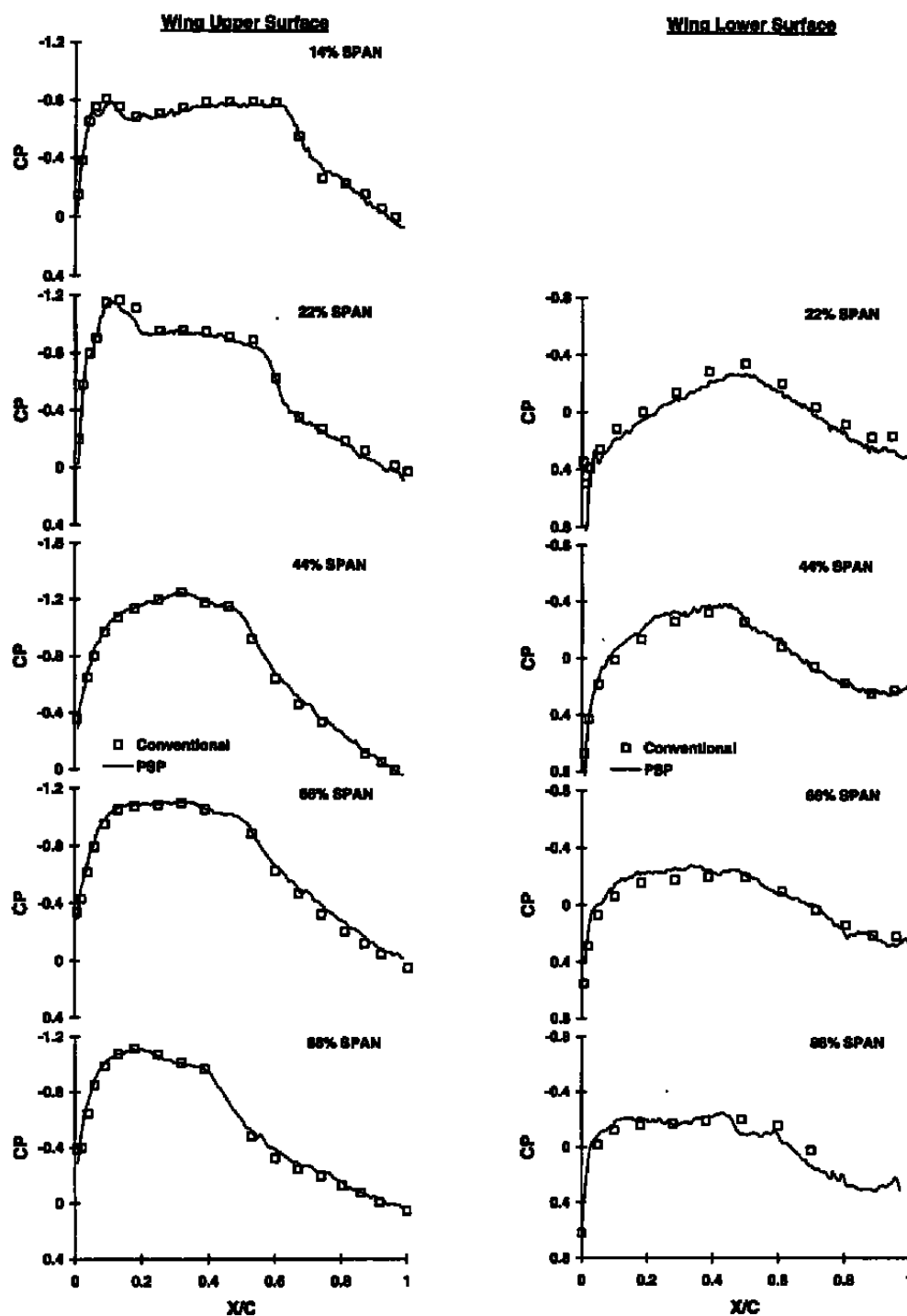
n. Alpha = 2 deg, Rec = 2.0

Figure 9. Continued.



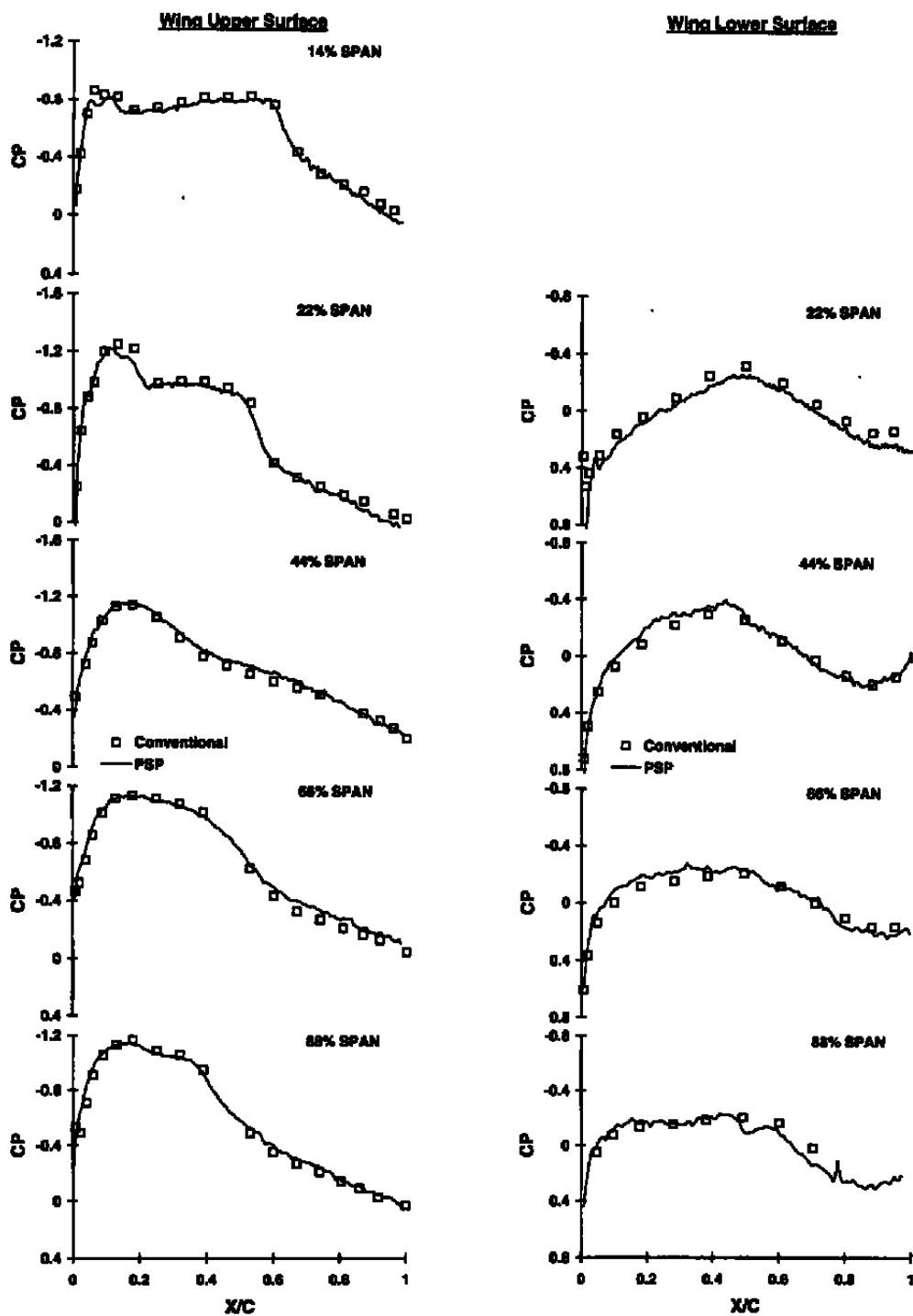
o. Alpha = 4 deg, Rec = 2.0

Figure 9. Continued.



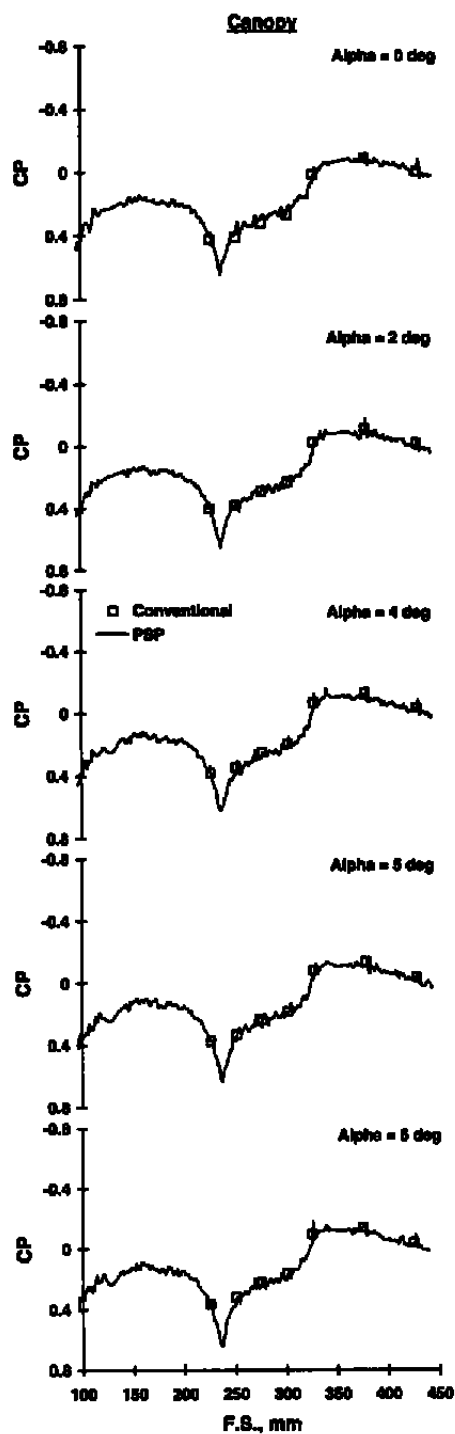
p. Alpha = 5 deg, Rec = 2.0

Figure 9. Continued.

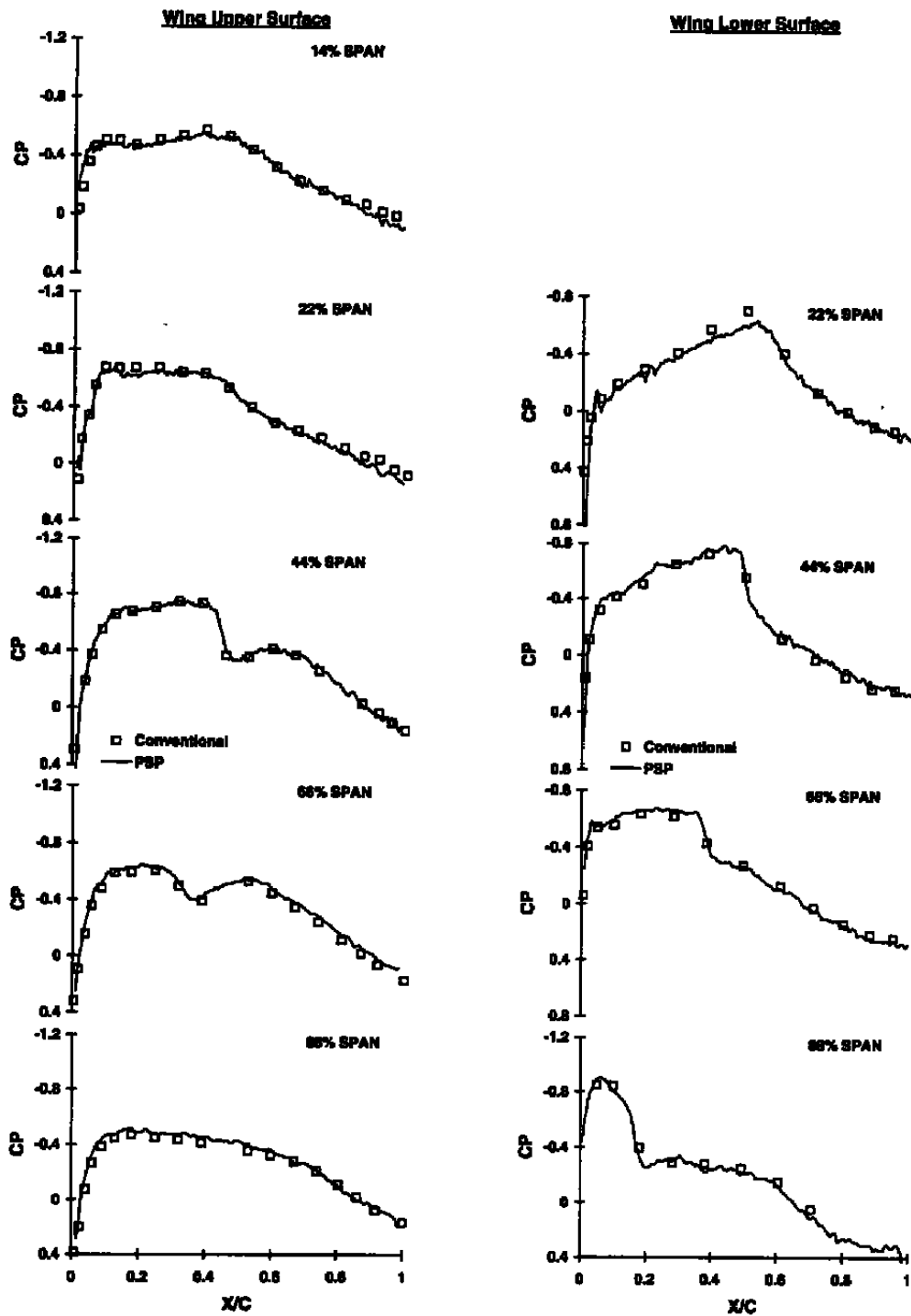


$\alpha = 6^\circ$, $Re_c = 2.0$

Figure 9. Continued.

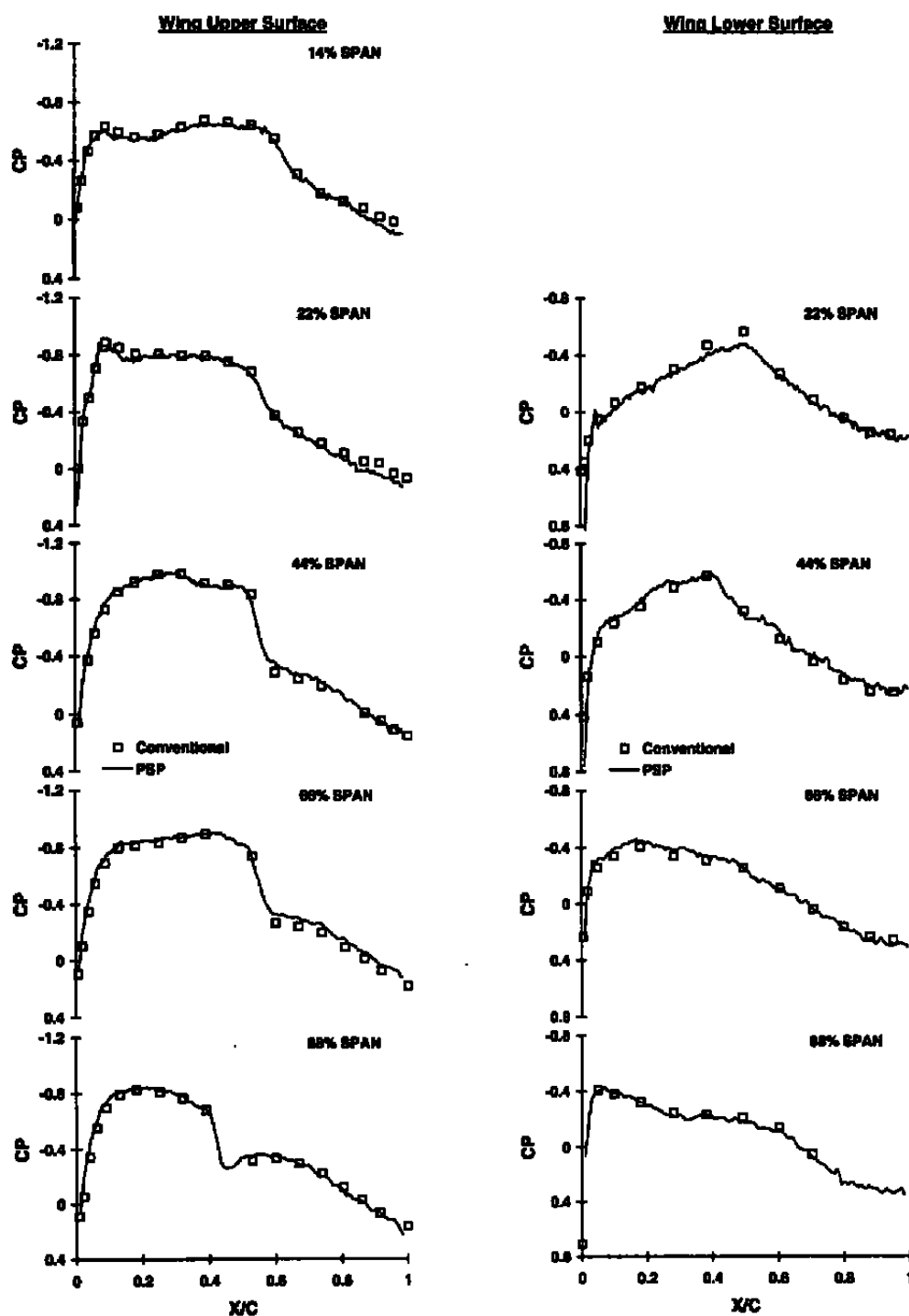


r. Canopy, Rec = 2.0
 Figure 9. Continued.

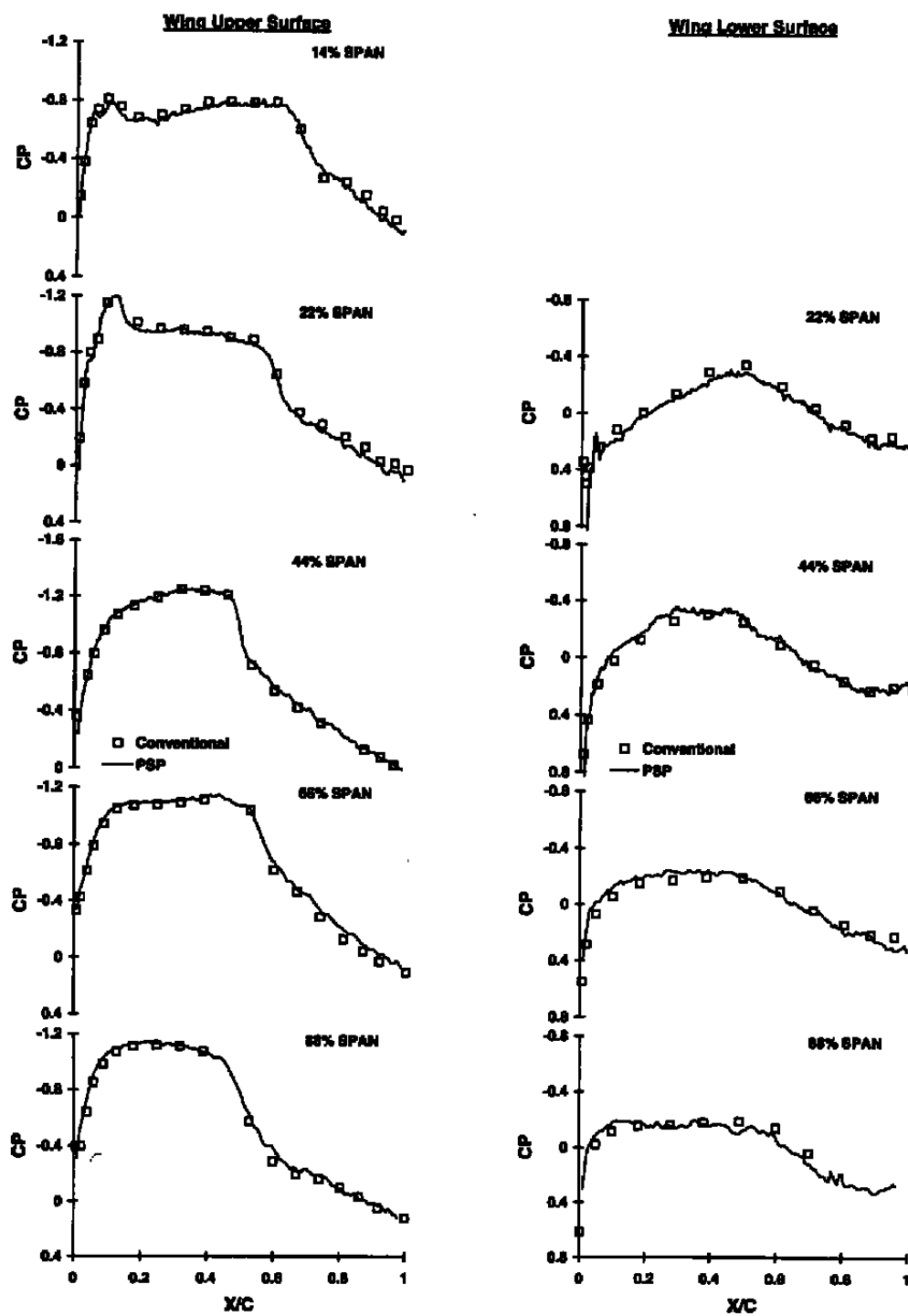


s. Alpha = 0 deg, Rec = 2.7

Figure 9. Continued.

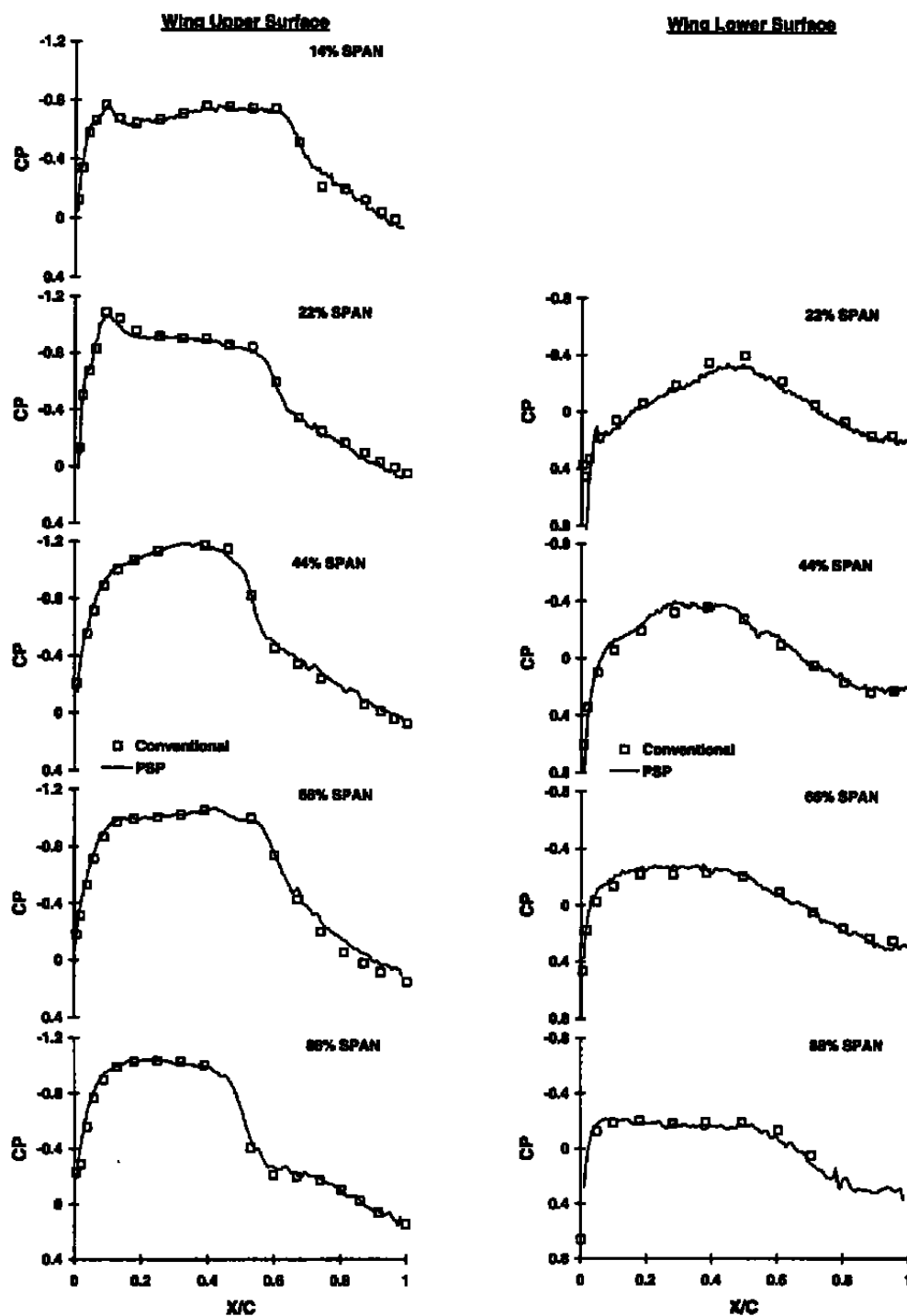


t. Alpha = 2 deg, Rec = 2.7
Figure 9. Continued.

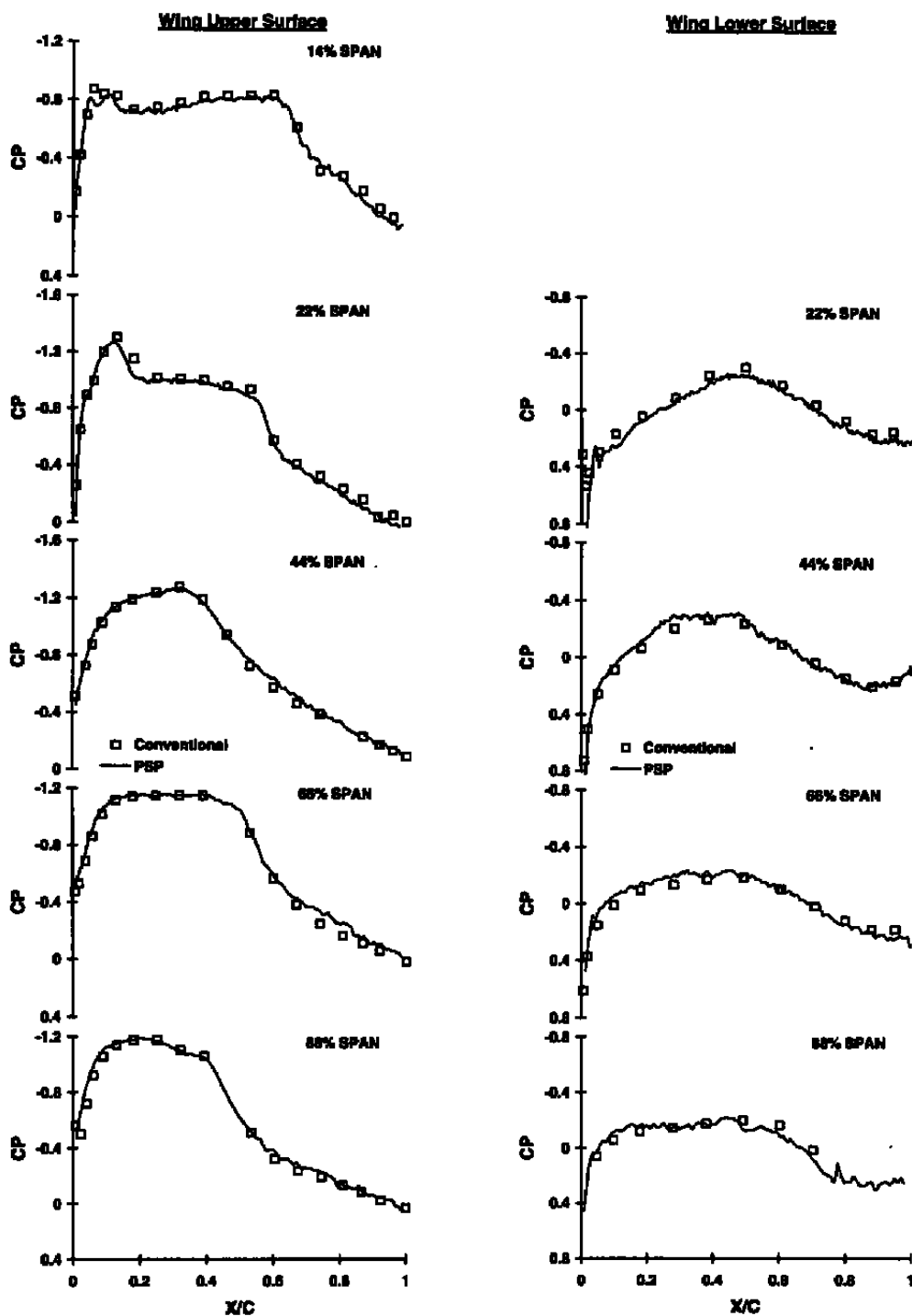


u. Alpha = 4 deg, Rec = 2.7

Figure 9. Continued.

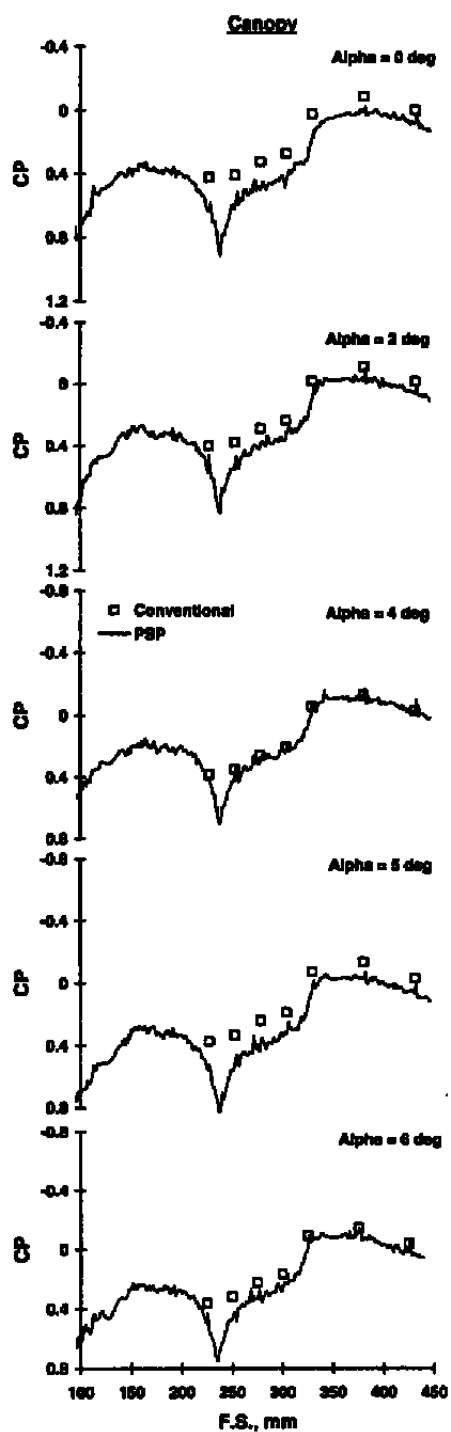


v. Alpha = 5 deg, Rec = 2.7
Figure 9. Continued.



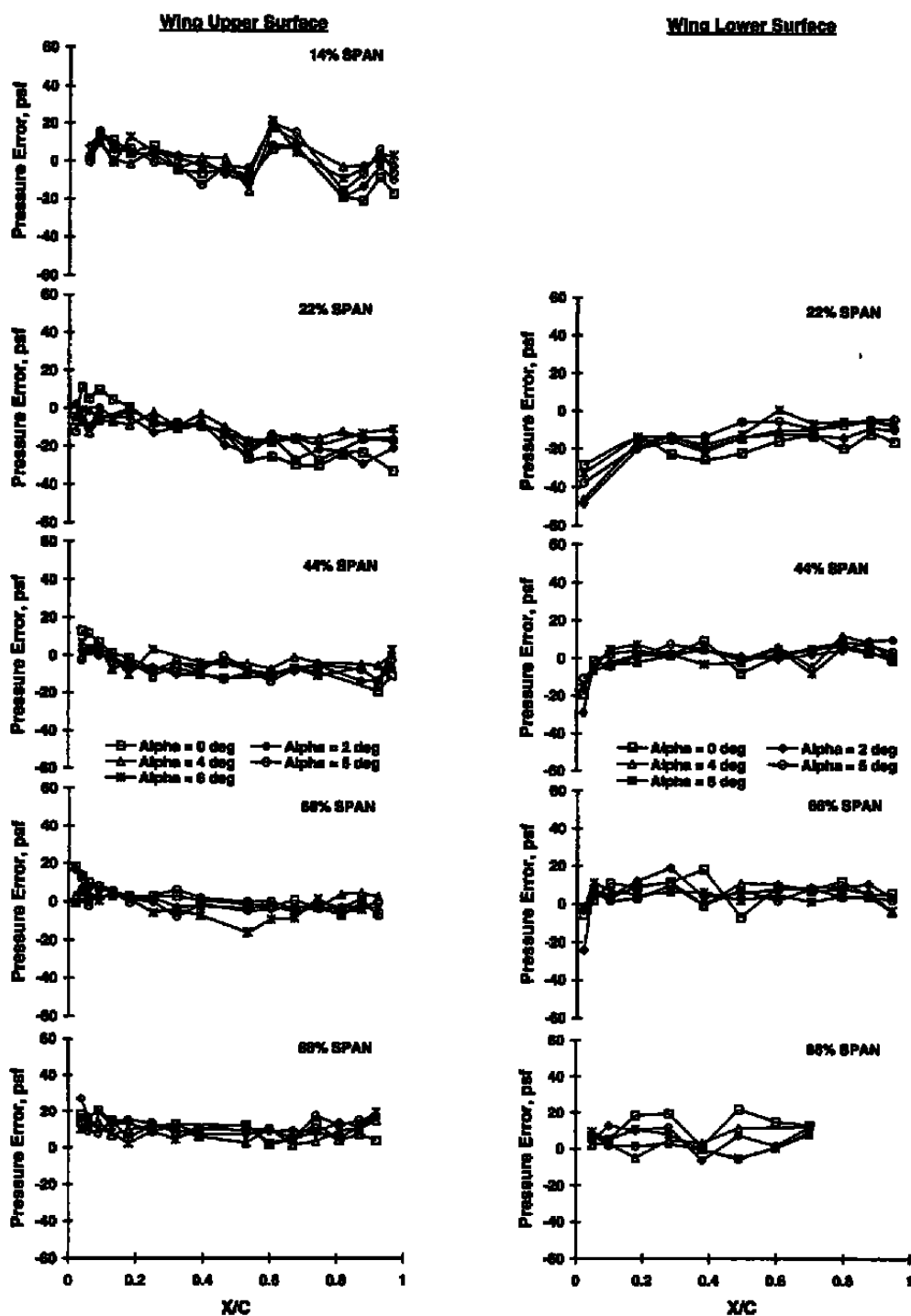
w. Alpha = 6 deg, Rec = 2.7

Figure 9. Continued.



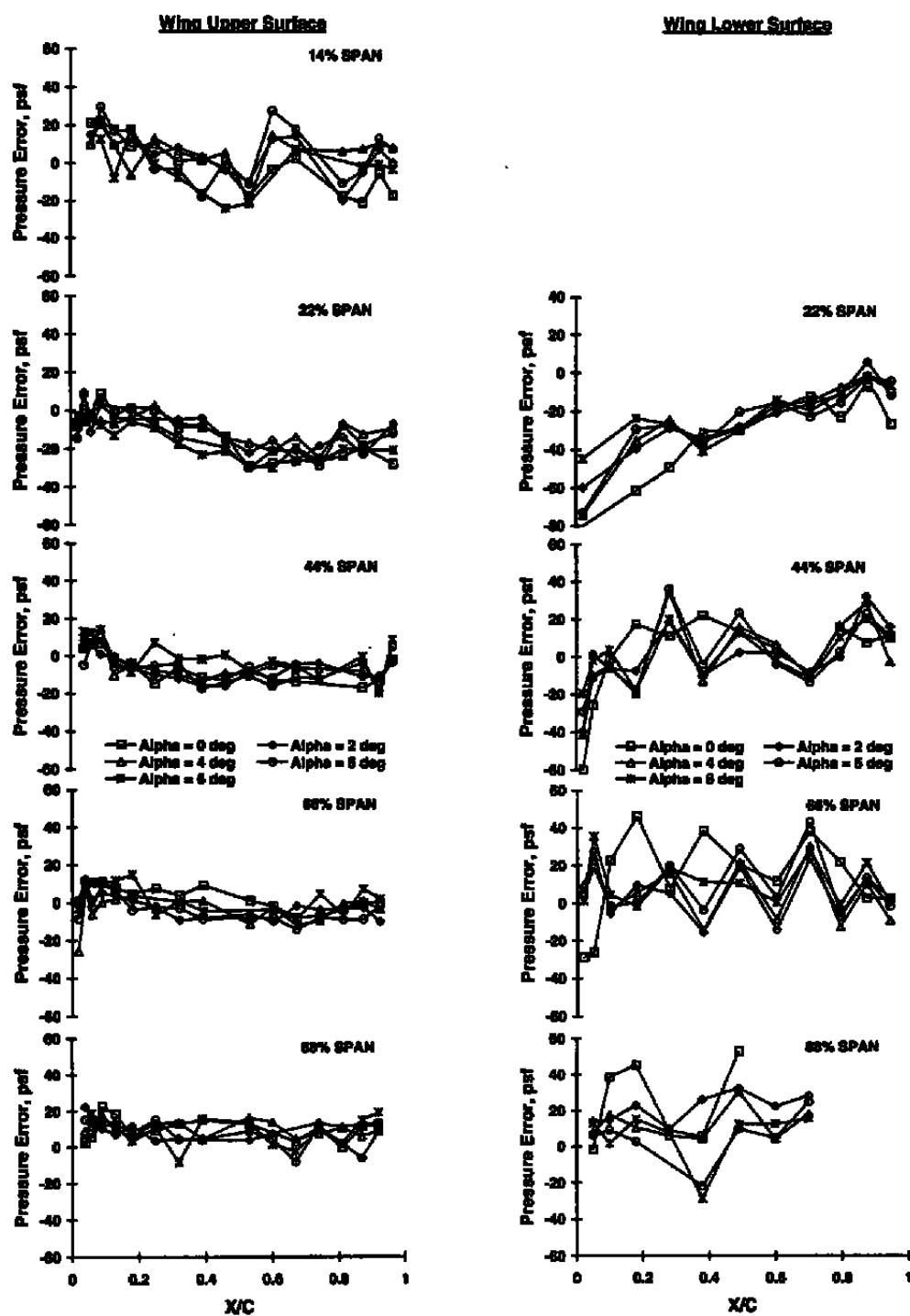
x. Canopy, Rec = 2.7

Figure 9. Concluded.

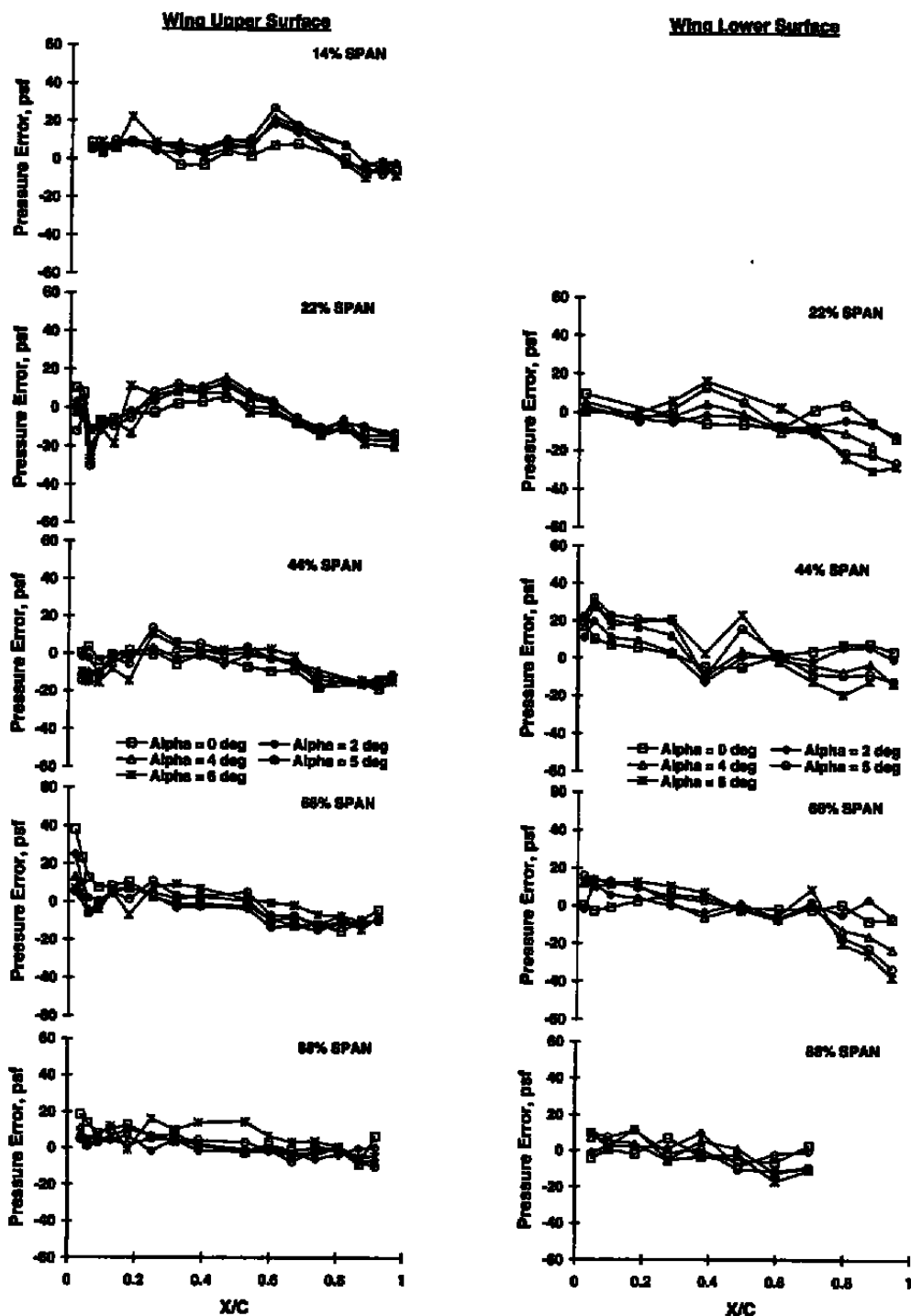


a. Mach = 0.3, Rec = 1.0

Figure 10. PSP measurement error compared to conventional measurement.

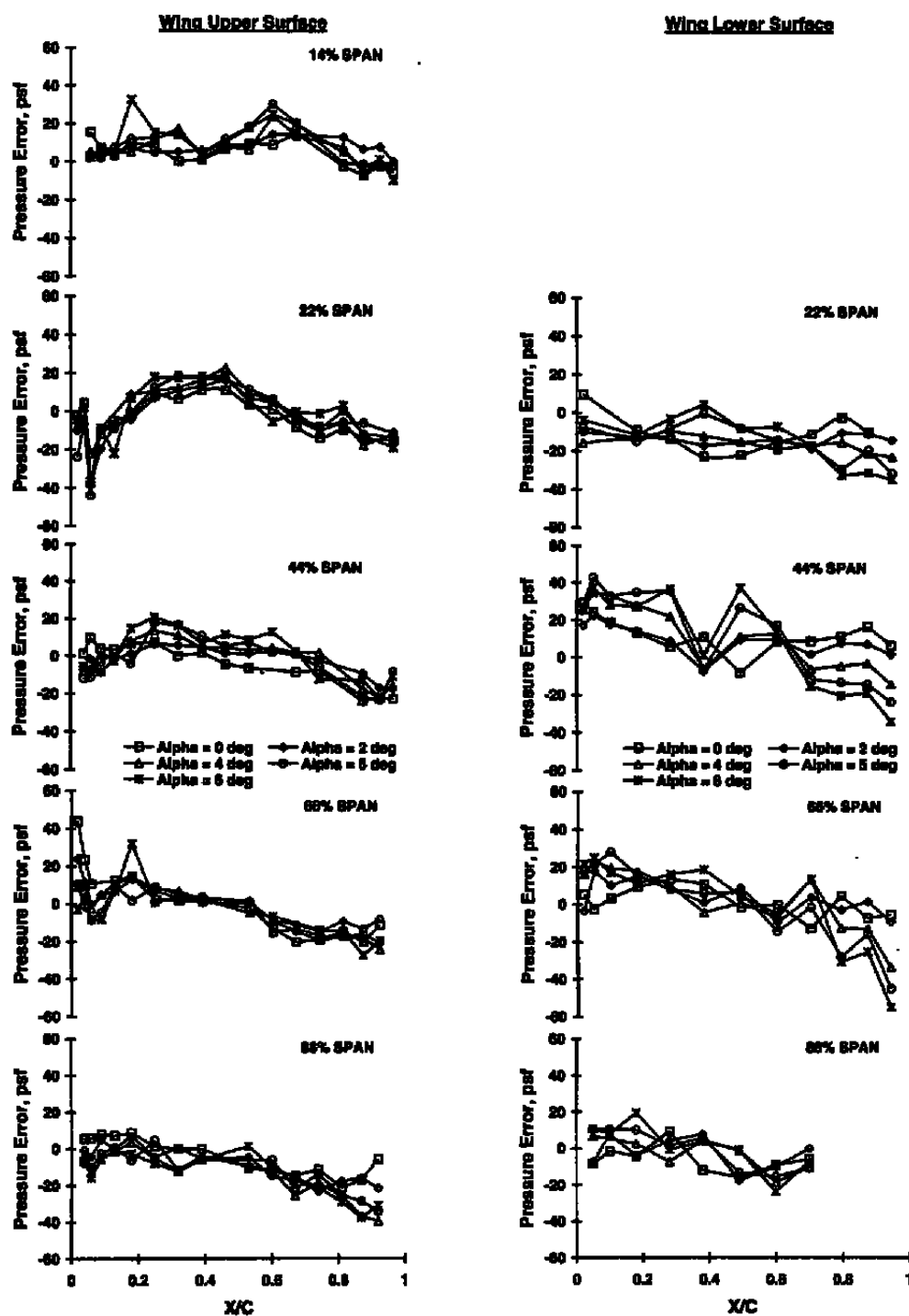


b. Mach = 0.3, Rec = 1.5
Figure 10. Continued.



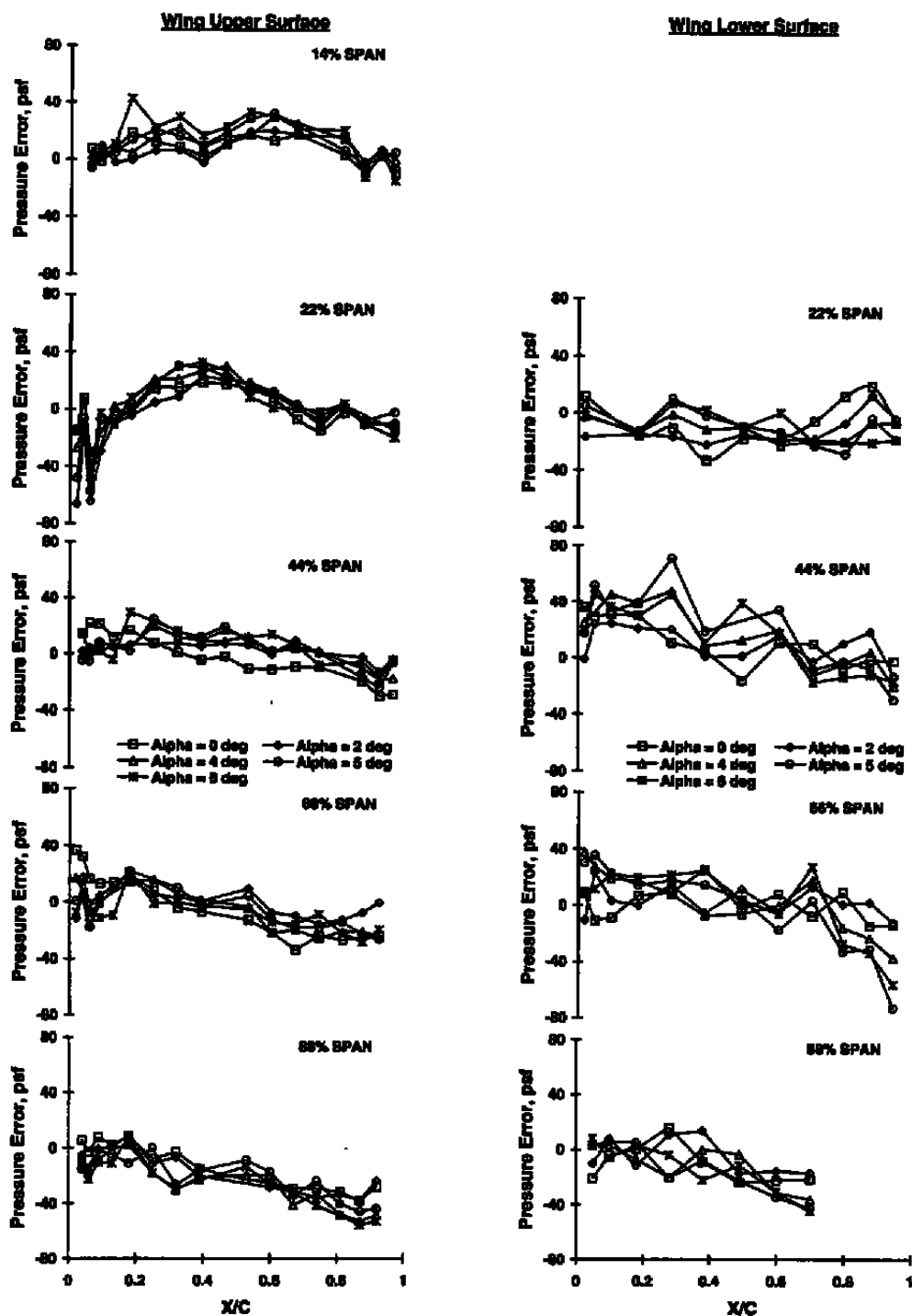
c. Mach = 0.6, Rec = 1.0

Figure 10. Continued.



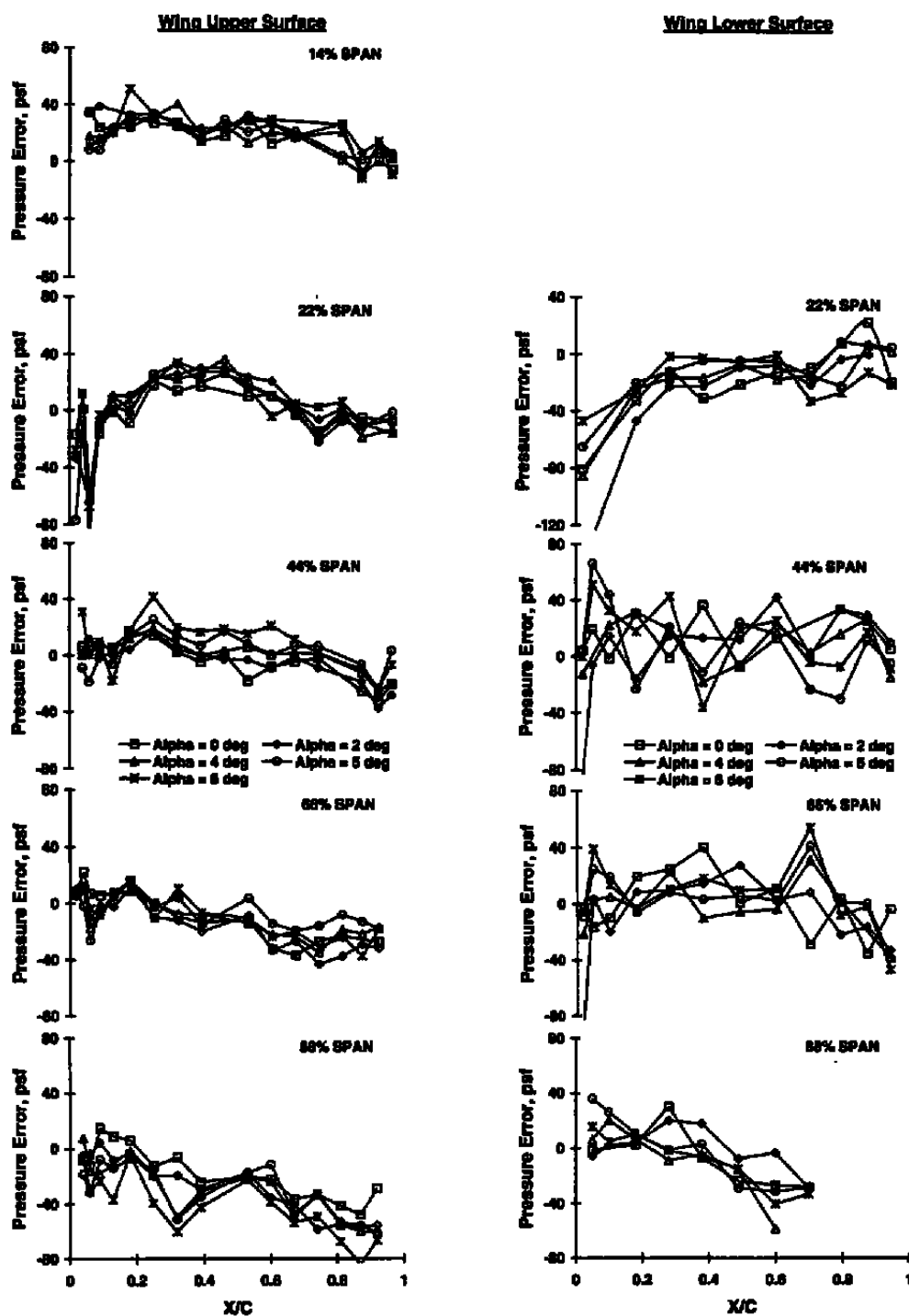
d. Mach = 0.6, Rec = 1.5

Figure 10. Continued.

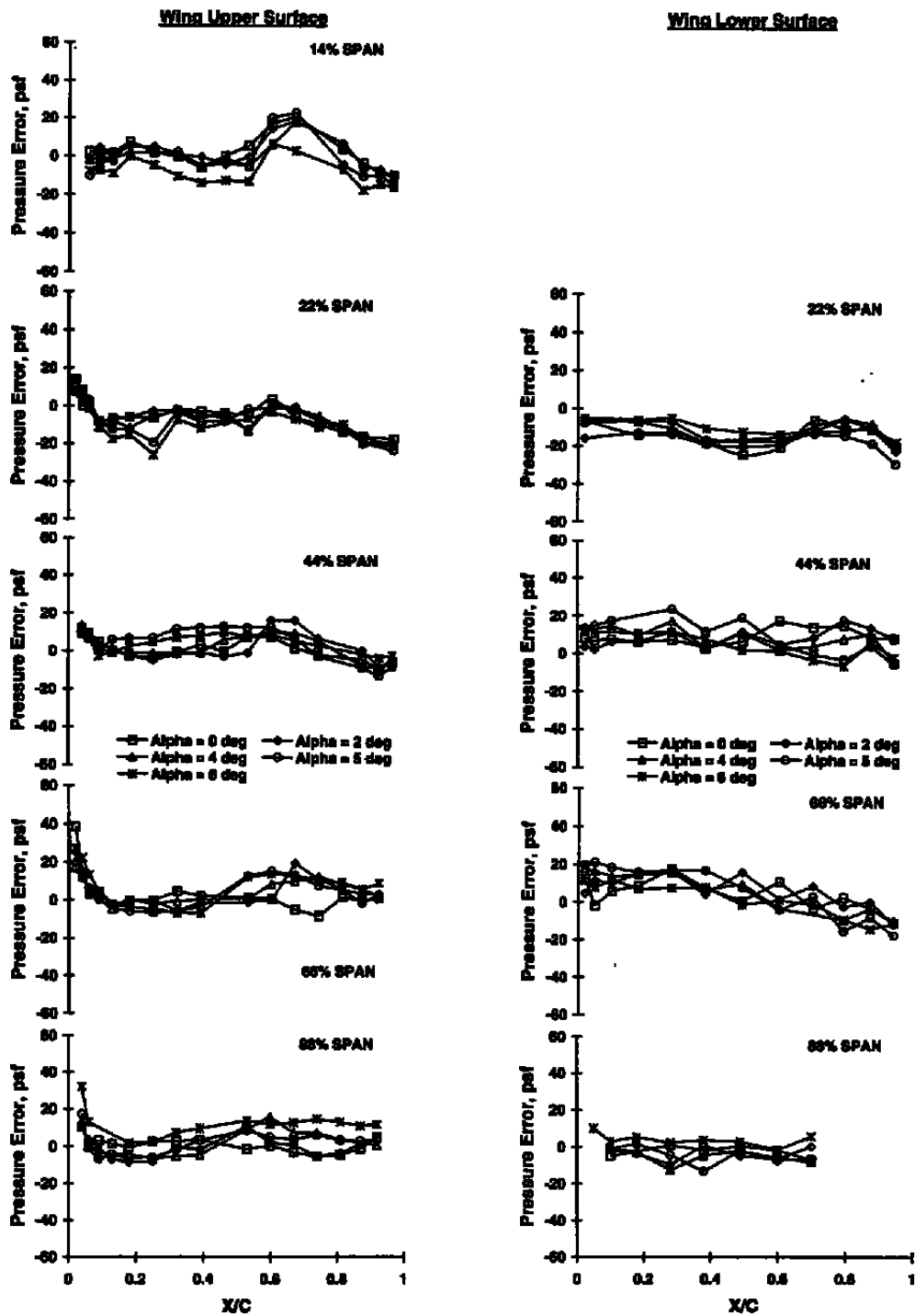


e. Mach = 0.6, Rec = 2.0

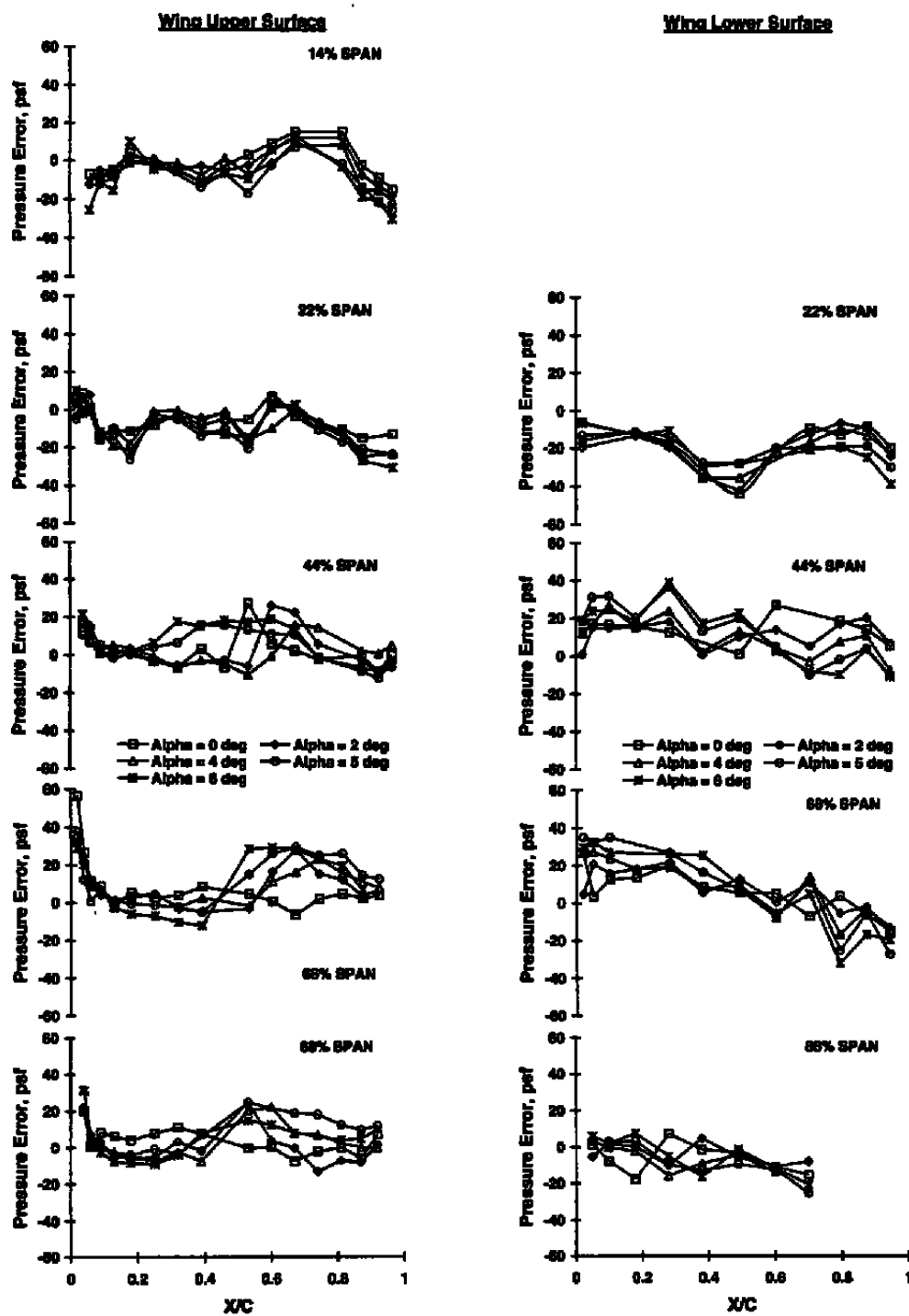
Figure 10. Continued.



f. Mach = 0.6, Rec = 2.7
Figure 10. Continued.

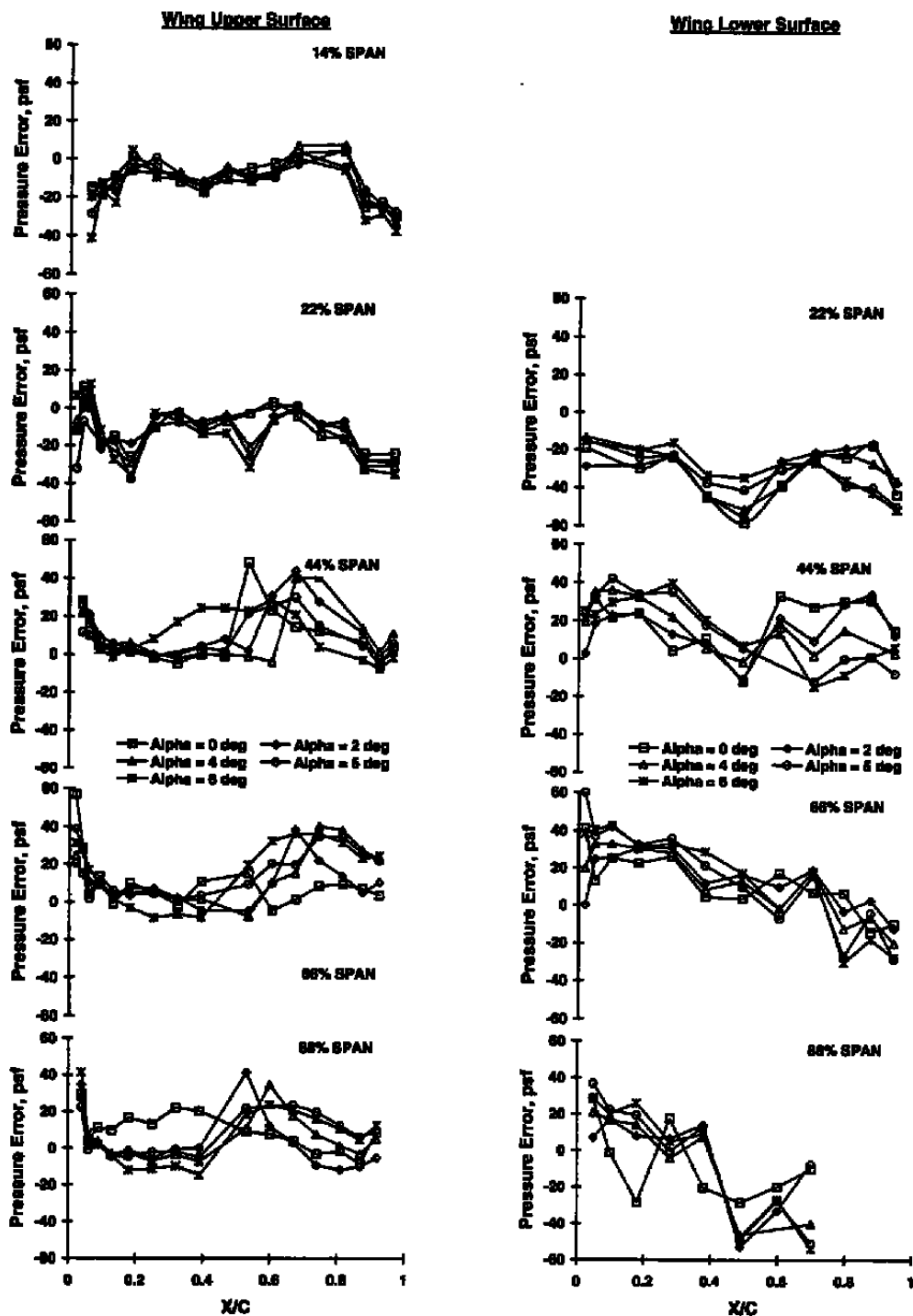


g. Mach = 0.835, Rec = 1.0
Figure 10. Continued.



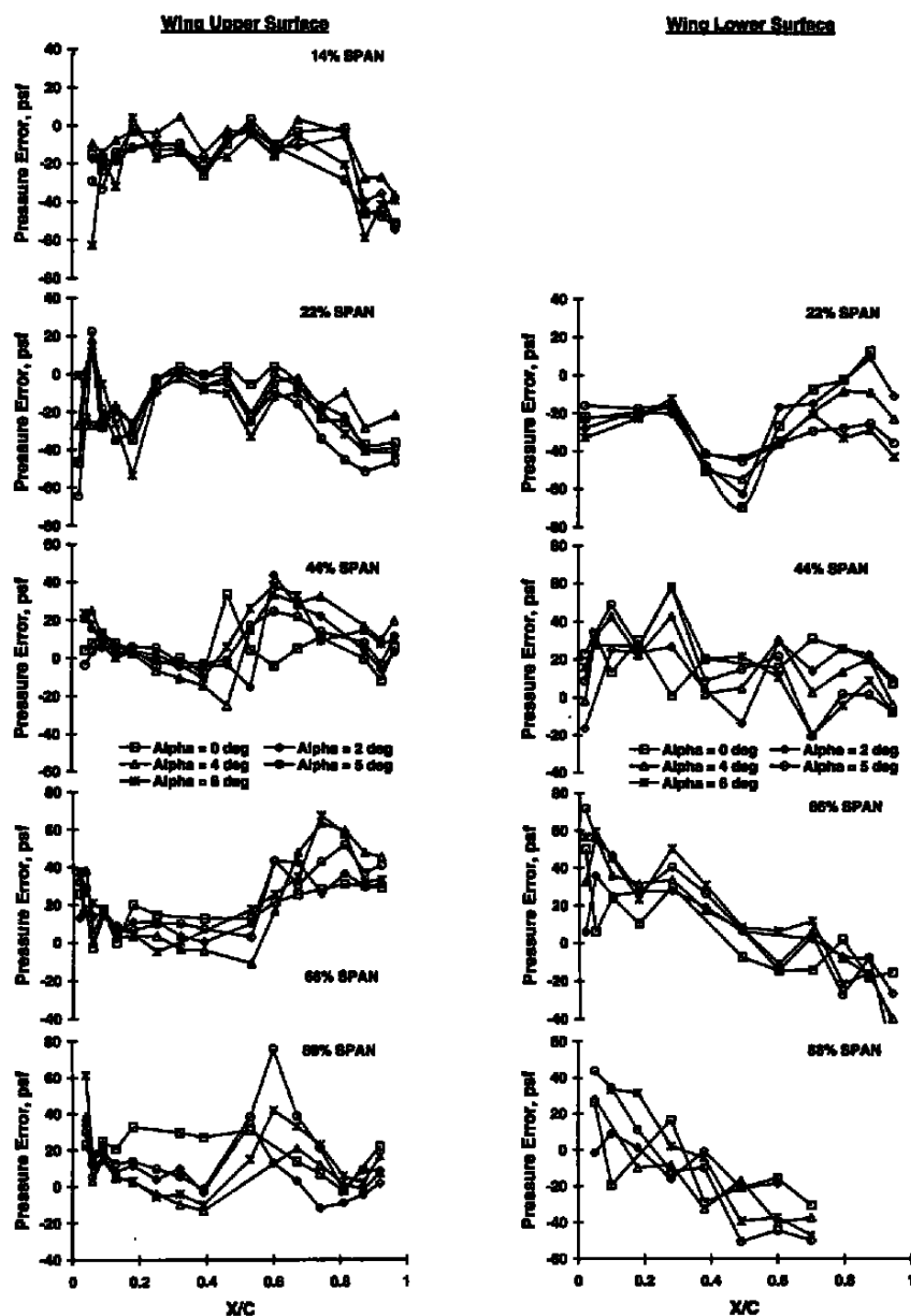
h. Mach = 0.835, Rec = 1.5

Figure 10. Continued.

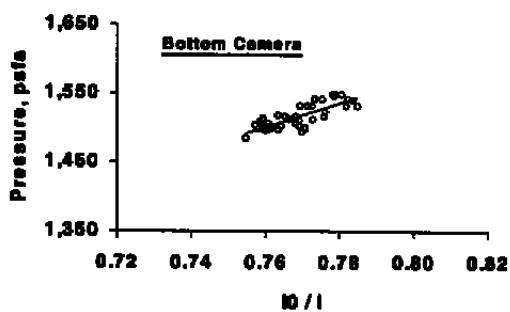
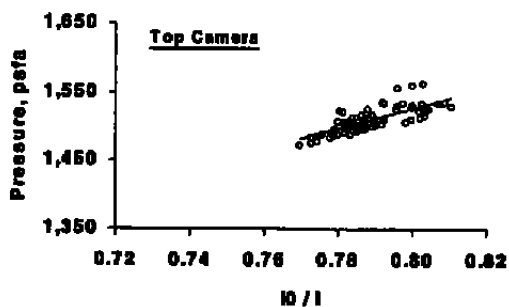


i. Mach = 0.835, Rec = 2.0

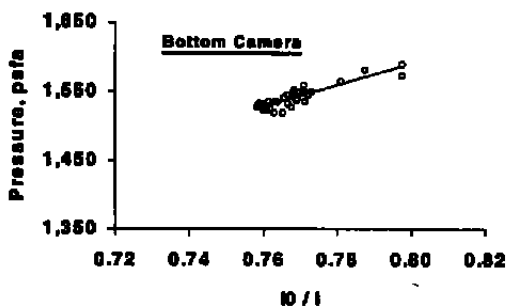
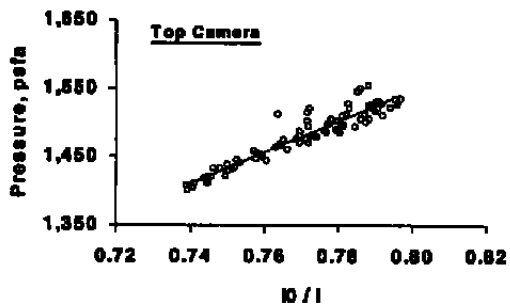
Figure 10. Continued.



j. Mach = 0.835, Rec = 2.7
Figure 10. Concluded.

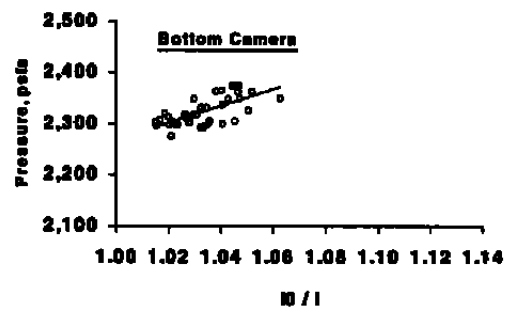
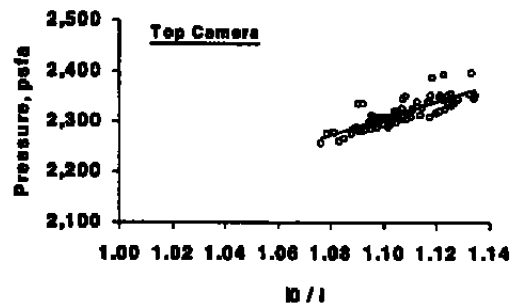


a. Mach = 0.3, Rec = 1.0, Alpha = 0 deg

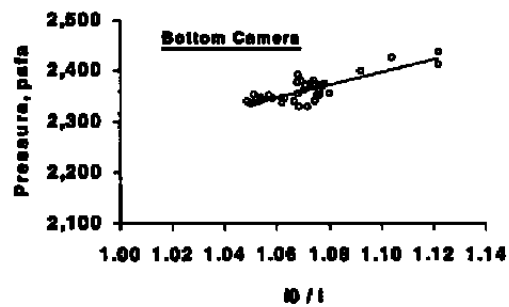
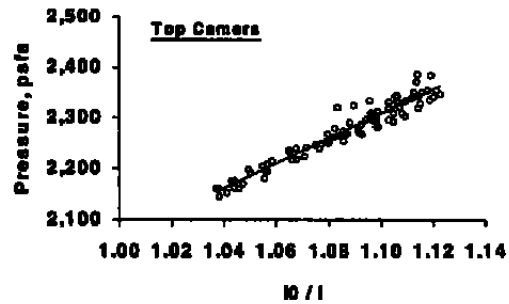


b. Mach = 0.3, Rec = 1.0, Alpha = 6 deg

Figure 11. Pressure vs. intensity ratio data.

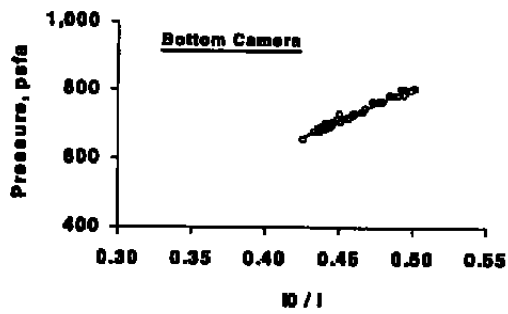
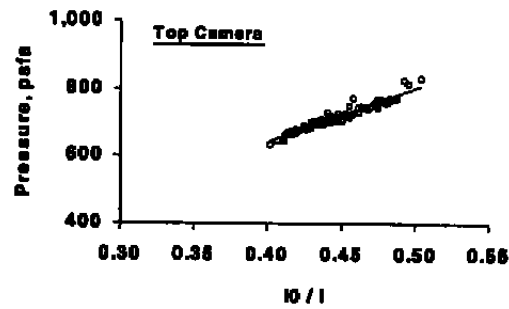


c. Mach = 0.3, Rec = 1.5, Alpha = 0 deg

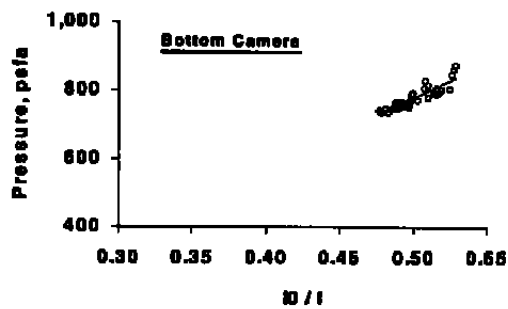
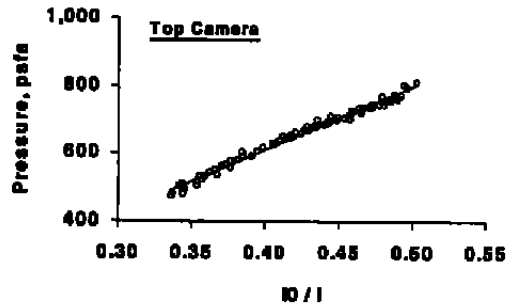


d. Mach = 0.3, Rec = 1.5, Alpha = 6 deg

Figure 11. Continued.

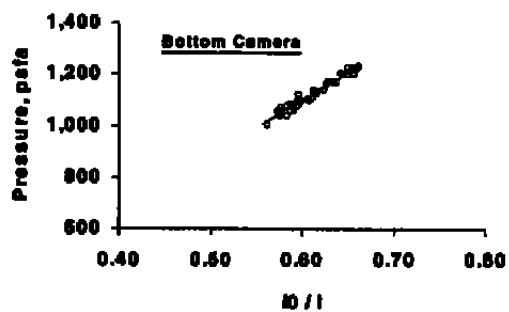
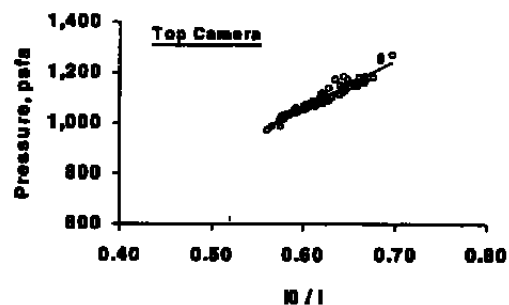


e. Mach = 0.6, Rec = 1.0, Alpha = 0 deg

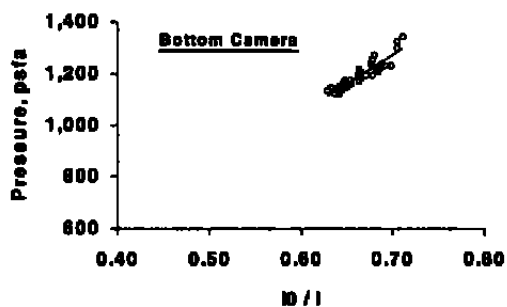
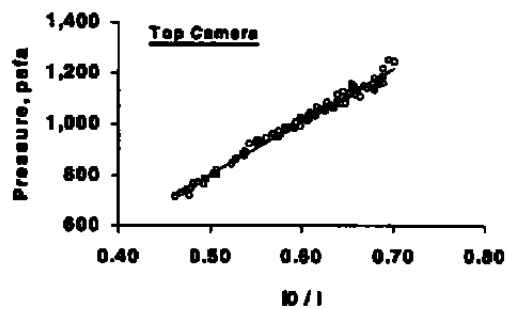


f. Mach = 0.6, Rec = 1.0, Alpha = 6 deg

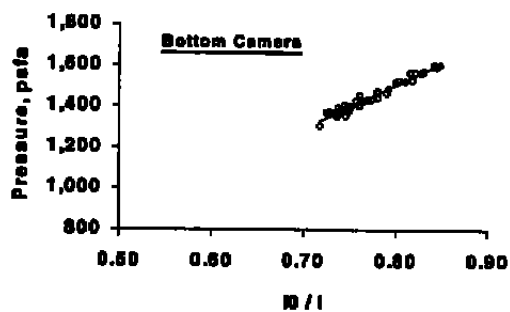
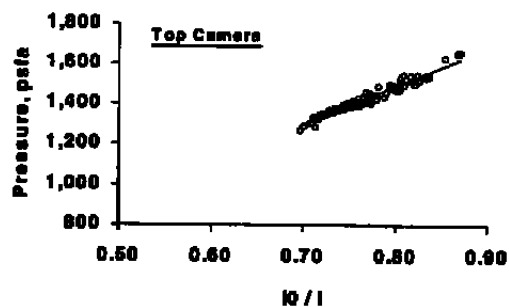
Figure 11. Continued.



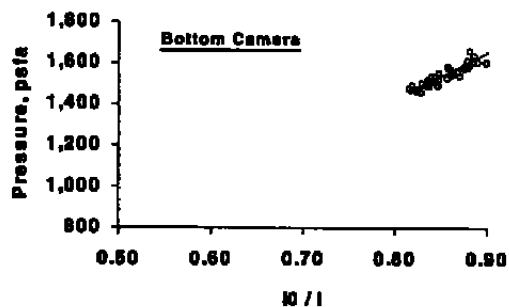
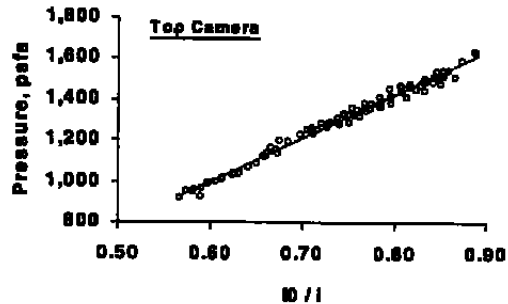
g. Mach 0.6, Rec = 1.5, Alpha = 0 deg



h. Mach = 0.6, Rec = 1.5, Alpha = 6 deg
Figure 11. Continued.

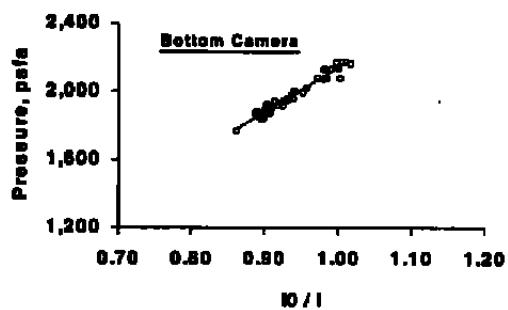
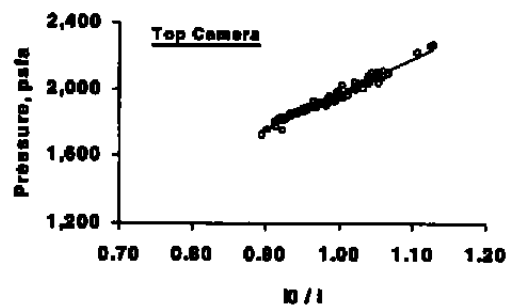


i. Mach = 0.6, Rec = 2.0, Alpha = 0 deg

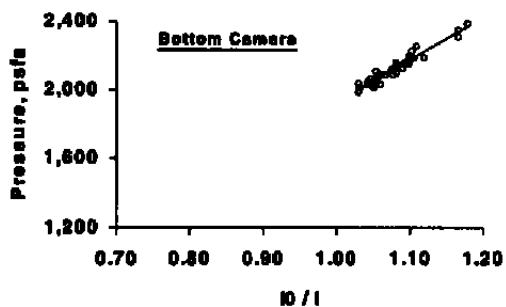
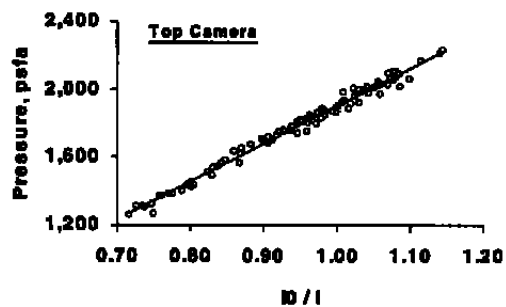


j. Mach = 0.6, Rec = 2.0, Alpha = 6 deg

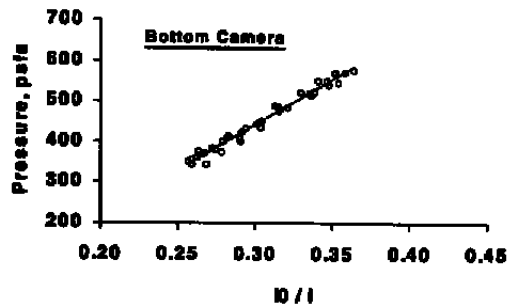
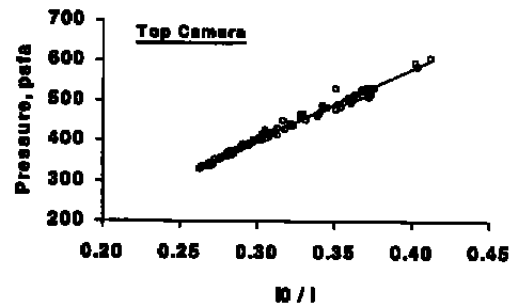
Figure 11. Continued.



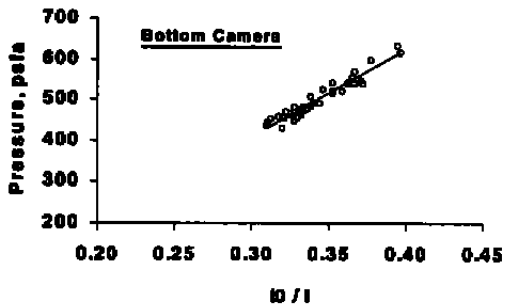
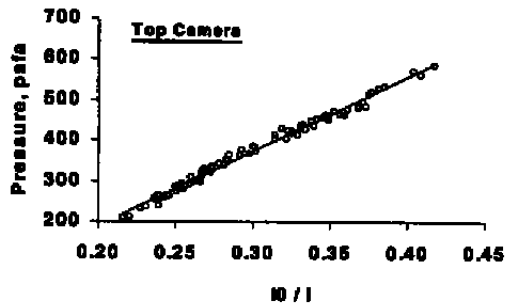
k. Mach = 0.6, Rec = 2.7, Alpha = 0 deg



l. Mach = 0.6, Rec = 2.7, Alpha = 6 deg
Figure 11. Continued.

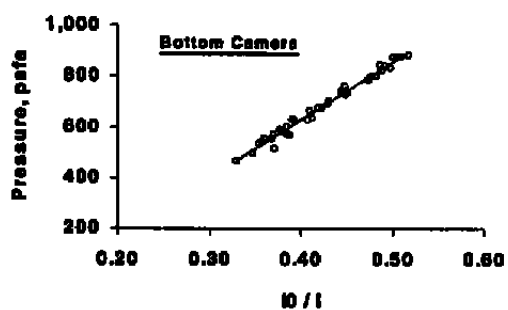
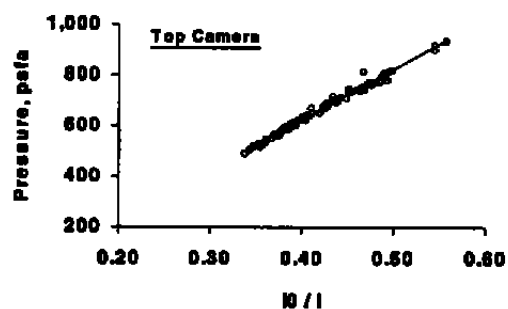


m. Mach = 0.835, Rec = 1.0, Alpha = 0 deg

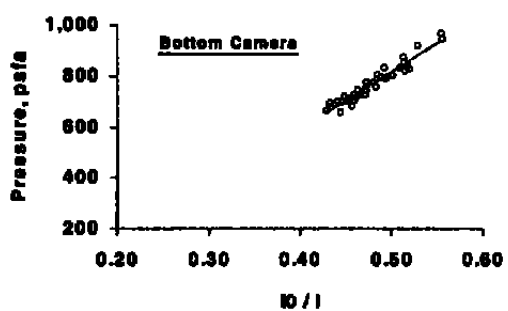
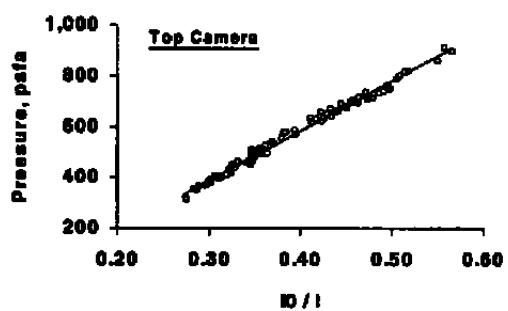


n. Mach = 0.835, Rec = 1.0, Alpha = 6 deg

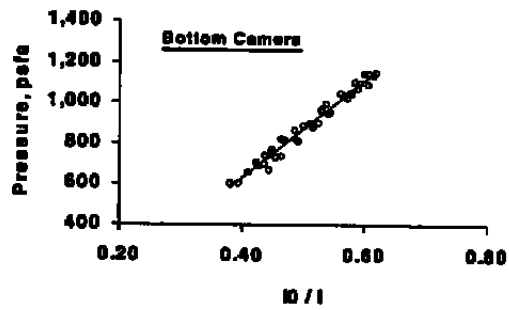
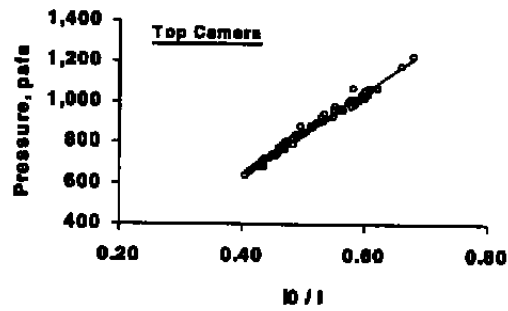
Figure 11. Continued.



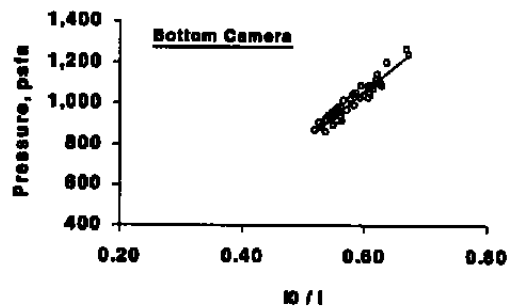
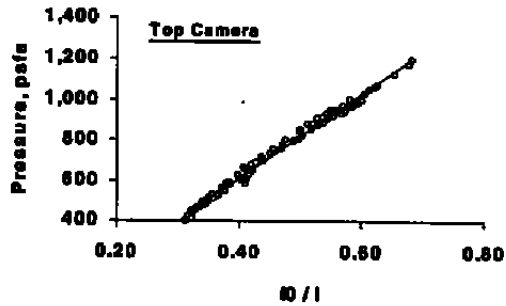
o. Mach = 0.835, Rec = 1.5, Alpha = 0 deg



p. Mach = 0.835, Rec = 1.5, Alpha = 6 deg
Figure 11. Continued.

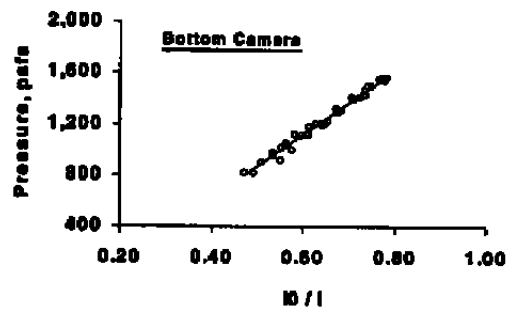
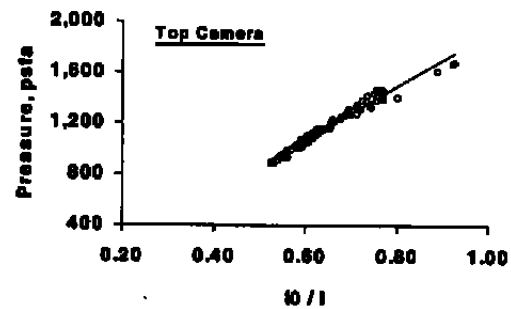


q. Mach = 0.835, Rec = 2.0, Alpha = 0 deg

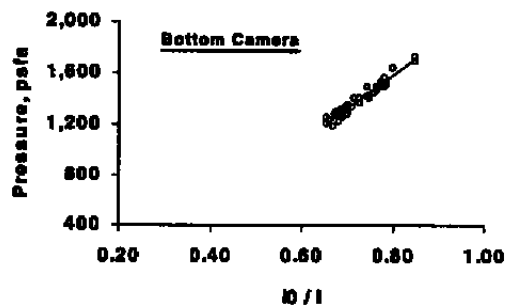
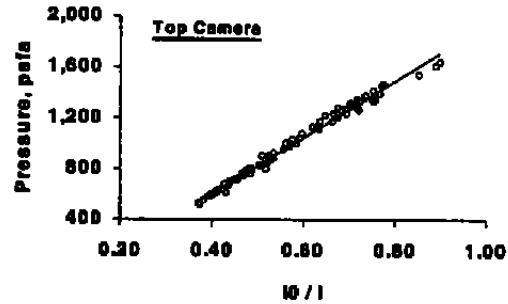


r. Mach = 0.835, Rec = 2.0, Alpha = 6 deg

Figure 11. Continued.

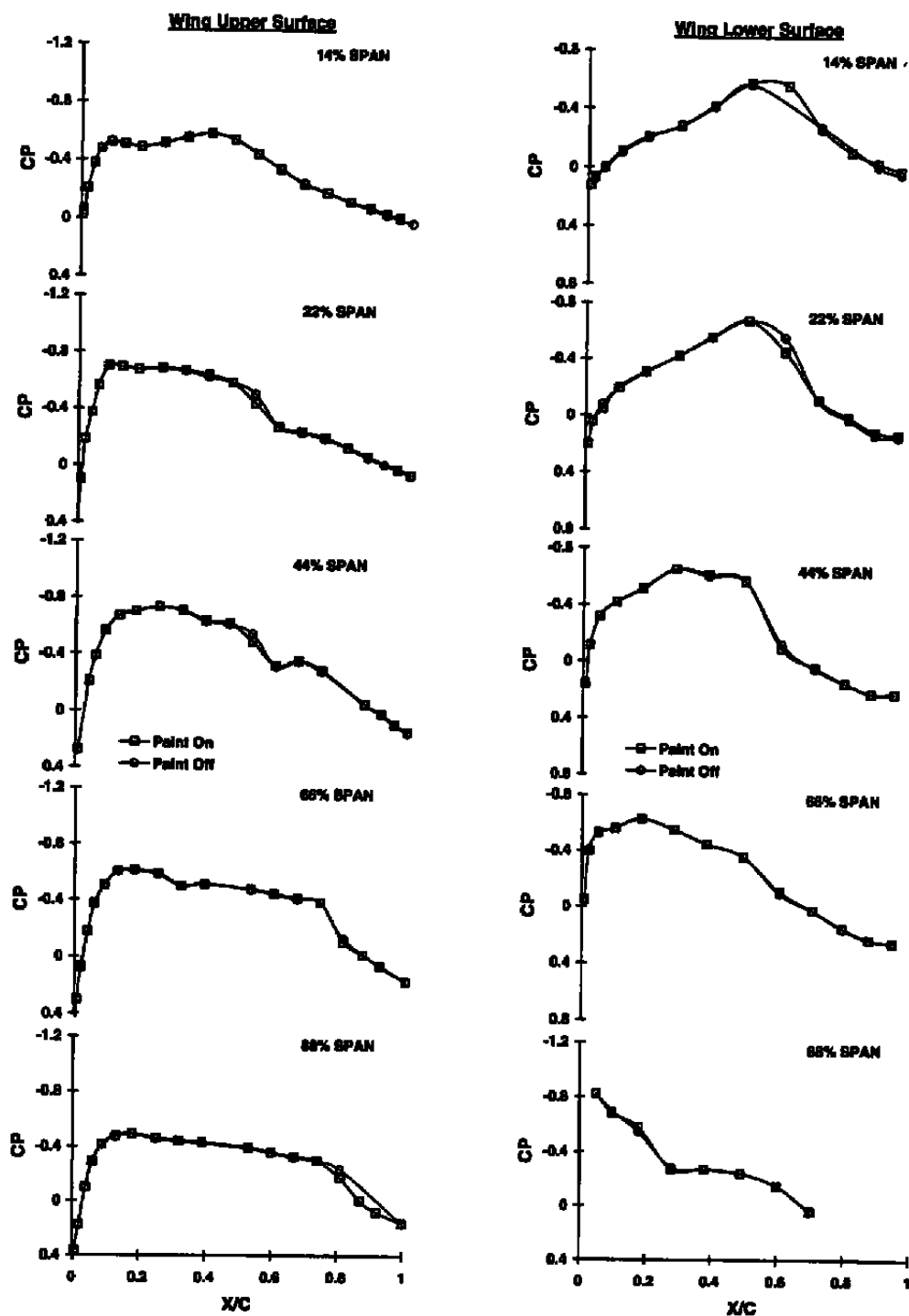


s. Mach = 0.835, Rec = 2.7, Alpha = 0 deg



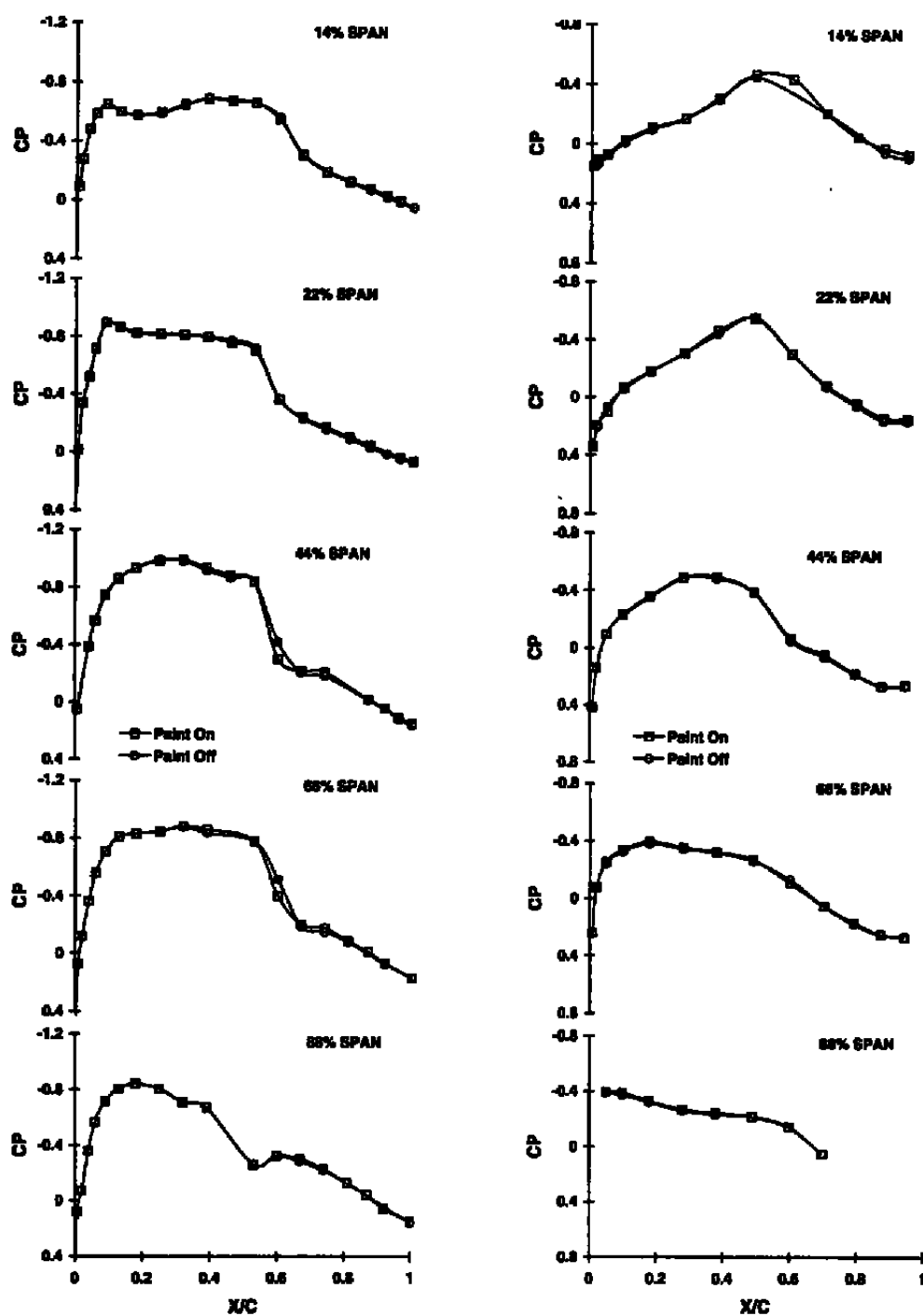
t. Mach = 0.85, Rec = 2.7, Alpha = 6 deg

Figure 11. Concluded.

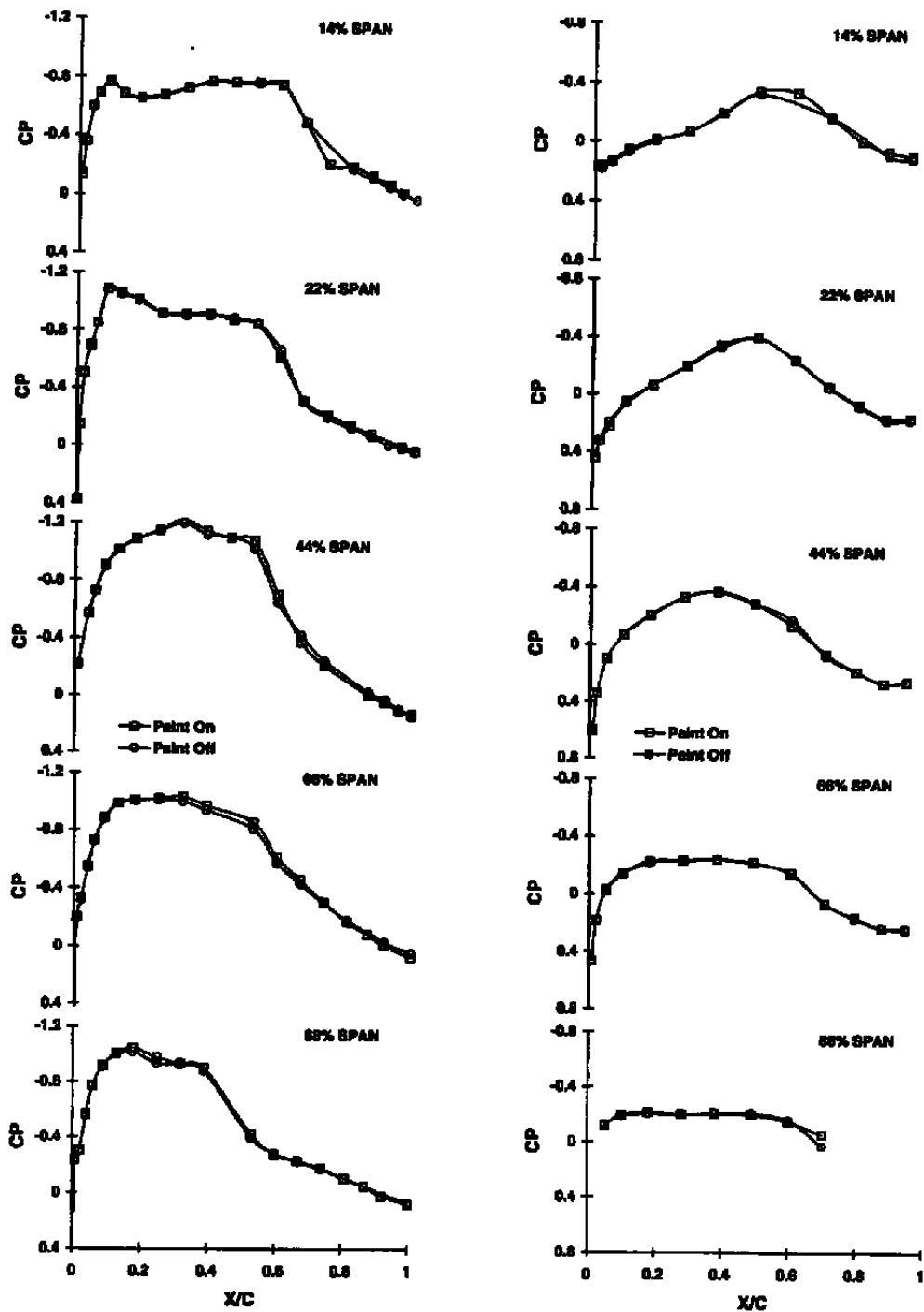


a. Alpha = 0 deg, Rec = 1.0

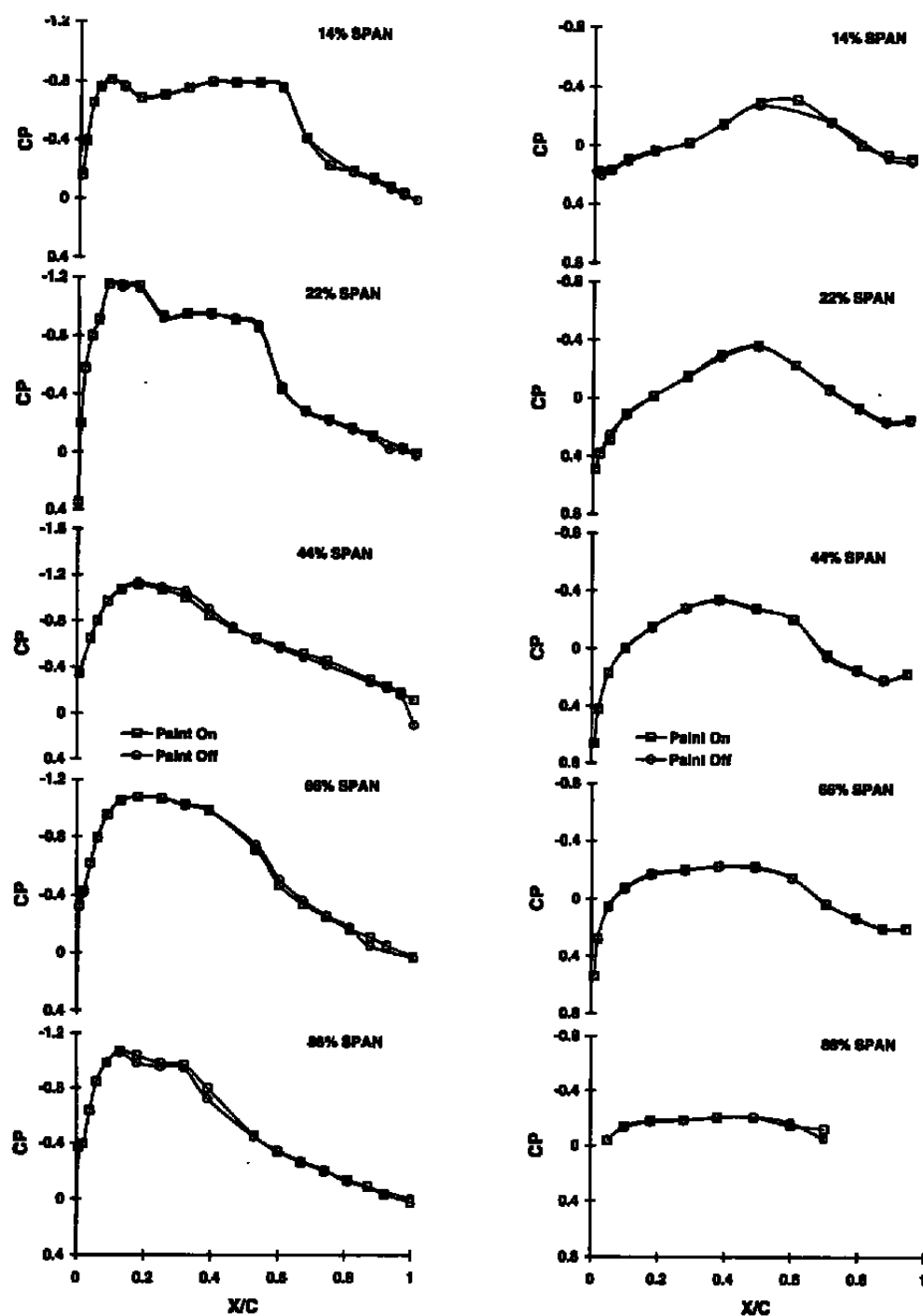
Figure 12. Effects of paint on pressure distribution at Mach number 0.835.



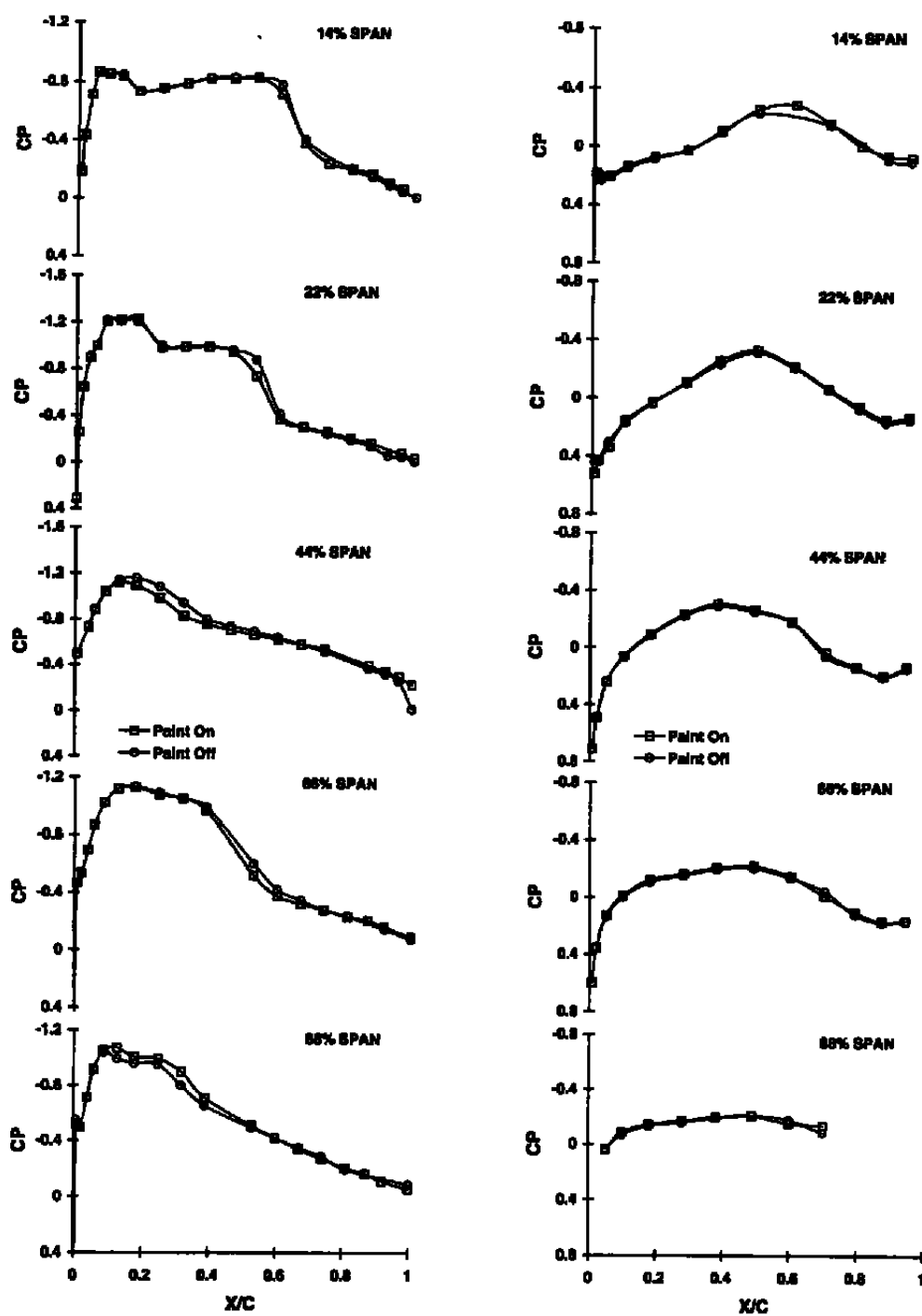
b. Alpha = 2 deg, Rec = 1.0
Figure 12. Continued.



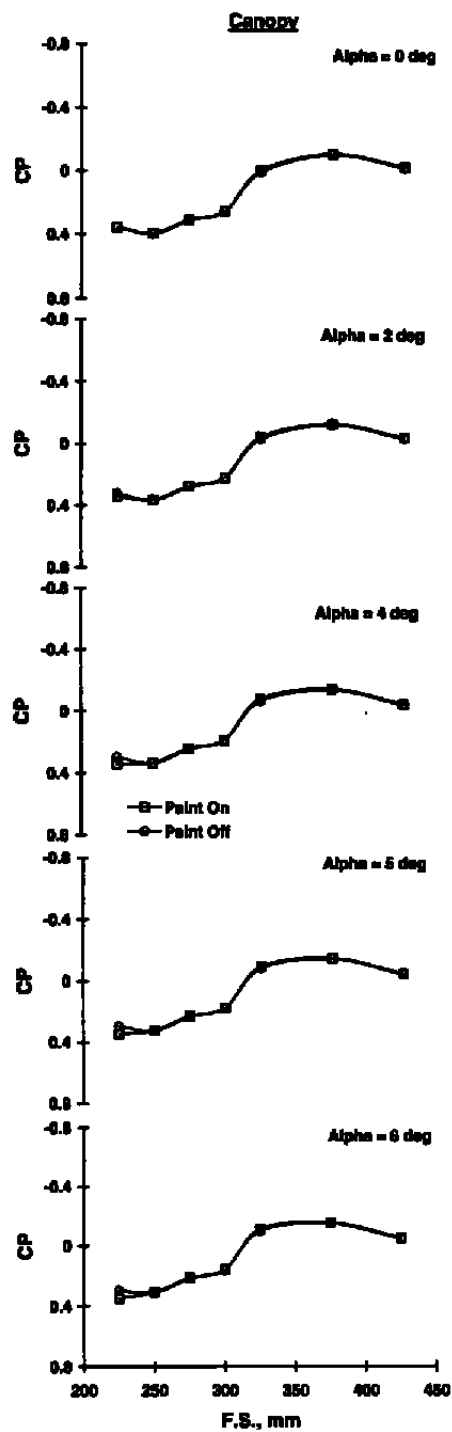
c. Alpha = 4 deg, Rec = 1.0
Figure 12. Continued.



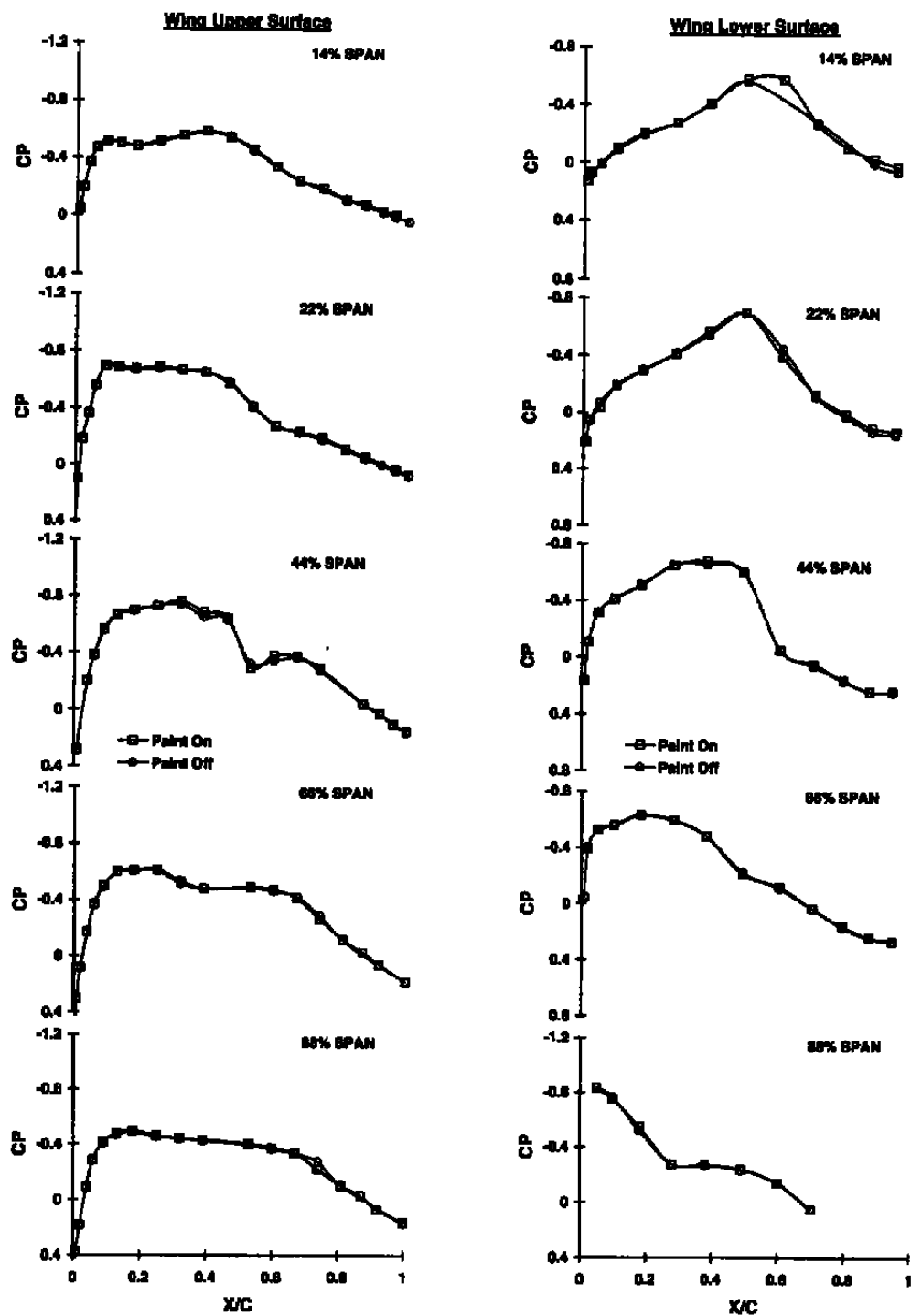
d. $\alpha = 5^\circ$, $Re_c = 1.0$
Figure 12. Continued.



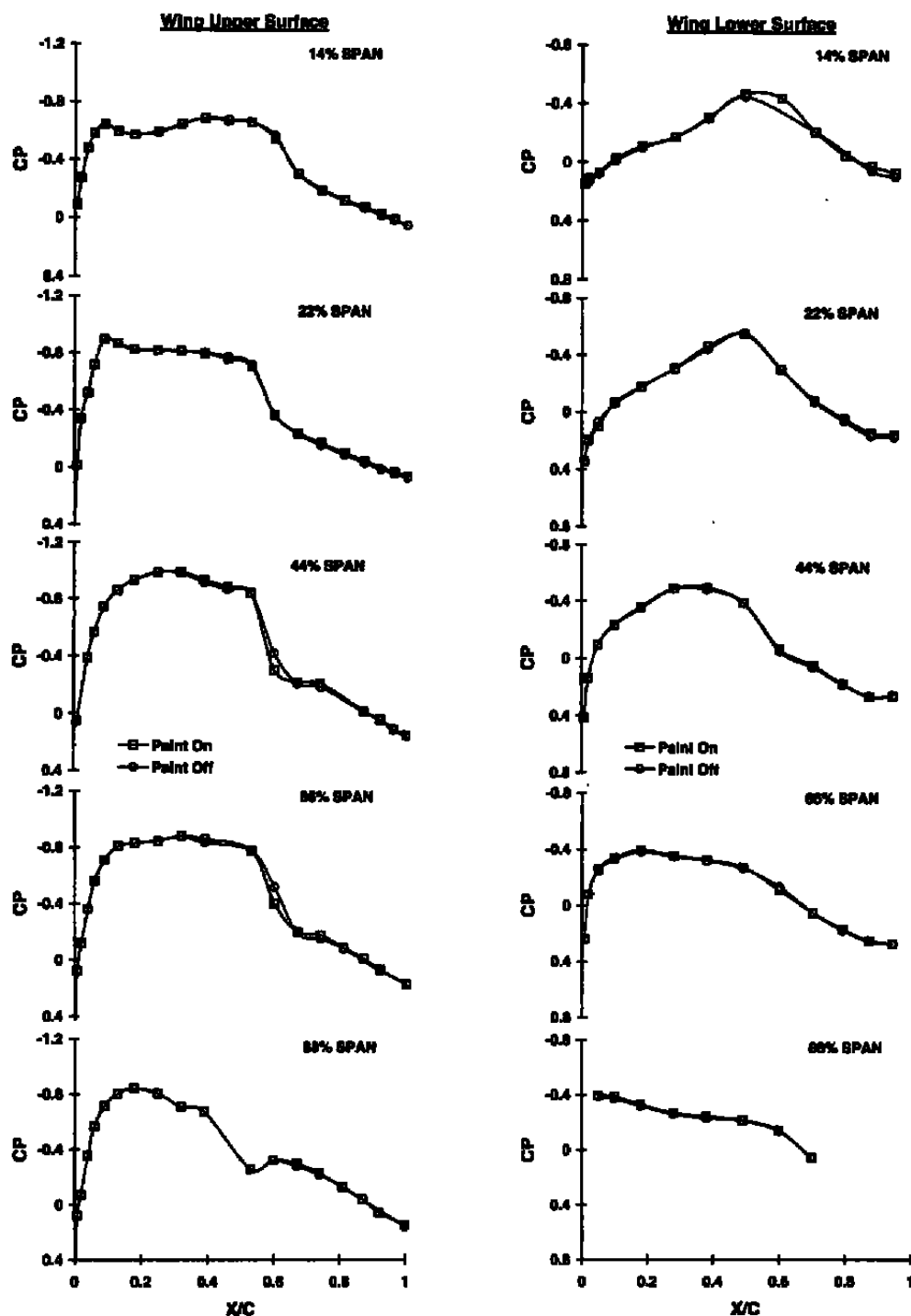
e. $\alpha = 6^\circ$, $Re_c = 1.0$
Figure 12. Continued.



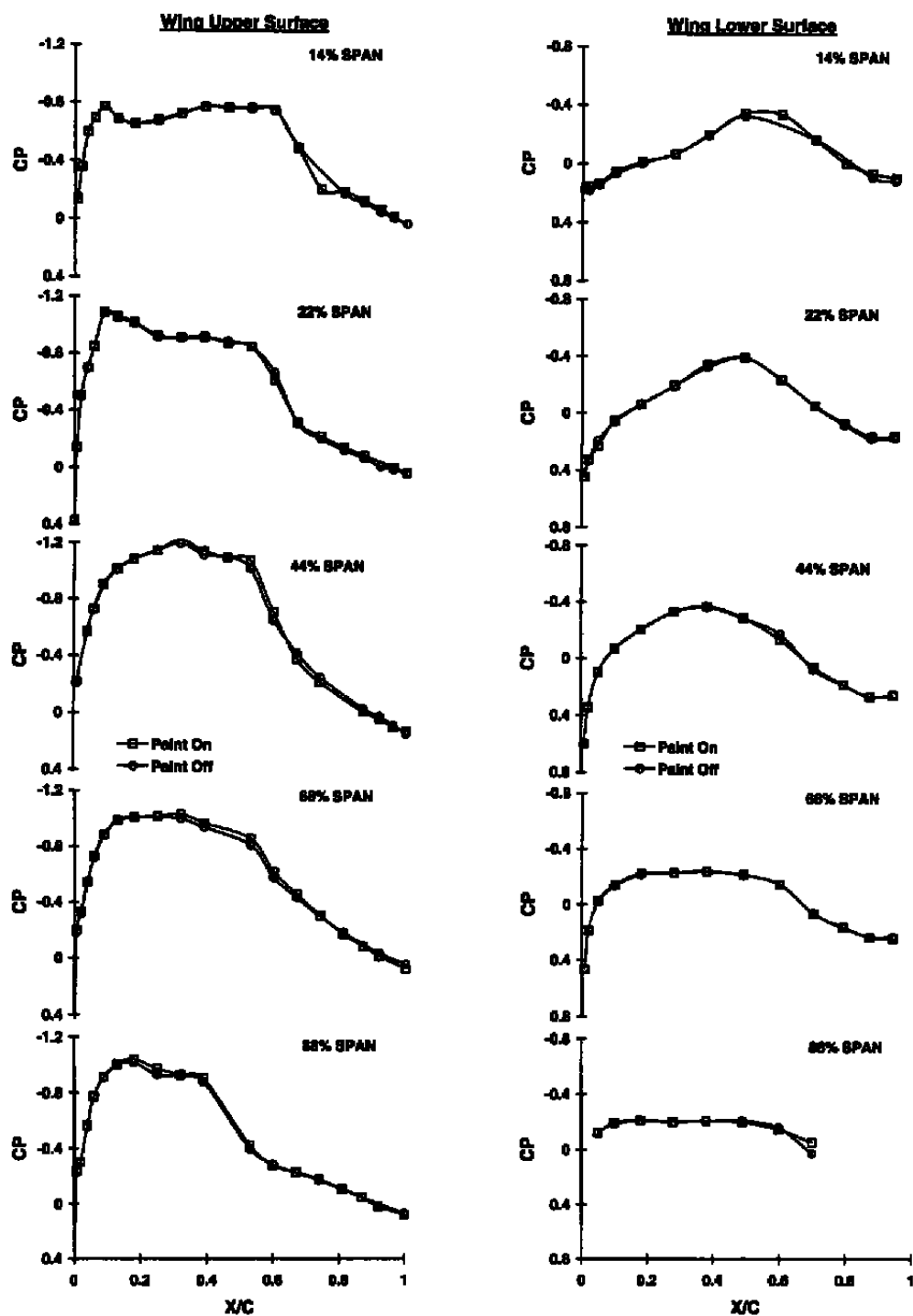
f. Canopy, Rec = 1.0
 Figure 12. Continued.



g. Alpha = 0 deg, Rec = 1.5
Figure 12. Continued.

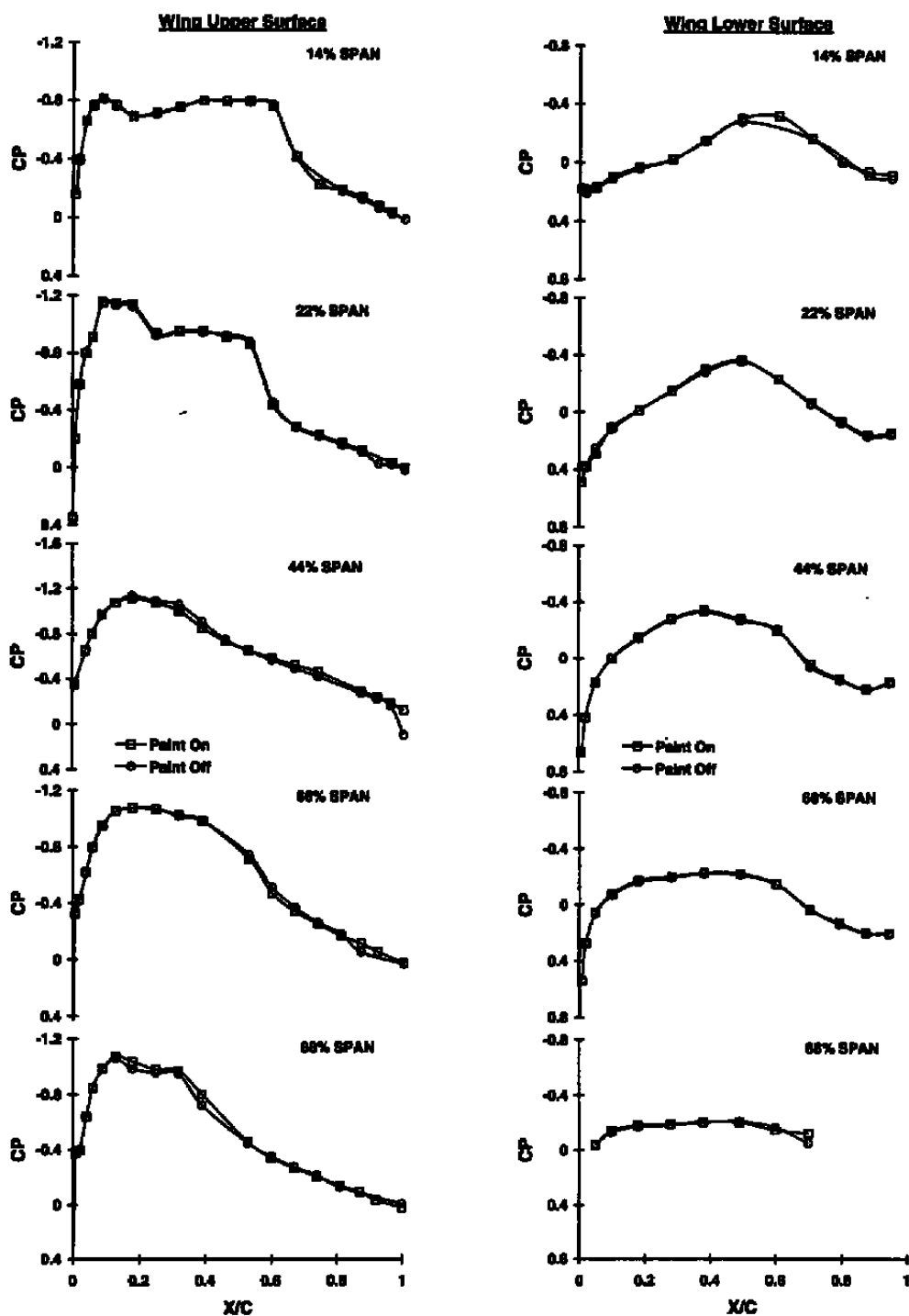


h. Alpha = 3 deg, Rec = 1.5
Figure 12. Continued.



i. Alpha = 4 deg, Rec = 1.5

Figure 12. Continued.



j. Alpha = 5 deg, Rec = 1.5
Figure 12. Continued.

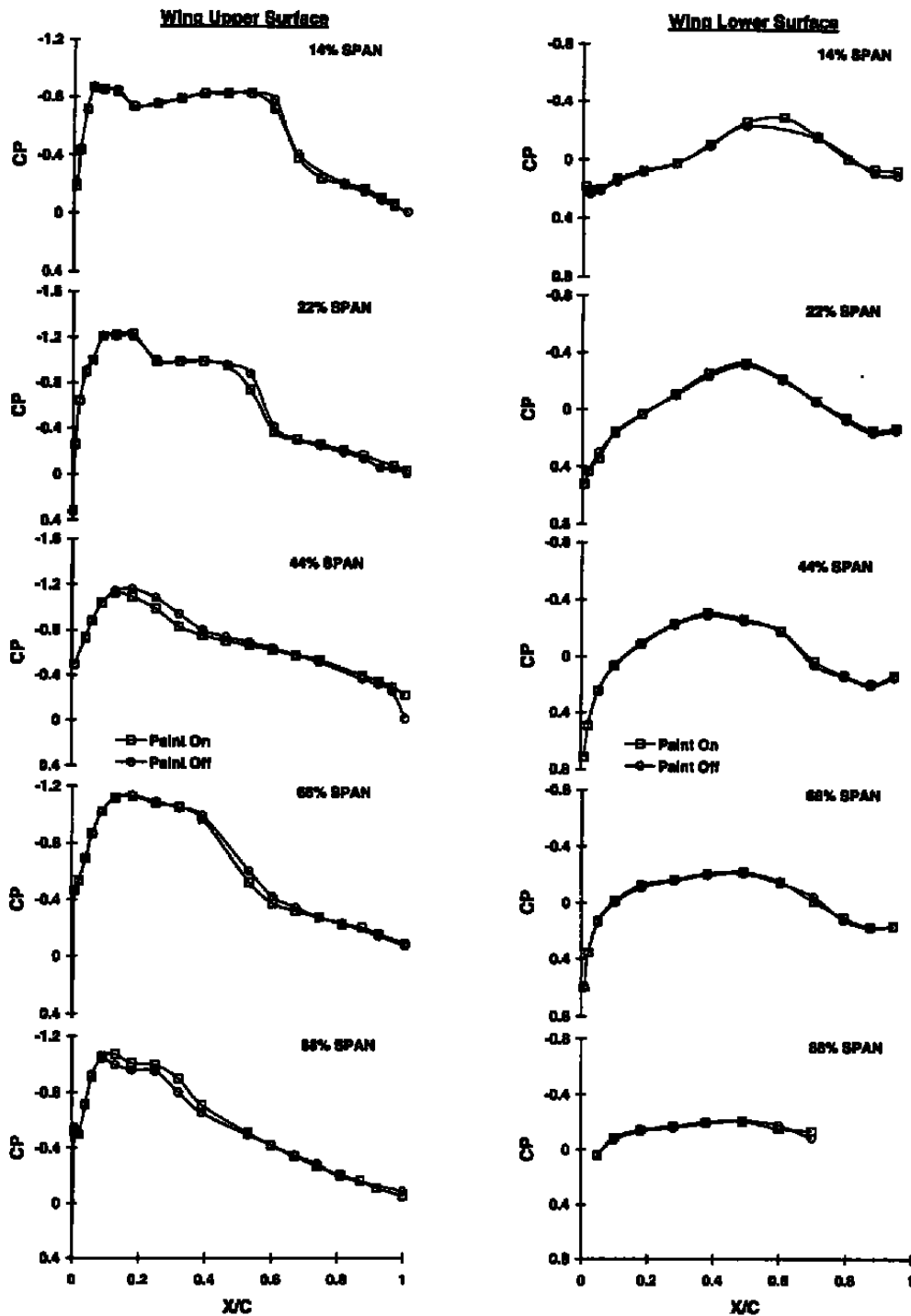
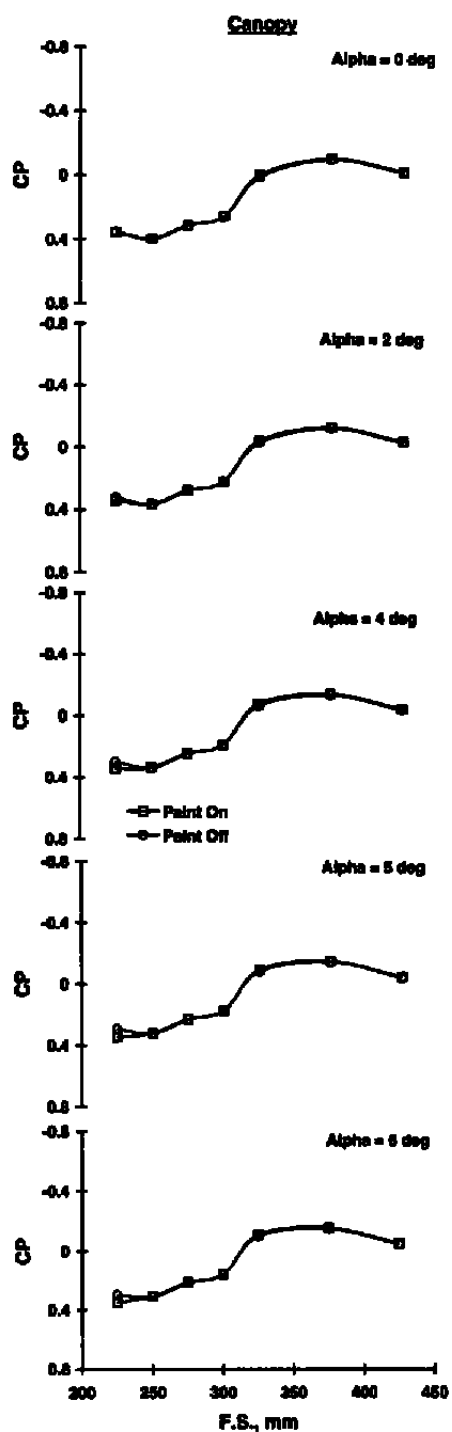
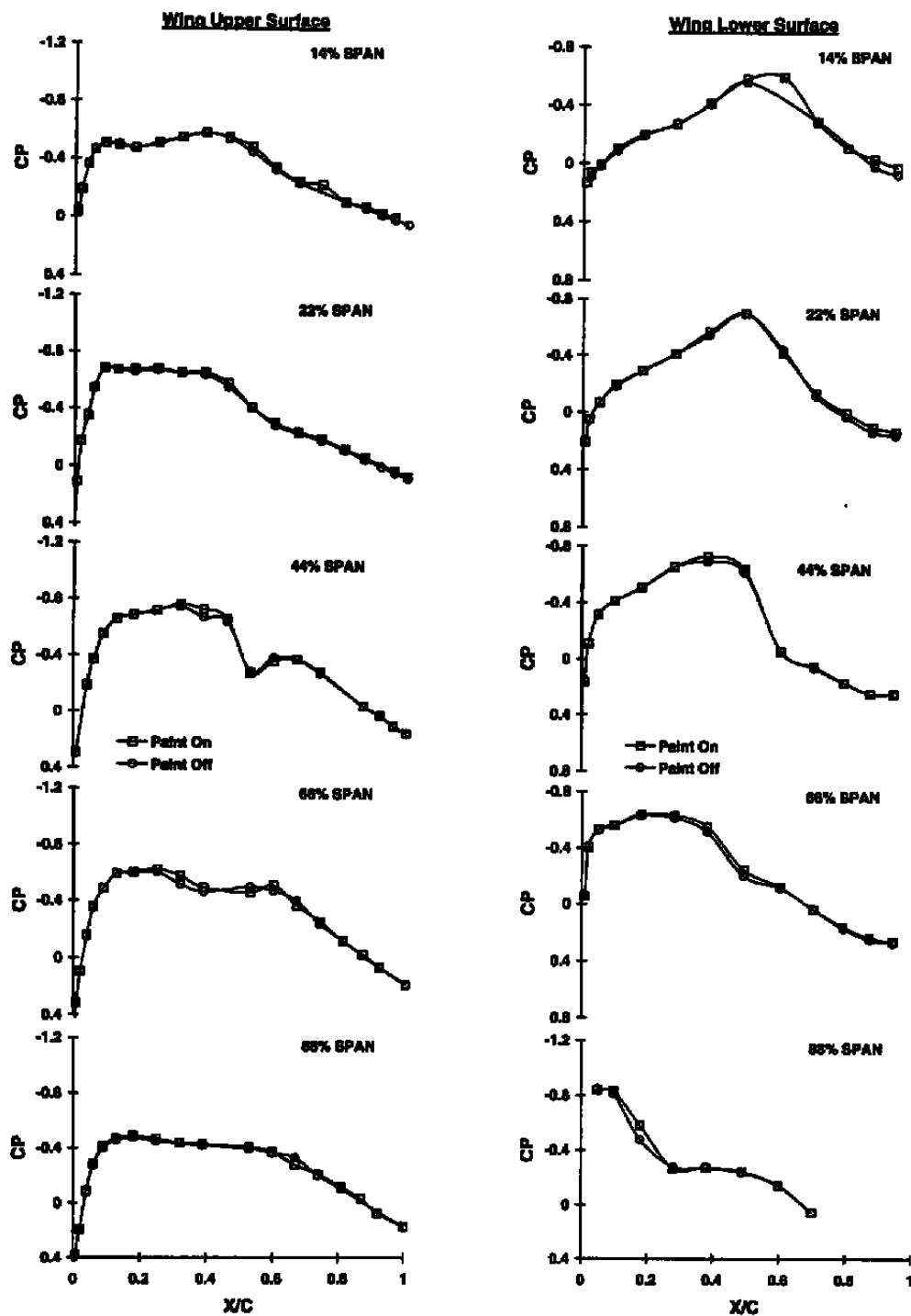
k. $\alpha = 6^\circ$, $Re_c = 1.5$

Figure 12. Continued.

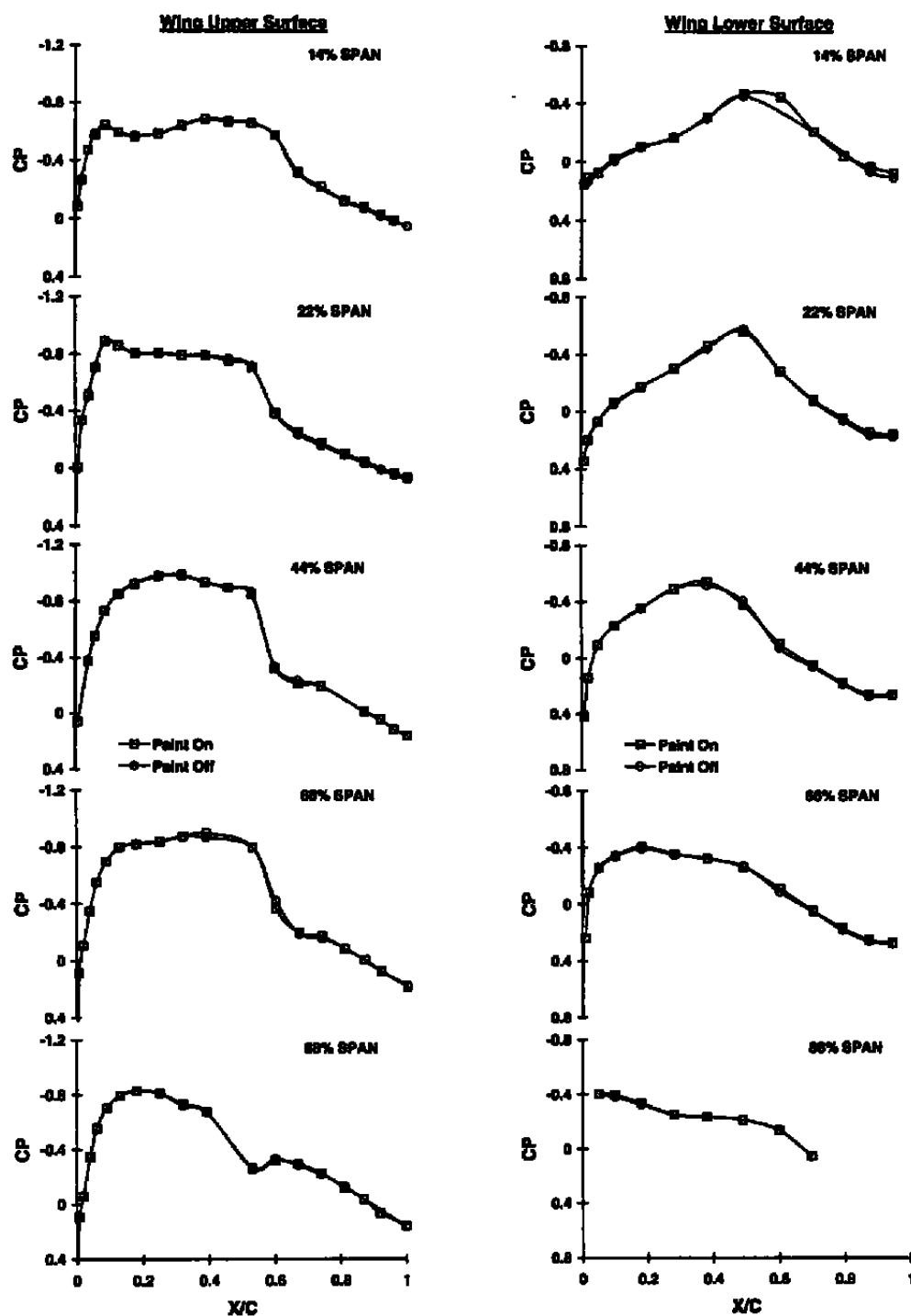


I. Canopy, Rec = 1.5
 Figure 12. Continued.



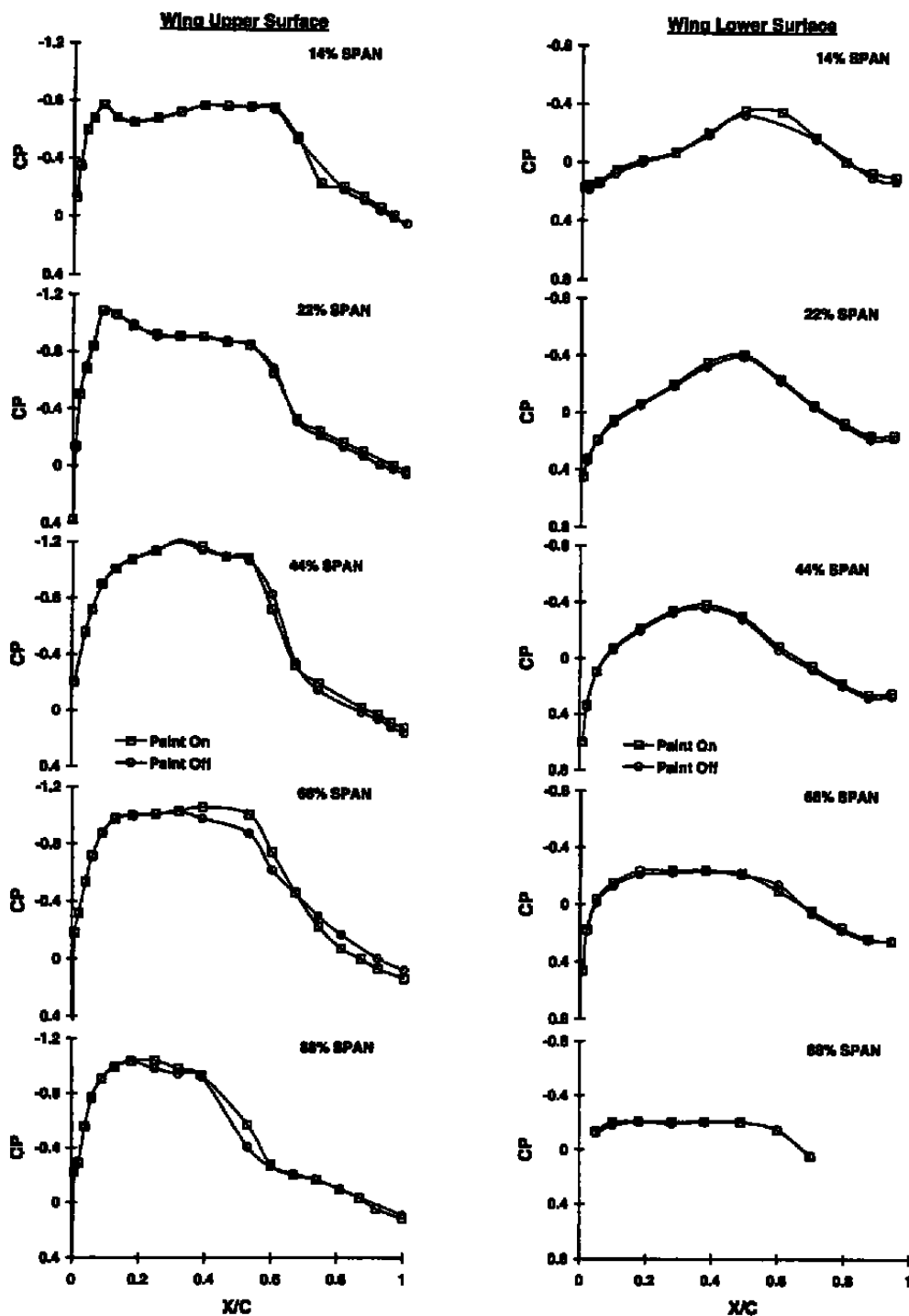
m. Alpha = 0 deg, Rec = 2.0

Figure 12. Continued.



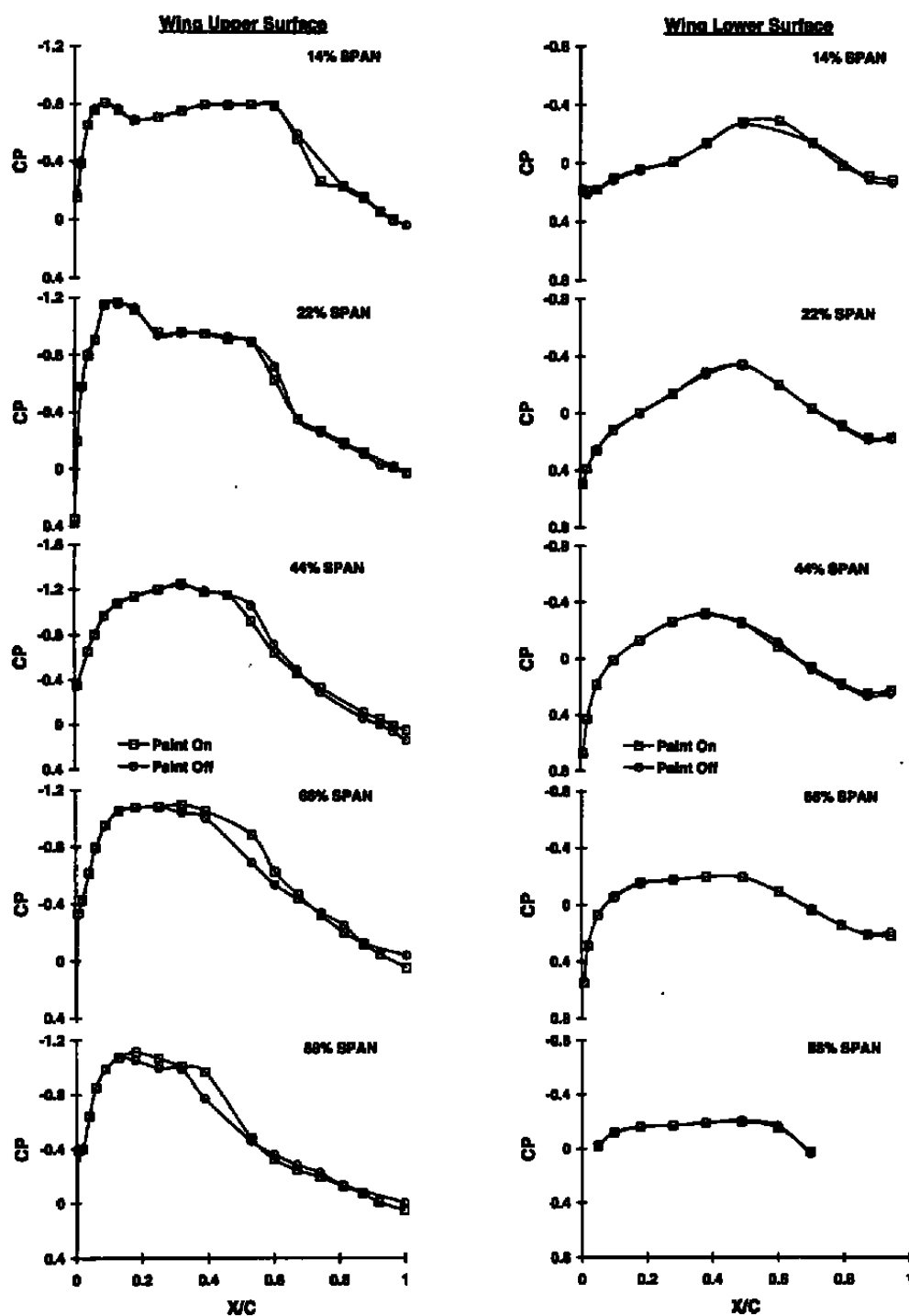
n. Alpha = 2 deg, Rec = 2.0

Figure 12. Continued.



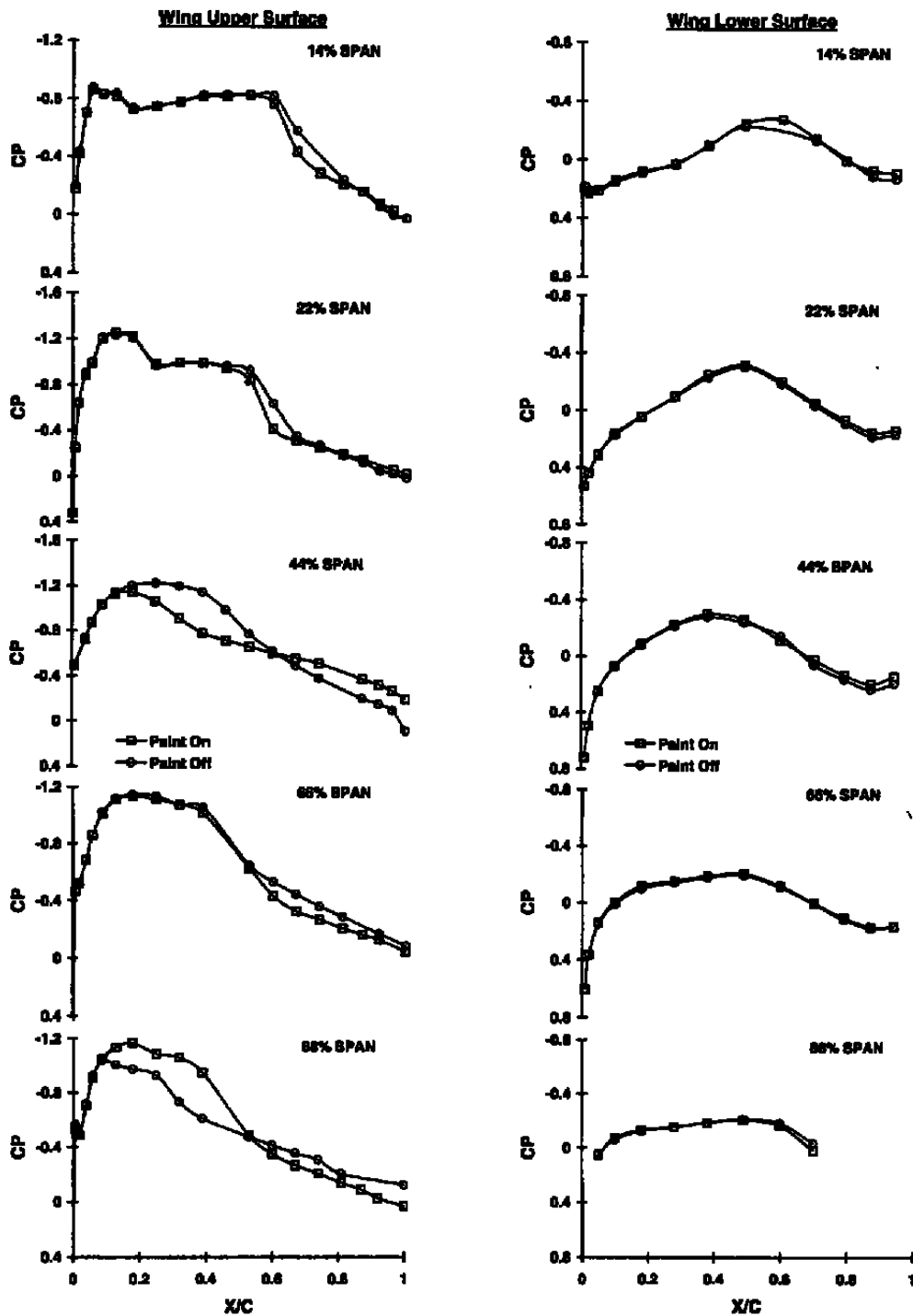
$\alpha = 4$ deg, $Re_c = 2.0$

Figure 12. Continued.

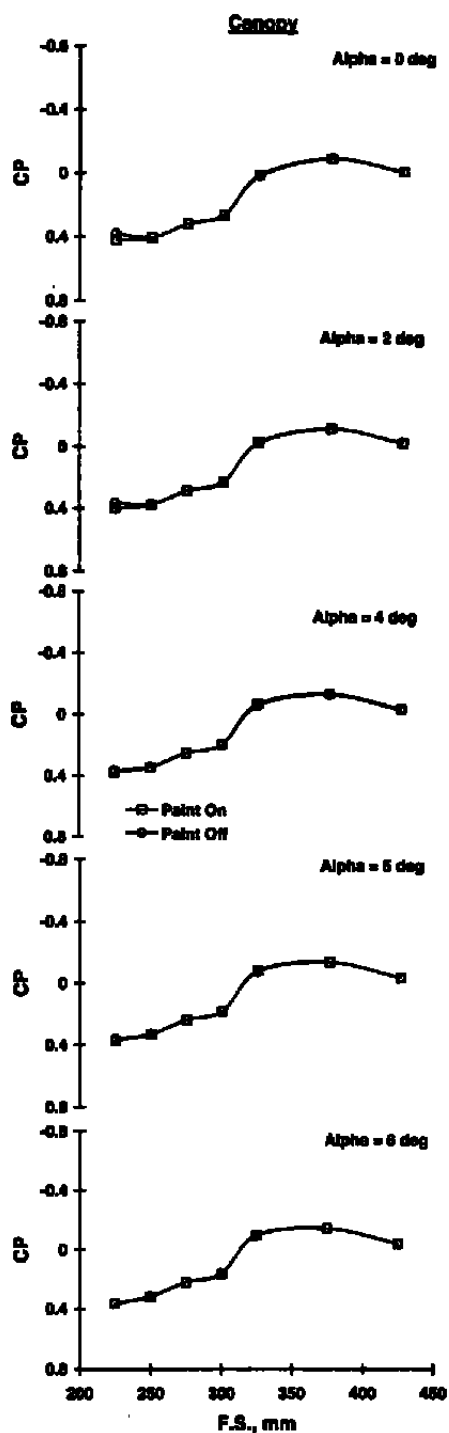


p. Alpha = 5 deg, Rec = 2.0

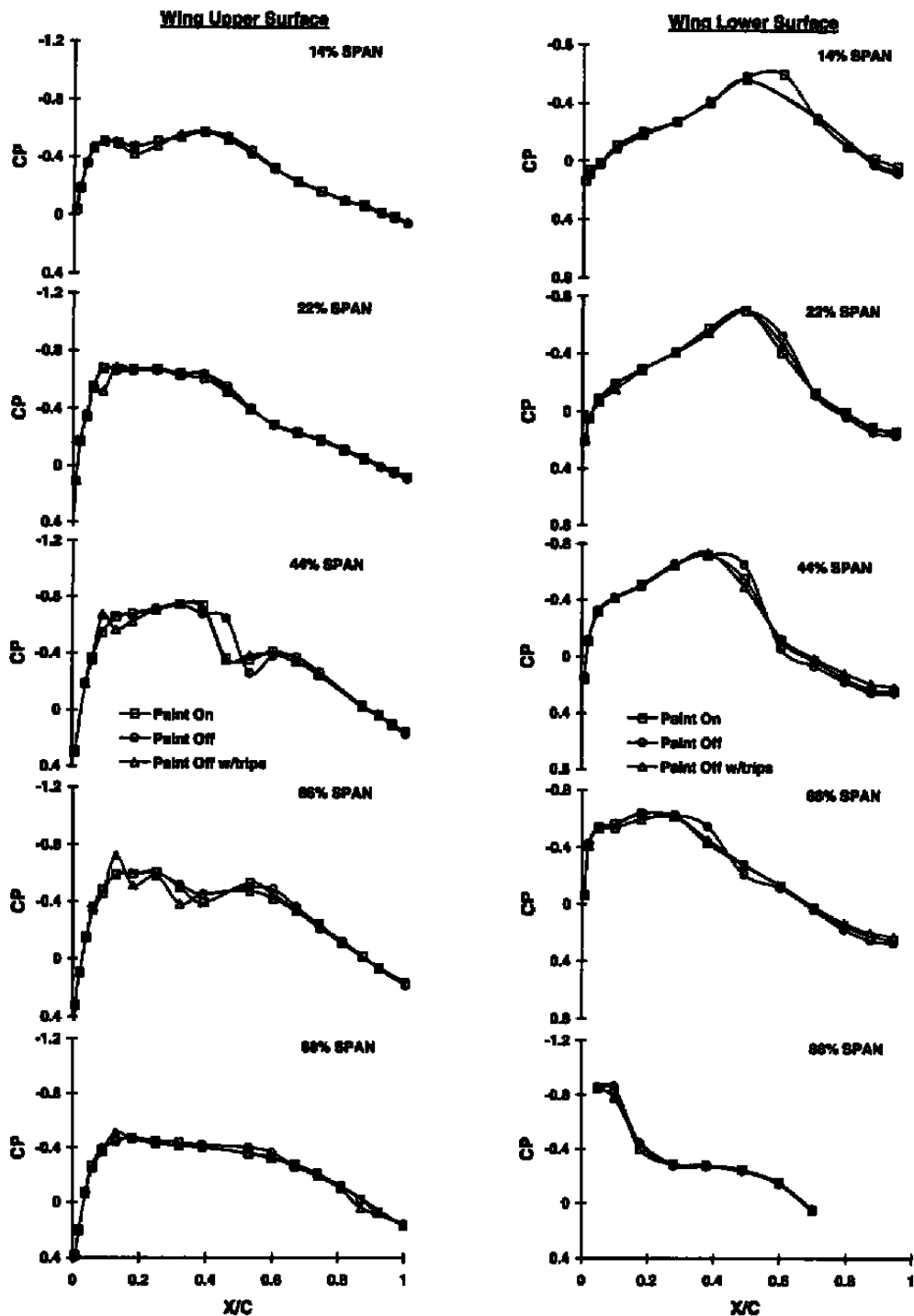
Figure 12. Continued.



q. Alpha = 6 deg, Rec = 2.0
Figure 12. Continued.

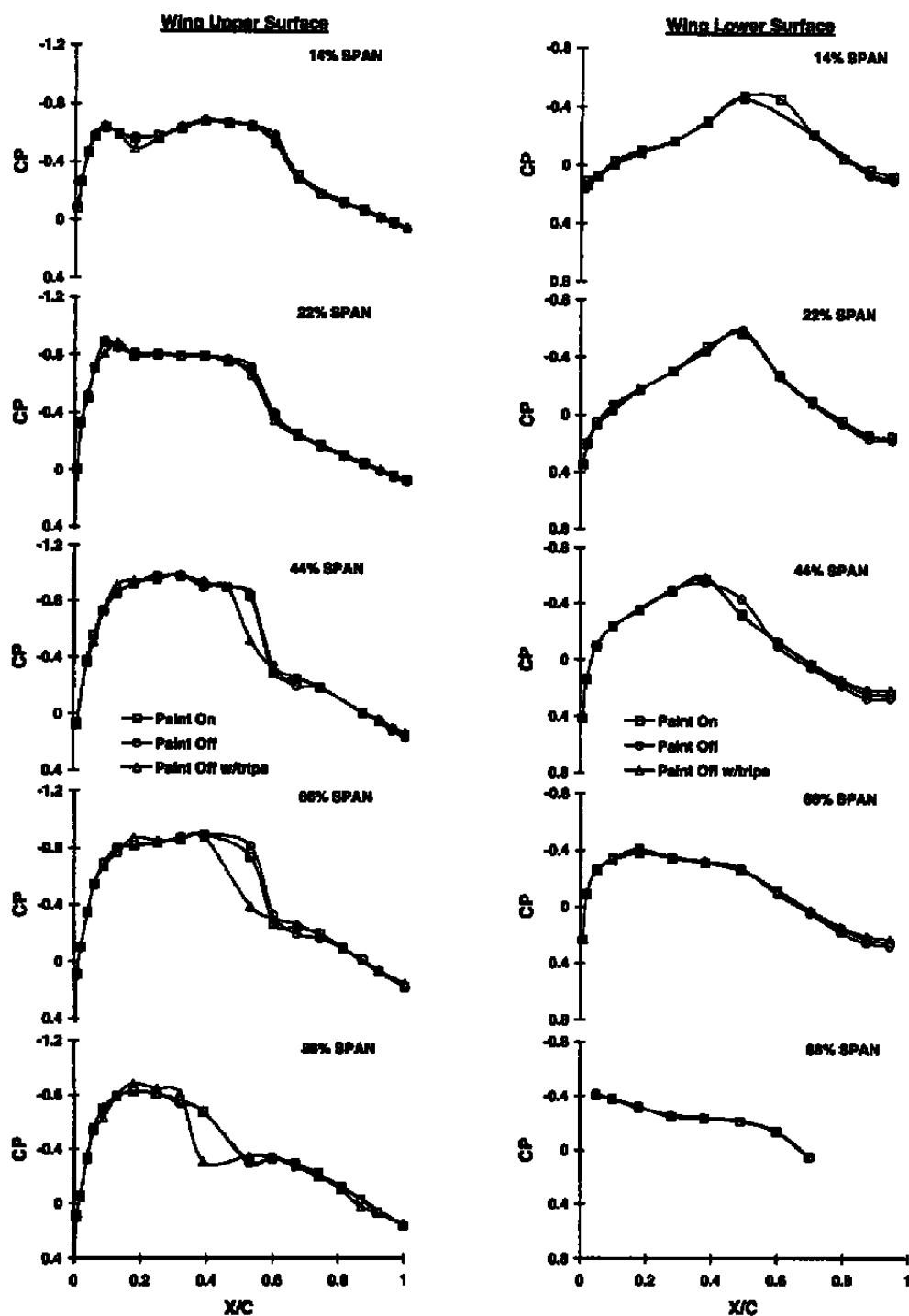


r. Canopy, Rec = 2.0
 Figure 12. Continued.



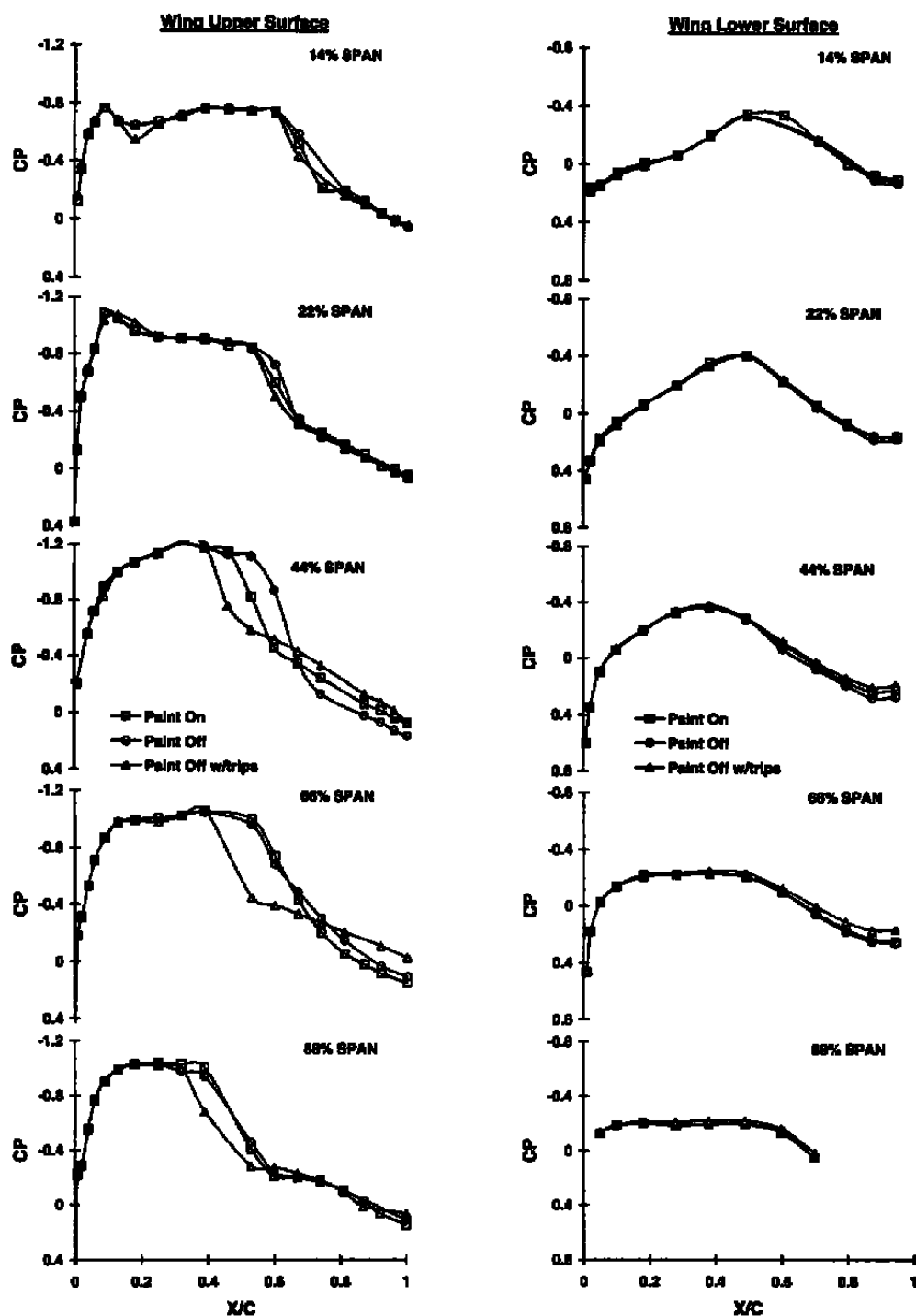
s. Alpha = 0 deg, Rec = 2.7

Figure 12. Continued.



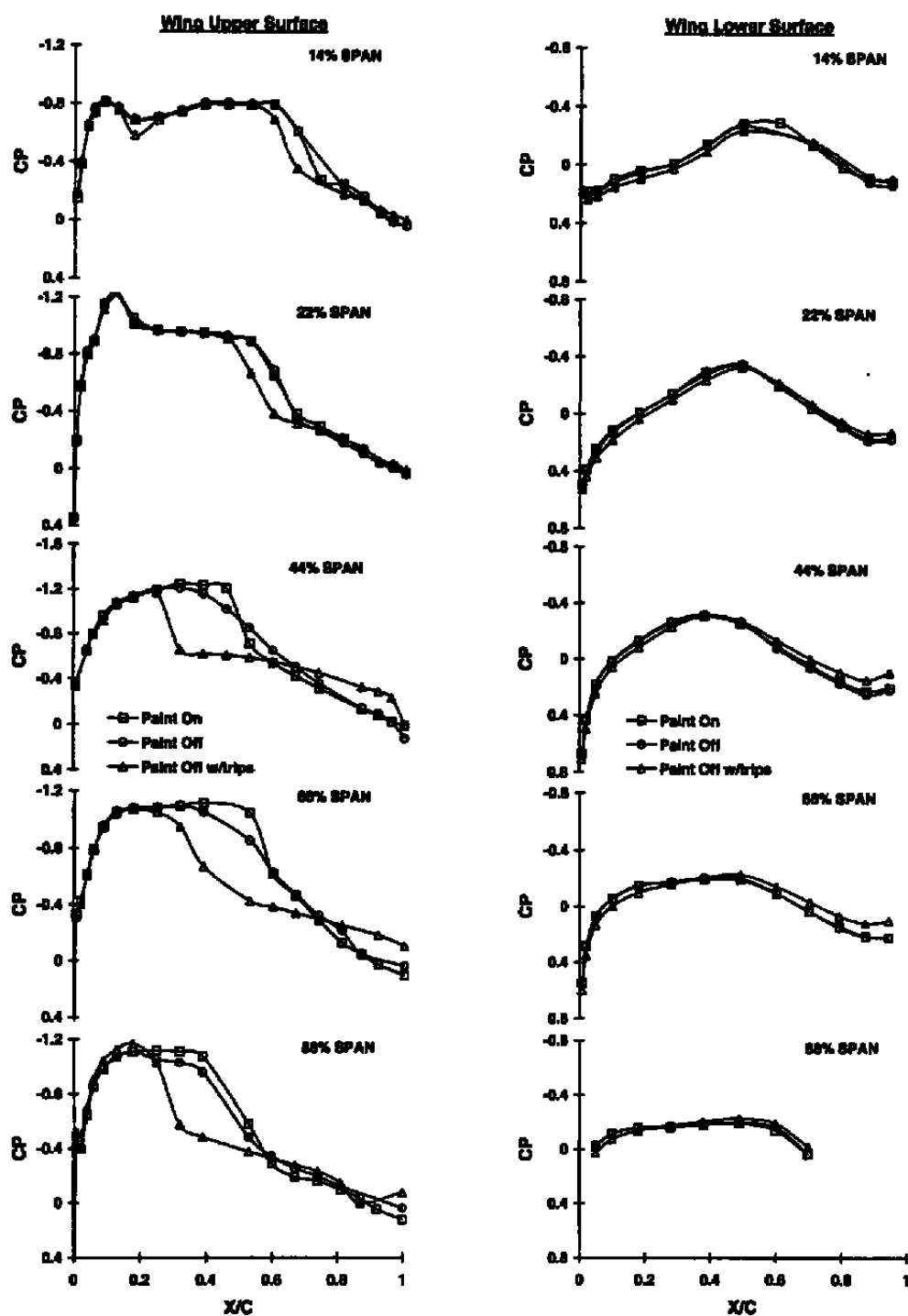
$t. \alpha = 2 \text{ deg}, \text{Rec} = 2.7$

Figure 12. Continued.



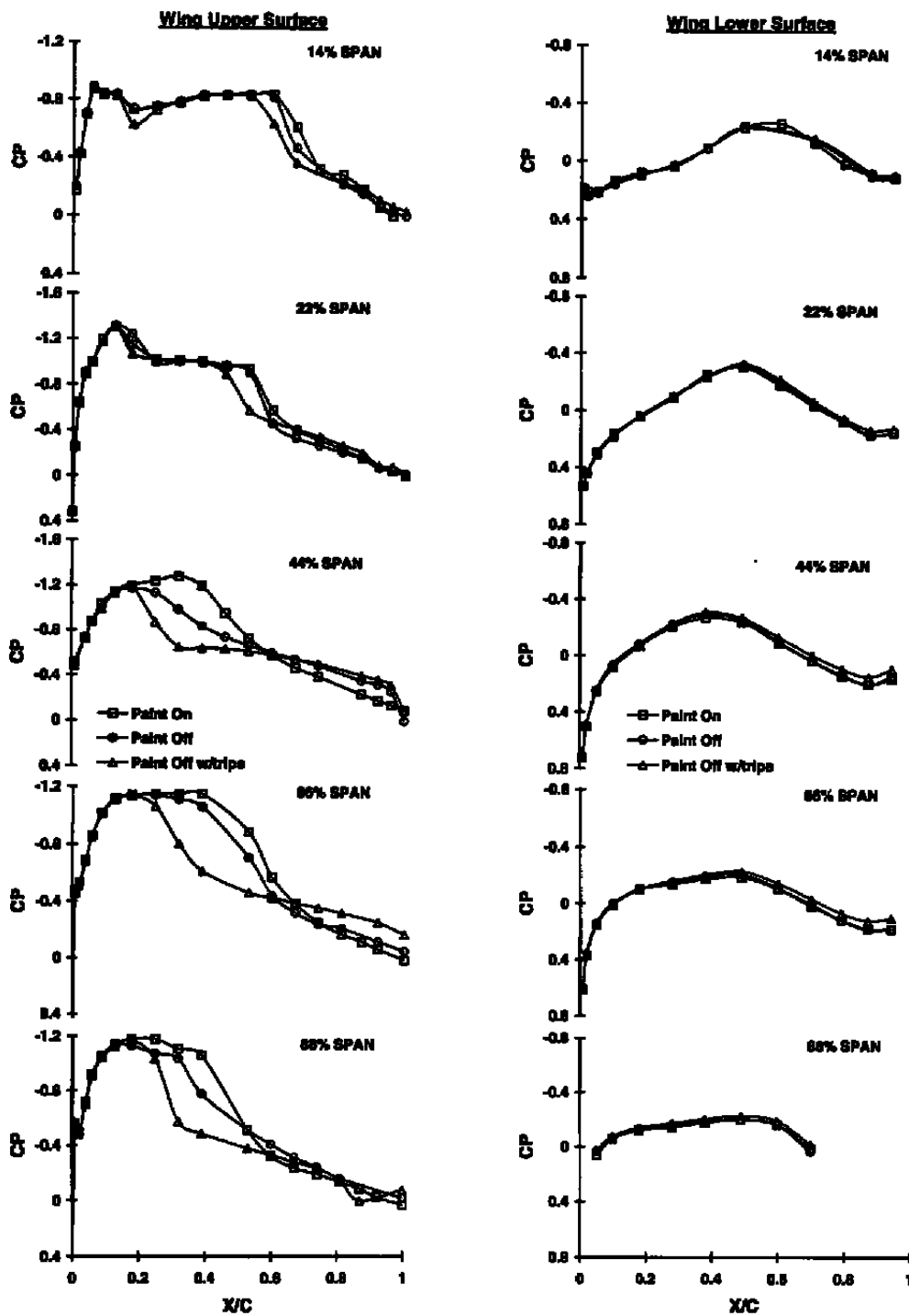
u. Alpha = 4 deg, Rec = 2.7

Figure 12. Continued.



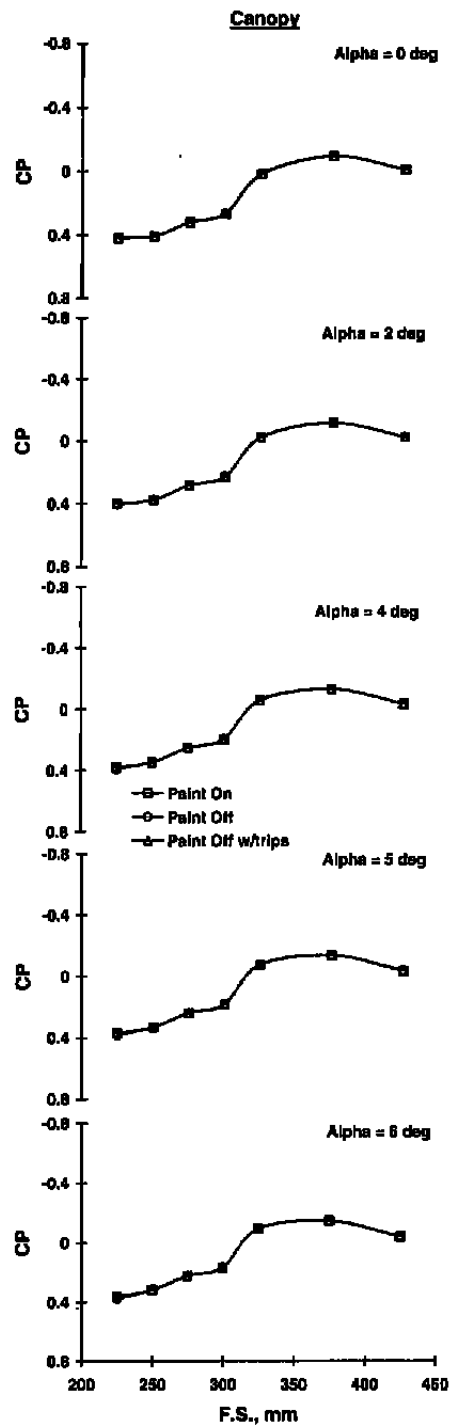
v. Alpha = 5 deg, Rec = 2.7

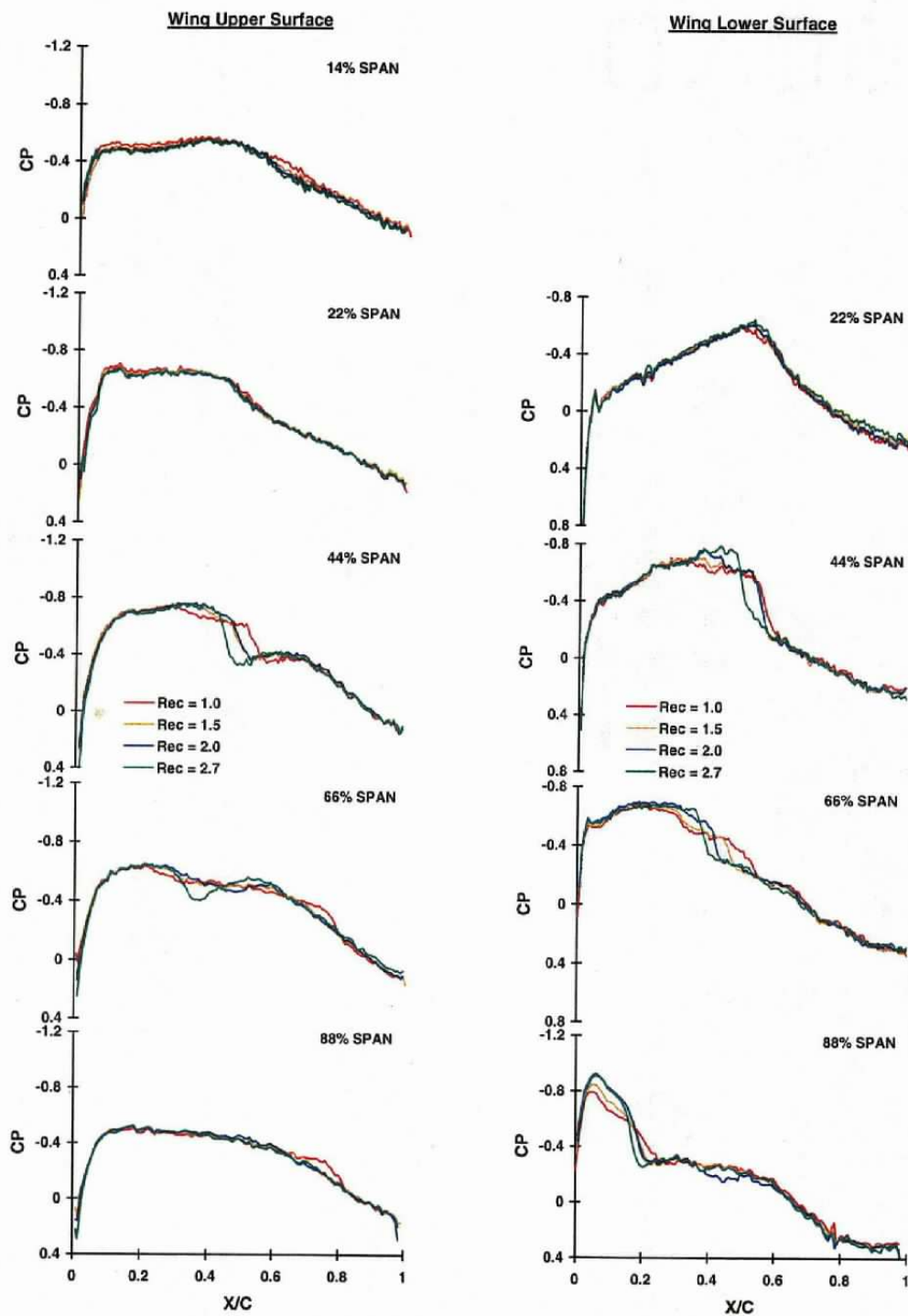
Figure 12. Continued.



w. Alpha = 6 deg, Rec = 2.7

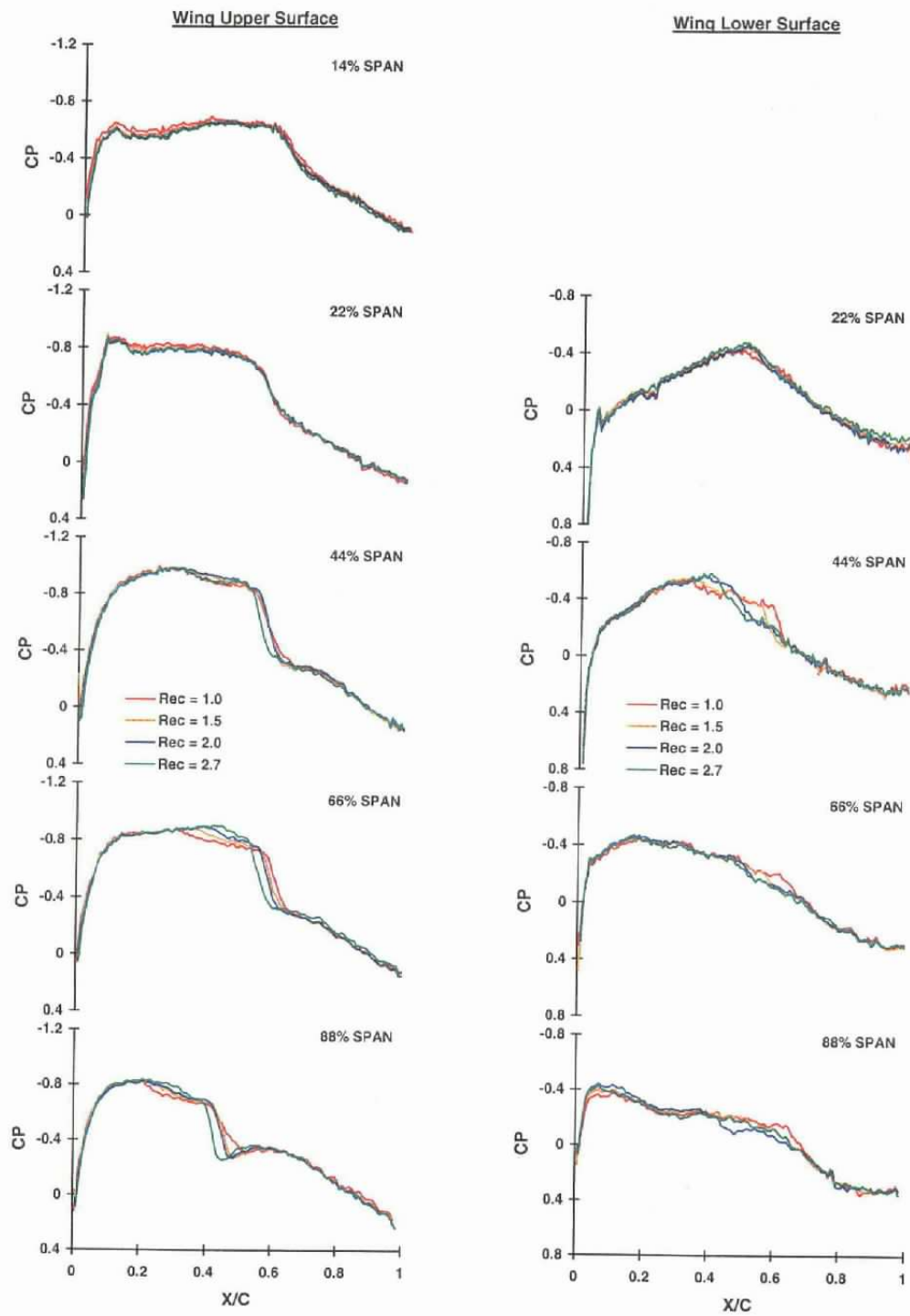
Figure 12. Continued.



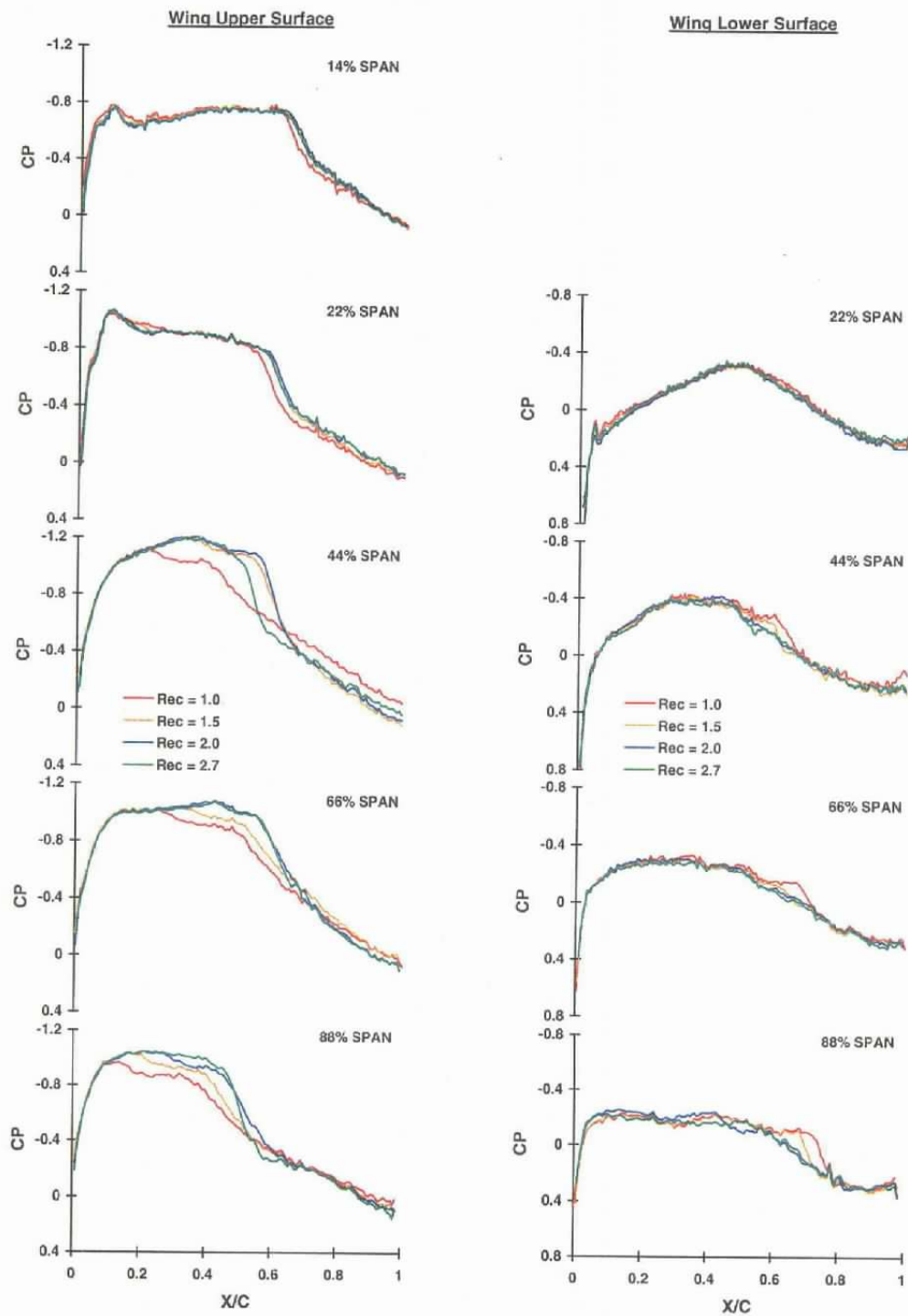


a. $\alpha = 0^\circ$

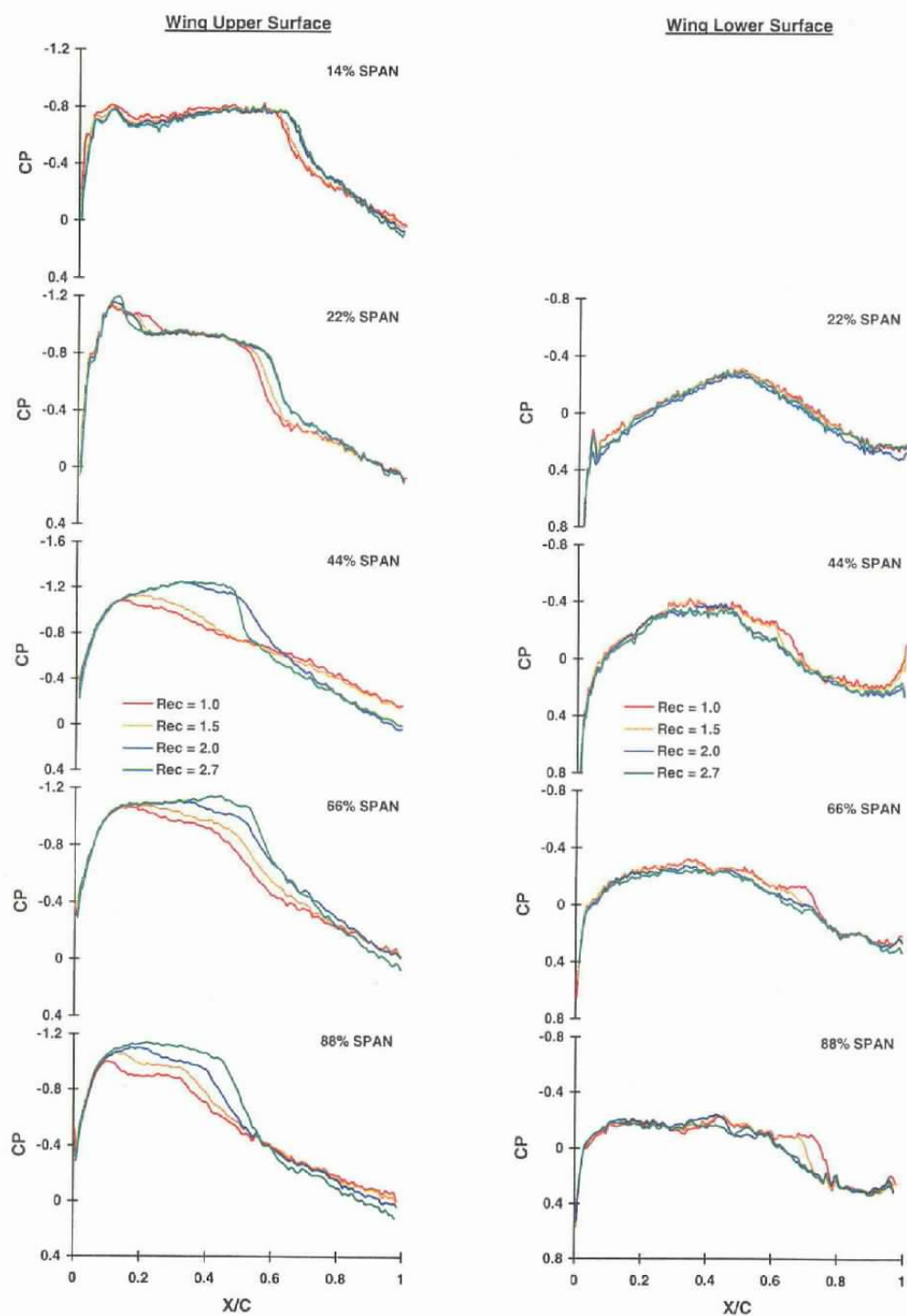
Figure 13. Reynolds number effects on PSP data at Mach number 0.835.



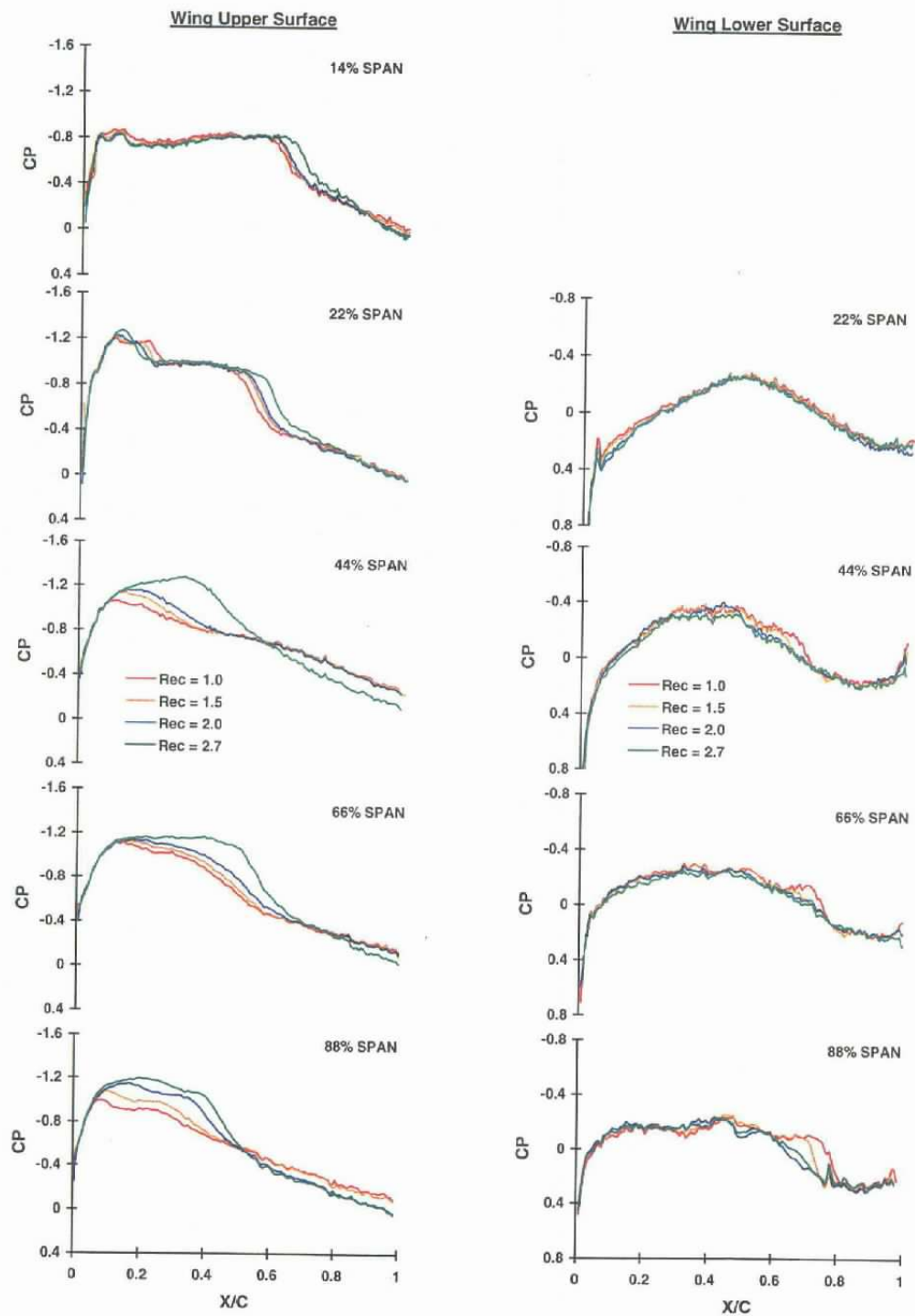
b. Alpha = 2 deg
Figure 13. Continued.



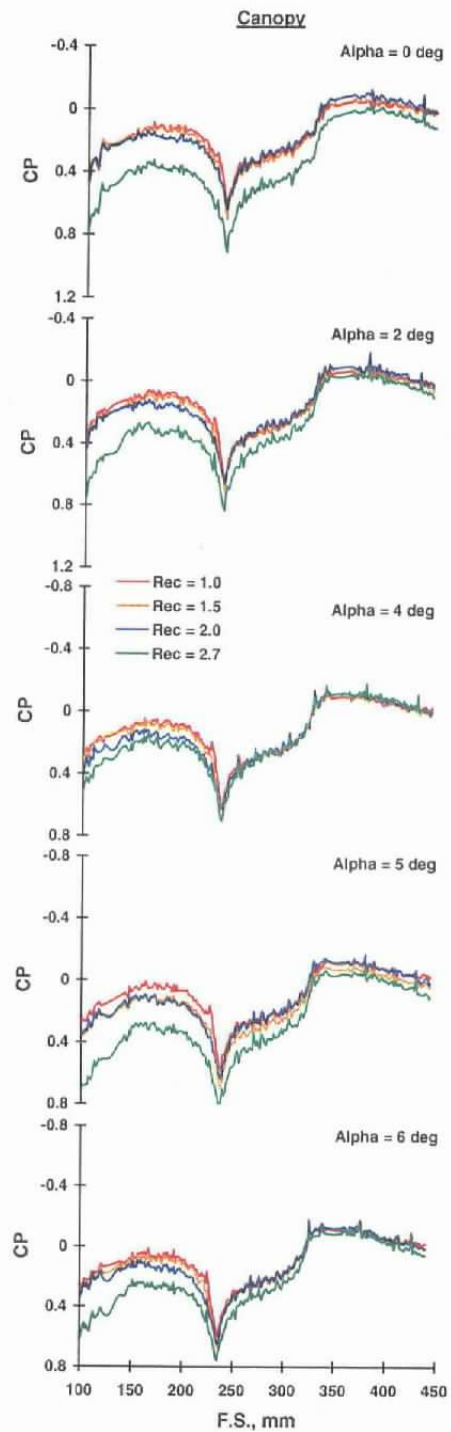
c. $\alpha = 4^\circ$
Figure 13. Continued.



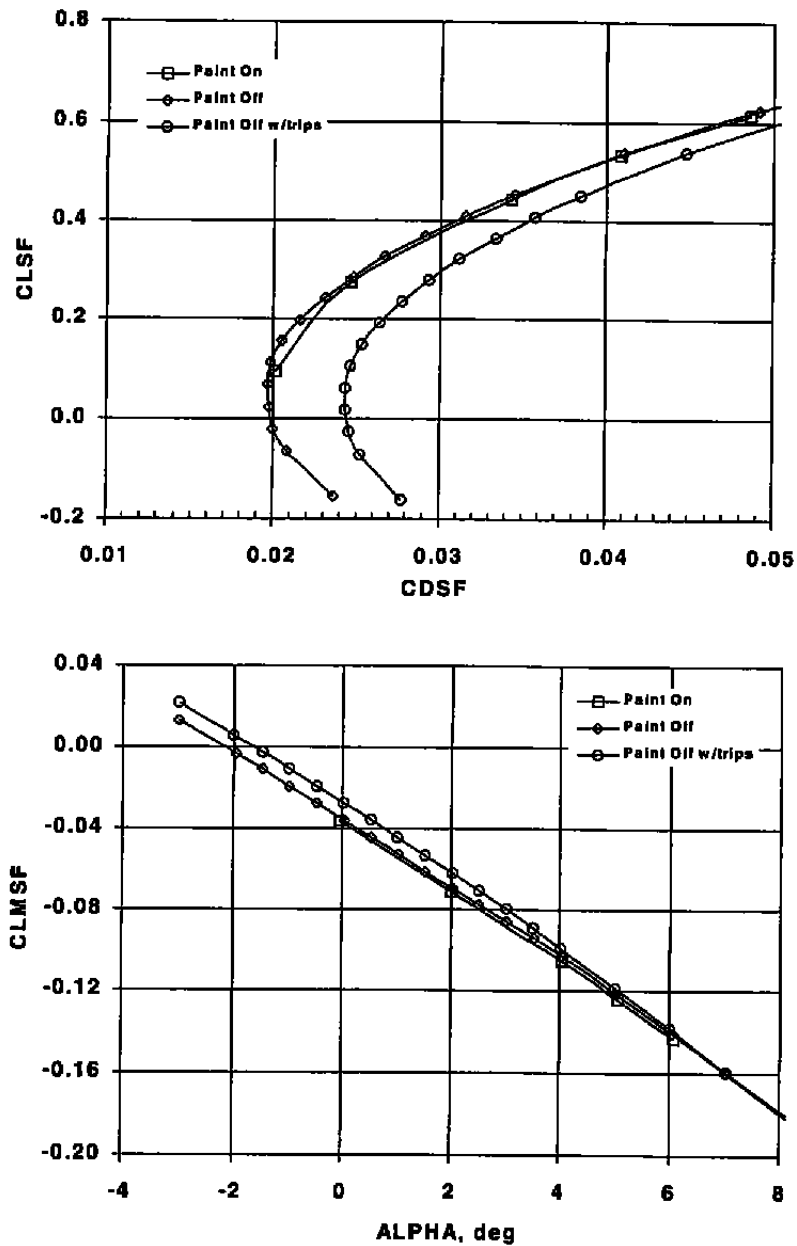
d. Alpha = 5 deg
Figure 13. Continued.



e. $\alpha = 6^\circ$
Figure 13. Continued.

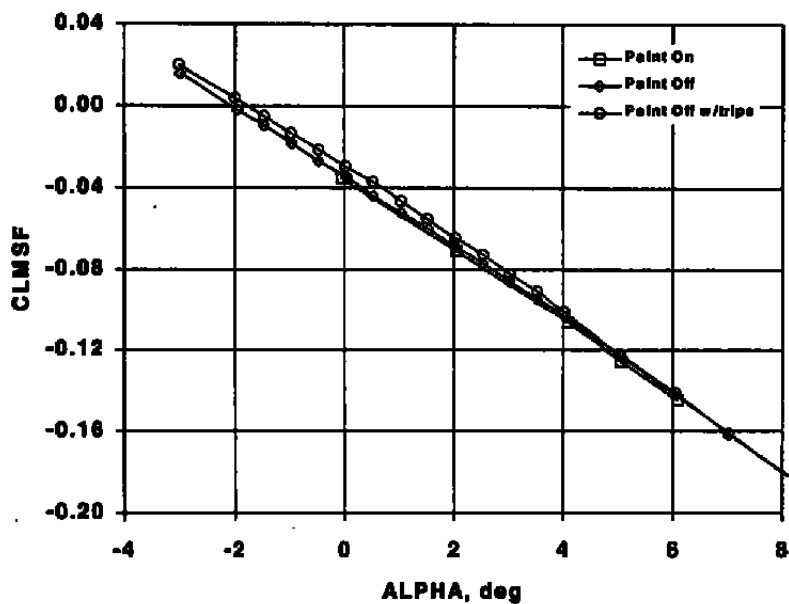
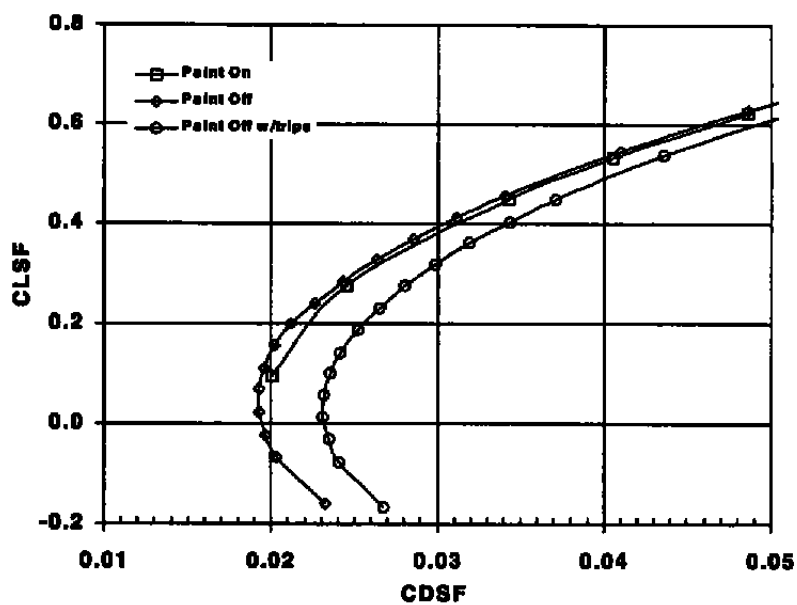


f. Canopy, Rec = 1.0
Figure 13. Concluded.

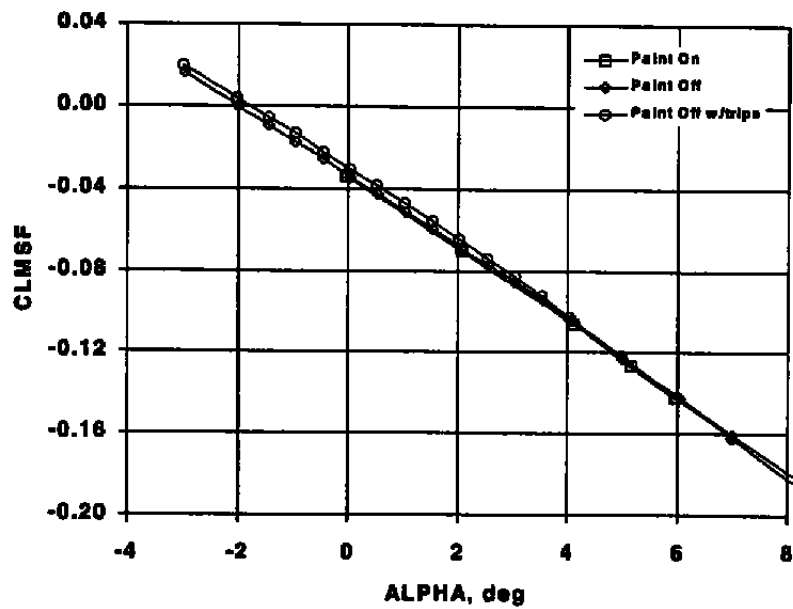
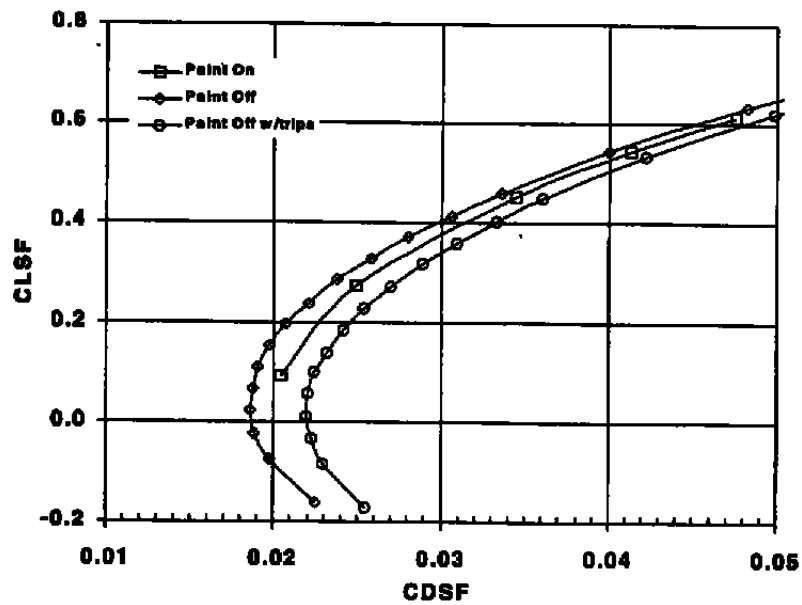


a. Mach = 0.6, Rec = 1.5

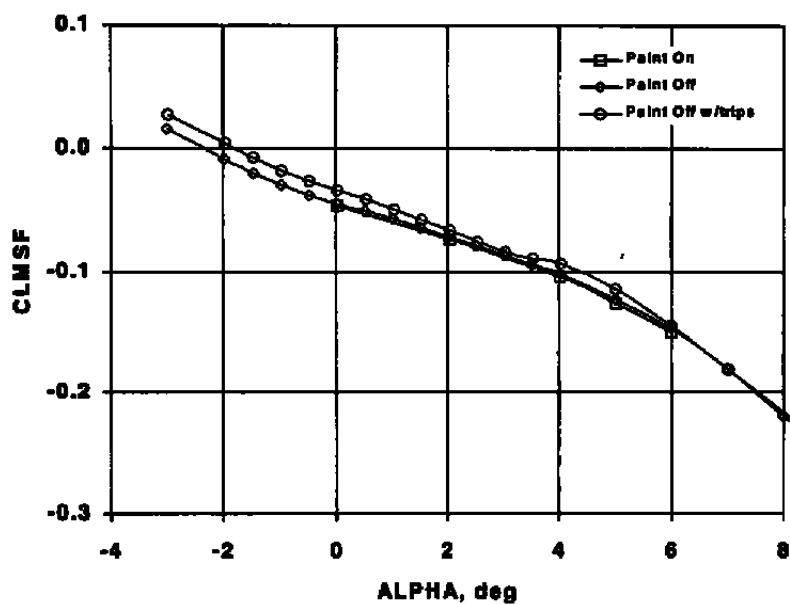
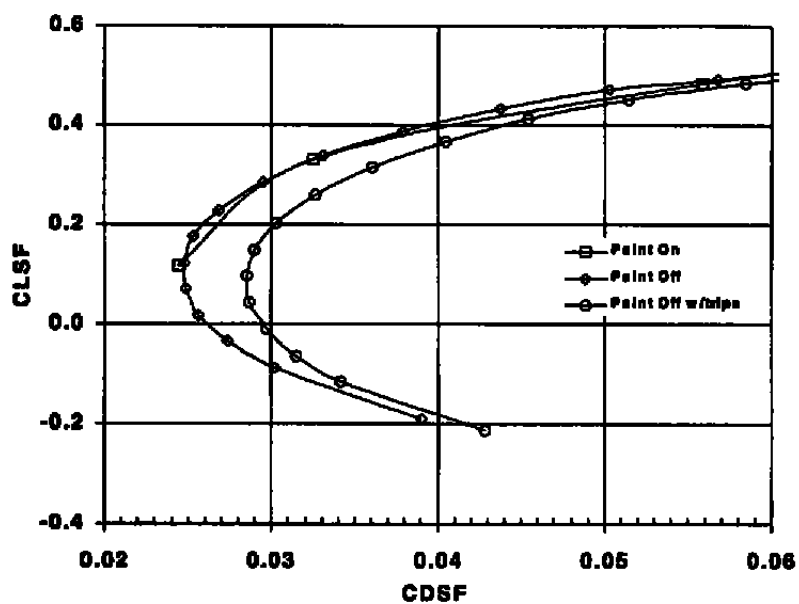
Figure 14. Effects of paint on model aerodynamic coefficients.



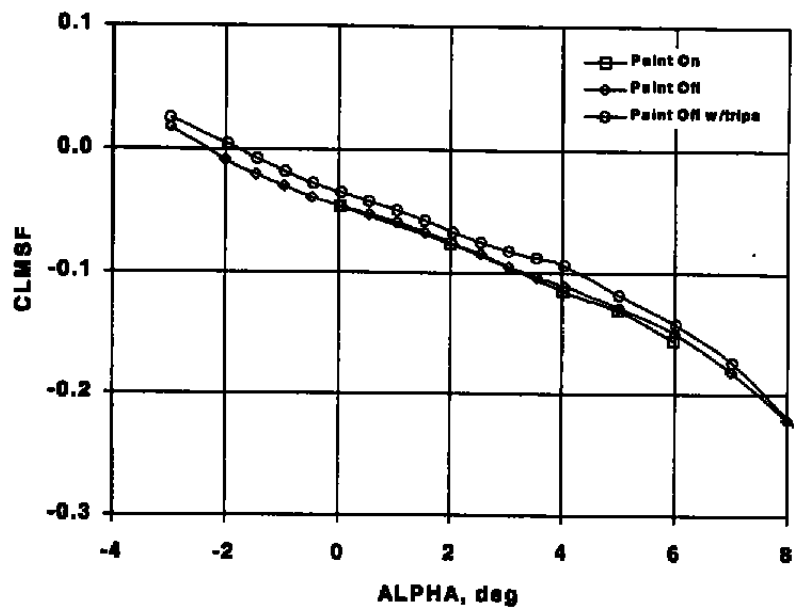
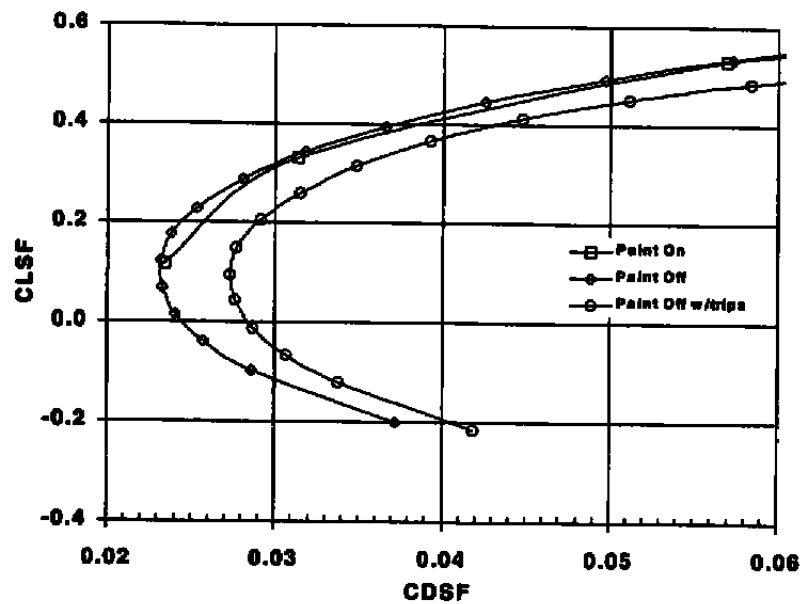
b. Mach = 0.6, Rec = 20
Figure 14. Continued.



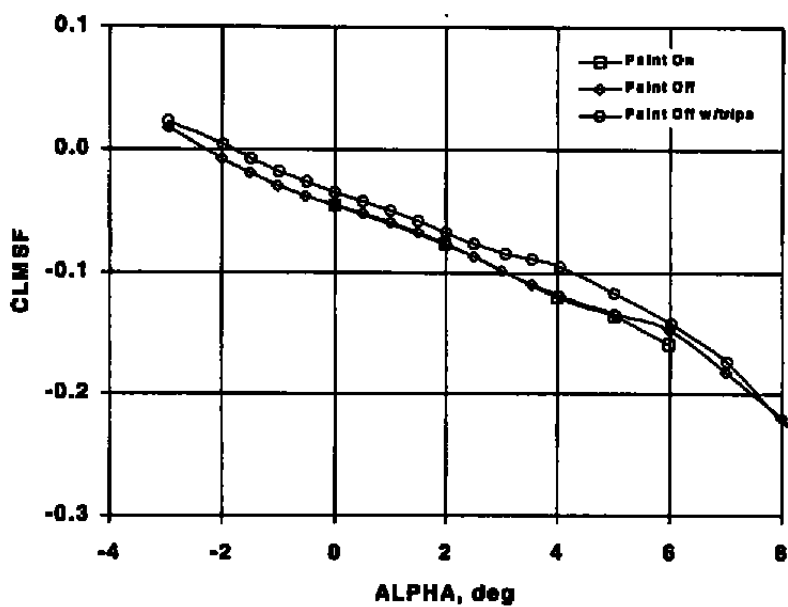
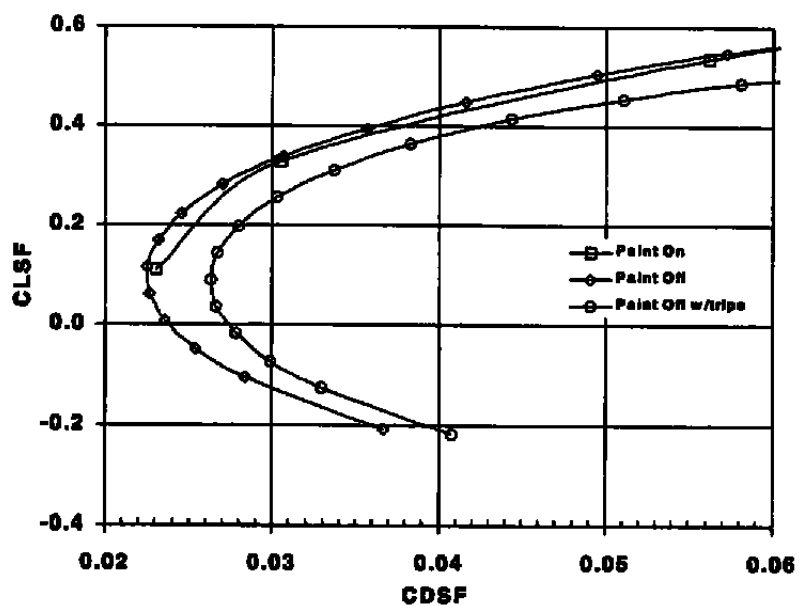
c. Mach = 0.6, Rec = 2.7
Figure 14. Continued.



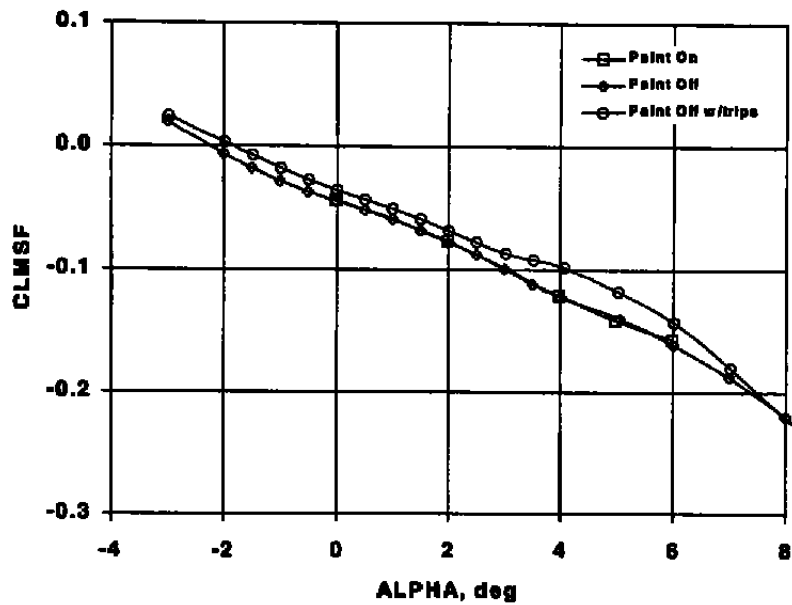
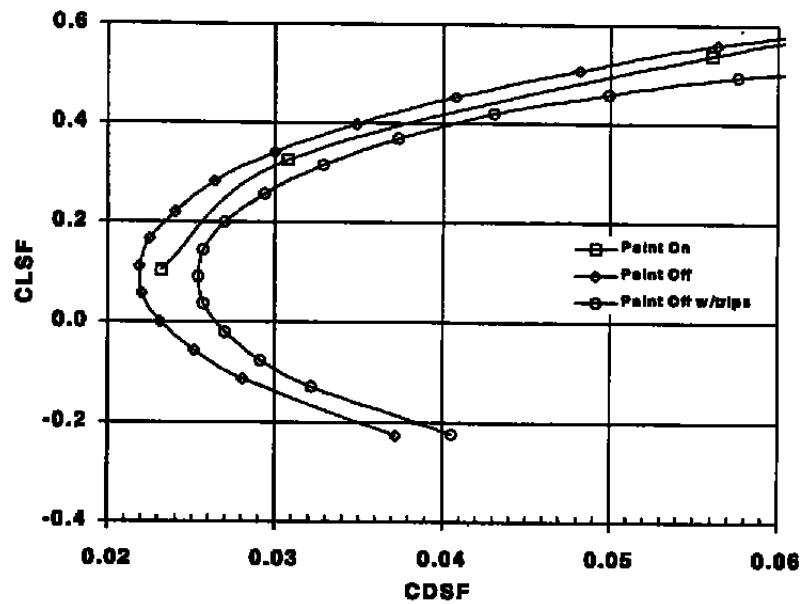
d. Mach = 0.835, Rec = 1.0
Figure 14. Continued.



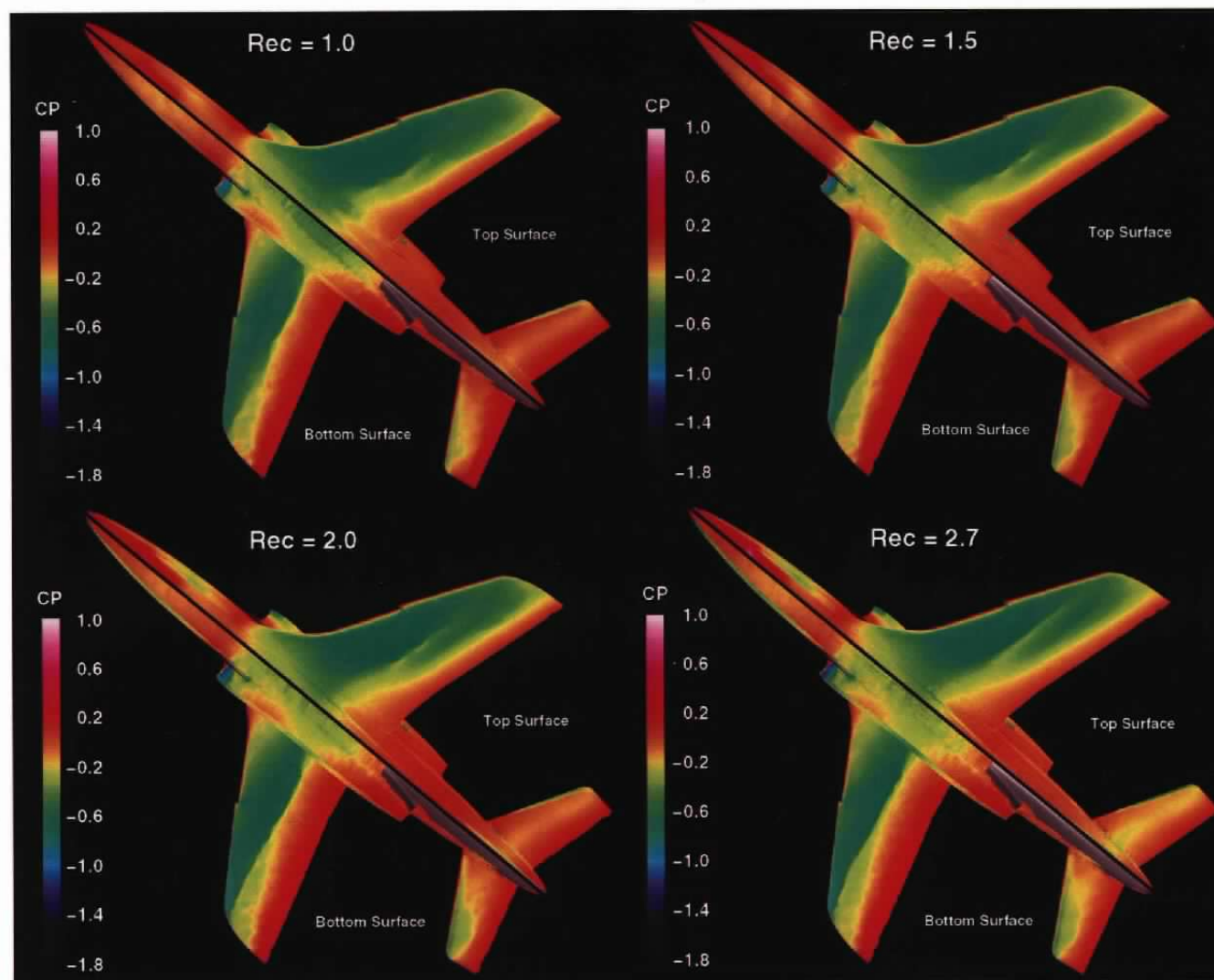
e. Mach = 0.835, Rec = 1.5
 Figure 14. Continued.



f. Mach = 0.835, Rec = 2.0
Figure 14. Continued.

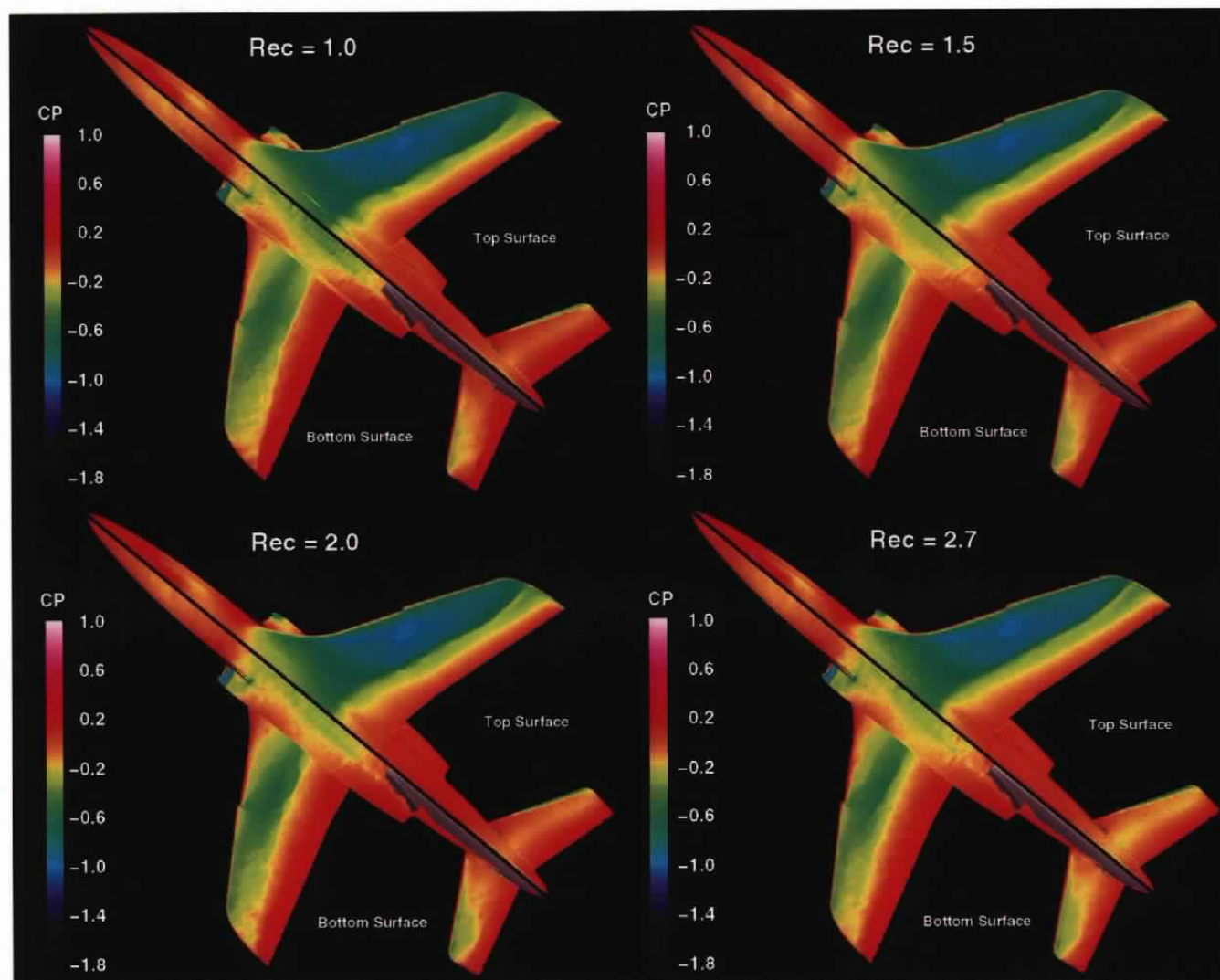


g. Mach = 0.835, Rec = 2.7
Figure 14. Concluded.

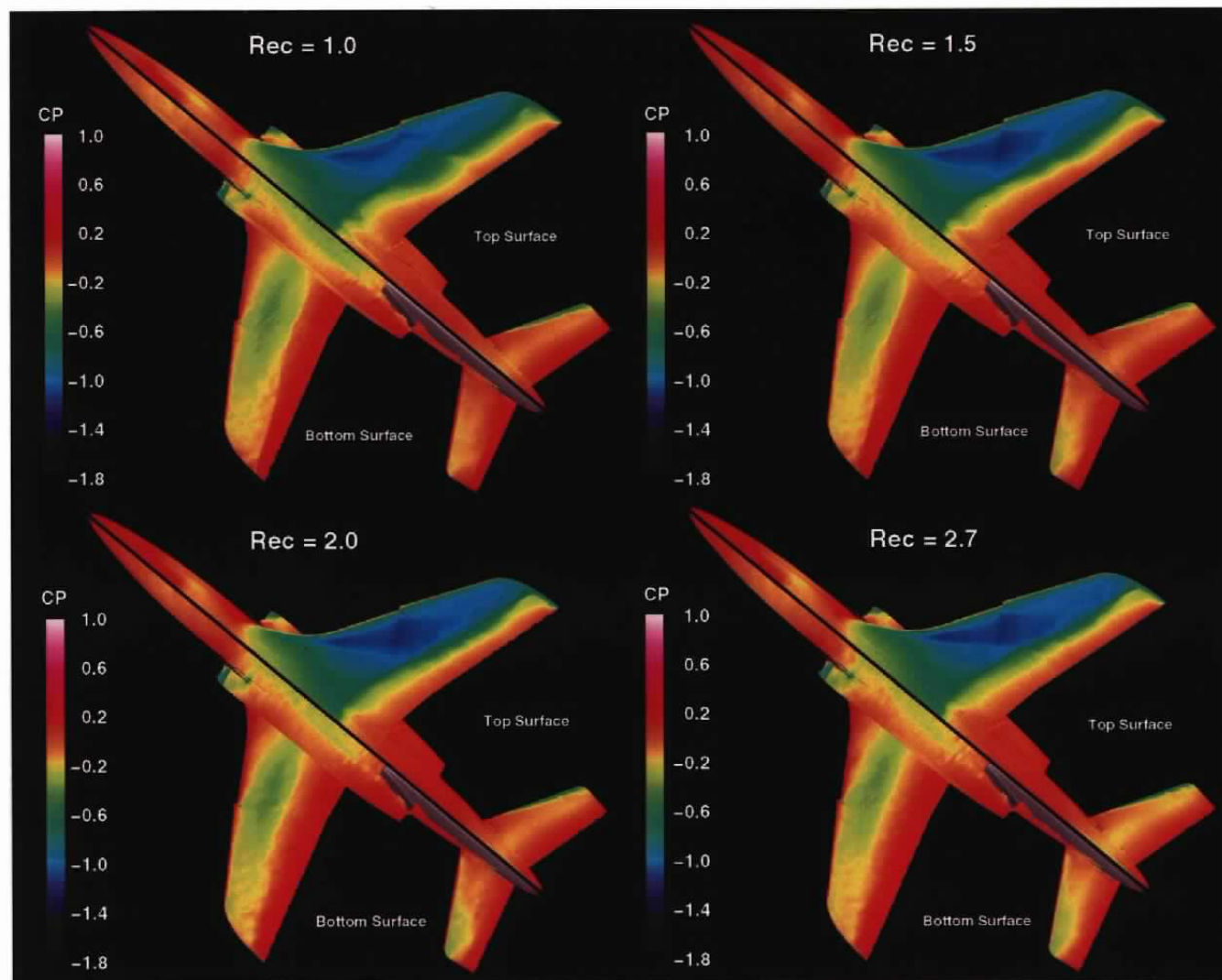


a. Alpha = 0 deg

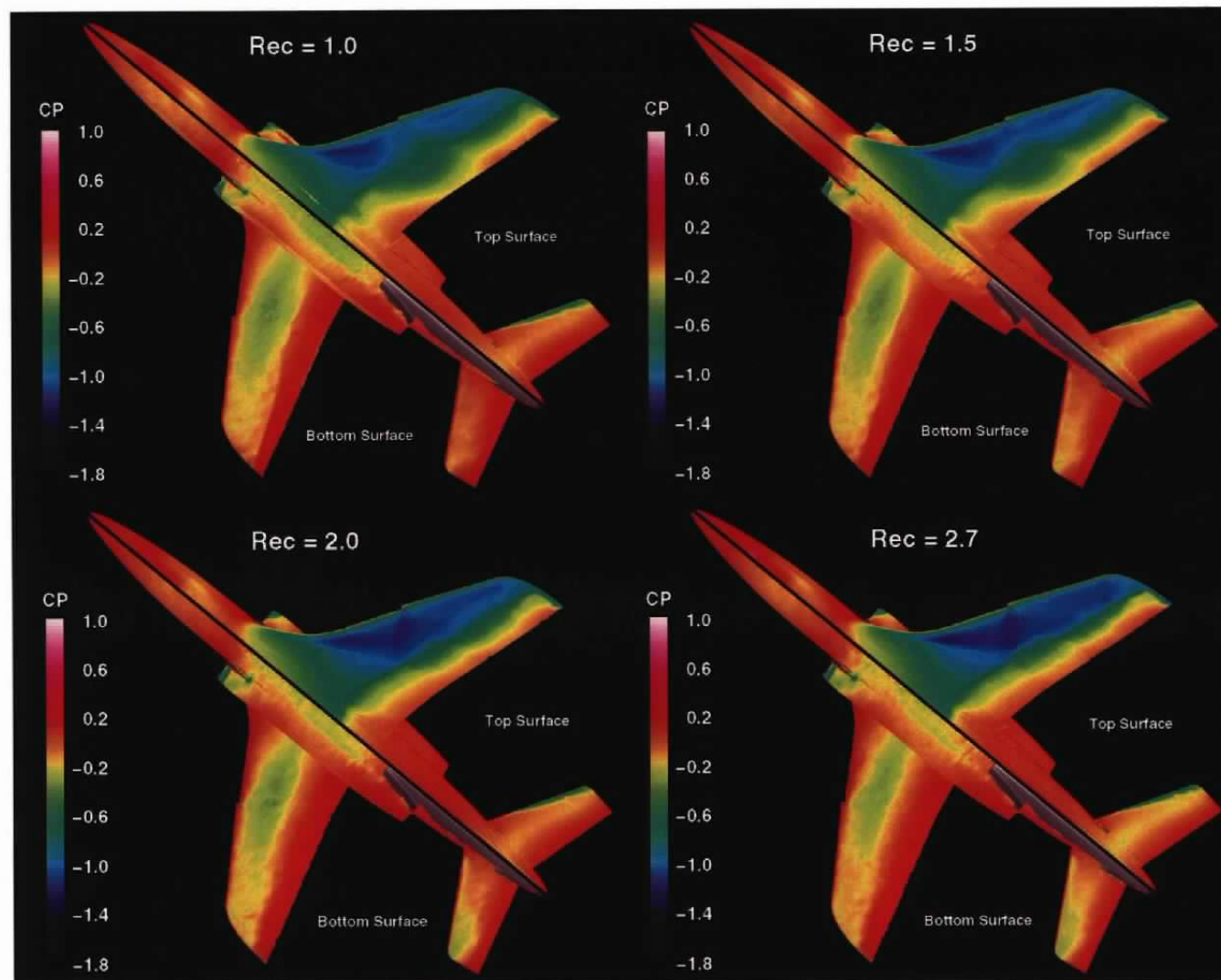
Figure 15. TST pressure coefficient distribution at Mach number 0.835.



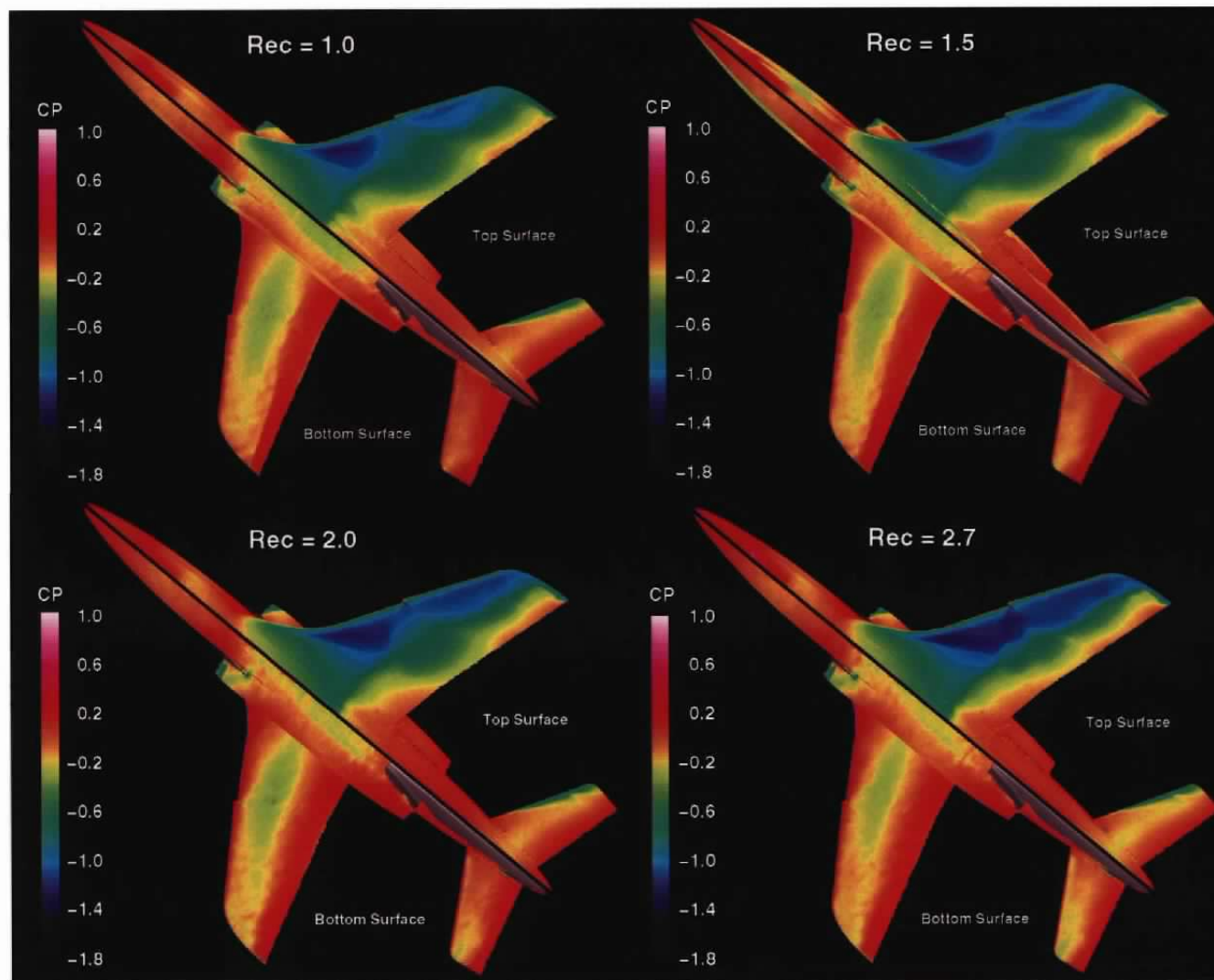
b. Alpha = 2 deg
Figure 15. Continued.



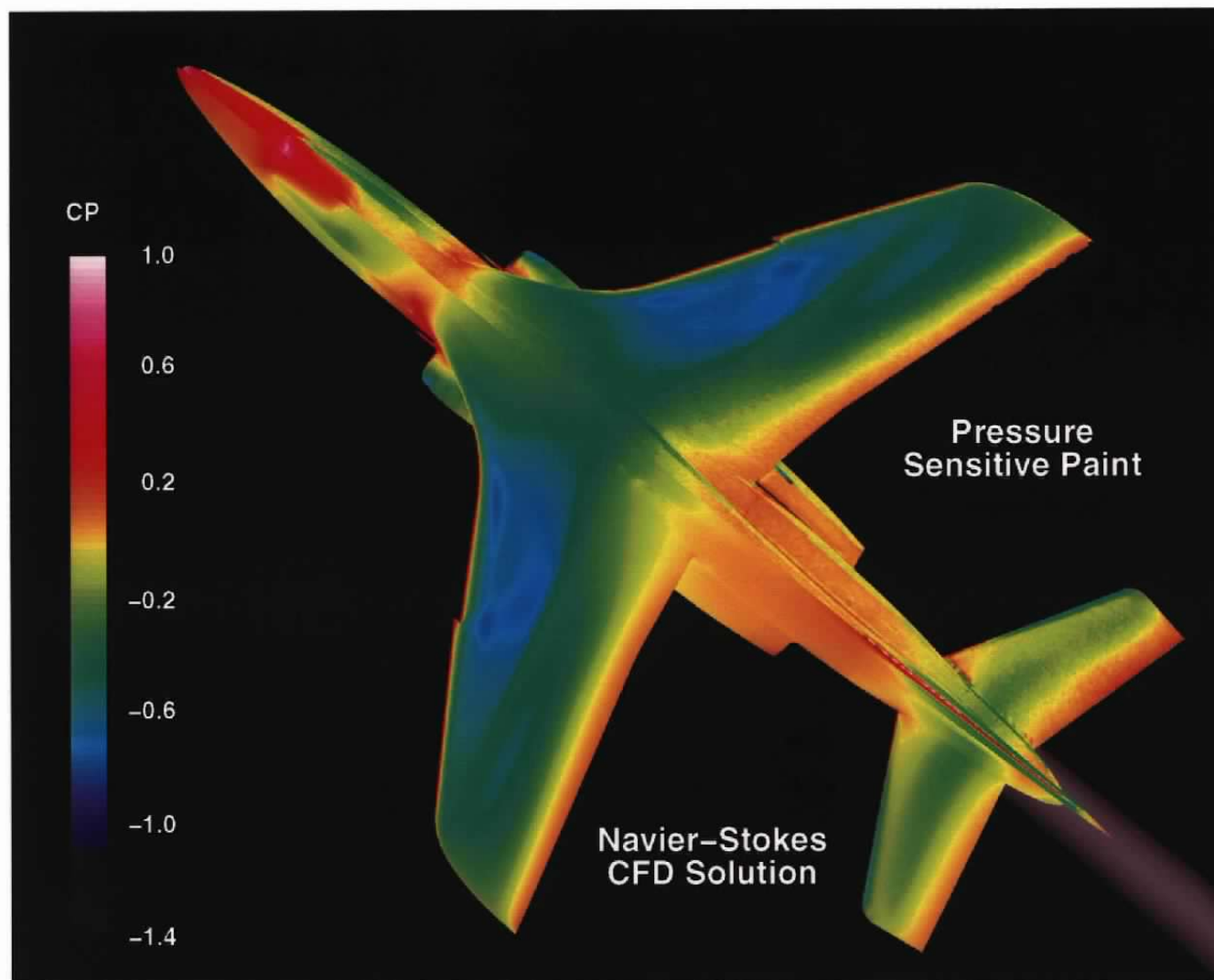
c. Alpha = 4 deg
Figure 15. Continued.



d. Alpha = 5 deg
Figure 15. Continued.

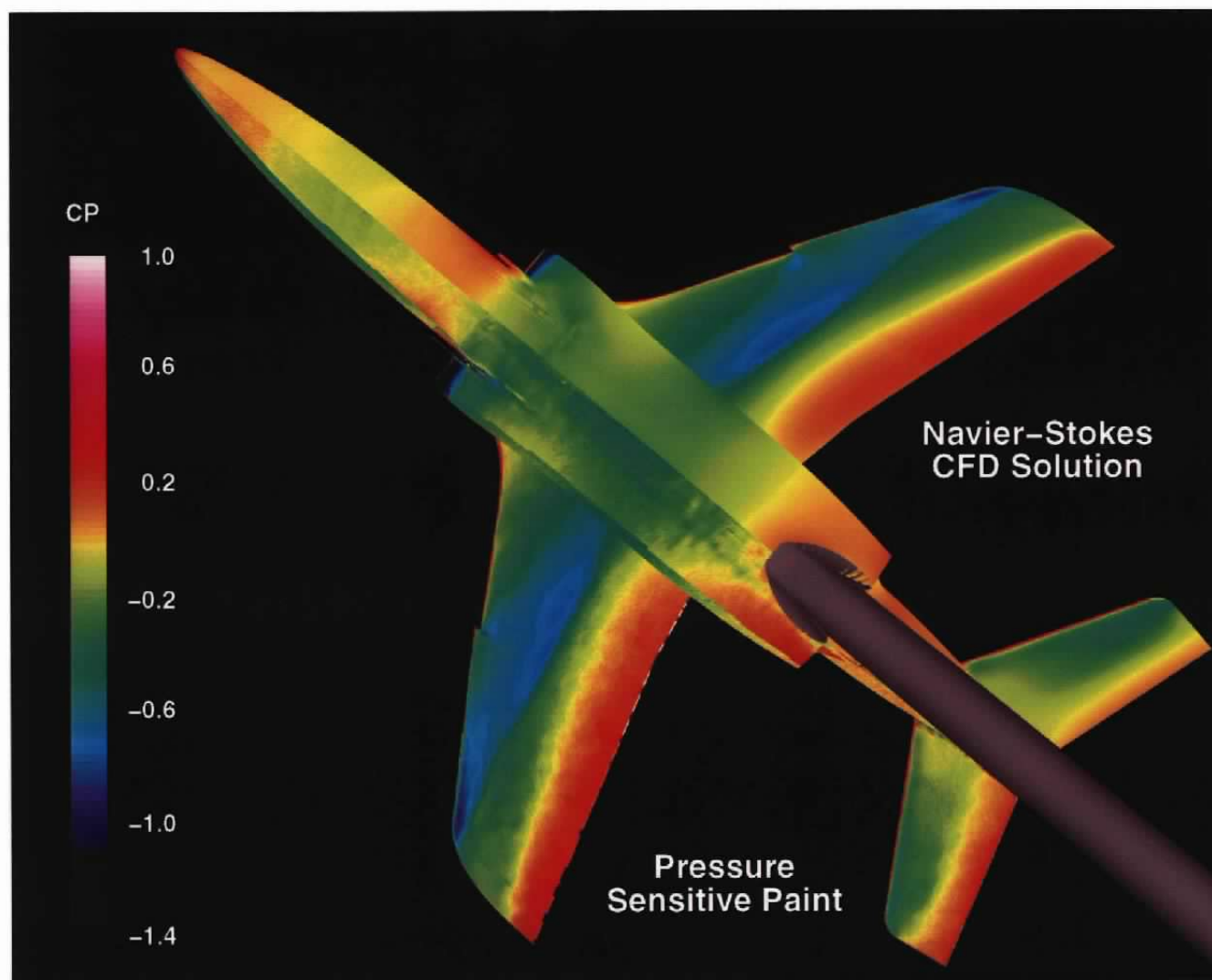


e. Alpha = 6 deg
Figure 15. Concluded

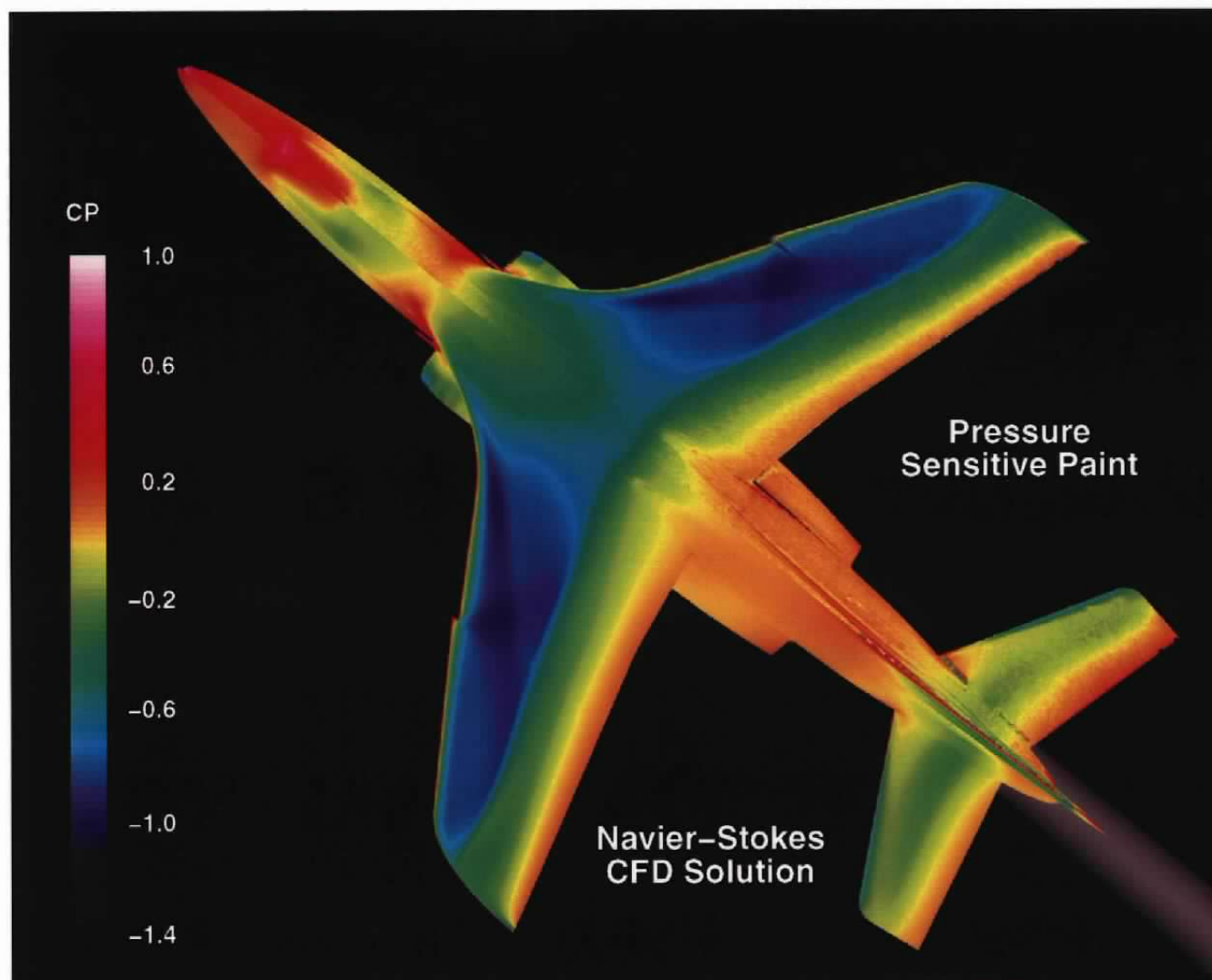


a. Upper Surface, $Re_c = 2.7$, $\alpha = 0^\circ$

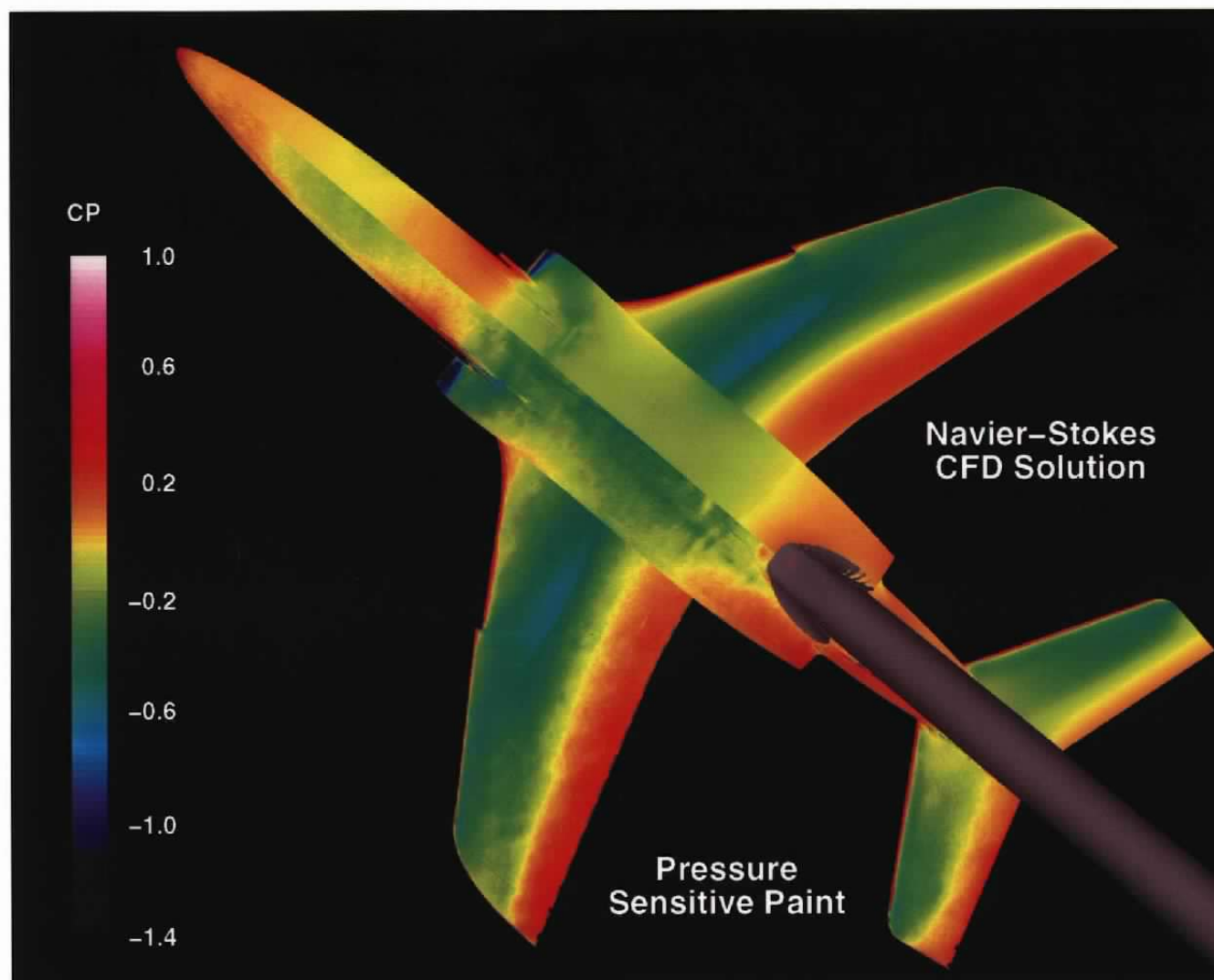
Figure 16. TST PSP and CFD pressure coefficient comparison at Mach number 0.835.



b. Lower Surface, $Re_c = 2.7$, $\alpha = 0^\circ$
Figure 16. Continued.



c. Upper Surface, $Re_c = 2.7$, $\alpha = 2^\circ$
Figure 16. Continued.



d. Lower Surface, $Re_c = 2.7$, $\alpha = 2^\circ$
Figure 16. Concluded.

Table 1. TST Wing, Canopy, and Fuselage Pressure Orifice Designation and Location

Section & Tap No.	X/C	F.S.	B.L.	W.L.	Section & Tap No.	X/C	F.S.	B.L.	W.L.
101	1.000	816.79	63.87	73.84	201	1.000	823.23	98.90	72.29
102	0.960	805.33	64.18	76.78	202	0.960	813.31	99.15	74.68
103	0.920	793.34	64.40	78.88	203	0.920	802.19	99.35	76.54
104	0.870	778.68	64.67	81.41	204	0.870	791.01	99.54	78.39
105	0.810	761.09	64.98	84.40	205	0.810	776.15	99.79	80.80
106	0.740	740.57	65.34	87.76	206	0.740	758.80	100.07	83.44
107	0.670	720.05	65.67	90.93	207	0.670	741.46	100.32	85.83
108	0.600	699.52	65.99	93.97	208	0.600	724.11	100.55	88.03
109	0.530	679.00	66.30	96.91	209	0.530	706.77	100.77	90.06
110	0.460	658.48	66.59	99.66	210	0.460	689.42	100.96	91.87
111	0.390	637.96	66.83	101.97	211	0.390	672.07	101.11	93.30
112	0.320	617.44	67.00	103.65	212	0.320	654.73	101.20	94.23
113	0.250	596.91	67.10	104.56	213	0.250	637.38	101.24	94.56
114	0.180	576.39	67.10	104.57	214	0.180	620.04	101.20	94.16
115	0.130	561.73	67.03	103.90	215	0.130	607.65	101.11	93.33
116	0.090	550.00	66.90	102.65	216	0.090	597.74	100.98	92.07
117	0.060	541.21	66.70	100.80	217	0.060	590.30	100.80	90.39
118	0.040	535.35	66.49	98.73	218	0.040	585.35	100.62	88.63
119	0.020	529.48	66.15	95.47	219	0.020	580.39	100.34	85.96
120	0.008	525.96	65.80	92.23	220	0.008	577.42	100.07	83.43
121	0.000	523.62	65.23	86.77	221	0.000	575.44	99.62	79.19
122	0.008	525.96	64.76	82.27	222	0.008	577.42	99.24	75.55
123	0.020	529.48	64.57	80.46	223	0.020	580.39	99.08	74.06
124	0.050	538.28	64.27	77.65	224	0.050	587.83	98.84	71.74
125	0.100	552.94	63.94	74.41	225	0.100	600.22	98.57	69.15
126	0.180	576.39	63.56	70.84	226	0.180	620.04	98.28	66.38
127	0.280	605.71	63.26	68.07	227	0.280	644.82	98.07	64.41
128	0.380	635.03	63.14	66.82	228	0.380	669.60	98.00	63.74
129	0.490	667.27	63.17	67.15	229	0.490	696.85	98.08	64.46
130	0.600	699.53	63.36	68.96	230	0.600	724.11	98.29	66.47
131	0.700	728.84	63.59	71.19	231	0.700	748.89	98.53	68.82
132	0.790	755.23	63.80	73.16	232	0.790	771.19	98.75	70.91
133	0.870	778.68	63.91	74.22	233	0.870	791.01	98.89	72.16
134	0.940	799.20	63.89	74.00	234	0.940	808.36	98.89	72.24

Table 1. Continued

Section & Tap No.	X/C	F.S.	B.L.	W.L.	Section & Tap No.	X/C	F.S.	B.L.	W.L.
301	1.000	846.00	198.76	65.75	401	1.000	873.90	293.32	56.57
302	0.960	837.96	198.95	67.54	402	0.960	866.89	293.47	58.01
303	0.920	829.98	199.09	68.82	403	0.920	859.89	293.58	59.03
304	0.870	819.98	199.25	70.41	404	0.870	850.98	293.71	60.30
305	0.810	807.94	199.44	72.23	405	0.810	840.61	293.86	61.70
306	0.740	793.91	199.64	74.10	406	0.740	828.35	294.01	63.15
307	0.670	779.89	199.80	75.61	407	0.670	816.09	294.13	64.27
308	0.600	765.87	199.20	76.75	408	0.600	803.82	294.21	65.04
309	0.530	751.84	200.00	77.56	409	0.530	791.56	294.26	65.49
310	0.460	737.82	200.06	78.08	410	0.460	779.30	294.28	65.66
311	0.390	723.80	200.08	78.27	411	0.390	767.04	294.27	65.56
312	0.320	709.77	200.07	78.15	412	0.320	754.77	294.23	65.22
313	0.250	695.75	200.01	77.65	413	0.250	742.51	294.16	64.60
314	0.180	681.72	198.91	76.67	414	0.180	730.25	294.06	63.64
315	0.130	671.71	199.79	75.52	415	0.130	721.49	293.96	62.65
316	0.090	663.69	199.64	74.13	416	0.090	714.48	293.84	61.50
317	0.060	657.68	199.48	72.61	417	0.060	709.22	293.71	60.23
318	0.040	653.68	199.34	71.24	418	0.040	705.72	293.58	59.05
319	0.020	649.67	199.15	69.39	419	0.020	702.22	293.42	57.48
320	0.008	647.27	198.98	67.82	420	0.008	700.11	293.27	56.13
321	0.000	645.66	198.68	64.94	421	0.000	698.71	293.00	53.52
322	0.008	647.27	198.39	62.24	422	0.008	700.11	292.75	51.10
323	0.020	649.67	198.27	61.03	423	0.020	702.22	292.64	50.09
324	0.050	655.68	198.08	59.25	424	0.050	707.47	292.51	48.84
325	0.100	665.70	197.90	57.56	425	0.100	716.23	292.39	47.72
326	0.180	681.72	197.74	56.07	426	0.180	730.25	292.30	46.89
327	0.280	701.76	197.66	55.24	427	0.280	747.76	292.28	46.70
328	0.380	721.79	197.67	55.39	428	0.380	765.28	292.31	46.98
329	0.490	743.83	197.81	56.67	429	0.490	784.55	292.42	47.98
330	0.600	765.87	198.05	58.93	430	0.600	803.82	292.61	49.79
331	0.700	785.90	198.31	61.43	431	0.700	821.34	292.84	51.97
332	0.790	803.93	198.54	63.67	432	0.790	837.11	293.06	54.06
333	0.870	819.96	198.70	65.13	433	0.870	851.13	293.22	55.56
334	0.940	833.98	198.74	65.55	434	0.940	863.39	293.29	56.24

Table 1. Concluded

Section & Tap No.	X/C	F.S.	B.L.	W.L.
501	1.000	904.73	397.88	46.90
502	0.960	898.16	398.01	48.09
503	0.920	893.44	398.87	48.89
504	0.870	885.75	398.17	49.60
505	0.810	878.18	398.26	50.53
506	0.740	869.38	398.35	51.37
507	0.670	859.86	398.42	51.03
508	0.600	850.34	398.47	52.46
509	0.530	840.82	398.49	52.66
510	0.460	831.30	398.49	52.64
511	0.390	821.78	398.46	52.39
512	0.320	812.26	398.41	51.94
513	0.250	802.75	398.34	51.27
514	0.180	793.22	398.25	50.36
515	0.130	786.42	398.15	49.45
516	0.090	780.98	398.05	48.46
517	0.060	776.90	397.94	47.44
518	0.040	774.19	397.84	46.51
519	0.020	771.75	400.11	44.14
520	0.008	769.75	394.27	45.99
521	0.000	768.75	397.40	42.26
522	0.008	769.83	397.21	40.53
523	0.020	771.47	397.14	39.82
524	0.050	775.54	397.05	38.93
525	0.100	782.34	396.98	38.27
526	0.180	793.22	396.94	37.93
527	0.280	806.82	396.95	38.01
528	0.380	820.42	396.99	38.40
529	0.490	835.38	397.08	39.24
530	0.600	850.34	397.23	40.69
531	0.700	863.94	397.45	42.76
532	0.790	877.48	397.67	44.90
534	0.940	896.58	397.84	46.53

Section & Tap No.	X/C	F.S.	B.L.	W.L.
701	-	225.00	0.00	30.94
702	-	250.00	0.00	42.96
703	-	275.00	0.00	58.58
704	-	300.00	0.00	74.20
705	-	325.00	0.00	89.55
706	-	375.00	0.00	109.39
707	-	425.00	0.00	119.87
801	-	853.00	28.00	88.10
802	-	925.00	28.00	86.10
803	-	997.00	28.00	84.30
804	-	1069.00	28.00	81.10

Table 2. Nominal Test Conditions

Mach Number	Total Pressure, psfa	Total Temperature, °F	Static Pressure, psfa	Dynamic Pressure, psf	Chord Reynolds Number, $\times 10^{-6}$
0.3	1,630	80	1,530	97	1.0
0.3	2,500	80	2,347	150	1.5
0.6	970	105	761	191	1.0
0.6	1,487	105	1,167	293	1.5
0.6	1,938	105	1,520	383	2.0
0.6	2,650	105	2,075	526	2.7
0.835	807	111	512	249	1.0
0.835	1,237	112	784	382	1.5
0.835	1,612	111	1,022	498	2.0
0.835	2,205	111	1,397	681	2.7

NOMENCLATURE

A	Intercept of paint luminescence calibration, psfa for pressure or non-dimensional for CP [see Eq. (3)]
Alpha	Model angle of attack, deg
B	Sensitivity of paint luminescence calibration, psf for pressure or non-dimensional for CP [see Eq. (3)]
B.L.	Model buttock line, mm
CDSF	Forebody drag coefficient, stability axis
CLMSF	Forebody pitching-moment coefficient, stability axis
CLSF	Forebody lift coefficient, stability axis
CP	Surface pressure coefficient
F.S.	Model fuselage station, mm
I	Paint luminescence intensity at pressure, wind-on condition
I₀	Paint luminescence intensity in the absence of oxygen
I_{ref}	Paint luminescence intensity at reference pressure, wind-off condition
K_q	Stern-Volmer constant
Mach	Free-stream Mach number
P	Pressure at wind-on condition, psfa
P_{O₂}	Partial pressure of oxygen, psfa
P_{ref}	Pressure at wind-off condition, psfa
Rec	Chord Reynolds number, $\times 10^{-6}$
W.L.	Model water line, mm
X/C	Ratio of pressure orifice position (as measured from wing leading edge) to local chord